T.C.
DOKUZ EYLUL UNIVERSITY
IZMIR INTERNATIONAL BIOMEDICINE AND GENOME INTSTITUTE

BIOLOGICAL FUNCTIONS OF FAM134B AND ITS ASSOCIATION WITH CANCER

UMUR KELEŞ

DEPARTMENT OF MOLECULAR BIOLOGY
AND GENETICS

DOCTOR OF PHILOSOPHY THESIS

İZMİR-2020

THESIS CODE: DEU.HSI.PhD-2016850042

T.C.
DOKUZ EYLUL UNIVERSITY
IZMIR INTERNATIONAL BIOMEDICINE AND GENOME INTSTITUTE

BIOLOGICAL FUNCTIONS OF FAM134B AND ITS ASSOCIATION WITH CANCER

MOLECULAR BIOLOGY AND GENETICS

DOCTOR OF PHILOSOPHY THESIS

UMUR KELEŞ

Advisor: Doç. Dr. Güneş Özhan

Co-advisor: Prof. Dr. Mehmet Öztürk

(This Project was supported by Dokuz Eylül University,
Department of Scientific Research Projects with the Project code 2014.KB.SAG.047)

THESIS CODE: DEU.HSI.PhD-2016850042

Dokuz Eylül University Izmir International Biomedicine and Genome Institute Department of Genomics and Molecular Biotechnology, Molecular Biology and Genetics graduate program Doctor of Philosophy student Umur Keleş has successfully completed his Doctor of Philosophy thesis titled "**BIOLOGICAL FUNCTIONS OF FAM134B AND ITS ASSOCIATION WITH CANCER**" on the date of 11/11/2020

Doç. Dr. Güneş ÖZHAN
Dokuz Eylül University
CHAIR

Prof. Dr. Semra KOÇTÜRK
Dokuz Eylül University
MEMBER

Prof. Dr. Kemal Sami KORKMAZ
Ege University
MEMBER

Assoc. Prof. Şerif ŞENTÜRK
Dokuz Eylül University
MEMBER

Prof. Dr. Petek BALLAR KIRMIZIBAYRAK
Ege University
MEMBER

Assoc. Prof. Kasım DİRİL
Dokuz Eylül University
SUBSTITUTE MEMBER

Prof. Dr. Hilmi ORHAN
Ege University
SUBSTITUTE MEMBER

Dokuz Eylül Üniversitesi İzmir Uluslararası Biyotıp ve Genom Enstitüsü
Genom Bilimleri ve Moleküler Biyoteknoloji Anabilim Dalı,
Moleküler Biyoloji ve Genetik Doktora programı öğrencisi Umur Keleş,
"FAM134B'NİN BİYOLOJİK İŞLEVLERİ VE KANSERLE İLİŞKİSİ"
konulu Doktora tezini 11/11/2020 tarihinde başarılı olarak tamamlamıştır.

Doç. Dr. Güneş ÖZHAN
Dokuz Eylül Üniversitesi
BAŞKAN

Prof. Dr. Semra KOÇTÜRK
Dokuz Eylül Üniversitesi
ÜYE

Prof. Dr. Kemal Sami KORKMAZ
Ege Üniversitesi
ÜYE

Doç. Dr. Şerif ŞENTÜRK
Dokuz Eylül Üniversitesi
ÜYE

Prof. Dr. Petek BALLAR KIRMIZIBAYRAK
Ege Üniversitesi
ÜYE

Doç. Dr. Kasım DİRİL
Dokuz Eylül Üniversitesi
YEDEK ÜYE

Prof. Dr. Hilmi ORHAN
Ege Üniversitesi
YEDEK ÜYE

TABLE OF CONTENTS

LIST OF TABLES ..... **iv**

LIST OF FIGURES ..... **v**

ABBREVIATIONS ..... **viii**

ACKNOWLEDGEMENTS **1**

ABSTRACT **2**

ÖZET **3**

1 INTRODUCTION AND AIM **5**

2 BACKGROUND INFORMATION & LITERATURE **7**

2.1 Endoplasmic reticulum **7**

2.2 Protein Turnover mechanisms **9**

2.3 Autophagy: a lysosomal degradation pathway **9**

2.4 Nutritional starvation as a canonical autophagy model **16**

2.5 Proteasomal degradation pathway **17**

2.6 Endoplasmic Reticulum Stress **18**

2.7 FAM134B and cancer **21**

2.8 Other implications of FAM134B in physiology **23**

3 MATERIALS AND METHODS **25**

3.1 Type of the study **25**

3.2 Place and time of the conducted study **25**

3.3 Test systems **25**

3.4 Variables of the Study **25**

3.5 Materials **26**

3.5.1 Common reagents 26

3.5.2 General Laboratory Reagents and kits 27

3.5.3 Cell culture solutions and materials 28

3.5.4 Antibodies 28

3.5.5 Oligonucleotides 29

3.5.6 Plasmid DNA 30

3.5.7 SDS-PAGE and western blot 31

3.5.8 PCR materials and reagents 31

3.6 Methods **31**

3.6.1 Cell passaging and culture routine 31

3.6.2 Chemical transfection of cells and generation of stable cell line 32

3.6.3 Molecular cloning 33

3.6.4 SRB cell viability assay 34

3.6.5 Colony forming assay with crystal violet staining 34

3.6.6 Cell fractionation experiments 35

3.6.7 Protein extraction and quantification 35

3.6.8 SDS-PAGE & western Blot 36

3.6.9 Immunofluorescence 37
3.6.10 Oil Red-O staining 37
3.6.11 Ethics 38
3.6.12 Animal maintenance 38
3.6.13 Animal starvation experiments 39
3.6.14 Tumor xenograft 39
3.6.15 Tissue collection/isolation 39
3.6.16 DNA and RNA extraction 40
3.6.17 Polymerase Chain Reaction (PCR) 40
3.6.18 RNA-Sequencing 41
3.6.19 Curation and organization of RNA-sequencing data 41
3.6.20 Differential gene expression analyses 42
3.6.21 Gene ontology analyses 42
3.6.22 Genomics, transcriptomics and proteomics data 43
3.6.23 Histopathology 43

4 RESULTS 44

***FAM134B IN PHYSIOLOGY* 44**

4.1 *FAM134B* gene and protein variants are highly conserved across species 44

4.2 *FAM134B* isoforms are differentially expressed in healthy human tissues 49

4.3 *FAM134B-2* is predominantly expressed in human liver, pancreas and skeletal muscle 50

4.4 FAM134B protein expression in bovine tissues is concordant with human 51

***4.5* All six *Fam134b* transcript isoforms are expressed in mouse tissues 53**

4.6 FAM134B-1 is the dominant form *in vitro* 57

4.7 FAM134B localizes to Endoplasmic Reticulum 58

4.8 Both isoforms can be recognized by autophagosomes 59

4.9 FAM134B-2 is located in lighter sub-cellular fractions 62

4.10 FAM134B-2 do not precipitate neither with Calnexin nor with GOPC 64

4.11 FAM134B-2 localizes to Golgi 65

***FAM134B RESPONSE TO STARVATION* 68**

4.12 Both FAM134B isoforms are degraded in response to nutrient starvation 68

4.13 Ectopic FAM134B-1 expression increases LC3BII formation 70

4.14 Upon starvation, *Fam134b*$^{-/-}$ mice display less weight loss and increased serum albumin levels along with disrupted amino acid release 72

4.15 Starvation stimulates FAM134B-2 and another protein variant expression in liver ... 82

4.16 *Fam134b*$^{-/-}$ animals exhibit disrupted lipid storage in liver 84

4.17 FAM134B-2 is expressed in liver of different species 87

4.18 Starvation stimulates FAM134B-2 expression in muscle and heart 88

4.19 Prolonged starvation further increases FAM134B-2 accumulation 89

4.20 Absence of *Fam134b*$^{-/-}$ alters liver gene expression related with lipid synthesis 91

***FAM134B RESPONSE TO ER-STRESS* 100**

4.21 Effects of ectopic FAM134B-1 expression upon Thapsigargin mediated ER-stress .. 100

4.22 Thapsigargin fails to stimulate endogenous FAM134B expression in epithelial-like cells 103

4.23 Ectopically expressed FAM134B-1 accumulates in vesicles upon Thapsigargin treatment 106

4.24 Ectopic FAM134B-1 expression alleviates Tunicamycin induced LC3B accumulation 110

4.25 Tunicamycin enhances FAM134B-2 accumulation in liver 113

***FAM134B IN CANCER* 115**

4.26 *FAM134B* expression is altered during carcinogenesis 116

4.27 *FAM134B* mRNA levels decrease during HCC development 118

4.28 Effect of FAM134B ectopic expression on cell proliferation 119

4.29 Ectopic FAM134B expression suppresses tumor formation *in vivo* 122

4.30 Ectopic expression of FAM134B-1 suppresses inflammatory response *in vivo* 129

4.31 Ectopic expression of FAM134B-1 slightly alters survival response against anti-cancer agents 130

4.32 FAM134B-1 slightly alters survival response against ER-stress agents 132

4.33 Proteasomal blockage leads to accumulation of FAM134B 133

4.34 FAM134B-2 is suppressed during epithelial to mesenchymal transition 134

4.35 Ectopic FAM134B expression alters hepatocyte lineage specific markers 137

4.36 Induced FAM134B expression increases albumin levels 140

4.37 Ectopic FAM134B expression does not alters tumoroid formation *in vitro* 141

5 DISCUSSION 144

5.1 FAM134B in physiology 144

5.2 FAM134B in cancer 162

6 CONCLUSION & FUTURE PERSPECTIVES 167

7 REFERENCES 171

8 APPENDIX 183

8.1 Ethics Approval from İBG Animal Experiments Local Ethics Committee (İBG-AELEC) 183

8.2 Curriculum Vitae in ARBIS format 184

LIST OF TABLES

Table 1: List of organelle specific autophagy receptors 12
Table 2: The list of common chemicals and commercial kits 26
Table 3: Common buffers and respective formula 26
Table 4: Primary and secondary antibodies used in biological assays 28
Table 5: primers for RT-PCR 29
Table 6: primers used for mouse genotyping 30
Table 7: Primers used for molecular cloning 30
Table 8: The list of plasmids used in this thesis 30

LIST OF FIGURES

Figure 1: The structural proteins shaping ER. 8
Figure 2: Core autophagy machinery is initiated by activation of ULK1 complex 11
Figure 3: ER-phagy is mediated through various receptors. 14
Figure 4: ER-phagy receptors exert their functions in response to various stimulation 16
Figure 5: Activation PERK, IRE1α or ATF6 branches of UPR affect different cellular mechanisms 19
Figure 6: Autophagy and UPR crosstalk via different pathways 20
Figure 7: The canonical hallmarks represents the capabilities of cancer 22
Figure 8: *FAM134B* isoforms are generated through alternative transcription start sites 44
Figure 9: *FAM134B* variants are highly conserved across species. 48
Figure 10: FAM134B-2 lacks a large hydrophylic N-terminal domain and a hydrophobic transmembrane domain 48
Figure 11: Human FAM134B-2 is predominantly expressed in skeletal muscle and heart 50
Figure 12: Expression of long and short *FAM134B* in healthy human tissues as shown by RT-PCR 51
Figure 13: FAM134B-2 is strongly expressed in bovine muscle and heart 52
Figure 14: *In vivo* knockout model lacks exon 6, 7 and 8. 53
Figure 15: Mouse brain, testis and fat express FAM134B-1 while heart and muscle express FAM134B-2 55
Figure 16: FAM134B-2 is strongly expressed in mouse pancreas, stomach, muscle and heart. 56
Figure 17: Mesenchymal-like HCC cells predominantly express FAM134B-1 58
Figure 18: FAM134B colocalizes with Calnexin (CNX). 59
Figure 19: FAM134B-1 and FAM134B-2 can colocalize with LC3B. 60
Figure 20: FAM134B-1 and FAM134B-2 mostly co-localize 62
Figure 21: FAM134B-2 localizes to lighter sub-cellular fractions 63
Figure 22: anti-FLAG antibody mediated pull down of FAM134B-2 in Hep3B-FAM134B-2-FLAG cells. 65
Figure 23: FAM134B-2 Co-immunoprecipitates with Golgi marker 58K 67
Figure 24: Response of FAM134B variants upon nutrient starvation. 69
Figure 25: HepG2-FAM134B-1 clones are inducible for FAM134B-1 expression 70
Figure 26: FAM134B-1 accumulates over time even under starvation 71
Figure 27: *Fam134b*$^{-/-}$ animals resist starvation induced weight loss. 74
Figure 28: Starvation induces abrupted serum amino acid levels in *Fam134b*$^{-/-}$ mice. 78
Figure 29: *Fam134b*$^{-/-}$ mice exhibits low basal levels of HDL cholesterol, and increased serum protein after starvation 80
Figure 30: *Fam134b*$^{-/-}$ animals resisted starvation induced hypocalcemia. 81
Figure 31: *Fam134b*$^{-/-}$ mice exhibits increased serum a-amylase levels upon 36h starvation. 82
Figure 32: Starvation stimulates FAM134B-2 accumulation in liver. 83
Figure 33: Expression of different mouse *Fam134b* isoforms in liver upon 48h starvation. 84
Figure 34: *Fam134b* deficiency lead to disrupted accumulation of lipid droplets. 86
Figure 35: Liver FAM134B protein expression in zebrafish, rat, human and mouse. 87
Figure 36: Response of *Fam134b* during 36h starvation shown in skeletal muscle, heart, pancreas and stomach. 88
Figure 37: FAM134B-2 expression is further stimulated at 72h of starvation 90

Figure 38: Principle component analyses and correlation heatmap of starved mouse livers... 92
Figure 39: Volcano plot representing gene expression levels according to their P value and Log_2 fold change 94
Figure 40: Absence of *Fam134b*$^{-/-}$ leads to alteration gene expression in both *ad libitum* and starvation groups 97
Figure 41: Absence of *Fam134b* alters expression of genes involved in lipid and cholesterol synthesis 99
Figure 42: Thapsigargin treatment causes further accumulation of ectopically expressed FAM134B-1 101
Figure 43: Accumulation of ectopically expressed FAM134B-1 was further verified in follow-up experiment. 102
Figure 44: Thapsigargin treatment of ancestral cell lines with little or no FAM134B expression. 103
Figure 45: Thapsigargin induces FAM134B-1 expression at early time points 105
Figure 46: Time dependent accumulation of FAM134B-1 in HepG2-FAM134B-1 cells upon thapsigargin treatment 108
Figure 47: Vesicular accumulation of FAM134B-1 in HepG2-FAM134B-1 cells upon thapsigargin treatment 109
Figure 48: Expressional change of ectopically expressed FAM134B and LC3B upon treatment with Tunicamycin 111
Figure 49: FAM134B-1 accumulates as punctae in response to Tunicamycin treatment 112
Figure 50: Effect of Tunicamycin and Dexamethasone on FAM134B-2 expression in liver. 115
Figure 51: *FAM134B* is dramatically decreased in major human cancers 117
Figure 52: *FAM134B* isoform expressions of human hepatocellular carcinoma tissues shown by Reverse Transcriptase PCR. 118
Figure 53: Colony formation assay of HepG2 cells inducible expressing FAM134B-1. 120
Figure 54: SRB experiments of HepG2-FAM134B-1 cells with or without doxycycline 120
Figure 55: Ectopically expressed FAM134B isoforms *in vitro* caused contradicting proliferation rates in different systems 121
Figure 56: FAM134B-1 expression suppresses *in vivo* tumor development 124
Figure 57: Doxycycline is capable of inducing FAM134B-1 *in vivo* 125
Figure 58: Both FAM134B isoforms suppresses tumor development *in vivo* 128
Figure 59: Mouse native immune response against Hep3B-FAM134B-1 cells 129
Figure 60: Effect of Sorafenib and Bortezomib on FAM134B expressing HCC cell lines 131
Figure 61: Effect of Tunicamycin and DTT on FAM134B expressing HCC cell lines 133
Figure 62: Bortezomib induced FAM134B expression 134
Figure 63: RNA sequencing and western blot results of NMuMG cells which undergo to EMT and MET 136
Figure 64: Ectopic expression of both isoforms alters hepatocyte lineage specific markers. 138
Figure 65: Liver specific differentiation markers under the inducible expression of FAM134B isoforms 140
Figure 66: Ectopic FAM134B expression does not affect tumoroid formation 142
Figure 67: Tissues classified according to their expression levels of FAM134B isoforms 146
Figure 68: FAM134B-1 involves in protein control mechanism of extracellular matrix 149
Figure 69: Proposed localization of FAM134B-1 and FAM134B-2 150
Figure 70: FAM134B-2 is not a partner of CNX 151
Figure 71: Both FAM134B-1 and FAM134B-2 is able to attract expanding phagophore 152

Figure 72: Shorter FAM134B isoform might be associated directly with starvation 154
Figure 73: Both FAM134B-1 and FAM134B-2 are possible actors in alleviating ER stress 161
Figure 74: Mesenchymal transition is compatible with FAM134B-1 but not FAM134B-2.. 165
Figure 75: Proposed mechanism for FAM134B mediated tumor suppression 169

ABBREVIATIONS

FAM134B: Family with sequence similarity 134, member B

RETREG1: Reticulophagy Regulator 1

LC3B: Also known as MAP1LC3B. Microtubule-associated proteins 1A/1B light chain 3B

ER: Endoplasmic Reticulum

UPR: Unfolded Protein Response

HSANIIB: Hereditary Sensory and Autonomic Neuropathy Type 2B

CMA: Chaperone Mediated Autophagy

HCC: Hepatocellular Carcinoma

ERAD: Endoplasmic Reticulum Associated Protein Degradation

UPS: Ubiquitin Proteasome System

ERLAD: ER Lysosome Associated Degradation

IC50: The Half Maximal Inhibitory Concentration

TM: Tunicamycin

TG: Thapsigargin

RTN: Reticulon proteins

RHD: Reticulon Homology Domain

FTCD: Formimidoyltransferase Cyclodeaminase. Also known as 58K.

ACKNOWLEDGEMENTS

I would like to start thanking all administrative personnel in IBG (Center) and DEU-IBG (Institute), who showed great effort to establish a functioning system for researchers.

All research laboratories in İBG were always generous about sharing lab materials and scientific knowledge, which is deeply appreciated. Atabey lab and Erdal lab deserve special thanks, since we shared not only lab materials and scientific knowledge, but also many memories with group members, who have always been great friends to us.

I would like to thank all Öztürk Lab. members who accompanied me while I walked through this long road: Umut Ekin, Erhan Bal, Evin İşcan, Tuğçe Batur, Aybike Erdoğan, Özden Öz, Huriye Erbak Yılmaz, Zeynep Mutlu, Seval Kılıç, Sıla Kahyaoğlu and Özgün Teksoy.

I would like to thank Bilge Kılıç as manager of all core facilities; Melek Üçüncü and Didem Çimtay from imaging core; Emre İnanç and İsmail Küçükbayram from biomedical engineering; Gözde Yeşilyurt from Histopathology core; Ahmet Bursalı from bioinformatics core; Alkan Gökçeoğlu from Vivarium core; Esra Türker from Dimitrov lab; Burcu Şengez from Alotaibi lab; Burcu Ekinci and Tutku Yaraş from Oktay lab; Hande Topel, Yeliz Yılmaz, Dehan Çömez and Peyda Korhan from Atabey lab; Soheil Akbari and Sanem Tercan Avcı from Erdal Lab; Yağmur Azbazdar from Özhan lab; Kerem Esmen from Diril lab.

Once again, I would like to thank my brothers Umut Ekin, Soheil Akbari and Erhan Bal who have been great companion both as skillful scientists and great friends since we met.

I would like to express my deepest gratitude for my advisor Prof. Mehmet Öztürk, as he always has been a great father and excellent mentor to us throughout our career. I also would like to thank my advisor Güneş Özhan, for guiding us through our graduate study with great patience.

Finally, none of these achievements would be meaningful without my family, who deserves the sincerest acknowledgments. As he honored our lives during the preparation of this thesis, I devote this thesis to my son, Deniz Keleş.

November, 2020 Umur Keleş

BIOLOGICAL FUNCTIONS OF FAM134B AND ITS ASSOCIACTION WITH CANCER

Umur Keleş, Dokuz Eylül University Izmir International Biomedicine and Genome Institute, umur.keles@ibg.edu.tr

ABSTRACT

Hepatocellular Carcinoma (HCC) is a major health problem worldwide and cause thousands of deaths each year. HCC development is mostly stemmed from the cirrhotic liver where hepatocytes escape cellular senescence to gain immortality. Our group has previously defined the expressional decrease of *FAM134B* as a hallmark for immortalization. Later, FAM134B was shown to be a receptor that mediates degradation of Endoplasmic Reticulum fragments through the autophagosome. However, how these properties are associated with development of cancer remains largely unknown. Therefore, we aimed to investigate the functional characterization of *FAM134B* in the context of physiology and cancer.

Using *in vitro* and *in vivo* models, expressional changes of *FAM134B* variants were tested in response to various cellular stresses such as fasting, ER-stress, and inhibition of proteasome machinery. In the context of cancer, the expression of *FAM134B* variants was screened using databases in different cancer types. The effect of FAM134B variants on HCC tumor formation was evaluated by *in vivo* xenograft model.

The findings have shown that there are at least two transcriptional isoforms in human, and bovine, and at least six isoforms in mouse. Starvation stimulated short FAM134B-2 expression in the skeletal and cardiac muscles as well as in the liver of *Fam134b*$^{+/+}$ mice. Fasted *Fam134b*$^{-/-}$ mice yielded significant changes in body weight, serum biochemistry and liver transcriptome. Ectopic expression of FAM134B variants altered ER-stress response *in vitro* and suppressed xenograft tumor growth *in vivo*. Finally, short *FAM134B* variant was found to be significantly changed variant during the development of different tumors, including HCC.

In conclusion, the short and long FAM134B isoforms were shown mediate different functions in physiology and cancer, play an important role in energy metabolism; and lastly, the short FAM134B-2 variant is the most altered in various cancers.

Keywords: ER-phagy, reticulophagy, ER-stress, HCC, autophagosome, RETREG1, FAM134B, JK-1

FAM134B'NİN BİYOLOJİK İŞLEVLERİ VE KANSERLE İLİŞKİSİ

ÖZET

Umur Keleş, Dokuz Eylül Üniversitesi İzmir Uluslararası Biyotıp ve Genom Enstitüsü, umur.keles@ibg.edu.tr

Hepatoselüler Karsinoma (HSK) dünya genelinde hala büyük bir sağlık problemidir ve her yıl binlerce insanın ölümüne neden olmaktadır. HSK gelişimi çoğunlukla sirotik karaciğerden köken alır ve bu süreçte hepatositler hücresel yaşlanmadan kaçarak ölümsüzlük kazanır. Grubumuz, bu geçişte *FAM134B'*in bir belirteç gen olduğunu ve ifadesinin azaldığını göstermiştir. Farklı çalışmalar ise FAM134B'nin Endoplazmik Retikulum'un spesifik olarak otofagozom aracılığıyla yıkımını sağlayan bir reseptör olduğunu göstermiştir. Bununla birlikte, bu özelliklerin kanser gelişimi ile nasıl ilişkili olduğu büyük ölçüde bilinmemektedir. Bu bilgiler ışığında bu tez çalışmasında, FAM134B'nin, fizyoloji ve kanser bağlamında fonksiyonel olarak karakterize edilmesi amaçlanmıştır.

Çalışmada *FAM134B* varyantlarının gen ifade değişimleri aç kalma, ER-stres indüksiyonu ve proteazom inhibisyonu gibi hücresel stres uyaranlarına karşı yanıt bakımından *in vitro* ve *in vivo* modeller kullanılarak karakterize edilmiştir. Kanser çalışmalarında ise öncelikle FAM134B varyantlarının ifadesi farklı kanser türlerinde veri tabanları kullanılarak taranmıştır. FAM134B varyantlarının HSK tümör oluşumu üzerindeki etkisi, *in vivo* ksenograft modeliyle değerlendirilmiştir.

Bulgular insan ve sığırda en az iki *FAM134B* transkript izoformu, farelerde ise en az altı farklı izoform olduğunu göstermiştir. Açlık sonucunda *Fam134b*$^{+/+}$ farelerde karaciğerin yanı sıra iskelet kası ve kalp kaslarında kısa FAM134B-2 izoformunun gen ifadesinin uyarıldığı gözlenmiştir. Açlık deneyine tabi tutulan *Fam134b*$^{-/-}$ farelerde ise vücut ağırlığı, serum biyokimya ve karaciğer transkriptom değerleri anlamlı düzeyde değişiklik göstermiştir. Devamındaki çalışmalarda FAM134B'nin ektopik ifadesinin ER-stres yanıtını etkilediği ve *in vivo* xenograft tümör gelişimini baskıladığı gösterilmiştir. Son olarak, FAM134B ifadesinin, HSK dahil farklı tümör tiplerinde değiştiği tespit edilmiştir.

Sonuç olarak, bu çalışmada kısa ve uzun FAM134B izoformlarının hem fizyolojide hem kanserde farklı fonksiyonlara aracılık ettiği, enerji metabolizmasında da önemli rol oynadığı ve son olarak da kısa FAM134B-2 varyantının çeşitli kanserlerde ifadesi en çok değişen gen olduğu, bunun da karsinojenez sırasında kritik rol oynadığı gösterilmiştir.

Anahtar kelimeler: ER-faji, retikülofaji, ER-stres, HSK, otofagozom, RETREG1, FAM134B, JK-1

1 INTRODUCTION AND AIM

Hepatocellular carcinoma is a major health threat representing 6th most common, and 4th deadliest cancer type with approximately 780.000 deaths worldwide every year [1]. Usually, HCC tumors develop on the background of massive liver inflammation and fibrin deposition, namely, cirrhosis[2]. Although several etiological factors have been defined, the net outcome of these factors is chronic liver injury, leading hepatocytes to exhaust from constant replication and become senescent[3]. Therefore, the majority of the cirrhotic tissue is predominantly composed of exhausted senescent hepatocytes which have the potential to escape from this stationary state and become malignant[4].

Our group has previously identified *FAM134B* as a significantly downregulated gene that involved in cellular process of transformation from senescent to cancerous state in hepatocellular carcinoma cell clones of Huh7[5,6]. In following studies, its remarkable decrease was shown as a reliable marker during hepatocellular carcinogenesis on the background of liver cirrhosis[6]. Later, these results were further recapitulated by our work, where replicative senescent clones of Huh7 exhibited enhanced *FAM134B* expression, while cells escaping from senescence showed decreased *FAM134B* levels[7]. In the same studies, *FAM134B* was shown to encode at least two distinct isoforms, which contain reticulon homology domain and correspond to Endoplasmic Reticulum (ER) specific localization pattern, as demonstrated by CNX staining[7].

It was later shown by others that FAM134B is primarily located in Golgi apparatus, and its mutations are associated with HSANIIB (Hereditary Sensory Neuropathy Type II B)[8]. In this article, human *FAM134B* was shown to encode two isoforms, however they focused on long, full-length isoform to define mutations and their effects in nervous system. HSANIIB is an autosomal recessive disorder characterized with early onset of disruption of nociceptive and autonomic neurons which results in sensory loss[9].

Based on the more comprehensive background information given below, the main goal of the study is the following:

1- Although FAM134B related studies are questions were founded on full-length transcript isoform in literature, other isoforms were not described in details except few studies.

Therefore, we aimed to identify expressed isoforms of FAM134B in terms of gene and protein similarity across different species.

2- Although FAM134B was first located in Golgi apparatus, the papers coming after usually contradicted about exact location of FAM134B in cell. Hence, we sought to find localization of FAM134B by using various markers of organelles such as Endoplasmic Reticulum, Golgi and autophagosome.

3- FAM134B has been shown as an autophagy receptor in different physiological context including survival of peripheric nerves. Since autophagy is a major energy recycling pathway in metazoa, it is strongly suggested that FAM134B plays important roles not only in nervous system, but also in other organs which are at the center of organism's energy homeostasis. Therefore, we aimed to evaluate behavior of FAM134B in normal physiology and also under nutritional challenges such as starvation.

4- It has long been known that autophagy machinery and UPR pathways crosstalk and work together to resolve ER-stress. As an autophagy receptor located in ER membrane, there is strong implication that FAM134B might be involved in ER-stress response. Therefore, we aimed to test cellular responses to ER-stress induction using FAM134B based genetic models.

5- Although FAM134B was associated with different cancer types including HCC in several studies, there is still a lack of comprehensive analyses regarding the expressional changes of *FAM134B* and its isoforms cancer. Furthermore, the mechanism underlying the tumor suppressor or promoter properties of FAM134B is still not well-defined. Hence, we sought ways to identify how expression of different FAM134B variants is associated in various cancers. We also aimed to discover causative roles of FAM134B isoforms in liver cancer.

2 BACKGROUND INFORMATION & LITERATURE

2.1 Endoplasmic reticulum

Eukaryotic cells are equipped with dynamic membrane systems which separates specialized milieu as compartments, which is also called as “endomembrane system”. The largest member of this system is Endoplasmic Reticulum which occupies a large space in cytosol by forming uninterrupted membrane network of nuclear envelope, ER sheets (or ER cisternae) and ER tubules[10]. Endoplasmic Reticulum plays pivotal roles in eukaryotic cells such as intra- and extracellular signaling, vesicular trafficking, Ca^{+2} homeostasis and energy storage.

Synthesis and processing of cellular proteins are one of the most well understood roles ascribed to Endoplasmic Reticulum. Proteins that are resident to Endoplasmic Reticulum as well as to other vesicular organelles that are secreted into extracellular space or integrated into plasma membrane are simultaneously translated by ribosomes and transferred into ER lumen by translocon complexes. Usually, this process takes place at ribosomes attached to cytosolic leaflet of the ER sheets, which is also called Rough-ER. Thanks to the ER resident chaperone proteins, ER lumen provides excellent environment for complex protein folding events. ER also mediates glycosylation and disulfide bond formation of proteins passing through ER lumen[10].

ER is a continuous membrane system composed of nuclear envelope (NE) and peripheral ER, which can be structurally categorized into flat sheets and branched tubule network. Usually, ER-processed molecules are translocated to Golgi apparatus for further processing such as vesicle maturation or post-translational modification[11]. The molecules are shuttled back and forth between ER and Golgi through transport vesicles. This is mediated in a transition region between ER and Golgi, which is also called ER-Golgi Intermediate Compartment (ERGIC) and represent primary site for synthesis of membrane lipids of various endomembrane compartments[12]. ER derived vesicles enter Golgi through Cis-Golgi site and are redistributed to their target location after exiting from Trans-Golgi site.

While the role of ER cisternae is associated primarily with protein synthesis, ER tubules involves in broader range of functions including lipid synthesis, inactivation of xenobiotics and Ca^{2+} uptake/release. Hence, depending on the properties of the cell, lumenal content of ER sheets and tubules show great variability. For example, pancreatic acinar cells, which stores and secretes bulk amounts of digestive enzymes, are rich in ER sheets due to high

demand of protein synthesis in the tissue. Liver, on the other hand, is equipped with more extensive tubular ER, since major cholesterol synthesis and inactivation of xenobiotics take place in hepatocytes.

The shape and structure of ER is adapted according to the functional role of respective ER region. Different architecture of ER is formed with the help of numerous ER shaping proteins. Climp63, for example, contains a transmembrane and a hydrophilic domain that face towards the ER lumen, which allows protein to anchor on ER membrane and form homodimers inside the ER lumen. Furthermore, proteins such as p180 and KTN1 (Kinectin) contains long hydrophilic domains that bind and overlay on the cytosolic leaflet of the ER, giving the flatness of the ER sheets (Figure 1). However, membranes at the edge of every sheets need to be connected, forming a bent shape. Reticulons (RTNs) and REEP proteins are known to undertake such structural functions through their specialized membrane bending Reticulon Homology Domains (RHDs), and forms convex shaped curvature at the edges of ER sheets[13] (Figure 1). Similar to the edges of ER sheets, majority of tubular structure takes help from RHD containing proteins for bending the ER membrane in order to keep luminal space constant along the ER sheets. In addition to tubule formation, adapter proteins are also required to connect tubules to form three-way-junctions. Atlastins (ATLs) and Lunapark (LNP1) protein localize such intersections and stabilize these connections[14]. Unlike the RTNs and REEPs, these proteins harbor only half of the reticulon homology domains (Figure 1). Even though how the curvature is shaped by these proteins are not very well understood, one hypothesis suggests that RHD harboring proteins forms homo- or hetero-oligomers for shaping curvatures of tubules.

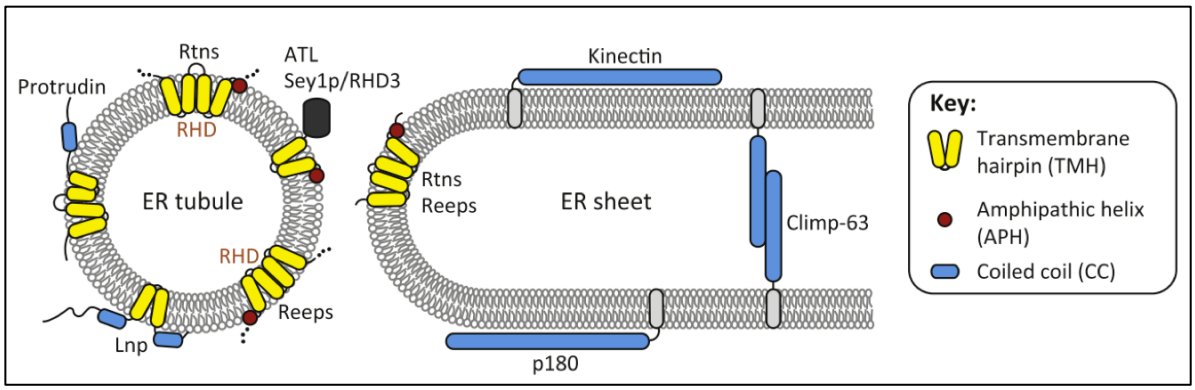


Figure 1: The structural proteins shaping ER.

While proteins such as Kinectin and Climp63 stabilize the flat structure of ER, RHD containing proteins including RTNs and ATLs tend form curvatures. The figure was adapted from Zhang et. al [13]

Similar to other ER shaping proteins, full length FAM134B has also been shown to harbor a RHD which bends ER[15,16]. Homo-oligomerization was also shown to be a necessity during the scission of ER fragments[17]. Furthermore, FAM134B was also shown to form hetero-dimers with Calnexin (CNX), an ER chaperone, in order to transfer vesicles filled with misfolded procollagen[18].

2.2 Protein Turnover mechanisms

Humans are usually advised to intake 60-80 gram of protein through daily diet in order to maintain the balance between anabolism and catabolism [19]. On the other hand, human body synthesize around 300-500 grams of protein every day. This gap is apparently compensated by intrinsic mechanisms by which endogenous proteins are recycled[19]. These two major protein turnover mechanisms are: 1- ubiquitin-proteasome system (UPS), by which intracellular proteins are tagged with short proteins called ubiquitin and destined to proteolytic cleavage in proteasome machinery; 2- Autophagy, which defines the sequestration of large cellular components, such as protein aggregates or even organelles, by autophagosome and degradation of segregated proteins via autophagosome-lysosome fusion [20].

As to be discussed below, discovery of the functional properties of FAM134B has greatly contributed to the understanding of organelle mediated autophagy, particularly in ER. Although autophagy and UPS are seemingly two distinct mechanisms, these pathways often intersect and work in harmony. Therefore, it is important to briefly introduce the two major protein degradation pathways.

2.3 Autophagy: a lysosomal degradation pathway

Lysosomes are cellular organelles enclosed in lipid bilayer and contain acid hydrolases for degradation of any macromolecule or organelle to contact with its lumen[21]. Lysosomes release their content usually by fusing with target vesicle such as late endosomes, phagosomes or autophagosomes. In addition to canonical organelles described above, there are also

examples of direct lysosomal uptake of other cellular structures such as DNA, RNA and proteins harboring KFERQ motif in their amino acid sequence[22].

Autophagy is a major protein recycling mechanism, through which cellular components are eventually degraded in lysosomes via proteolytic enzymes. So far, three distinct autophagy mechanisms have been described: microautophagy, macroautophagy and chaperone mediated autophagy (CMA).

The process of microautophagy refers to engulfment of cytosolic molecules through invagination of lysosomes or late endosomes[23]. Unlike the non-selective cargo processing abilities of macro- and microautophagy, chaperone mediated autophagy (CMA) is highly selective. Substrate of CMA is a pentapeptide, KFREQ, which is common to approximately 30% of cytosolic proteins. Target molecules carrying this consensus sequence is recognized by chaperones, unfolded and translocated into lysosomes, where proteolytic degradation takes place. Macroautophagy, on the other hand, represent a bulk autophagy process, in which an insulating membrane is generated to sequester target structures. This *de novo* organelle is called autophagosome and is able to wrap structures of different sizes ranging from single molecules to whole organelles[23]. Unless stated otherwise, macroautophagy will be referred as "autophagy" in following sections.

The process of autophagy starts with the generation of autophagosomes. Anatomically, autophagosomes are initiated mostly through budding from ER site, which is called omegasomes due to the shape of budding membrane similar to Greek letter omega (Ω). Then, membrane bilayer elongates, which is also called phagophore, and wraps target structures (e.g. organelle and protein aggregates) by recognizing organelle specific molecular receptors. Autophagosome formation is completed by fusion of open ends of phagophore. In the final form, cargo is completely surrounded by lipid bilayer and ready to fuse with lysosomes. After fusion with lysosomes, sequestered cargo and inner membrane of autophagosome is degraded by hydrolases, and molecular components are released back to the cytosol, where they are re-purposed as either building blocks or energy source[24] (Figure 2) . In mammals, autophagosomes may also fuse with early or late endosomes before fusing with lysosomes.

At molecular level, one of the main stimulants of autophagy cascade is depletion of amino acids, which is tightly sensed and regulated by mTOR protein. Under basal conditions, ULK1 and ATG13 proteins are attached to the mTOR complex 1 (mTORC1) as inactive form. Upon starvation, ULK1 undergoes autophosphorylation which is followed by ATG13 and

FIP200 phosphorylation. This triggers the phosphorylation of another protein complex consisted of VPS34, Beclin1, ATG14, AMBRA1 and p115. This is the initial step for phagophore nucleation which stimulates increase of local PI3P production. PI3P attracts WIPI and DFCP1 proteins via their PI3P binding domains, which in turn recruits other autophagosome precursors forming ATG16L~ ATG12 ~ ATG5 complex. This complex enhances the ATG3 mediated lipidation of ATG8 family proteins (e.g. LC3s and GABARAPs) with hydrophobic phosphatidylethanolamine (PE) groups. PE conjugated ATG8 family proteins (only LC3B is discussed in following sections) have long been considered as hallmark of active autophagosomes. ATG8-PE proteins not only can recognize any intracellular aggregate, organelle or complex through LC3-interacting region (LIR) on target molecule, but also are necessary for elongation of the phagophore membrane. During phagophore elongation, increased demand for lipid bilayer is supplied by other endomembrane system members such as Golgi complex, plasma membrane, mitochondria and endosomes through ATG9-containing shuttling vesicles. When elongated membranes are sealed, the structure is now called autophagosome and is ready to be fused with lysosomes.

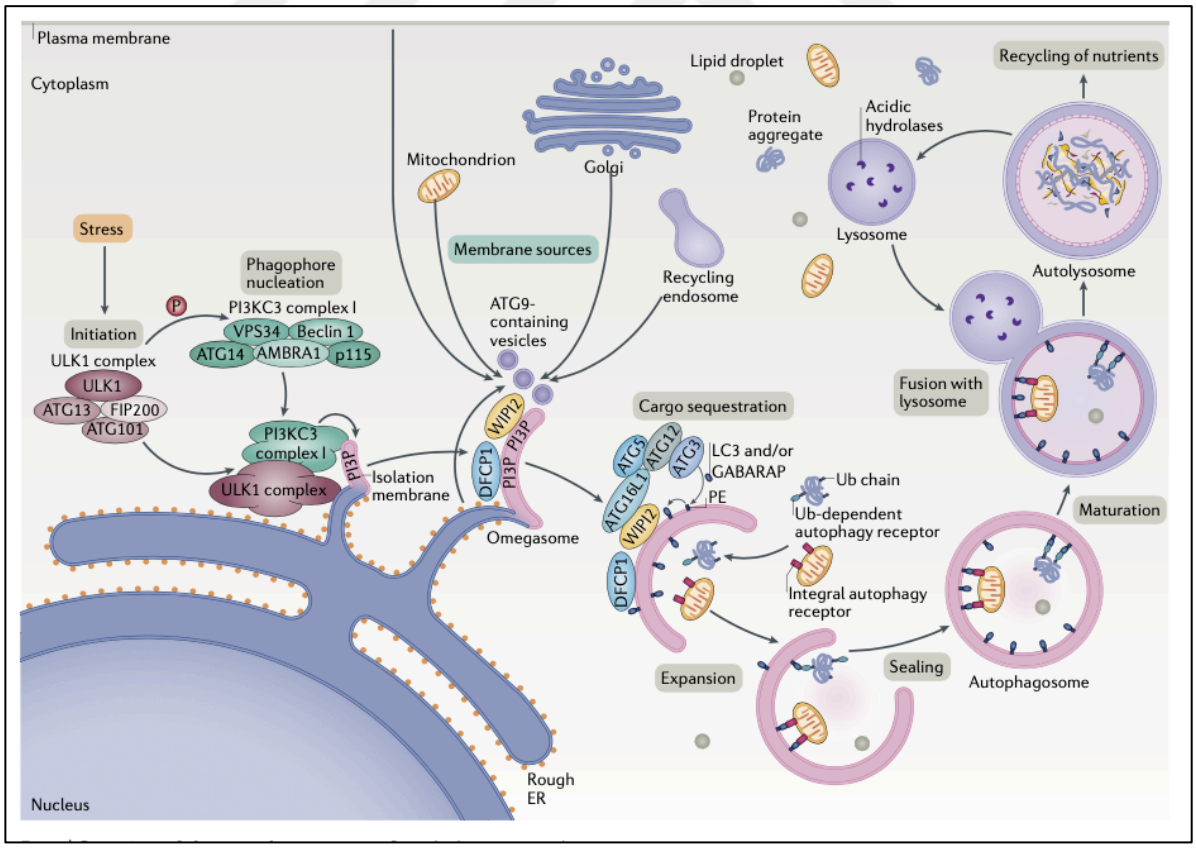


Figure 2: Core autophagy machinery is initiated by activation of ULK1 complex

The figure was adapted from Dikic et. al[24]

During nutrient starvation, increased demand for energy is compensated by activating autophagy, through which cellular molecules or more complex structures are engulfed and degraded into micro molecules. Although this process is usually considered as a non-selective response due to bulk degradation of intracellular structures, cells are equipped with various molecular mechanisms which facilitates highly selective sequestration of cellular components such as mitochondria, endoplasmic reticulum, invading bacteria or cellular aggregates by helping autophagy machinery to select respective structure (Table 1). This process is called "selective autophagy" and the selectivity is mediated through structure or organelle specific cargo receptors which are recognized by autophagosome/phagophore associated ATG8 family proteins (e.g. LC3B and GABARAP) [24]. Even though the nutrient deficiency initiates autophagy cascade, some intracellular structures undergo constant turnover via autophagy without stimulation. Since the studied gene in this study was mainly associated with endoplasmic reticulum mediated autophagy, no further discussion will be made on other selective autophagy types.

Table 1: List of organelle specific autophagy receptors.
The table was adapted from Johansen T. et. al. [25]

Target	**Mammalian autophagy receptors.**
Protein aggregate	p62, NBR1, OPTN
Mitochondria	NDP52, OPTN, p62, TAX1BP1, AMBRA1, NIX, BNIP3, FUNDC1, Bcl2L13, FKBP8, PHB2, NLRX1, AMBRA1, cardiolipin, ceramide
Peroxisome	NBR1, p62
Lysosome	TRIM16, NDP52
Secretory granule	p62
ER	FAM134B, SEC62, RTN3, CCPG1, ATL3, TEX264
Ferritin	NCO4A
Glycogen	Stbd1
Nuclear lamina	Lamin B1
Bacteria	NDP52, p62, OPTN, TAX1BP1

Viral capsids	TRIM5α, p62
Ribosomes	NUFIP1
Midbody rings	p62, NBR1, TRIM17

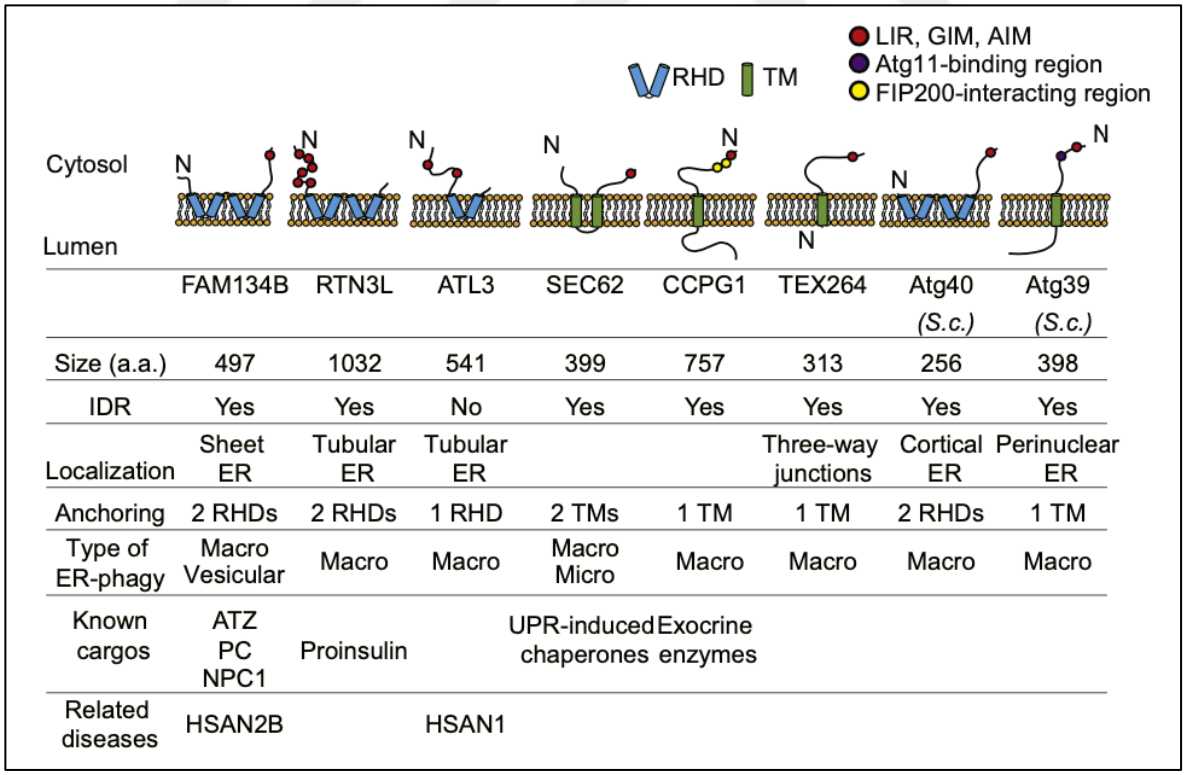
Endoplasmic Reticulum mediated autophagy can be defined as selective engulfment of ER fragments into autophagosomes followed by lysosomal fusion and degradation of the sequestered ER fragment. Although we have just started to understand the molecular insights of this process, the ER-phagy was nicely demonstrated for the first time almost half a century ago[26]. In the study, ultrastructure of rat liver was inspected during and after the treatment of phenobarbital. Phenobarbital treatment was shown to expand peripheral tubular ER in rat liver. However, during the recovery phase after treatment, ER fragments were observed encapsulated in double membrane vesicles[26].

Despite the striking discovery of ER-phagy, molecular understanding of the ER phagy has come decades after. Bernales et al. have shown that expanded ER sheets in yeast cells due to ER stress can be alleviated by ER sequestration and degradation via autophagy machinery[27]. In 2015, the receptors of ER mediated autophagy have been described for yeast and mammals by two groups in the same issue of Nature Journal. Khaminets et. al, described FAM134B as an ER localized protein, facilitating the autophagosome binding through LC3BII, thereby targeting ER fragments for lysosomal degradation[16]. This process was found to takes place under normal conditions without autophagy stimulation, which is also called ER-turnover. In association with HSANIIB, silencing of FAM134B resulted in expanded endoplasmic reticulum sheets which eventually lead neuronal death. In addition, they nicely recapitulated the HSANIIB phenotype by a knockout mouse *Fam134b*$^{-/-}$ model, which exhibited delayed and weakened response to pain stimulation in aged animals. In the same issue of the journal, yeast specific ER-phagy receptors Atg39 and Atg40 were described by others[28]. The former was shown to be responsible for degradation of ER regions near nucleus (Nuclear ER), while the latter was demonstrated to be a receptor for degradation of peripheric ER and its structure is highly similar to FAM134B (Figure 3).

Following its discovery, the mechanistic role of FAM134B has been further elaborated by various studies in the context of ER-phagy. One prominent example is the FAM134B mediated quality control of procollagen with the help of ER chaperone Calnexin[18]. In this study, Forrester et al. has shown that FAM134B is essential for the degradation of misfolded

procollagen, which is the precursor of one of the most abundant protein in the metazoan (Figure 4). Thanks to this study, the crosstalk between ER quality control and ER-phagy pathways has been demonstrated for the first time. Similarly, another group has demonstrated that alpha-antityripsin aggregated polimers (ATZ) in endoplasmic reticulum are degraded via FAM134B mediated lysosomal degradation[29]. Interestingly, however, FAM134B was shown to facilitate ER fragmentation and degradation via lysosomes, but without induction of core autophagy machinery. The process is called ER-to-lysosome associated degradation (ERLAD) which mainly represents LIR-independent formation of ER vesicles destined to fuse with endo-lysosomes with the help of LC3BII.

One of the most striking roles has been identified as a molecular defense mechanism against viruses which hijack the ER physiology in the favor of viral replication. Zika and Dengue viruses was shown to cleave the FAM134B at R142, resulting in a truncated version of FAM134B which fails to function as ER turnover receptor[30]. In following years, more articles elaborating the novel ER-phagy receptors with distinct functional roles have been published (Figure 4).



	FAM134B	RTN3L	ATL3	SEC62	CCPG1	TEX264	Atg40 *(S.c.)*	Atg39 *(S.c.)*
Size (a.a.)	497	1032	541	399	757	313	256	398
IDR	Yes	Yes	No	Yes	Yes	Yes	Yes	Yes
Localization	Sheet ER	Tubular ER	Tubular ER			Three-way junctions	Cortical ER	Perinuclear ER
Anchoring	2 RHDs	2 RHDs	1 RHD	2 TMs	1 TM	1 TM	2 RHDs	1 TM
Type of ER-phagy	Macro Vesicular	Macro	Macro	Macro Micro	Macro	Macro	Macro	Macro
Known cargos	ATZ PC NPC1	Proinsulin		UPR-induced chaperones	Exocrine enzymes			
Related diseases	HSAN2B		HSAN1					

Figure 3: ER-phagy is mediated through various receptors.

List of ER-phagy receptors, their respective structure, size, localization, anchoring style, cargo type and related diseases. Please note the structural similarity between mammalian FAM134B and yeast Atg40. The figure was adapted from Chino et. al [31]

Despite their structural and amino acid sequence differences, all ER-phagy receptors share some common features. All receptors: 1- are anchored to ER membrane either via RHDs which do not completely spans lipid bilayer or via membrane spanning TM domains; 2- have water soluble cytosolic domains, which might interact other cytosolic proteins or organelles to mediate protein specific functions[32]; 3- have at least one autophagosome binding motif as LIR and/or FIR (F200 interacting region) (Figure 3). These features together show that, besides the autophagosome binding ability, these proteins are involved in ER membrane shape. Among these receptors, despite the large difference in protein size, mammalian FAM134B and yeast Atg40 share quite similar structural organization (i.e. RHD and LIR motif). This strongly indicates that ER-phagy mediated by FAM134B-like proteins are highly conserved.

One of the recently discovered ER-phagy receptors was Sec62, which had been previously known as a component of ER-translocon complex. According to study, cells treated with ER stress agents such as cyclopiazonic acid (CPA) exhibits expanded ER due to unfolded protein response, which is relieved by Sec62 mediated autophagy after treatment is ceased[33]. Similarly, ER-phagy receptor CCPG1 was reported as a critical player in ER-recovery in cells challenged by ER-stress. Furthermore its deletion lead to increased expression of other ER-phagy receptor such as FAM134B and RTN3[34] along with formation of insoluble enzyme aggregates in pancreatic acinar cells[34]. Another receptor TEX264 was discovered as a key protein in ER-phagy, particularly in nutrient starvation[35]. RTN3 and ATL3 proteins were shown to be predominantly located on ER tubules and mediate tubular autophagy[32,36] (Figure 4).

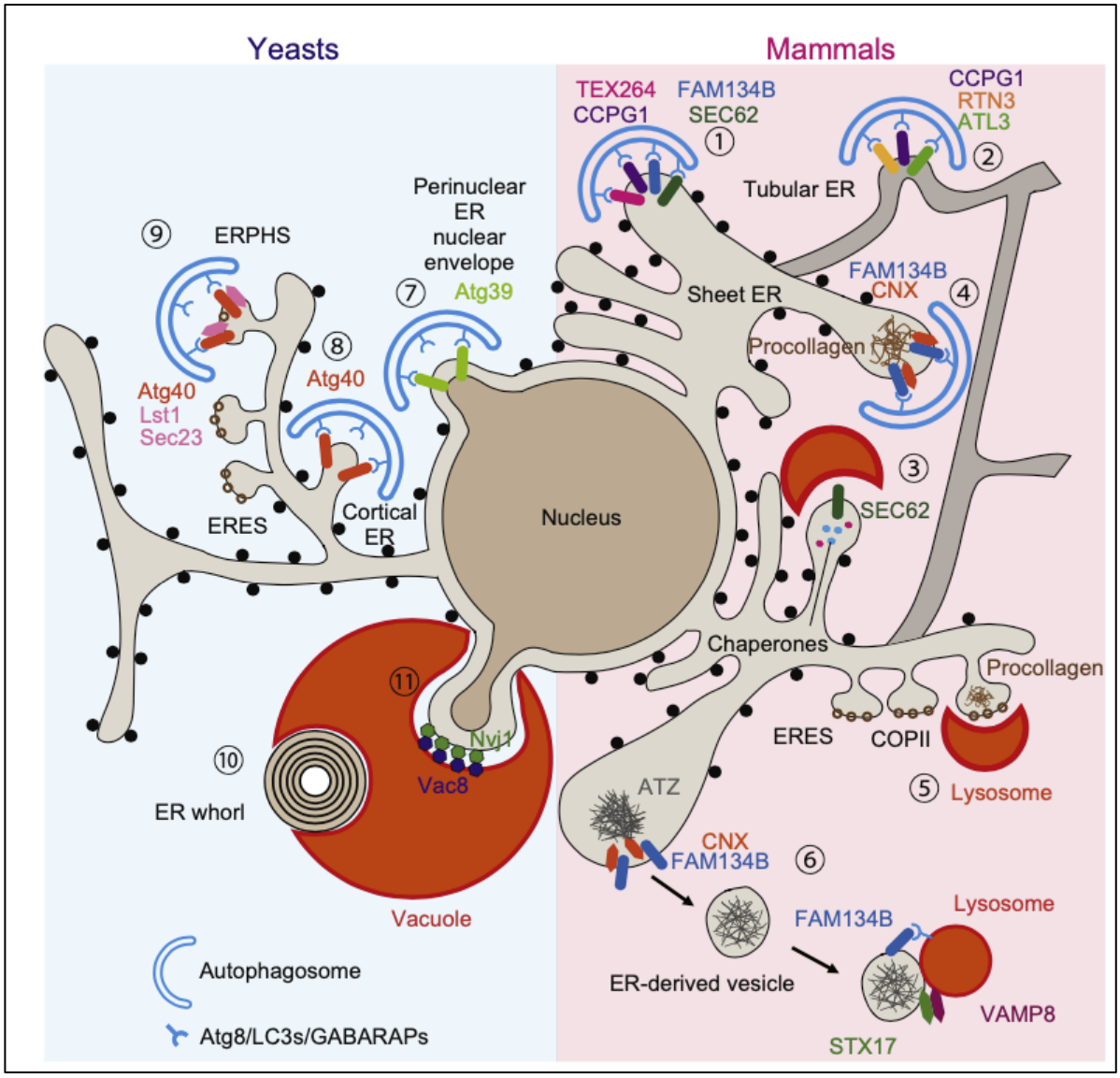


Figure 4: ER-phagy receptors exert their functions in response to various stimulation
The figure was adapted from Chino et al. [31]

2.4 Nutritional starvation as a canonical autophagy model

As previously described, canonical autophagy cascade is controlled by mTOR complex, which is highly responsive to cytosolic amino acid levels. Although it is possible to block or induce autophagy at different molecular levels by using physical, chemical or genetic tools, nutrient deprivation in both *in vitro* and *in vivo* has long been utilized as a reliable model for autophagy studies[37].

Starvation induced autophagy has been intensively studied *in vitro* using yeast and mammalian cell lines as models, which provided vast amount of information about autophagy

mechanisms at cellular level. However, induction of autophagy in a complex organism such as mammals initiates series of events, all of which are strictly organized to protect whole organism rather than protecting individual cells or organs. For example, besides the ketone body which is consumed at relatively little amounts, the primary fuel of the mammals' brain is glucose; therefore, energy expenditure of whole body is readjusted to maintain blood glucose levels at certain levels during starvation [38]. Liver stands at the center of energy homeostasis, as it both reads the signals about metabolic requirements of the body and meticulously orchestrate blood glucose, lipid and amino acid levels[39]. The early response of liver against starvation is the utilization of glycogen storage and maintain blood glucose. However, glycogen reserves can easily be depleted in prolonged fasting, and other micronutrients such as lipids and amino acids are used by liver for generating glucose, which is also called gluconeogenesis[40]. The lipids are also converted to ketone bodies (β-hydroxybutirate and acetoacetate) and released into bloodstream by the liver as a secondary carbon source after glucose. Since the ketone body production is increased during prolonged starvation, fatty acid storage also temporarily increase in hepatocytes in the form of lipid droplets, which is also called starvation induced steatosis[41].

2.5 Proteasomal degradation pathway

The initiation of autophagy cascade helps cells recycle large macromolecules composed of not only proteins but also lipids, complex sugars and even nucleic acids. However, when cells need to degrade individual proteins, they mostly take advantage of the Ubiquitin-Proteasome System (UPS), which represents major protein degradation pathway. In fact, this machinery is responsible degradation of around 80-90% of cellular proteins[20] and involves in critical cellular processes such as DNA damage repair, cell stress response and apoptosis. In order for proteasomal degradation to take place, target proteins must be tagged with 76-amino acid peptide, Ubiquitin. The Ubiquitin protein is ligated to target protein via core machinery composed of E1 (Activating Enzyme), E2 (conjugating enzyme) and E3 (ligating enzyme). Proteins tagged with certain ubiquitin motif, which is mostly poly ubiquitin polymers, can be recognized by proteasome complex.

For the homeostasis of ER, UPS is of particular importance, since one of the earliest responses to unfolded protein is the retro translocation of misfolded proteins into the cytosol which is followed by ubiquitination and degradation of target protein via proteasome

machinery[42]. Therefore, UPS blockage by proteasome inhibitors such as bortezomib and lactacystin[43] would cause ER-stress and eventually Unfolded Protein Response (UPR)

2.6 Endoplasmic Reticulum Stress

Although ER is equipped with a robust protein folding mechanism backed up with a strong arsenal of chaperones, the delicate homeostasis of ER can easily be disrupted by various factors resulting in accumulation of misfolded proteins in ER lumen, which is also called "ER-stress"[44]. In order to boost folding environment, one of the earliest response to ER stress is expansion of ER membrane[45]. However, membrane expansion alone may not be sufficient to alleviate ER-stress, where a cascade of events is initiated in order to either decrease the burden of total protein load, and/or increase the efficacy of protein folding properties of the ER. The mechanism is called Unfolded protein response (UPR) which is composed of three major pathways initiated by sensors anchored to ER membrane: Inositol-requiring protein 1α (IRE1α); Protein kinase RNA-like endoplasmic reticulum (ER) kinase (PERK); and Activating transcription factor 6 (ATF6)[46].

PERK signaling is one of the earliest responses to ER stress, in which PERK kinase phosphorylates translational initiation factor subunit 2α (eIF2α) resulting in attenuation of global protein translation. On the other hand, eIF2α selectively initiates translation of particular mRNAs that encodes stress response proteins. One such example is transcription factor ATF4 which initiates expression of genes involved in amino acid metabolism, redox homeostasis, apoptosis and autophagy.

IRE1α also senses disrupted ER homeostasis; but unlike the PERK pathway, IRE1α directly process cytosolic mRNAs or miRNAs. In order to reduce the protein load of ER, cytosolic mRNAs and miRNAs are degraded via regulated IRE1α dependent decay (RIDD). IRE1α also mediates the alternative splicing of *XBP1* mRNA, which encodes XBP1s protein, a transcription factor that transcriptionally activates set of genes involved in ER protein folding, translocation and ERAD (Figure 5).

Full length ATF6 protein translocate to Golgi upon ER stress, and cleaved by certain Golgi proteases (S1P and S2P) to release cytosolic fragment which translocate to nucleus and induce transcription of genes which are assigned in protein folding, ERAD, and ER biogenesis (Figure 5).

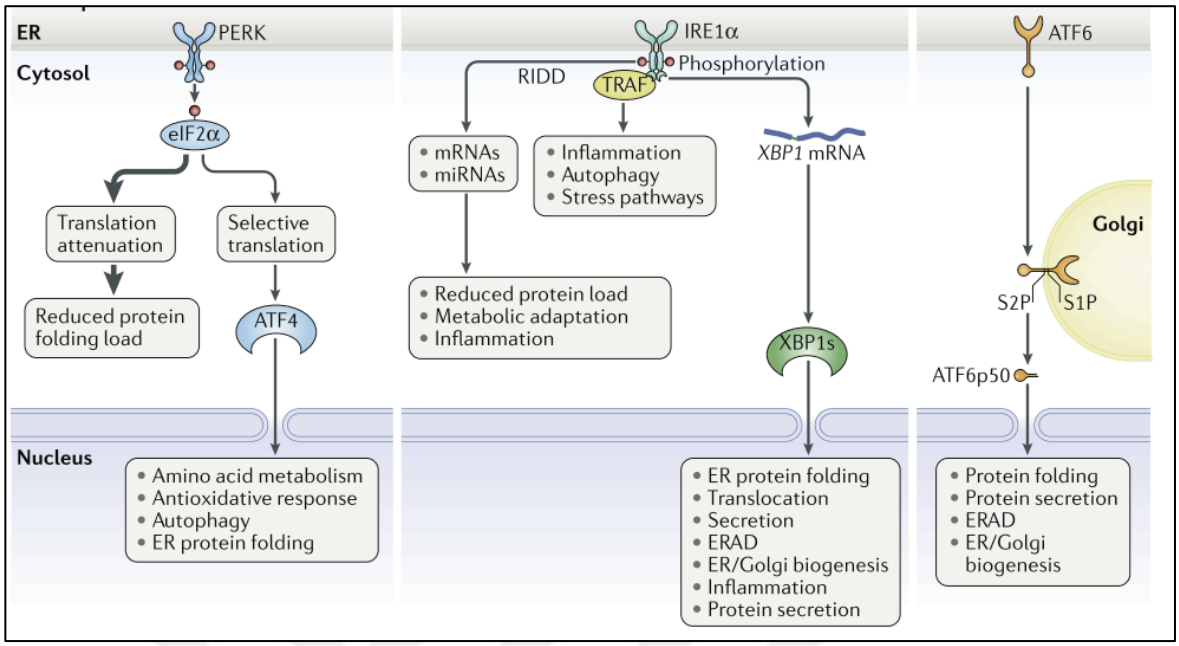


Figure 5: Activation PERK, IRE1α or ATF6 branches of UPR affect different cellular mechanisms

Besides the increased efficiency of protein folding, degradation of misfolded proteins is another major outcome of activated UPR. This is achieved by activation of both proteasomal and autophagy mediated degradation of misfolded protein in ER lumen (Figure 5).

ER associated translocon complexes mediate the shuttling of the misfolded proteins back to the cytosol, where they are simultaneously ubiquitinated and degraded through UPS. This pathway is named as ER associated degradation (ERAD) and alleviates the ER-stress by removing total protein burden of ER[47].

Although the comprehensive molecular mechanism is yet to be further delineated, ER-stress also stimulates the activation autophagy machinery in order to help cells recover from ER-stress by sequestering bulk amount of misfolded protein from ER[48]. This is mediated by various transcription factors activated in UPR (Figure 6). For example, ATF4 from PERK cascade and XBP1 from IRE1α is able to activate autophagy associated Beclin1 and ATG proteins (Figure 6).

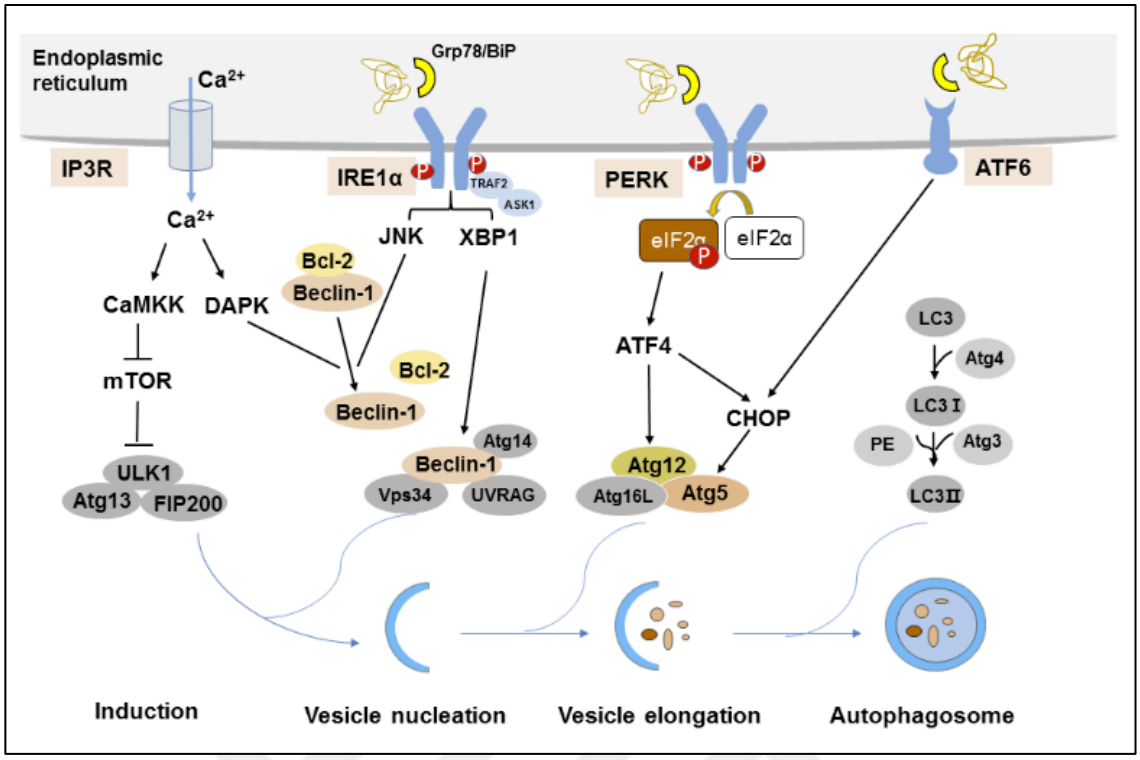


Figure 6: Autophagy and UPR crosstalk via different pathways

The figure was adapted from Song et al. [48]

Before its discovery as an ER-phagy receptor, our group had performed several studies in order to illuminate possible relationship between FAM134B and ER-stress response. One of the most critical findings shown that shRNA mediated FAM134B silencing dramatically increases the susceptibility of Snu449 cells to undergo apoptosis upon treatment with ER stressor Thapsigargin (TG)[49]. Furthermore, Huh7 cells treated with ER-stress agents such as Tunicamycin or Thapsigargin exhibited elevated levels of FAM134B transcript[50].

After the role of FAM134B was discovered as ER-phagy receptor, few papers were able to establish the connection between FAM134B and ER-stress response. A mechanistic study from Jiang et al. has demonstrated that ER-stress activated CAMK2B phosphorylates the reticulon homology domain of the FAM134B, facilitating the protein homo-oligomerization thereby the ER-phagy[17]. Similarly, seizure induced apoptotic cell death and ER-stress in hippocampal neurons were shown to be decreased through FAM13B induced ER-phagy[51]. In another study, FAM134B expression was shown to be upregulated as a response to procollagen IV accumulation in ER, which is caused by enzyme inhibitory effect of 2-Hydroxygluterate in

glioma cells [52]. On the other hand, a controversial role of FAM134B was revealed in another study that, when excessive ER phagy is stimulated via chemical Z36, robust degradation of ER through autophagy leads to disrupted ER homeostasis, ER-stress and eventually cell death[53].

2.7 FAM134B and cancer

Cancer remains to be a major health problem and leading cause of death worldwide. The expectation as of 2018 is around 17 million new cancer diagnosis and 8 million deaths due to cancer [54]. In order to tackle this ever-challenging task, a comprehensive understanding of the molecular mechanisms underlying the cancer development is essential. Despite the fact that development of cancer depends on numerous variables, the long-known hallmarks of cancer are still guiding cancer researchers to pave the way for gaining new insights about cancer biology. These hallmarks are six different capabilities of cancer: Resisting cell death, inducing angiogenesis, sustaining proliferative signaling, evading growth suppressors, activating invasion and metastasis, enabling replicative immortality[55] (Figure 7). Additional properties of cancer such as deregulating cellular energetics and avoiding immune destruction are considered as emerging hallmarks.

In order to survive and thrive, tumor must tackle some critical environmental challenges such as hypoxia, lack of glucose and other nutrients due to poor vascularization[56]. All these challenges directly or indirectly affect protein folding capacity of ER. For example, activity of disulphite isomerases which catalyzes post-translational formation of disulphite bonds are oxygen dependent and can be directly affected by hypoxia. Since glucose acts as a donor for protein glycosylation in ER, its absence prevents the proper glycosylation of proteins, causing protein retention in ER. In such challenging conditions, activation of UPR is a key survival factor for cancer cells, because the UPR cascade increases protein folding capacity, degradation of misfolded proteins through ERAD and autophagy.

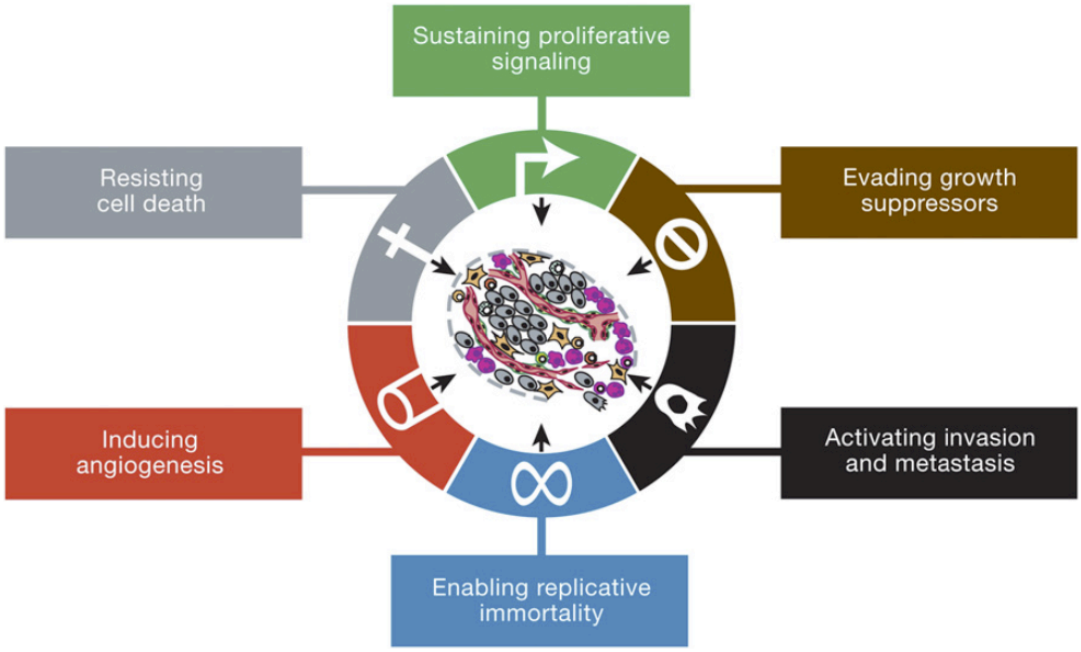


Figure 7: The canonical hallmarks represents the capabilities of cancer
The figure was adapted from Hanahan et al. [55]

Earliest insights of FAM134B has actually come from oncology studies. Tang et al. discovered that JK-1 (later named as FAM134B) located at chromosome 5p is amplified in esophageal squamous cell carcinoma (ESCC) and its overexpression promoted cell growth of NIH3T3 and Hek293 cells[57,58]. In line with this, silencing of FAM134B in ESCC cell lines abrogated the proliferating capacity[59]. A more recent study has also shown that FAM134B overexpression leads to Epithelial to Mesenchymal transition through Akt signaling in hepatocellular carcinoma[60].

Contrary to the studies delineating its tumor promoting role, there are several studies supporting the role of FAM134B as a tumor suppressor. Working on a large patient cohort, Kasem et al. has shown for the first time that copy number of FAM134B is decreased in colon tumors[61]. In following studies, they also demonstrated that the expression level of FAM134B is decreased in patients diagnosed with colorectal carcinoma[62,63] and silencing of FAM134B in colon cancer cell lines significantly increases tumor forming capacity[64,65]. As much as decreased expression is attributed to decreased copy number, FAM134B was also shown to be silenced via promoter methylation[66] and micro RNA (miR-142-5p and miR-186-5p)[67,68].

Furthermore, loss of FAM134B has also been defined as a diagnostic marker for colorectal cancer[69,70]. Although the type of mutations were not attributed as gain- or loss-of-function, *FAM134B* gene was shown to mutated in all metastatic cases of ESCC[71]. However, it also must be noted that, in the same study, around 37% of the patients exhibited increased gene copy number whereas there was copy number decrease in 35% of the patients.

As stated in the first section of the introduction, our group has previously identified FAM134B as one of the key expression marker that distinguish HCC from cirrhosis by decreased expression in HCC[6]. This notion was further verified by senescent Huh7 cell clones, which exhibited increased FAM134B expression. Cells gaining immortality through escaping senescence has shown decreased FAM134B expression[7], which strongly favors the tumor suppressor function of the molecule.

Further investigation on the role of FAM134B in cancer revealed that FAM134B is expressed almost exclusively in poorly differentiated liver cancer cell lines which exhibit morphological and molecular characteristics of mesenchymal cells such as spindle shaped morphology and expression of EMT markers [72]. Among these cell lines, Snu449 was also picked as a model cell line, since it strongly expresses FAM134B, shows outstanding drug resistance activity among other cell lines and proliferates robustly. Strikingly, when *FAM134B* expression was silenced through RNAi, cell morphology and proliferative capacity was shown to be deeply affected in Snu449 cells. Firstly, although cells tended to gain more mesenchymal-like morphological characteristics, they became less proliferative shown by wound healing assay[49]. Resistance against TG, TM and Adriamycin induced cell death greatly reduced upon RNAi silencing of *FAM134B*[49]. Furthermore, cancer cells responded TGF-β treatment with decreased FAM134B levels[49,50].

Although there are multiple studies demonstrating mechanistic role or its association with cancer, to our knowledge, FAM134B could not have been directly linked with cancer in the context of ER phagy. Furthermore, FAM134B has been associated with both tumor suppressor and tumor promoting properties.

2.8 Other implications of FAM134B in physiology

In addition to its well-studied role in ER-phagy and diseases such as cancer and neuropathy, FAM134B has also been associated with other physiological contexts. One

interesting example is the fat deposition in adipose tissue. *FAM134B* has been shown as a key regulator of fat deposition in adipose tissue in pigs and its activity is regulated via adenosine methylation of mRNA[73,74]. Same group has demonstrated that this adipogenic activity can be achieved by enhancing the differentiation of adipocytes[75]. They further detailed the underlying mechanism by claiming that overexpressing *FAM134B* in mouse tissues and in differentiating 3T3-L1 preadipocytes result in increased mitophagy, which in turn cause increased fat deposition[76].

Association of FAM134B with lipids was also investigated in another study, where FAM134B levels were shown to be increased upon nutrient starvation[77]. The researchers identified that nutrient starvation in mice transcriptionally activates expression of a truncated short *Fam134b* isoform in liver, through autophagy related C/EBPβ transcription factor. Proteomics analyses has revealed that absence of *Fam134b* during starvation rescues ApoIIIC from degradation which is a structural protein of lipid carrier VLDL[77]. Since liver is the main manufacturing and scavenging center of serum lipoproteins, this study represents critical evidence regarding the role of *Fam134b* on energy homeostasis of whole organism.

3 MATERIALS AND METHODS

3.1 Type of the study

This study is based completely on experimental methods.

3.2 Place and time of the conducted study

This study was performed between June 2016 and September 2020, at laboratories of İzmir Biomedicine and Genome Center. All animal experiments were performed at Laboratory animal facility of İBG.

3.3 Test systems

Both cell culture and animal models were utilized as test systems in this study. HCC cell lines were used from cell stocks of Prof. Mehmet Öztürk's group. Heterozygous *Fam134b*$^{-/+}$ animals were kindly gifted by Christian Hübner from Friedrich Schiller University Jena, Germany and previously described [16]. Animals were housed and bred in iBG-Vivarium Rodent Facility.

3.4 Variables of the Study

In this study, depending on the context, FAM134B has been considered both as dependent and independent variable.

In experiments where FAM134B is overexpressed or knocked out, different physiological or cellular parameters were monitored in order to understand the role of the molecule. Therefore, FAM134B was considered as independent variable. However, it is also a dependent variable, since its expression levels are sensitive to other factors such as starvation, ER stress and proteasome blockage etc.

Some of the main independent variables are ER-stress, nutrient starvation (both *in vivo* and *in vitro*) and proteasome inhibition. Serum metabolytes, lipid levels, LC3B-II/LC3B-I ratio and relative levels, amino-acid levels, all biological parameters retrieved from animal studies are dependent variables.

3.5 Materials

3.5.1 Common reagents

The common reagents used in study are listed in Table 2 and buffers are listed in Table 3

Table 2: The list of common chemicals

Reagent Name	**Brand**	**Catalog No**	**Storing temperature**
NaCl	BioShop	SOD001.1	RT
Tris	Amresco	826	RT
Tris-HCl	BioShop	TRS002.500	RT
EDTA	Bioshop	EDT001.500	RT
Sodium Dodecyl Sulfate (SDS)	BioShop	SDS001.1	RT
Skim Milk Powder	BioShop	SKI400.250	RT
Nonidet P-40 Substitute	Amresco	E109	RT
Tween-20	Amresco	0777	RT
Tryptone	Amresco	J859	RT
Proteniase K	ThermoScientific	17916	-20°C
Safe View	ABM	G108	+4°C
Tunicamycin	Sigma	T7765	-20°C
Oil Red O	Sigma	OO625	RT
Paraformaldehyde	Serva	31628.02	RT
Acrylamide	Sigma	A3553	RT
Bisacrylamide	Sigma	294381	RT
Methanol	Milipore	1060092511	RT
2-propanol	Sigma	24137	RT

Table 3: Common buffers and respective formulations

RIPA protein lysis buffer:	150mM NaCl, 1% Nonidet P-40, 0.5% Sodium deoxycholate, %0.1 SDS, amd 25mM pH7.4 Tris
Tail Buffer:	50mM Tris-HCl pH8.0, 100mM EDTA pH8.0, 100mM NaCl, 1% SDS.
1X PBS:	137mM NaCl, 2.7mM KCl, 8mM Na2HPO4, and 2mM KH2PO4, pH 7.4,
1X PBS-T:	1X PBS with 0.1% Tween-20
1X TBS:	50mM Tris-HCl, pH 7.5, 150mM NaCl,
1X TBS-T:	1X TBS with 0.5% Tween-20
LB(Luria-Bertani) medium:	10g BactoTryptone, 5 gr yeast extract, 5gr NaCl dissolved in 1L ddH_2O
LB(Luria-Bertani) agar:	10g BactoTryptone, 5 gr yeast extract, 5gr NaCl, 15g bacto agar dissolved in 1L ddH_2O
Oil Red O Stock Solution:	2.5 g of ORO is added into 99% Isopropyl alcohol solution (v/v) and mixed by a magnetic stirrer for 2 hours at room temperature. The solution can be stored at RT for 6 months.
SRB staining solution:	0.04% (weight/vol) SRB powder is dissolved in 1% Acetic acid

3.5.2 General Laboratory Reagents and kits

The reagents used in this dissertation were purchased from various chemical companies. Ethanol, methanol, Bovine Serum Albumin (BSA), Dexamethasone, Oil Red O, Sulfarhodamine B (SRB) and DMSO were purchased from Sigma-Aldrich (St. Louis, MO, USA). Midi and maxi plasmid isolation kits and NucleoSpin total RNA isolation kits were purchased from Machery-Nagel (Düren, Germany). Agarose and non-fat milk powder were purchased from Bioshop (Canada). For water compatible glass mounting, Prolong Gold Antifade Mountant was purchased from Invitrogen (Carlsbad, CA, USA). For protein quantification Bicinchoninic Acid (BCA) kit was purchased from ThermoFisher (Waltham, MA, USA). Gel extraction kit was purchased from Qiagen.

3.5.3 Cell culture solutions and materials

Cell culture medium is composed of basal Roswell Park Memorial Institute-1640 (RPMI-1640) media, supplemented with 10% GIBCO Fetal Bovine Serum, 1x Penicillin/ Streptomycin (100U/ml), 1x MEM non-essential amino acids, trypsin-EDTA 0.25%, all purchased from ThermoFisher Scientific (Waltham, MA, USA). Tunicamycin and thapsigargin were purchased from Sigma-Aldrich (St. Louis, MO, USA). For plasmid transfection to mammalian cells, FuGENE HD was purchased from Promega (Medison, WI, USA). Cell culture grade 1x PBS without calcium or magnesium was purchased from Serox GmbH (Mannheim, Germany)

3.5.4 Antibodies

Antibodies used for biological assays are listed in Table 4:

Table 4: Primary and secondary antibodies used in biological assays

Primary Antibody	Host Species	Brand	Catalog Number	Western Blot	IF
α-FAM134B	Rabbit	Sigma	HPA012077	1:2000	1:200
α-LC3B	Rabbit	Cell Signaling	2775S	1:2000	1:200
α-Calnexin	Mouse	Santa Cruz	sc23954	1:1000	1:200
α-β-Actin	Mouse	Abcam	Ab6276	1:5000	-
α-FLAG	Mouse	Sigma	F3165	1:5000	1:200
α-58K	Mouse	Abcam	ab27043	1:2000	1:200
α-GOPC	Rabbit	Cell Signaling	cs8576	1:1000	-
α-Syntaxin 6	Mouse	Cell Signaling	cs2869	1:1000	1:200
α-AFP	Mouse	Sigma	A8452	1:1000	-
α-ALB	Mouse	Santa Cruz	sc271605	1:1000	-
α-GM130	Mouse	Abcam	ab31561	1:1000	-
α-AAT1	Mouse	Santa Cruz	sc166018	1:2000	-
α-PARP	Rabbit	Cell Signaling	cs9542	1:2000	
α-ATL2	Rabbit	MyBiosource	MBS7001027	1:2000	-

α-Mouse-HRP	Horse	Cell signaling	7076S	1:10000	
α-Rabbit-HRP	Goat	Invitrogen	31360	1:5000	
α-Mouse-Alexa488	Goat	Invitrogen	A11029	-	1:5000
α-Mouse-Alexa594	Goat	Invitrogen	A11005	-	1:5000
α-Rabbit-Alexa488	Goat	Invitrogen	A11008	-	1:5000
α-Rabbit-Alexa594	Goat	Sigma	77671	-	1:5000

3.5.5 Oligonucleotides

Oligonucleotides used for RT-PCR are listed in Table 5; for genotyping PCR, Table 6; for molecular cloning, Table 7.

Table 5: Primers for RT-PCR

Primer ID	Sequence
mm_Fam134B_Isoform1_F	TTCTGGTTCCTTGCCTTGAC
mm_Fam134B_Isoform2_F	TGCTGGAGTGAGAGAGCCTGT
mm_Fam134B_Isoform3_F	CATAATAGTCCACTCCTCGGC
mm_Fam134B_Isoform4_F	TCACGGTGCTGGAGTGAGAGC
mm_Fam134B_Isoform5_F	CTCTGAGGTAATAGGCTCCTG
mm_Fam134B_Isoform6_F	AGTGTTATGAAATGGGTCACAG
mm_Fam134B_common_R	CAGAAGGTAGCTGAGTATGAC
murine_hprt_F	CACAGGACTAGAACACCTGC
murine_hprt_R	GCTGGTGAAAAGGACCTCT
mm_Fam134B_X1_F	TCCTGTGCGTGCTTCTTGTGAG
mm_Fam134B_X1_R	AAGCGCTCCTCCTCTCTC
mm_Fam134B_X2_R	AAAGCGCTCCTCCTCTAC
hs_Fam134B_Isoform1_F	GAGAAGCCTCAGTGAAAGCTG
hs_Fam134B_Isoform2_F	TTTGGACCAGGCAAAAGCTGG
hs_Fam134B_common_R	GCAACCGTGAGGCTAATCTTAGGA
murine β-actin_F	AAGGCCAACCGTGAAAAGAT
murine β-actin_R	GTGGTACGACCAGAGGCATA
murine IL6_F	GTGGTATCCTCTGTGAAGTCT

murine IL6_R	AAGAGCTTCCAGCCAGTTGCC
murine TNF- α_F	GTGCCACTTCATACCAGGAGAA
murine TNF- α_R	TCACAGACGAATGACTCCAA

Table 6: Primers used for mouse genotyping

Primer ID	Sequence
Fam134b_mut_F	CATGGCAATGACATTTCTCC
Fam134b_wt_F	ACCCCATAGTTCATACTAGGC
Fam134b_wt_R	CGTAACAGAGGTTGGTGAGG

Table 7: Primers used for molecular cloning

Primer ID	Sequence
Famb1_mchc1_F	CCTCGAGAAGCTTCTATGGCGAGCCCGGCGCCTCC
Famb2_mchc1_F	CTCGAGAAGCTTCTATGCCTGAAGGTGAAGACTT
Famb_common_Rev	GAATTCGGATCCTTAATGGCCTCCCAGCAGAT

3.5.6 Plasmid DNA

Plasmids used in this study listed in Table 8

Table 8: The list of plasmids used in this thesis

Plasmid	**Mammalian Selection**	**Bacterial Selection**	**Tag**	**Location**
pcDNA4TO-FAM134B-1	Zeocin	Amp.	NA	-
pcDNA4TO-FAM134B-2	Zeocin	Amp.	NA	-
p3xFLAG-CMV-14-FAM134B-1	Neomycin	Amp.	FLAG	C-Term
p3xFLAG-CMV-14-FAM134B-2	Neomycin	Amp.	FLAG	C-Term
pEGFP-FAM134B-1	Neomycin	Kanamycin	EGFP	N-Term
pEGFP-FAM134B-2	Neomycin	Kanamycin	EGFP	N-Term
pmCherry-FAM134B-1	Neomycin	Kanamycin	mCherry	N-Term
pmCherry-FAM134B-2	Neomycin	Kanamycin	mCherry	N-Term

3.5.7 SDS-PAGE and western blot

Polyacrylamide gel casting, protein running and wet transfer workflow is performed using Bio-Rad mini-PROTEAN Tetra Cell system (Hercules, CA, USA). PVDF membranes were purchased from Millipore (Burlington, MA, USA) and Nitrocellulose membranes were purchased from GE healthcare (Chicago, IL, USA). For the Enhanced Chemiluminescence (ECL) procedure, SuperSignal West Dura Extended Duration Substrate and SuperSignal West Pico Plus Chemiluminescent Substrate were purchased from ThermoFisher Scientific (Waltham, MA, USA). Protein marker was also purchased from ThermoFisher Scientific (Waltham, MA, USA).

3.5.8 PCR materials and reagents

For cDNA synthesis, Revert-aid First Strand cDNA kit was purchased from ThermoFisher Scientific (Waltham, MA, USA). For conventional PCR reactions, MyTaq DNA polymerase kit was purchased from Bioline (London, England). 1kb and 100bp DNA ladders were purchased from ThermoFisher Scientific (Waltham, MA, USA).

3.6 Methods

3.6.1 Cell passaging and culture routine

Cell lines were manipulated using standard aseptic cell culture techniques under Class II type A biosafety cabinets and incubated in 5% CO2 incubators.

Frozen cells were thawed by incubating frozen vials in 37C water bath for one minute. In order to dilute and discard freezing medium, fresh complete medium was added in a 15ml falcon tube and centrifuged at 200xg for 5 minutes. After supernatant was discarded, fresh complete media was added on cell pellet and gently resuspended. Then, cells were seeded on flasks or dishes.

Routine cell culture manipulation technique for monolayer cell lines was performed by following steps: 1- cells were checked for confluency and passaged when 70-90 % confluent; 2- culture medium was removed using air vacuum system and cells were washed with warm, Calcium or Magnesium free PBS; 3- PBS was discarded using vacuum and cells were incubated with 0.25 % Trypsin-EDTA in CO2 incubator in order to detach from the surface; 4- in order

to inactivate trypsin, fresh complete media is added on cells with at least 1:4 trypsin to medium ratio; 5- cells were mixed with trypan blue dye with 1:1 ratio and counted on a hemocytometer; 6- required amount of cell suspension is transferred to clean cell container (well-plate, flask or petri dish); 7- if downstream wet-lab assays were planned (e.g. RNA isolation, protein extraction etc.) cell suspension was centrifuged, washed with warm PBS and centrifuged again, and PBS is removed, which results in cell pellet.

Organoid forming experiment was performed by mixing growth factor reduced Matrigel® with cell culture media with 20:80 ratio. 10.000 inducible Hep3B-FAM134B cells were seeded into 12 well plate in total 200µl Matrigel-Media mixture. After mixture is solidified, fresh complete media was added. Cell cluster formation was observed every day. 1µg/ml doxycycline was added with fresh media after 4th day of culture. After culturing, cells were embedded in fibrin in order to facilitate microtome slicing from paraffin blocks.

In order to take advantage of tetracycline inducible system, we transfected Tet repressor expressing Hep3B-Trex or HepG2-Trex cells with pcDNA4TO-Fam134B vectors. In experiments, cells are treated with 1ug/ml Doxycycline, a potent analog of tetracycline, for at least 24 hours.

3.6.2 Chemical transfection of cells and generation of stable cell line

One day before the transfection procedure, monolayer cells were seeded at 70-80% confluency. On the day of transfection, the cell medium was changed with fresh complete media. Then, intact plasmid DNA was mixed with FuGENE HD (Promega, USA) at 1:6 ratio (ug:ul) in serum free Gibco OPTIMEM (Invitrogen,) medium. After mixing well and incubating for 10-15 minutes, mixture was slowly dropped on cells (submerged in complete medium)

After 48h of transfection, antibiotics for mammalian cell positive selection were added with fresh media. Mammalian selection markers are indicated in materials section. The cell type and the antibiotic concentration required for selection and maintenance is as followed: For zeocin, Hep3B cells 10ug/ml and HepG2 cells 100ug/ml; for neomycin, Hep3B cells 300ug/ml. Cell media and antibiotics were replaced in every three days.

Approximately 2-3 weeks after selection cells were either checked for colony formation in 10cm plate, or single-cell sorted into 98 well plate in order to facilitate single cell clone formation.

Cell colonies in 10cm plate are first labeled by a marker pen from the bottom of the plate. Cells were washed with PBS and all liquid remnant was removed. Then, colonies were gently picked by a fast drop-draw movement with a small volume of trypsin using tip of 200ul micropipette plastic tip. Picked colonies were immediately put in complete medium.

Single cell sorting procedure was done by İBG-Flow Cytometry core facility using FACS Aria III device (Becton and Dickinson, Franklin Lakes, NJ, USA). Cells formed 200-300 cell colonies after 3 weeks.

All selected cells were maintained in complete medium supplemented with antibiotics. All clones were screened for stable expression via western blot or immunofluorescence.

3.6.3 Molecular cloning

Human FAM134B-1 and FAM134B-2 were previously cloned into p3xFLAG-CMV vectors by Nilgün Taşdemir. cDNA sequences of FAM134B isoforms and target vector pcDNA4TO were excised by using HindIII and BamHI restrictions enzymes and the digestion product was run on %1.5 agarose gel. Both vector and insert were gel purified using gel purification kit as per manufacturer's manual. Ligation was performed using T4 Ligase according to manual overnight at 16°C via thermal cycler. Resulting product was transformed into competent bacteria using following steps: 1) 5µl of ligation mixture was added on 50µl competent and kept on ice for 30 minutes; 2) bacteria and ligation mix were heat shocked at 42°C for 45 seconds; 3) immediately put tubes on ice and wait 2 minutes; 4) 1ml LB media without antibiotic was added on transformed bacteria and incubated in a heated orbital shaker at 37 °C for 1 hour; 5) 200µl of bacteria suspension is spread on LB agar plates and left for incubation at 37°C overnight; 6) colonies were picked by 200µl sterile pipette tips and put into 5ml of LB liquid media supplemented with antibiotics for 8 hours; 7) either plasmid DNA is isolated using a MN miniprep kit or seeded into LB liquid media with antibiotics for large scale plasmid isolation.

Positive clones were screened by digesting isolated plasmids with restriction enzymes used for cloning. Digestion products were run in 1.5% agarose gel and positive clones are identified by excision of insert from vector, both of which gives correct band size.

For bacterial selection, antibiotic concentrations were 100µg/ml for ampicillin and 50µg/ml for kanamycin.

3.6.4 SRB cell viability assay

Cells were seeded in 96 well plate at low confluency, exact amount of which was determined based on the experiment type (e.g. drug treatment, gene expression etc). Briefly, cell media was first gently discarded without disturbing the cells. Wells were gently washed with PBS once. 100µl Ice cold 10 % Trichloroacetic Acid (TCA) was gently added on wells and incubated at -20°C for 20 minutes. Then, plates were washed with tap water, gently tapped on tissues to discard excess water and left for air drying.

After wells were air dried, Sulforhodamine B solution (0,4 %, w/v) is added on wells and incubated for 20 minutes at room temperature. Wells were then washed with 1% acetic acid (acetic acid/water; v/v) solution, gently tapped on tissues and left for drying.

Retained stains were dissolved by adding 50µl of Tris buffer with pH 10.5 on wells followed by incubation on a rocking platform at room temperature for 20 minutes. After dye is completely dissolved, plates were analyzed at 510nm using MultiSkanGo (ThermoScientific) spectrophotometer.

While performing cell viability assays, same experimental conditions were repeated as triplicate or quadruplicate.

3.6.5 Colony forming assay with crystal violet staining

Tet inducible HepG2-FAM134B-1 cells were seeded on 6 well plates as 500 cells per well. 24 hours after seeding, culture media was replaced with fresh media supplemented with 1µg/ml Doxycycline (For Dox + condition). Culture media was replaced every other day for 15 days.

After culture period is finished, cells were washed with PBS and fixed with 100% ice cold methanol for 10 minutes. Cells were stained with 0.5% Crystal Violet staining solution for 10 minutes at room temperature. Excessive dye was removed and the plate was washed with water several times, until the dye is washed off from the plate (cells must remain stained). Cells were left air dry overnight.

The picture of the plate was taken and colony numbers were counted by using Fiji cell counter.

3.6.6 Cell fractionation experiments

Fractionation experiment was performed using a slightly modified version of a previously established protocol[78]. Briefly, equal amounts (5x10^6 from each) of FAM134B-1 and FAM134B-2 expressing Hep3B cell pellets were homogenized in 5 ml 0.35M sucrose containing homogenization buffer with 50mM Tris-HCL pH 7.6, 25mM KCL, 10mM MgCl2, 2mM DTT using a motor homogenizer (Stuart). After centrifugation at 14.000xg, 4 °C for 10 minutes, the supernatant was carefully loaded on top of discontinuous sucrose gradient, which is made up 10ml 1,5M sucrose (top) and 10ml 2M sucrose (bottom). Samples were centrifuged at 70.000xg, 4°C for 16h using SW32 Ti rotor (Beckman Coulter). By puncturing the bottom of the tubes, 500ul fractions were collected. Fraction samples were mixed with 4x Laemmli loading buffer (with 2-mercaptoethanol), making the total loading buffer concentration to 1x. Samples were directly loaded on polyacrylamide gel.

3.6.7 Protein extraction and quantification

Prior to protein isolation, standard RIPA buffer was freshly supplemented with 25x Protease inhibitor tablets, 1nM NaF (Sodium Floride) and 1nM NaOV3 (Sodium Orthovanadate). All protein extraction procedures were performed by keeping tissue samples on wet ice.

Solid tissue fragments and pellets were kept in -80°C until homogenization. Solid tissues were directly dipped into liquid nitrogen which is immediately followed by grinding using mortar and pestle. Ice cold RIPA buffer was then added on fine tissue powder and mixture is vortexed thoroughly. For homogenization of cultured cells, ice cold RIPA buffer was directly added on cell pellets and vortexed.

After homogenization, protein lysates were vortexed in every 5 minutes for 30 minutes. Homogenates were then centrifuged at 17.000xg for 30 minutes at +4°C. Without touching the pellet, supernatant was transferred into clean microfuge tubes. Protein samples were measured by BCA and stored in -80°C for further use.

For protein quantification, BSA protein standard supplied by manufacturers (2mg/ml) was loaded in wells of 96 well plates with a linear increase in protein concentration (0, 2, 4, 8 and 16 ug/ well). Proteins of interest were loaded in each well as 2µl/well. BCA reagent was prepared as per manufacturer's manual and added on wells, making total volume of each well

100µl. Plates were incubated at 60°C for 10 minutes and absorbance values were obtained at 562nm using MultiSkanGo (ThermoScientific).

A linear regression curve is calculated based on OD (Optical Density) values of protein standards and the slope formula of the curve is used to calculate protein concentration of samples by using OD values.

3.6.8 SDS-PAGE & western Blot

All polyacrylamide gels were self-casted according to standard gel concentration tables. Usually resolving gel was prepared using single gel concentration. However, in cases where the small molecules (e.g. LC3B, 15kDa) variants and larger molecules (e.g. FAM134B, 70kDa) were expected to be observed in single blot, gradient gels composed of 15% (bottom half) and 10% (upper half) gels were casted in single mold. Briefly, after the gel matrix is prepared, 15% of gel is gently poured on a single spot using a plastic pastor pipette until the half of the space between two glasses are filled. Without hesitation, 10% gel matrix is poured on 15% gel using a micropipette by slowly moving both sides and pouring at the same time.

Protein lysates were run at 70V for 30 minutes and 110V for 120-180 minutes depending on the size and the expected resolution of the protein bands.

Proteins were wet transferred from gel to PVDF or nitrocellulose membrane at 400mA for 2 hours.

Membranes are incubated for 1 hour at room temperature with blocking solution which is composed of 5% Non-Fat Milk Powder dissolved in Tris Buffer Saline with 0.5% Tween (TBS-T). Primary antibodies were diluted in blocking solution incubated with membranes for overnight at +4°C. Membranes were washed with TBS-T for 3 times and incubated with secondary antibody, which is also diluted in blocking solution, for 1 hour at room temperature. This is followed by a washing step as mentioned above.

Protein bands are visualized using enhanced chemiluminescence technique using a western blot imaging device. After peroxidase buffer and enhancer buffers were mixed, immediately poured on membrane. Then, pictures were taken under different exposure times in a dark chamber. Photographs of membranes are also taken under visible light in order to obtain general template of the membrane and take protein ladder image.

All adjustments of the western blot photographs are performed using FIJI, an expanded version of Image J.

3.6.9 Immunofluorescence

Cells were seeded on sterile glass cover slips inside well plates (e.g. 12 or 24 well plates). After overnight incubation, depending on the experimental requirements, cells were either subjected to further experimentation (e.g. drug treatment, starvation etc.) or directly fixed. Before fixation, cells were washed with PBS.

Depending on the compatibility of the antibodies, cells were fixed either with 4% paraformaldehyde for 10 minutes or 100% ice cold methanol for 20 minutes. If cells were fixed with a crosslinking agent such as paraformaldehyde, membranes are permeabilized using PBS buffer with 0.3 % Triton-X 100 detergent on a rocking platform for 5 minutes at room temperature. Fixed cells were washed with PBS at least 3 times and blocked by using 5% BSA in PBS for 1 hour.

Both primary and secondary antibodies were diluted in antibody diluting solution composed of 2% BSA in PBS with 0.1 % tween (PBS-T). Cells were incubated with primary antibody, overnight at +4°C. Slides were washed three times with PBS-T and incubated with secondary antibody for 1 hour at room temperature. Slides were then washed three times with PBS-T and washed once more with distilled water.

For counterstaining, cells were stained by DAPI with concentration of 100ng/ml for 1 minutes at room temperature. Cells were then washed with distilled water excess water on cover slips is absorbed on a filter paper and mounted on slide using mounting media.

3.6.10 Oil Red-O staining

Oil Red-O staining protocol was performed as described before[79]. Tissues were snap frozen in liquid nitrogen and stored in -80°C until the staining procedure. Staining procedure was performed according to a previously described protocol[79]. Tissues were placed in TissueTek® Cryomolds® and embedded in TissueTek® O.C.T.™ Compound immediately after transfer from -80°C.

For freezing embedded tissue, molds were placed on nitrogen frozen Hexane until O.C.T. ™ is completely frozen. 8µm thick frozen sections were taken using Leica Cryostat and placed on lysine coated slides. Oil Red O working solution is prepared by adding 1.5 part of Oil Red O stock solution and 1 part of distilled water. Solution was kept at 4°C for 10 minutes, or until solution becomes thicker. The solution was then filtered through 45µm syringe filter.

Using a hydrophobic pen, tissue borders were drawn which is followed by adding Oil Red O solution by covering all tissue. After 5 minutes incubation at room tempereature, tissues were counterstained with hematoxylin for 15 seconds. Tissues were washed under running tap water for 30 minutes. Slides were mounted with water soluble mounting media.

3.6.11 Ethics

All animal studies performed in this thesis was approved by İBG Animal Experiments Local Ethics Committee (İBG-AELEC), with the approval code of 10/2017. Since used animal strains and animal numbers were expanded, we revised the ethical application with the approval code of 2020-011. Human samples used in the RT-PCR were approved by the Ethics Committee of Dokuz Eylul University. Written consent was obtained from all patients prior to liver transplantation.

3.6.12 Animal maintenance

All animal breeding, maintenance and experimental procedures were performed in İBG-Vivarium Rodent Facility (İVRF). Heterozygous *Fam134b*$^{-/+}$ animals were kindly gifted by Christian Hübner from Friedrich Schiller University Jena, Germany and previously described [16]. In order not to compromise experimental results with any possible reason due to animal background, all homozygous mutant and wild type animals were derived from these heterozygous founder animals by inbreeding. This mouse strain lacks exon 6, 7 and 8 on *Fam134b* genomic sequence which is found on chromosome 15 in mouse. All animals were housed in individually ventilated cages and maintained under 12 hours light/dark cycle, with 22 ±2 ambient temperature and %55 ±10 humidity. Unless otherwise is stated, animals were fed *ad libitum* with standard irradiated chow and steam sterilized drinking water.

3.6.13 Animal starvation experiments

Before starvation experiments, all animals were weighed and individually housed in clean rodent cages. For starvation, food pellets were removed from cages, but animals were allowed to access water *ad libitum*.

Starvation procedure is continued for the indicated periods of time. Animal health was checked and all animals were weighed in every 12-24 hours until the experiment was finished.

After the starvation procedure was completed, animals were euthanized by exsanguination through cardiac puncture under deep anesthesia. Blood samples were collected in regular microcentrifuge tubes and kept for 20-30 minutes at room temperature to accelerate blood clotting. Blood samples were then centrifuged for 10 minutes at 4 C in 5000xg. Serum biochemistry analyses were performed using spectrophotometric methods by an automated analyzer, Architect c16000 (Abbott).

3.6.14 Tumor xenograft

Nude mice (*Foxn1*^{nu}) were obtained from Bilkent University Laboratory Animal Facility and Nod Scid Gamma (NSG, NOD.Cg-*Prkdc*^{scid} *Il2rg*^{tm1Wjl}/SzJ) mice were obtained from Jackson Laboratory. These strains were bred and utilized in İVRF.

Before tumor injection, animals were immobilized using anesthesia. Cells were suspended in 100 µl PBS and subcutaneously injected to rear flanks of the animals.

After the tumor bulges were detected on the skin, shortest and longest diameter of the tumor size was measured weekly by analog caliper. The tumor volume was calculated with following formula V=(Long x Short^2)/2.

3.6.15 Tissue collection/isolation

Tissues obtained from animal studies were either fixed in PBS buffered 10%formalin (%3.7 formaldehyde) or snap frozen using liquid nitrogen and stored in -80°C.

Bovine tissues were collected from local slaughterhouse by cutting samples from fresh carcass and immediately dipped in liquid nitrogen, and stored in -80°C.

Samples for genotyping were collected by snipping tail tips from mice pups no older than one week. Until the day for DNA isolation, samples in microcentrifuge tubes were stored in -20°C.

3.6.16 DNA and RNA extraction

DNA extraction for genotyping was performed using in-house made tail buffer. 750µl tail buffer was added on tail samples along with 20µl of 10mg/ml Proteinase K solution and samples were incubated in 55°C water bath overnight. After 5 minutes vortex with maximum frequency, 250µl saturated NaCl was added and vortexed again. Tubes were centrifuged for 30 at 4°C minutes, maximum speed, 13.300 rpm. 750µl of supernatant was transferred to another microcentrifuge tube and added 500µl isopropanol. Samples were centrifuged again, which makes DNA visible at the bottom of the tube. After supernatant was discarded, 70% ethanol was added on tubes and centrifuged again. Supernatant was discarded and tube caps were left open at room temperature for 30 minutes. DNA pellet was dissolved in 30µl DNase free water. After one day incubation at 4°C overnight, DNA concentration and quality are measured using Nanodrop (ThermoScientific).

3.6.17 Polymerase Chain Reaction (PCR)

For *Fam134b* genotyping, PCR was performed under the following conditions: 3 minutes at 94°C (initial denaturation), 1 cycle; 30 seconds at 94°C (denaturation), 30 seconds at 60 °C (annealing), 30 seconds at 72°C (extension), 35 cycles; 3 minutes at 72°C (final extension), 1 cycle. Samples were incubated at 4°C until further processing.

RT-PCR conditions for mouse and human *FAM134B* mRNA isoforms, RT-PCR was performed under the following conditions: 3 minutes at 94°C (initial denaturation), 1 cycle; 30 seconds at 94°C (denaturation), 30 seconds at 58 °C (annealing), 30 seconds at 72°C (extension), 35 cycles; 3minutes at 72°C (final extension), 1 cycle. Samples were incubated at 4°C until further processing. For human *FAM134B* isoforms, total 28 cycles of the same reaction (denaturation, annealing and extension) was performed.

For TNF and IL6 mRNA, RT-PCR was performed under the following conditions: 2 minutes at 94°C (initial denaturation), 1 cycle; 10 seconds at 94°C (denaturation), 10 seconds

at 58 °C (annealing), 30 seconds at 72°C (extension), 40 cycles; 5 minutes at 72°C (final extension), 1 cycle. Samples were incubated at 4°C until further processing.

3.6.18 RNA-Sequencing

Before RNA sequencing, RNA samples taken from livers of 36 hours starved animals (n=12) were tested for their integrity by using Agilent Bioanalyzer (Santa Clara, CA, USA). RNA Integrity Number (RIN) values and virtual gel images were evaluated. Samples with RIN values above 7.0 or clean gel images (without any smear, degradation product etc.) were sent Eurofins Genomics laboratories. Samples were subjected to company's quality control prior to sequencing. Samples were then processed with one-way 50bp reading using Illumina HiSeq4000 Next Generation Sequencing device. Depth of reading was minimum 30 million read per sample.

3.6.19 Curation and organization of RNA-sequencing data

All bioinformatic analyses were performed by İBG Bioinformatics core facility under the supervision of Gökhan Karakülah.

Quality control of the reads of sequencing libraries was carried out via FastQC v0.11.5 [https://www.bioinformatics.babraham.ac.uk/projects/fastqc/] software. Trimmomatic v0.39 [http://www.usadellab.org/cms/?page=trimmomatic] software "Trimmomatic PE -threads 24 {input fastq} {output fastq} ILLUMINACLIP: {adapter Fasta file }: 2: 30: 10 LEADING: 3 TRAILING: 3 SLIDINGWINDOW: 4: 15 MINLEN: 36 "command. Sequences belonging to the GRCm38 mouse reference genome were obtained in fasta format from the Ensembl database [https://www.ensembl.org/index.html/] and from these sequences R v3.5.1 in the statistical computing environment Rusbread v1.34.7 [https: // bioconductor. An index was created with the "buildindex (basename, reference)" command of the org / packages / release / bioc / html / Rsubread.html] package. Using this index created, RNA sequencing reads are "align (index = {index file}, readfile1 = {input_1.fastq}, readfile2 = {input 2.fastq} type =" rna ", input_format =" gzFASTQ ", output_format =" BAM ", output_file = {output file}, nthreads = numParallelJobs)" is aligned to the corresponding reference genome. The obtained BAM files were then sorted with the sortBam () and indexBam () commands and their indexes were created. Then, from the raw sequencing data "featureCounts (files = {infile.bam}, annot.ext =" {infile.gtf} ", isGTFAnnotationFile = T, GTF.featureType =" exon ", GTF.attrType =" gene_id

", useMetaFeatures Gene level expression levels were determined using the commands and parameters = T, countMultiMappingReads = T, isPairedEnd = T, nthreads = numParallelJobs). The statistical significance of the differences in gene expression levels between the groups was achieved with the edgeR package (v3.24.3) in the R calculation environment (v3.5.2). In this step, the counting values determined by RSEM were normalized with The trimmed mean of M-values (TMM) normalization method and their statistical significance was calculated with the glmFit function by estimating the distribution with estimateDisp. In the visualization of the gene expression data, Fragments Per Kilobase of transcript per Million (FPKM) values obtained from the featureCounts function and measured by the edgeR package were used. In the visualization of the expression data, the ggplot2 package was used in the R environment.

3.6.20 Differential gene expression analyses

It is the stage performed in order to determine the statistical significance of the differences in gene expression levels between groups. In order to interpret the statistical significance of the differences in gene expression levels between groups, a script was written with the edgeR package (v3.24.3) in the R computing environment (v3.5.2). The purpose of this script is to determine the statistical significance of the raw count values determined via featureCounts by subjecting them to various processes. While performing this analysis, edgeR package was used. A data set suitable for analysis was obtained by using the raw counting values of each sample. Then, the required pairs of groups were formed to perform differentiated expression analysis. Genes showing increasing and decreasing expression were drawn according to the FDR value of 0.05, and the gene names were combined with the table containing the genes with expression differences. Then, heat maps (heatmaps) were drawn for easy interpretation of the expressions of each pair of groups.

3.6.21 Gene ontology analyses

Gene Ontology (GO) Analyzes were performed using the results obtained from the differentiated expression analysis, separately using RDAVIDWebService (version 1.20.0) and Cluster Profiler (version 3.10.1) tools. Gene Set Enrichment Analysis (GSEA) (https://www.gsea-msigdb.org/gsea/index.jsp) software developed by Broad Institute was used for Gene Set Enrichment Analysis.

3.6.22 Genomics, transcriptomics and proteomics data

The illustration of human and mouse FAM134B transcript variants was recreated using the NCBI reference sequence (RefSeq) database with the following accession codes: human FAM134B-1, NM_001034850.2; human FAM134B-2, NM_019000.4; mouse isoform1, NM_001034851.2; mouse isoform2, NM_025459.3; mouse isoform3, NM_001277315.1; mouse isoform 4, NM_001277316.1; mouse isoform5, NM_001277317.1; mouse isoform6, NM_001277318.1. The exon annotation was based on the UCSC genome browser.

The expression data of FAM134B variants in human healthy tissues were retrieved from the Genotype Tissue Expression (GTEx) database, version 3 as RPKM (Reads Per Kilobase Million) values [80]. Bar graphs were generated using Log2(RPKM+1) excluding the standard deviation.

Cancer and normal tissue expression data of human FAM134B isoforms were downloaded directly from The Cancer Genome Atlas Splicing Variant Database (TSVdb) as RSEM values [81]. This database provides isoform level expression value of any human gene across 33 tumor types, and researchers can retrieve and interpret the isoform expression variations between or across clinical subgroups. Statistical analyses of tumor and non-tumor groups were performed using nonparametric Mann-Whitney U test and $P<0.01$ was accepted as significant.

3.6.23 Histopathology

İBG-Histopathology Unit undertook the frozen sectioning, paraffin embedding, tissue staining and mounting procedures of any cell culture and animal materials required for histological examination.

4 RESULTS

FAM134B IN PHYSIOLOGY

4.1 *FAM134B* gene and protein variants are highly conserved across species

To better understand the role of *FAM134B,* we first investigated genomic architecture of *FAM134B* in both mouse and human. Human *FAM134B* is located on chromosome 5, p15.1 between 16,473,054-16,617,058 base positions and spans 144kb region while mouse *Fam134b* is located on chromosome 15, 15qB1 between chr15:25,843,180-25,973,687 base positions and spans 130kb. The nearest protein coding gene neighbors flanking *FAM134B* are *ZNF622* on 3' side and MYO10 on 5' side for both mouse and human.

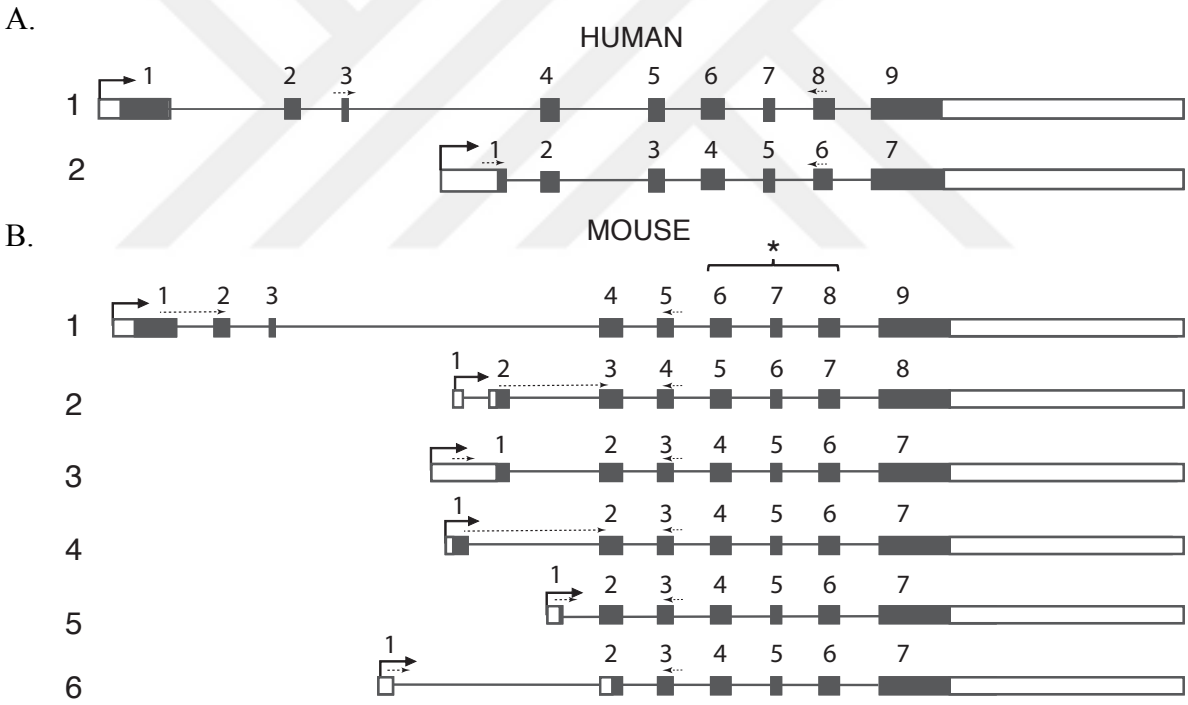


Figure 8: *FAM134B* isoforms are generated through alternative transcription start sites

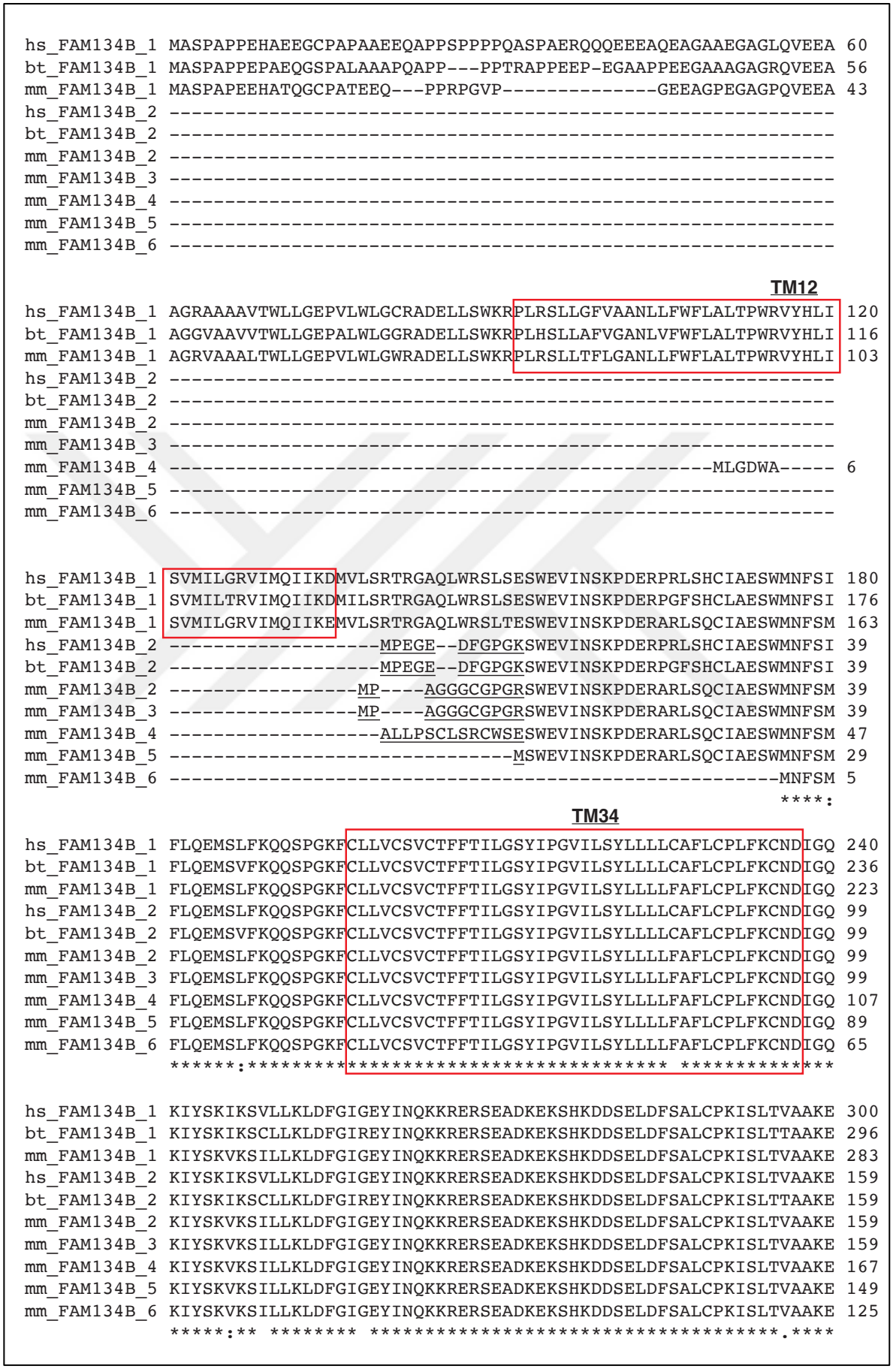
A. human *FAM134B* transcript variants. B. mouse *Fam134b* transcript variants. Blank boxes are untranslated regions. Angled arrows show putative transcription start sites. Dashed arrows show the location of primer pairs for the RT-PCR. The exons excised for generating *Fam134b* knockout mice are indicated with asterisk.

Based on the genomic structure, FAM134B is composed of nine exons giving rise to different transcript variants all of which are generated via transcription from alternative transcription start sites residing in intron 3 (Figure 8A and B, angled arrows). Human *FAM134B* encodes one long and one short isoforms. Mouse *Fam134b*, on the other hand, can generate at least 6 protein coding transcripts, one of which is the homolog of human long isoform and the other 5 isoforms are the homolog of human short variant (Figure 8A, B). There are putative and unverified *FAM134B* transcript variants in RefSeq and Ensembl assemblies which will not be detailed further in the thesis.

For simplicity, human and bovine transcript variants are labeled as *FAM134B-1* (long) and *FAM134B-2* (short), while mouse long transcript variant will be marked as *Fam134b-1* and all short isoforms together are mentioned as *Fam134b-2.* When particular notification is needed, mouse mRNA isoforms from -2 to -6 will be specified with *isoform* prefix (i.e. *isoform-1, -2, -3, -4, -5 and -6*). Protein isoforms of all species are labeled FAM134B-1 for long, and FAM134B-2 for short isoforms.

We further analyzed *FAM134B* by looking into protein structure of transcript variants from different species *in silico*. Total length of the long isoform is 497 amino acid for human, 480 amino acid for the mouse and 493 amino acid for the bovine (Figure 9). Although *FAM134B-2* coding sequence generates single protein for both human and bovine, mouse *Fam134b-2* transcripts give rise to at least five protein sequences, two of which are translated from *isoform-2* and *-3*, but encodes same amino acid sequences (Figure 9).

Next, we aligned FAM134B amino acid sequences of different species. Alignment results has shown that both FAM134B-1 and FAM134B-2 are highly conserved across species especially for previously defined transmembrane regions (i.e. TM12 and TM34) and LC3 Interactive Region (LIR) (Figure 9). Interestingly, truncated FAM134B-2 (*isoform-2* and *-3* in mouse), contains a 11 amino acid-long peptide at the N-terminal, which is not found in full length *FAM134B* in all species (Figure 9). Mouse *isoform-4*, *-5* and *-6,* on the other hand, show quite variable N-terminal regions with different length and amino acid sequences (Figure 9).


hs_FAM134B_1 MASPAPPEHAEEGCPAPAAEEQAPPSPPPPQASPAERQQQEEEAQEAGAAEGAGLQVEEA 60
bt_FAM134B_1 MASPAPPEPAEQGSPALAAAPQAPP---PPTRAPPEEP-EGAAPPEEGAAAGAGRQVEEA 56
mm_FAM134B_1 MASPAPEEHATQGCPATEEQ---PPRPGVP--------------GEEAGPEGAGPQVEEA 43
hs_FAM134B_2 ----------
bt_FAM134B_2 ----------
mm_FAM134B_2 ----------
mm_FAM134B_3 ----------
mm_FAM134B_4 ----------
mm_FAM134B_5 ----------
mm_FAM134B_6 ----------
TM12
hs_FAM134B_1 AGRAAAAVTWLLGEPVLWLGCRADELLSWKRPLRSLLGFVAANLLFWFLALTPWRVYHLI 120
bt_FAM134B_1 AGGVAAVVTWLLGEPALWLGGRADELLSWKRPLHSLLAFVGANLVFWFLALTPWRVYHLI 116
mm_FAM134B_1 AGRVAAALTWLLGEPVLWLGWRADELLSWKRPLRSLLTFLGANLLFWFLALTPWRVYHLI 103
hs_FAM134B_2 ----------
bt_FAM134B_2 ----------
mm_FAM134B_2 ----------
mm_FAM134B_3 ----------
mm_FAM134B_4 ----------MLGDWA----- 6
mm_FAM134B_5 ----------
mm_FAM134B_6 ----------
hs_FAM134B_1 SVMILGRVIMQIIKDMVLSRTRGAQLWRSLSESWEVINSKPDERPRLSHCIAESWMNFSI 180
bt_FAM134B_1 SVMILTRVIMQIIKDMILSRTRGAQLWRSLSESWEVINSKPDERPGFSHCLAESWMNFSI 176
mm_FAM134B_1 SVMILGRVIMQIIKEMVLSRTRGAQLWRSLTESWEVINSKPDERARLSQCIAESWMNFSM 163
hs_FAM134B_2 ----------MPEGE--DFGPGKSWEVINSKPDERPRLSHCIAESWMNFSI 39
bt_FAM134B_2 ----------MPEGE--DFGPGKSWEVINSKPDERPGFSHCLAESWMNFSI 39
mm_FAM134B_2 ----------MP----AGGGCGPGRSWEVINSKPDERARLSQCIAESWMNFSM 39
mm_FAM134B_3 ----------MP----AGGGCGPGRSWEVINSKPDERARLSQCIAESWMNFSM 39
mm_FAM134B_4 ----------ALLPSCLSRCWSESWEVINSKPDERARLSQCIAESWMNFSM 47
mm_FAM134B_5 ----------MSWEVINSKPDERARLSQCIAESWMNFSM 29
mm_FAM134B_6 ----------MNFSM 5
TM34
hs_FAM134B_1 FLQEMSLFKQQSPGKFCLLVCSVCTFFTILGSYIPGVILSYLLLLCAFLCPLFKCNDIGQ 240
bt_FAM134B_1 FLQEMSVFKQQSPGKFCLLVCSVCTFFTILGSYIPGVILSYLLLLCAFLCPLFKCNDIGQ 236
mm_FAM134B_1 FLQEMSLFKQQSPGKFCLLVCSVCTFFTILGSYIPGVILSYLLLLFAFLCPLFKCNDIGQ 223
hs_FAM134B_2 FLQEMSLFKQQSPGKFCLLVCSVCTFFTILGSYIPGVILSYLLLLCAFLCPLFKCNDIGQ 99
bt_FAM134B_2 FLQEMSVFKQQSPGKFCLLVCSVCTFFTILGSYIPGVILSYLLLLCAFLCPLFKCNDIGQ 99
mm_FAM134B_2 FLQEMSLFKQQSPGKFCLLVCSVCTFFTILGSYIPGVILSYLLLLFAFLCPLFKCNDIGQ 99
mm_FAM134B_3 FLQEMSLFKQQSPGKFCLLVCSVCTFFTILGSYIPGVILSYLLLLFAFLCPLFKCNDIGQ 99
mm_FAM134B_4 FLQEMSLFKQQSPGKFCLLVCSVCTFFTILGSYIPGVILSYLLLLFAFLCPLFKCNDIGQ 107
mm_FAM134B_5 FLQEMSLFKQQSPGKFCLLVCSVCTFFTILGSYIPGVILSYLLLLFAFLCPLFKCNDIGQ 89
mm_FAM134B_6 FLQEMSLFKQQSPGKFCLLVCSVCTFFTILGSYIPGVILSYLLLLFAFLCPLFKCNDIGQ 65
hs_FAM134B_1 KIYSKIKSVLLKLDFGIGEYINQKKRERSEADKEKSHKDDSELDFSALCPKISLTVAAKE 300
bt_FAM134B_1 KIYSKIKSCLLKLDFGIREYINQKKRERSEADKEKSHKDDSELDFSALCPKISLTTAAKE 296
mm_FAM134B_1 KIYSKVKSILLKLDFGIGEYINQKKRERSEADKEKSHKDDSELDFSALCPKISLTVAAKE 283
hs_FAM134B_2 KIYSKIKSVLLKLDFGIGEYINQKKRERSEADKEKSHKDDSELDFSALCPKISLTVAAKE 159
bt_FAM134B_2 KIYSKIKSCLLKLDFGIREYINQKKRERSEADKEKSHKDDSELDFSALCPKISLTTAAKE 159
mm_FAM134B_2 KIYSKVKSILLKLDFGIGEYINQKKRERSEADKEKSHKDDSELDFSALCPKISLTVAAKE 159
mm_FAM134B_3 KIYSKVKSILLKLDFGIGEYINQKKRERSEADKEKSHKDDSELDFSALCPKISLTVAAKE 159
mm_FAM134B_4 KIYSKVKSILLKLDFGIGEYINQKKRERSEADKEKSHKDDSELDFSALCPKISLTVAAKE 167
mm_FAM134B_5 KIYSKVKSILLKLDFGIGEYINQKKRERSEADKEKSHKDDSELDFSALCPKISLTVAAKE 149
mm_FAM134B_6 KIYSKVKSILLKLDFGIGEYINQKKRERSEADKEKSHKDDSELDFSALCPKISLTVAAKE 125


hs_FAM134B_1 LSVSDTDVSEVSWTDNGTFNLSEGYTPQTDTSDDLDRPSEEVFSRDLSDFPSLENGMGTN 360
bt_FAM134B_1 LSVSDTDVSEVSWTDNGTFNLSEGYTPQTDTSDDLDRPSEEVFSRDLSDFPSLENGTGTN 356
mm_FAM134B_1 LSVSDTDVSEVSWTDNGTFNLSEGYTPQTDTSDDLDRPSEEVFSRDLSDFPSLENGTGTN 343
hs_FAM134B_2 LSVSDTDVSEVSWTDNGTFNLSEGYTPQTDTSDDLDRPSEEVFSRDLSDFPSLENGMGTN 219
bt_FAM134B_2 LSVSDTDVSEVSWTDNGTFNLSEGYTPQTDTSDDLDRPSEEVFSRDLSDFPSLENGTGTN 219
mm_FAM134B_2 LSVSDTDVSEVSWTDNGTFNLSEGYTPQTDTSDDLDRPSEEVFSRDLSDFPSLENGTGTN 219
mm_FAM134B_3 LSVSDTDVSEVSWTDNGTFNLSEGYTPQTDTSDDLDRPSEEVFSRDLSDFPSLENGTGTN 219
mm_FAM134B_4 LSVSDTDVSEVSWTDNGTFNLSEGYTPQTDTSDDLDRPSEEVFSRDLSDFPSLENGTGTN 227
mm_FAM134B_5 LSVSDTDVSEVSWTDNGTFNLSEGYTPQTDTSDDLDRPSEEVFSRDLSDFPSLENGTGTN 209
mm_FAM134B_6 LSVSDTDVSEVSWTDNGTFNLSEGYTPQTDTSDDLDRPSEEVFSRDLSDFPSLENGTGTN 185
hs_FAM134B_1 DEDELSLGLPTELKRKKEQLDSGHRPSKETQSAAGLTLPLNSDQTFHLMSNLAGDVITAA 420
bt_FAM134B_1 DEDELSLGLPTELKRKKEQLDGGPRRSTEKKSAAGLSLPLSSDQTLHLMSDLAGDVITAA 416
mm_FAM134B_1 DEDELSLGLPTELKRKKQQLDSAHRPSKERQSAAGLSLPLKSDQALHLMSNLAGDVITAA 403
hs_FAM134B_2 DEDELSLGLPTELKRKKEQLDSGHRPSKETQSAAGLTLPLNSDQTFHLMSNLAGDVITAA 279
bt_FAM134B_2 DEDELSLGLPTELKRKKEQLDGGPRRSTEKKSAAGLSLPLSSDQTLHLMSDLAGDVITAA 279
mm_FAM134B_2 DEDELSLGLPTELKRKKQQLDSAHRPSKERQSAAGLSLPLKSDQALHLMSNLAGDVITAA 279
mm_FAM134B_3 DEDELSLGLPTELKRKKQQLDSAHRPSKERQSAAGLSLPLKSDQALHLMSNLAGDVITAA 279
mm_FAM134B_4 DEDELSLGLPTELKRKKQQLDSAHRPSKERQSAAGLSLPLKSDQALHLMSNLAGDVITAA 287
mm_FAM134B_5 DEDELSLGLPTELKRKKQQLDSAHRPSKERQSAAGLSLPLKSDQALHLMSNLAGDVITAA 269
mm_FAM134B_6 DEDELSLGLPTELKRKKQQLDSAHRPSKERQSAAGLSLPLKSDQALHLMSNLAGDVITAA 245
LIR
hs_FAM134B_1 VTAAIKDQLEGVQQALSQAAPIPEEDTDTEEGDDFELLDQSELDQIESELGLTQDQEAEA 480
bt_FAM134B_1 VTAAVKDQLAGVRQALSQAAPSLGEDTDTEEGDDFELLDQSELDQIESELGLSQDQEAEA 476
mm_FAM134B_1 MTAAIKDQLEGARQALTQVAPTAGEDTDTEEGDDFELLDQAELDQIESELGLTQDQGAEA 463
hs_FAM134B_2 VTAAIKDQLEGVQQALSQAAPIPEEDTDTEEGDDFELLDQSELDQIESELGLTQDQEAEA 339
bt_FAM134B_2 VTAAVKDQLAGVRQALSQAAPSLGEDTDTEEGDDFELLDQSELDQIESELGLSQDQEAEA 339
mm_FAM134B_2 MTAAIKDQLEGARQALTQVAPTAGEDTDTEEGDDFELLDQAELDQIESELGLTQDQGAEA 339
mm_FAM134B_3 MTAAIKDQLEGARQALTQVAPTAGEDTDTEEGDDFELLDQAELDQIESELGLTQDQGAEA 339
mm_FAM134B_4 MTAAIKDQLEGARQALTQVAPTAGEDTDTEEGDDFELLDQAELDQIESELGLTQDQGAEA 347
mm_FAM134B_5 MTAAIKDQLEGARQALTQVAPTAGEDTDTEEGDDFELLDQAELDQIESELGLTQDQGAEA 329
mm_FAM134B_6 MTAAIKDQLEGARQALTQVAPTAGEDTDTEEGDDFELLDQAELDQIESELGLTQDQGAEA 305
hs_FAM134B_1 QQNKKSSGFLSNLLGGH 497
bt_FAM134B_1 QQNKKSSGFLSNLLGGH 493
mm_FAM134B_1 QQSKKSSGFLSNLLGGH 480
hs_FAM134B_2 QQNKKSSGFLSNLLGGH 356
bt_FAM134B_2 QQNKKSSGFLSNLLGGH 356
mm_FAM134B_2 QQSKKSSGFLSNLLGGH 356
mm_FAM134B_3 QQSKKSSGFLSNLLGGH 356
mm_FAM134B_4 QQSKKSSGFLSNLLGGH 364
mm_FAM134B_5 QQSKKSSGFLSNLLGGH 346
mm_FAM134B_6 QQSKKSSGFLSNLLGGH 322

Figure 9: *FAM134B* variants are highly conserved across species.

Underlined sequences show the different N-terminal regions of FAM134B-2. The components of reticulon domains are marked with red rectangles labeled as TM12, which is peculiar to full length protein; TM34 which is found in both isoforms. Autophagosome cargo recognition signal motif, LC3 interacting region (LIR), is maked with green rectangle. The peptide sequence used as antigen for the development fof anti-FAM134B antibody (HPA012077) development, which is marked with orange rectange in "hsFAM134B-1" row. Identical, high and low similarity amino acids are marked with asterisk, colon and dots, respectively, at the bottom of the alignment lane. Amino acids that do not show any similarity is not marked. Abbreviations: hs, *homo sapiens*; bt, *bos taurus*; mm, *mus musculus*.

Protein organization of human FAM134B-1 has been previously defined in several studies[15,77,82,83]. The main functional unit of native FAM134B-1 is composed of two transmembrane hairpin domains (i.e. TM12 and TM34) separated by a linker sequence, and a single LIR motif by which GABARAP/LC3B decorated phagophores are recognized[82]. The short protein, on the other hand, lacks the TM12 region, yet, contains the rest of the linker region, TM34 and full C-terminal region including LIR motif (Figure 10).

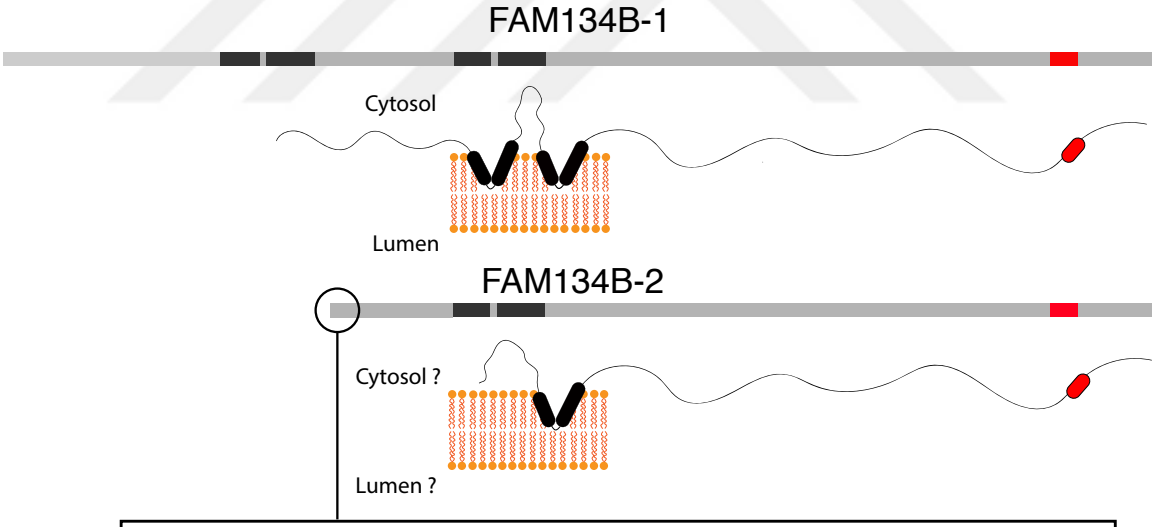


Figure 10: FAM134B-2 lacks a large hydrophylic N-terminal domain and a hydrophobic transmembrane domain

Functional units of long (top) and short (down) isoforms are represented by linear and native form. FAM134B-2 difference across species in amino acid level. Black rods: the subunits of reticulon hairpin domains. Red rod: LC3B binding LIR motif.

4.2 *FAM134B* isoforms are differentially expressed in healthy human tissues

The physiological relevance of FAM134B emerged as a key player in nervous system, where it acts as a key ER-phagy receptor and mediates ER turnover. Besides its role in nervous system, there are also studies reporting the role of FAM134B in various normal and cancerous tissues, yet with little implication about how broadly the *FAM134B* and its variants are expressed in different tissues. Therefore, we studied the expression levels of *FAM134B* in healthy tissues on isoform level.

We started analyzing the tissue distribution of *FAM134B* transcript variants in a web based tool, Genotype Tissue Expression portal (GTEx), which harbors the RNA-sequencing catalogue of various tissues collected from 175 healthy individuals (version 3)[80].

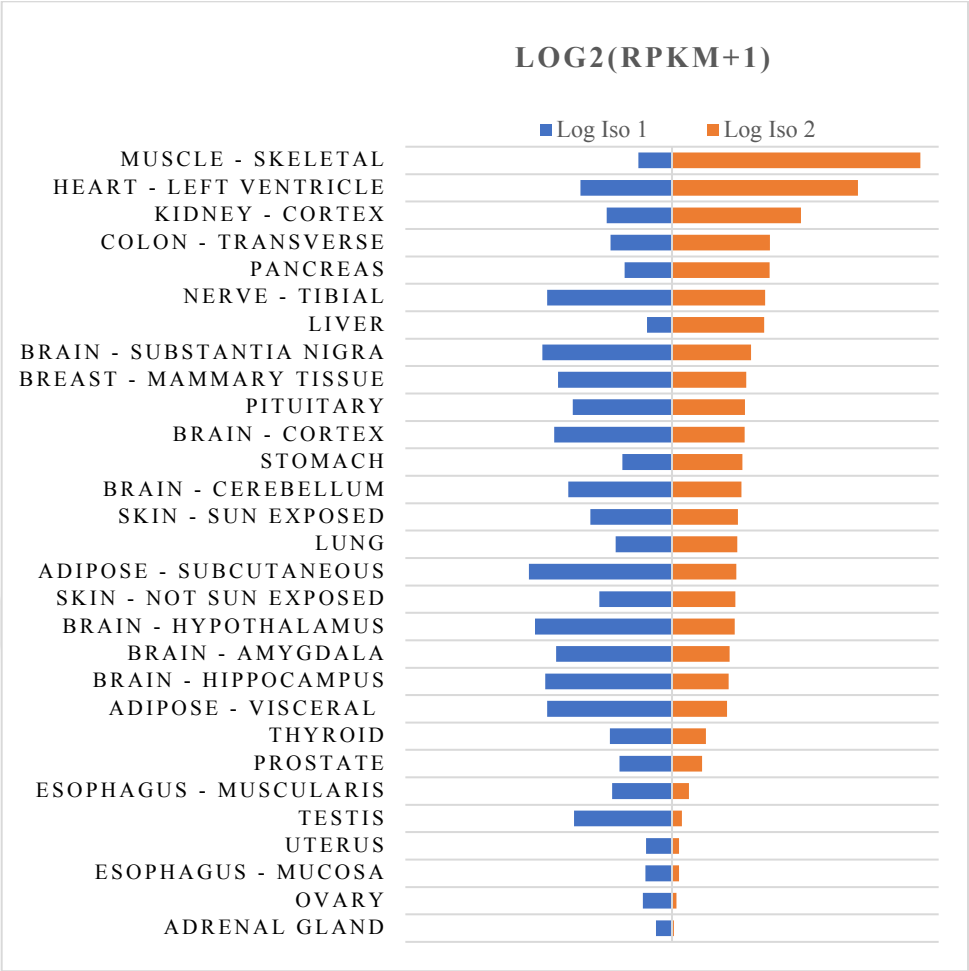


Figure 11: Human FAM134B-2 is predominantly expressed in skeletal muscle and heart
Mean (Log_2RPKM+1) values retrieved from GTEx dataset were used to generate this figure. Standard deviations were not shown.

As shown in Figure 11, *FAM134B-1* is predominantly expressed in nervous tissue, as expected. Adipose, breast, testis also follows similar expression preference on *FAM134B-1*. However, *FAM134B-2* to *FAM134B-1* ratio is strikingly high in muscle and heart tissues, which are followed by kidney, colon, pancreas and liver.

4.3 *FAM134B-2* is predominantly expressed in human liver, pancreas and skeletal muscle

After discovering that the FAM134B isoforms are differentially expressed in tissues, we experimentally tested the tissue expression levels on healthy tissue cDNA panel.

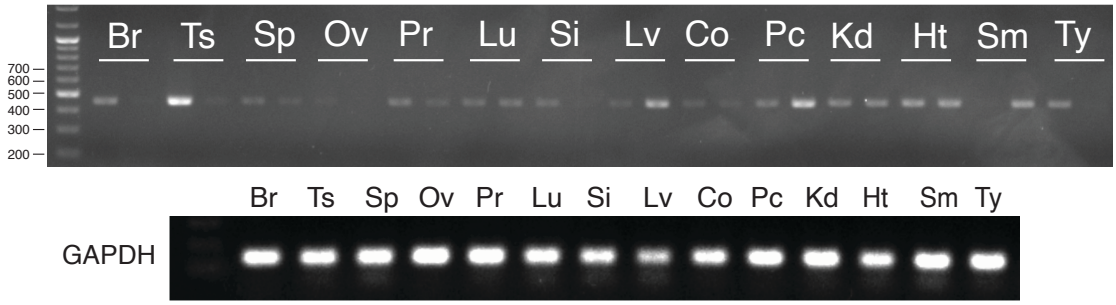


Figure 12: Expression of long and short *FAM134B* in healthy human tissues as shown by RT-PCR

The PCR bands are FAM134B-1 (left) and FAM134B-2 (right) for each organ, respectively. Equal loading control PCR was performed by using GAPDH primers.Tissue name coding is as followed: Br: Brain; Ts: Testis; Sp; Spleen; Ov: Ovaries; Pr: prostate; Si: Small intestine; Lv: Liver; Co: Colon; Pc: Pancreas; Kd: Kidney; Ht: Heart; Sm: Skeletal Muscle; Ty: Thymus; Ctr: Control.

As seen in Figure 12, brain and testis verify the GTEx data with a strong expression of *FAM134B-1*. In silico data was further supported with high *FAM134B-2* expression in liver, pancreas and skeletal muscle. Kidney, heart, colon, lung and spleen, however, failed to show the preference on particular isoform, and demonstrated similar levels of both isoforms.

4.4 FAM134B protein expression in bovine tissues is concordant with human

Although human results strongly indicate that the FAM134B isoforms are differentially expressed in various tissues, we sought to verify these results using a model system for three main reasons: 1- Despite the usefullness of the cDNA pool, PCR is still susceptible to contaminations, which may lead to false results; 2- Determining the protein levels of related transcripts in human materials are difficult due to tissue availability and ethical issues 3- *FAM134B* and its isoforms was shown to be highly conserved across species; therefore, using a model organism would provide an important clue regarding its protein expression in human.

As a model organism, bovine has drawn our particular attention, because tissue sampling is readily available in local slaughterhouses, sampling from slaughtered animal does not require ethical approval, and most importantly, *FAM134B* encodes two isoforms in bovine, as in humans. Bovine tissues were selected based on their expression profile of *FAM134B* isoforms in humans and screened for FAM134B expression via western blot. In this experiment,

we tested both the compatibility of the antibody with bovine tissues, and if so, how selected tissues express FAM134B protein isoforms.

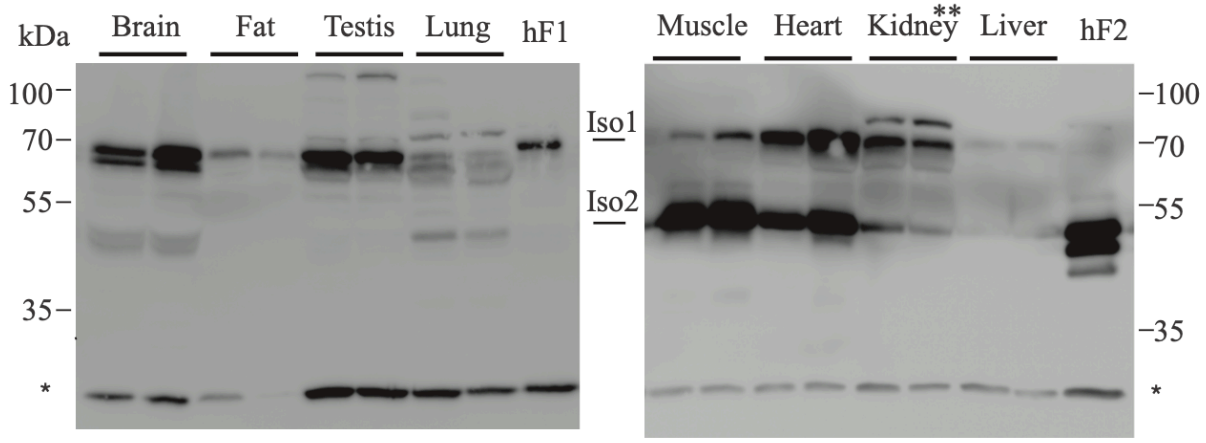


Figure 13: FAM134B-2 is strongly expressed in bovine muscle and heart

hF1 and hF2 lanes are human FAM134B isoforms ectopically expressed in cell lines, as positive control. Asterisks represent nonspecific antibody binding and used as loading control.

Western blot results (Figure 13, left) displayed a similar expression pattern as of human; brain demonstrates a predominant FAM134B-1 along with a weak FAM134B-2 expression, fat and testis solely express FAM134B-1 at different strength, and lung shows weak but similar expression of both isoforms.

Other organs (Figure 13, right), however, exhibited FAM134B expression somewhat similar to human. As expected, FAM134B-2 protein levels are most strongly observed in muscle and heart tissues, which are followed by weaker expression in kidney. Interestingly, discordant to GTEx data, FAM134B-1 is also dominantly expressed in heart, and even more strongly expressed in kidney tissue. Furthermore, in the liver, FAM134B-2 expression is almost not detected, while there is little to no expression of FAM134B-1.

Indeed, when interpreting the data presented above, we have to consider the following facts: 1- mRNA expression may not be followed with similar profile of protein expression due to many mechanisms that can affect the translation; 2- expression of FAM134B variants might serve different physiological processes in different species, therefore, is differentially expressed in various tissues.

Nevertheless, these data have shown that FAM134B protein expression profile is mostly concordant with the transcript data of human, and, the antibody is able to recognize bovine FAM134B in addition to hFAM134B.

4.5 All six *Fam134b* transcript isoforms are expressed in mouse tissues

Spatial expression of FAM134B was further elaborated by using mouse as model organism. Thanks to the kind gift from Christian Hübner, we were able to import and breed *Fam134b*$^{-/-}$ knockout mice in İzmir Biomedicine and Genome Center Vivarium Rodent Facility.

Imported mouse model was established on mixed mouse genetic background of 129SvJ/ C57BL/6 and mutant animals lacks Exon 6, 7 and 8 which corresponds to almost all domain of TM34. Wild type and mutant animals were characterized by PCR based genotyping protocol (Figure 14).

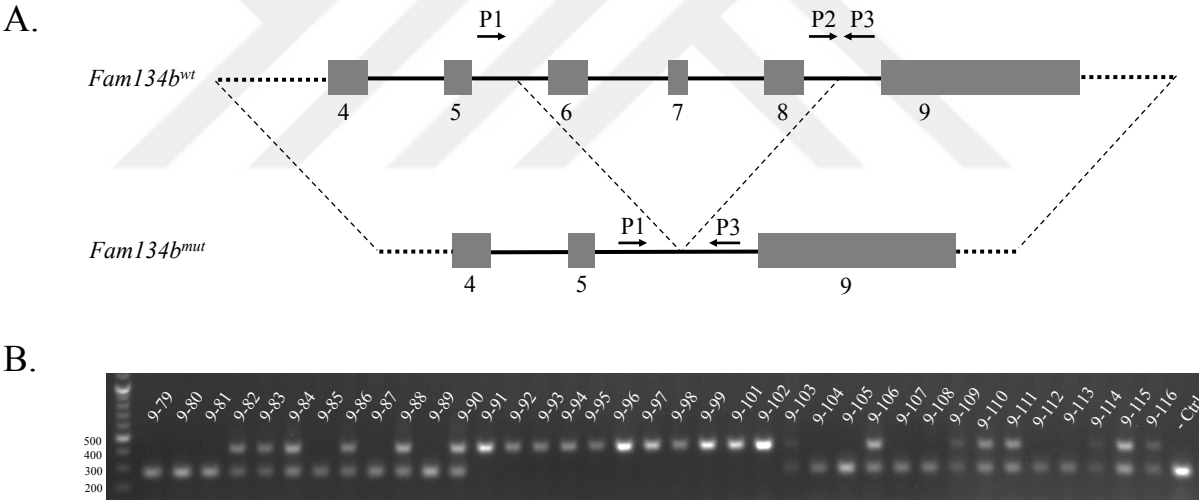


Figure 14: *In vivo* knockout model lacks exon 6, 7 and 8.

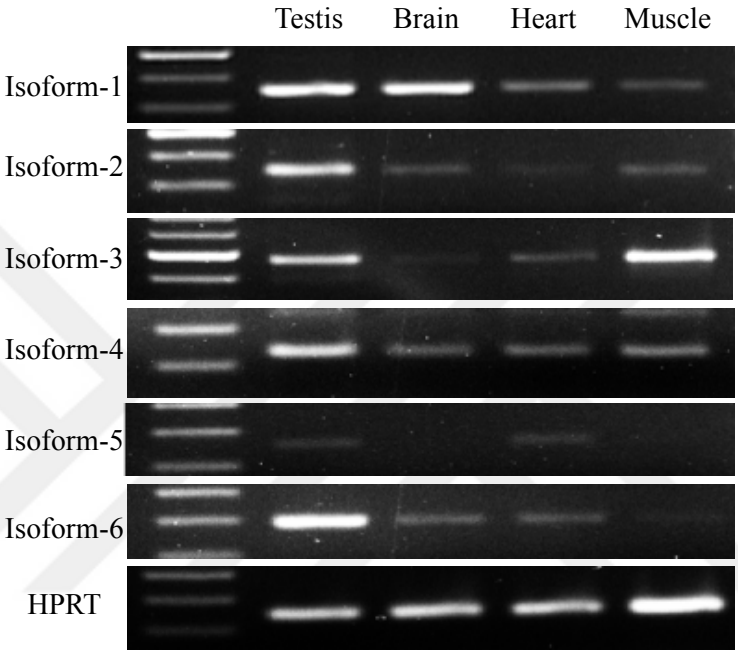
A. Demonstration of deleted exons. Black arrows show the primers used for genotyping. In wild type allele, P2 and P3 is close to each other and yields 280bp product, while in deleted allele, P1 is brought in close proximity to P3 and PCR yields 420bp amplicon. B. Wild type (280bp) and mutant (420bp) alleles demonstrated by conventional PCR. Numbers represent the identification of individual mice.

As stated above, Mouse *Fam134b* encodes at least 6 transcript isoforms. Accordingly, we hypothesized that some, if not all, tissues might differentially express *Fam134b* transcripts.

Therefore, we performed Reverse Transcriptase PCR (RT-PCR) in search of differential expression of the mouse isoforms.

Next, we tested whether anti-FAM134B antibody recognize the mouse proteins via western blot experiment. The subjected tissues were selected according to their FAM134B isoform expression in human and bovine counterparts.

A.



B.

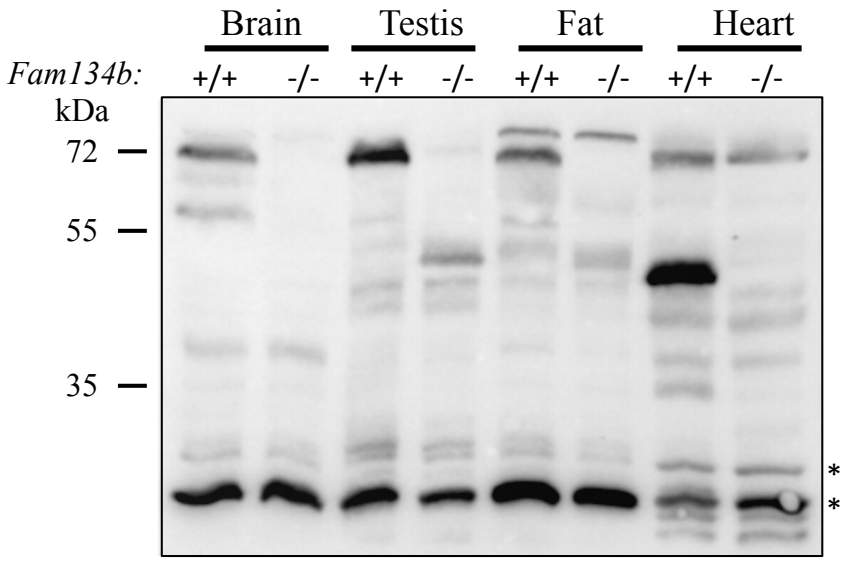


Figure 15: Mouse brain, testis and fat express FAM134B-1 while heart and muscle express FAM134B-2

A. Gel image of reverse transcriptase PCR results. The respective *Fam134b* isoform and size of the amplicons are as following: Isoform1, 354bp; isoform 2, 343bp; isoform 3, 474bp; isoform 4, 231bp; isoform5, 256bp; and isoform6, 286bp. HPRT (Hypoxantine Phosphorybosyltransferase) was used for loading control. B: Western blot images of brain, testis, fat and heart tissues. *Fam134b* wild type and mutant mice are represented by +/+ and -/- respectively. Asterisks show the nonspecific binding of anti-FAM134B antibody and used for loading control.

As seen in Figure 15, anti-FAM134B antibody was able to recognize wild type mouse FAM134B, which is clearly absent in mutant counterparts. Similar to the observations made on human samples, mouse brain and muscle tissues show dominant expression of FAM134B-1 around 70kDa (mouse *isoform-1*) and FAM134B-2 around 55kDa (mouse *isoform-2 and -3*) respectively in mouse tissues (Figure 15, A). RNA levels in mouse testis, however, showed strong expression of short mouse *isoform-2*, *-3*, *-4* and *-6*. Interestingly, besides the long isoform, short variants in testis could not be observed in western blot. It was also intriguing that FAM134B isoforms in heart tissue did not exhibit an isoform specific expression in RT-PCR but gives strong short isoform expression around 55kDa in western blot.

These results showed that, protein levels of FAM134B isoforms in mouse tissues exhibit great similarity to RNA levels from human GTEx and RT-PCR, where FAM134B-1 is predominantly expressed in Brain, testis and fat; whereas FAM134B-2 is exclusively expressed by heart and muscle. Western blot data has also shown that primary antibody is compatible to work with mouse tissues in western blot.

Verification of FAM134B isoform expression on small number of tissues urged us to test FAM134B levels in an extended mouse tissue panel. Hence, tissues from healthy wild type and mutant mice were analyzed for the FAM134B presence using western blot.

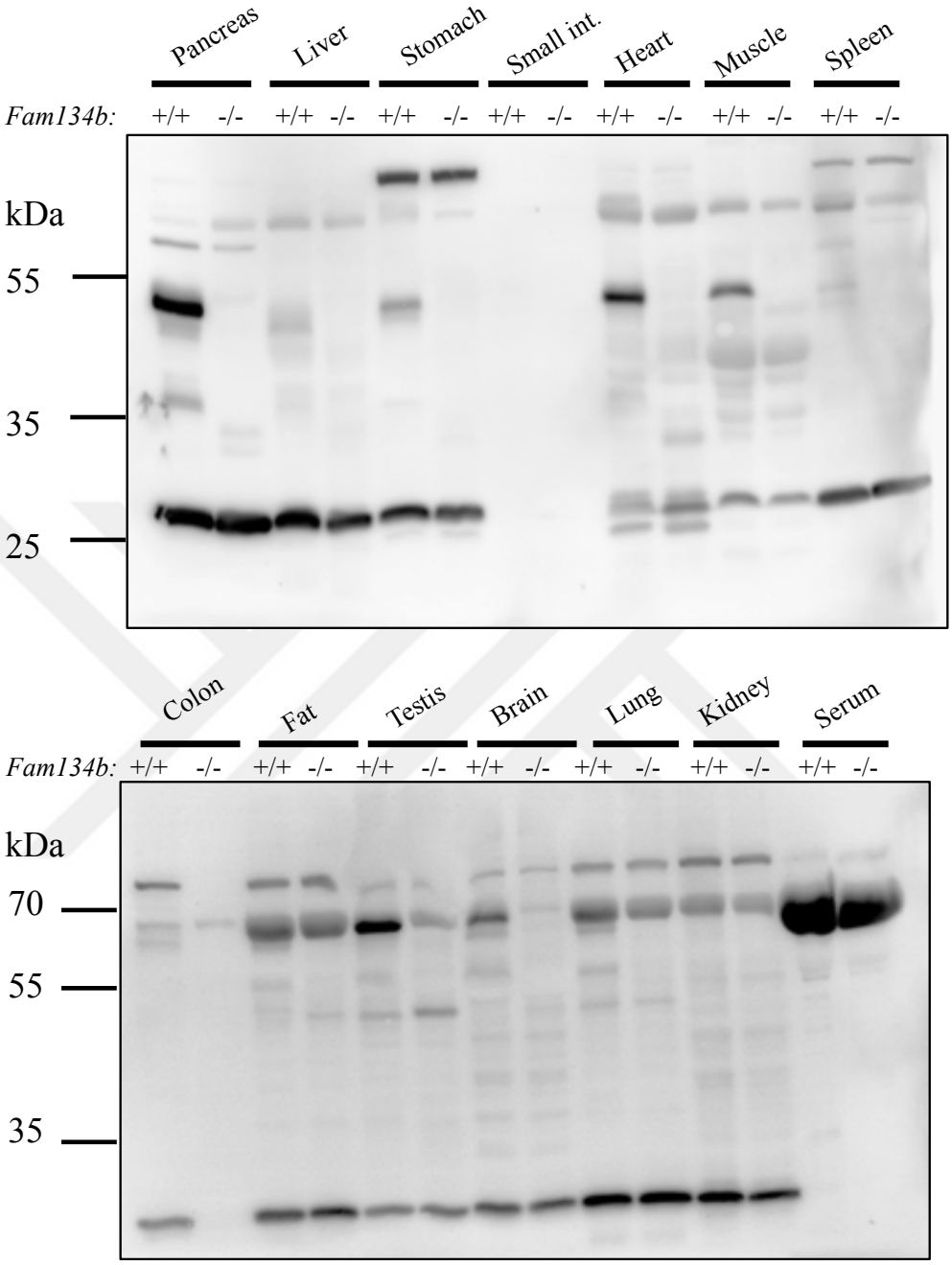


Figure 16: FAM134B-2 is strongly expressed in mouse pancreas, stomach, muscle and heart.

To better separate long and short isoforms, 10% and 12% SDS gels were used respectively and run over 2 hours 30 minutes.

As seen in Figure 16, upper panel; pancreas, liver, stomach, heart and muscle express short FAM134B-2 at different levels. Interestingly, heart, muscle and pancreas are quite distinctive in their high FAM134B-2 levels. In addition to expected ~55kDa short form, extra

bands were observed at 35kDa in pancreas, liver and heart. In heart, long isoform at 70kDa was also visible.

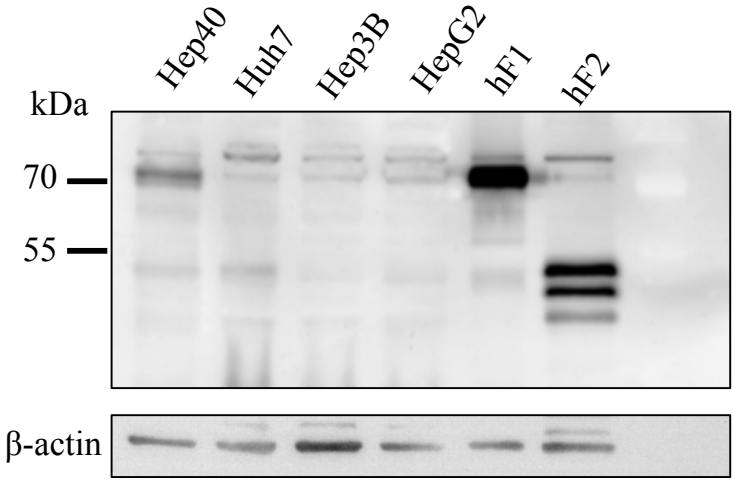
FAM134B-1 bands in brain and testis were detected as expected. However, due to the masking effect of nonspecific antibody binding, long isoform in other tissues could not be interpreted.

Although overall these data have shown that differential expression of FAM134B variants are similar across different mammals, we failed to show visible expression of FAM134B in mouse kidney.

4.6 FAM134B-1 is the dominant form *in vitro*

Discovering the differential roles of FAM134B variants requires strong *in vitro* models which are easier to manipulate and modify for mechanistic studies. Therefore, we first screened the protein levels of FAM134B isoforms in hepatocellular carcinoma cell lines. Despite wide variety of phenotypic characteristics of the cells, they could be roughly subdivided into two previously defined phenotypes: epithelial- and mesenchymal- like cells [72]. Accordingly, we screened the presence of FAM134B isoforms in these subsets using western blot technique.

A.



B.

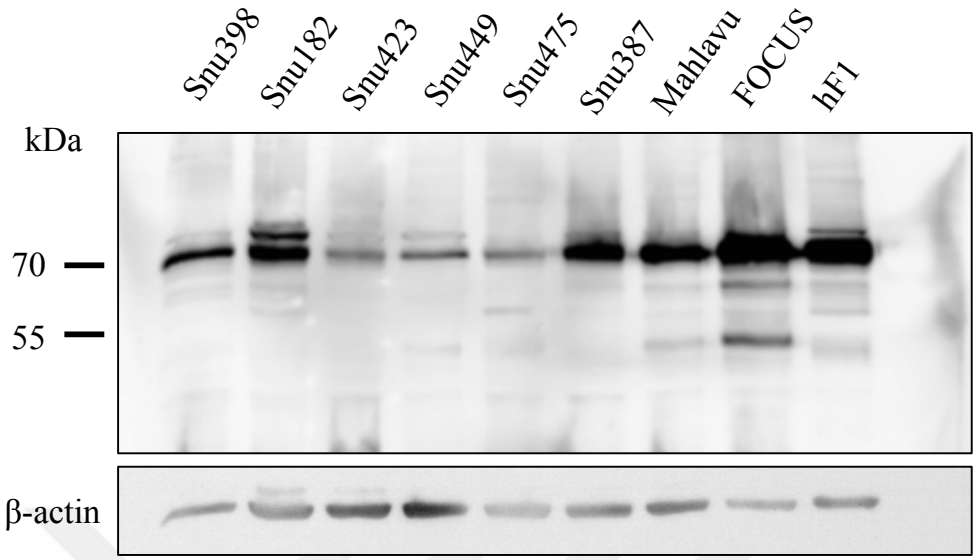


Figure 17: Mesenchymal-like HCC cells predominantly express FAM134B-1
A. Well-differentiated (epithelial-like), and B. poorly-differentiated (mesenchymal-like) HCC cell lines.

Epithelial-like cell lines (Figure 17, A) showed FAM134B-1 only in Hep40 and weak expression of FAM134B-2 in Hep40 and Huh7, whereas mesenchymal-like cell lines predominantly expressed long isoform near 70kDa, with weaker expressions of FAM134B-2 in FOCUS and Mahlavu (Figure 17, B). This result indicates that FAM134B isoforms, particularly FAM134B-1, is peculiar to mesenchymal-like cancer cells, while epithelial like cells express little or no *FAM134B* of any isoform, except Hep40 cells.

4.7 FAM134B localizes to Endoplasmic Reticulum

The localization of full length FAM134B in Golgi Apparatus and/or Endoplasmic Reticulum has been demonstrated by our group and other groups [16,83]. The differences in N-terminal structure of short FAM134B-2, especially lack of half of the reticulon domain, has urged us to compare the co-expression of FAM134B isoforms with Calnexin (CNX) using immunofluorescence techniques.

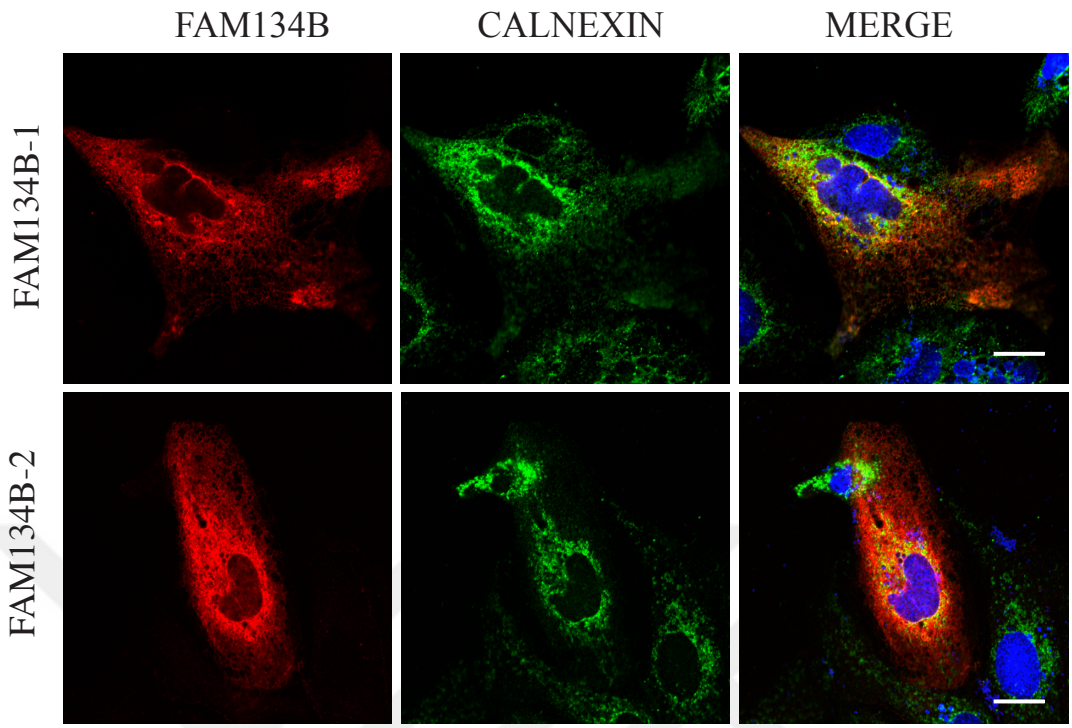


Figure 18: FAM134B colocalizes with Calnexin (CNX)

Huh7 cells transiently transfected either with FAM134B-1-FLAG or FAM134B-2-FLAG vectors, co-stained with FAM134B and CNX. Scale bar represents 20µm.

Since CNX is a chaperone enhancing the folding of misfolded proteins stacked in Endoplasmic reticulum, its expression was expected more intensely on perinuclear, where usually the rough endoplasmic reticulum is observed. According to our results, both FAM134B isoforms were co-localized with CNX particularly on perinuclear area. However, both FAM134B isoforms were stained more expanded in the cytosol, where CNX staining is lacking (Figure 18).

4.8 Both isoforms can be recognized by autophagosomes

Differences in protein size and structure of FAM134B variants indicates functional diversity. Although recognition of FAM134B-1 coated ER fragments by LC3B attached phagophores has been a *de facto* mechanistic role, the involvement of FAM134B-2 in the same context requires a further clarification. Hence, in order to observe FAM134B variants and LC3B co-localization status, we starved Huh7 cells transiently transfected with FAM134B-1-

FLAG and FAM134B-2-FLAG vectors (Figure 19) and stained with LC3B and FLAG antibodies.

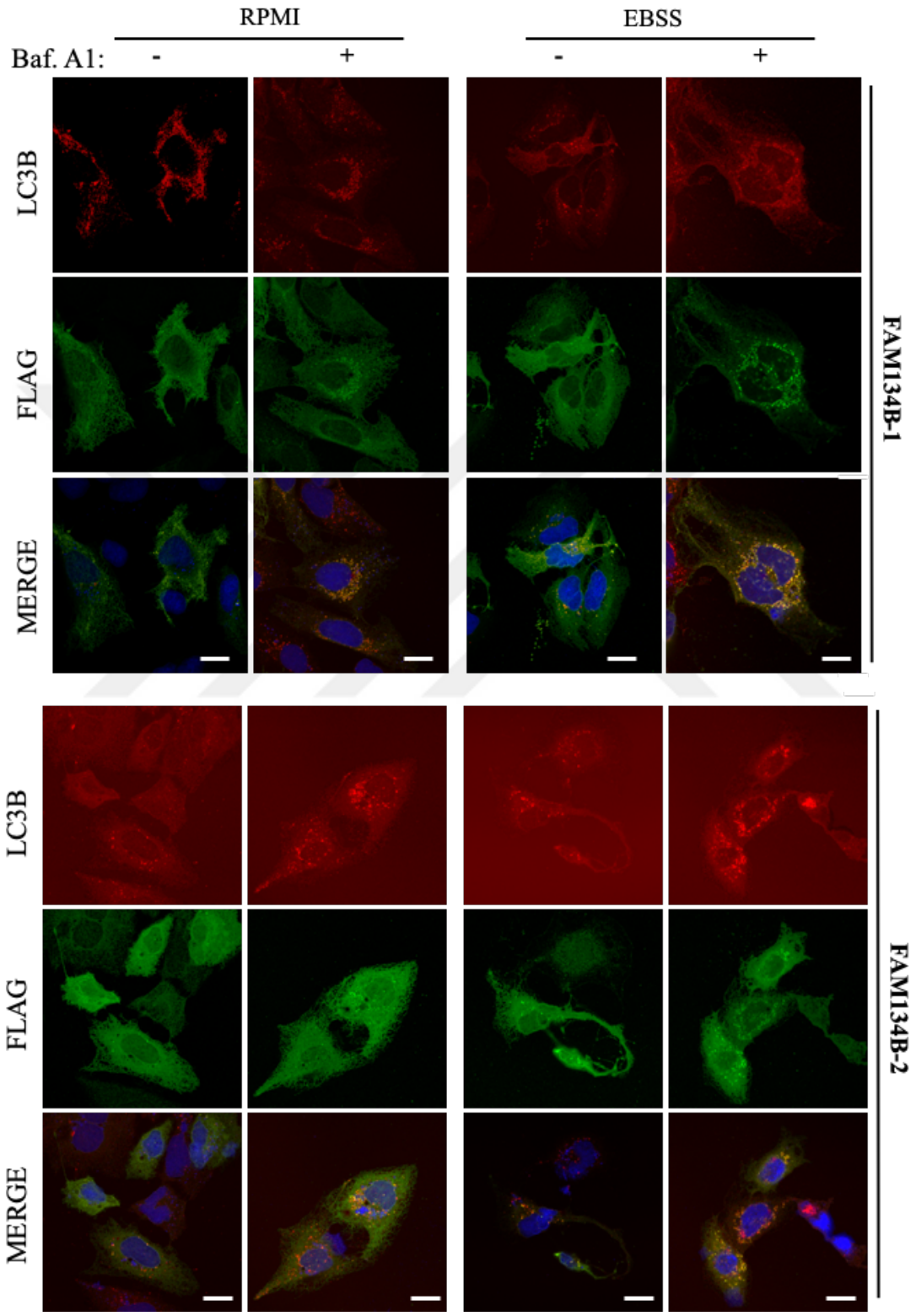


Figure 19: FAM134B-1 and FAM134B-2 can colocalize with LC3B

Huh7 cells were transiently transfected with FAM134B-1-FLAG and FAM134B-2-FLAG plasmids. After 48 hours of transfection, starvation induced with EBSS with or without the 200nM Bafilomycin A1 treatment for 4 hours. Scale bar, 20μm.

Under normal culture conditions (complete medium, no starvation) without bafilomycin, both FAM134B-1 and FAM134B-2 diffusely spread across the cytosoplasm with only a few FLAG positive punctae co-stained with LC3B. When the cells were treated with a lysosomal proton pump blocker, Bafilomycin A1, however, massive accumulation of both LC3B and two FAM134B isoforms were observed. Since these punctae were co-stained with both FAM134B isoforms and autophagosome marker LC3B, we concluded that both FAM134B isoforms are segregated into autophagosomes. Similar co-staining pattern with fewer number of punctae was also visible when cells were treated with EBSS only (Starvation medium, without Bafilomycin A1), indicating that both isoforms are destined to LC3B mediated segregation under starvation conditions. When starvation is combined with Bafilomycin A1, the number of LC3B and FAM134B co-stained punctae dramatically increased (Figure 19).

The Bafilomycin A1 treated cells under normal conditions have shown that, cells constantly undergo an ER turnover mediated by both FAM134B isoforms. Starvation alone has induced the similar accumulation, but weakly, likely due to unblocked lysosomal degradation. Accordingly, when starved cells were treated with Bafilomycin A1, number of punctae has greatly increased. We could not observe any difference of punctae accumulation between FAM134B-1 and FAM134B-2, which strongly suggests that, despite the major structural differences, both isoforms may exert similar roles at least in the context of autophagy.

The functional similarity of two isoforms has made us curious about their co-localization status, as isoforms may exclude each other from different compartments. In order to visualize the differential expression of two isoforms, we co-transfected Huh7 cells with fluorescent protein conjugated FAM134B-1 (mCherry-FAM134B-1) and FAM134B-2 (EGFP-FAM134B-2).

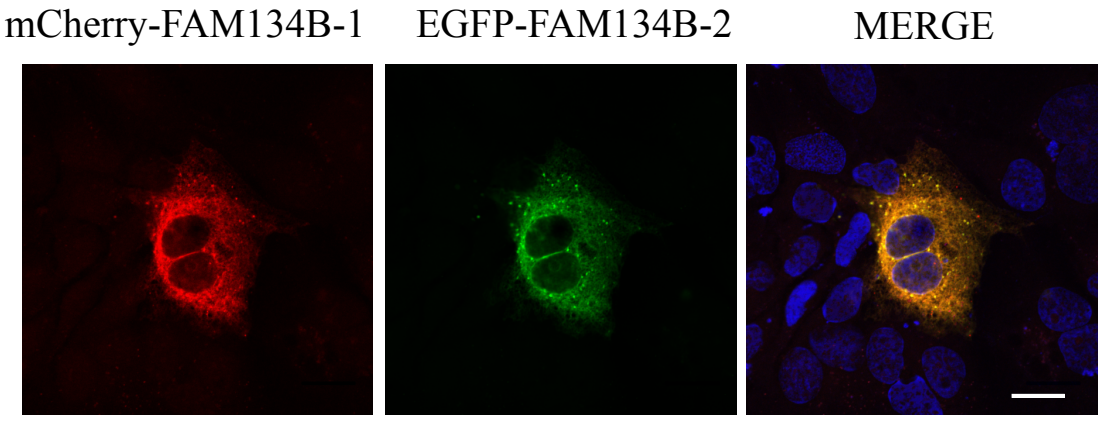


Figure 20: FAM134B-1 and FAM134B-2 mostly co-localize

Fluorescence imaging of mCherry-FAM134B-1 and EGFP-FAM134B-2 co-transfected Huh7 cells. Scale bar represents 20µm.

Confocal imaging has shown that, mCherry-FAM134B-1 and EGFP-FAM134B-2 proteins are mostly co-expressed across the cytoplasm with only few exceptions, where some punctae exhibits either mCherry-FAM134B-1 or EGFP-FAM134B-2 only (Figure 20).

4.9 FAM134B-2 is located in lighter sub-cellular fractions

Although immunofluorescence is invaluable tool to demonstrate cellular localization of proteins, obtained data needed further delineation with biochemistry methods. In order to do so, first, we generated Hep3B single cell clones stably expressing FAM134B-1-FLAG or FAM134B-2-FLAG. The expression of the proteins was verified by using western blot technique (Figure 21, A). Next, both cell lines were subjected to sucrose gradient discontinuous cellular fractionation via ultracentrifugation. The collected fractions were tested by western blot method to show co-localization of FAM134B isoforms with various organelle specific markers.

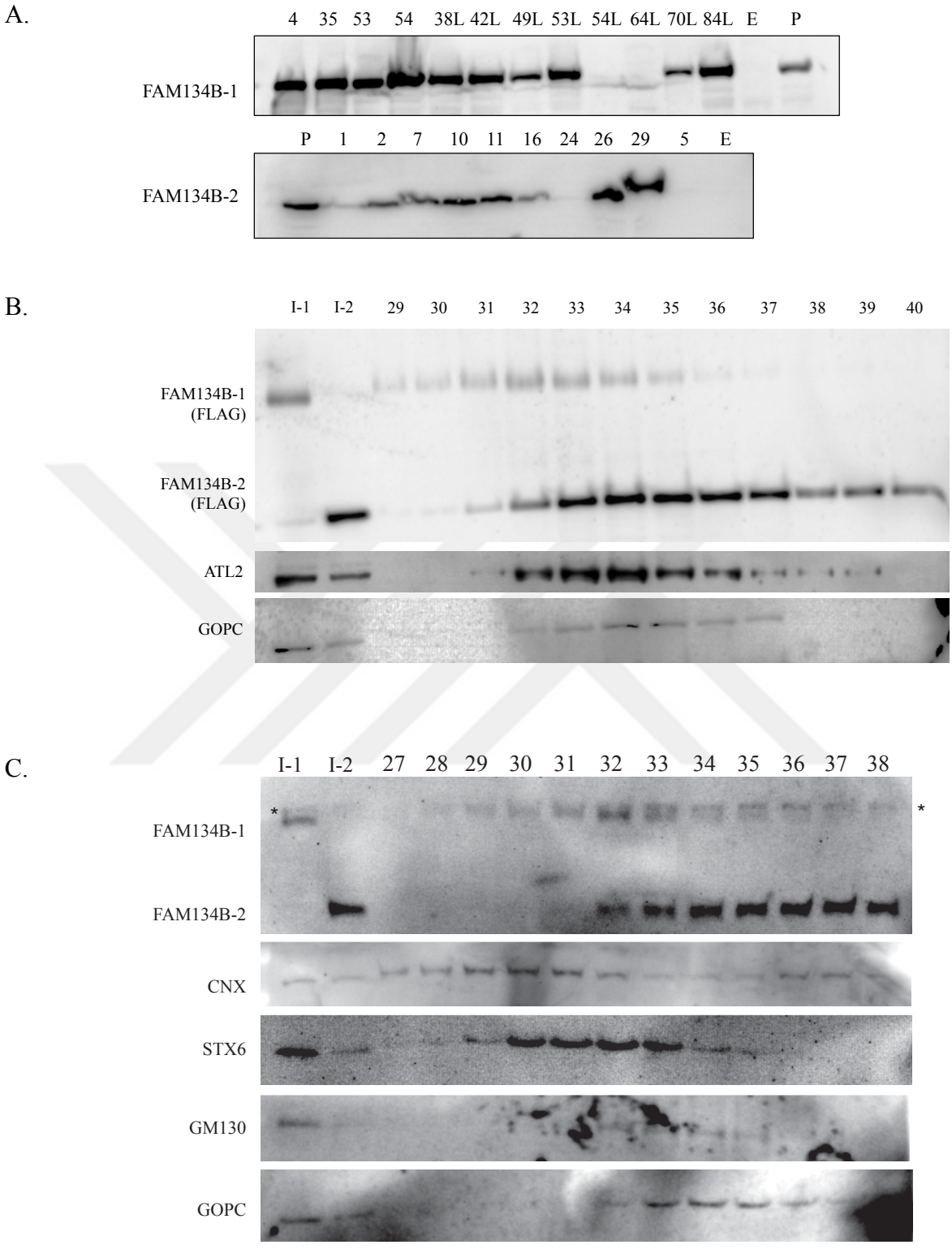


Figure 21: FAM134B-2 localizes to lighter sub-cellular fractions

A. Generation of stable Hep3B cells expressing FAM134B-1-FLAG and FAM134B-2-FLAG proteins. Bands represents FLAG immunoblotting. Numbers indicate single cell derived clones. P, polyclone control; E empty vector transfected Hep3B. B. Discontinuous Sucrose

gradient of FAM134B-1 and FAM134B-2 expressing Hep3B cells. ATL2, Atlastin-2; CNX, Calnexin; GOPC, Golgi Associated PDZ and Coiled-Coil Motif Containing. ATL2 and CNX proteins were used as ER markers; GOPC is used as Golgi marker. I-1 and I-2 represents input for FAM134B-1 and FAM134B-2 respectively. Fraction numbers are lined according to transition from heavier to lighter fractions, from left to right.

FLAG immunoblotting of stable cell clones has shown that we successfully generated FAM134B-1 and FAM134B-2 expressing stable Hep3B cell lines.

In fractionation experiment, gradual increasing and decreasing of all markers have clearly showed that the cellular compartments were successfully fractioned in gradients according to their centrifugal density. Interestingly, FAM134B-1-FLAG and FAM134B-2-FLAG gradients exhibited slightly different fractionation gradient based on the fact that the peak protein densities differ from each other (Figure 21, B Lane 32 and 34). Although CNX signal extended to fractions which contains both FAM134B isoforms, another ER resident protein, ATL2 (Atlastin2) and cis-Golgi marker GOPC exhibited peak at fractions where FAM134B-2-FLAG proteins are more dominantly expressed.

According to these results, FAM134B-2-FLAG isoform is preferably localized in lighter fractions along with the ATL2 and GOPC, while both isoforms co-exist with CNX.

4.10 FAM134B-2 do not precipitate neither with Calnexin nor with GOPC

FAM134B-1 was previously shown to be directly interacting with Calnexin, by which the autophagic degradation of ER fragments filled with procollagen molecules is mediated[18]. The interaction between FAM134B-1 and Calnexin occurs through hydrophobic transmembrane domains of both molecules. Therefore, we hypothesized that the same interaction would be applicable to truncated FAM134B-2 molecule, since it still contains half of the reticulon structure, which could possibly be interacting calnexin. Hence, we performed co-immunoprecipitation on stable Hep3B-FAM134B-2-FLAG cells by using anti-FLAG antibodies, which is followed by western blot.

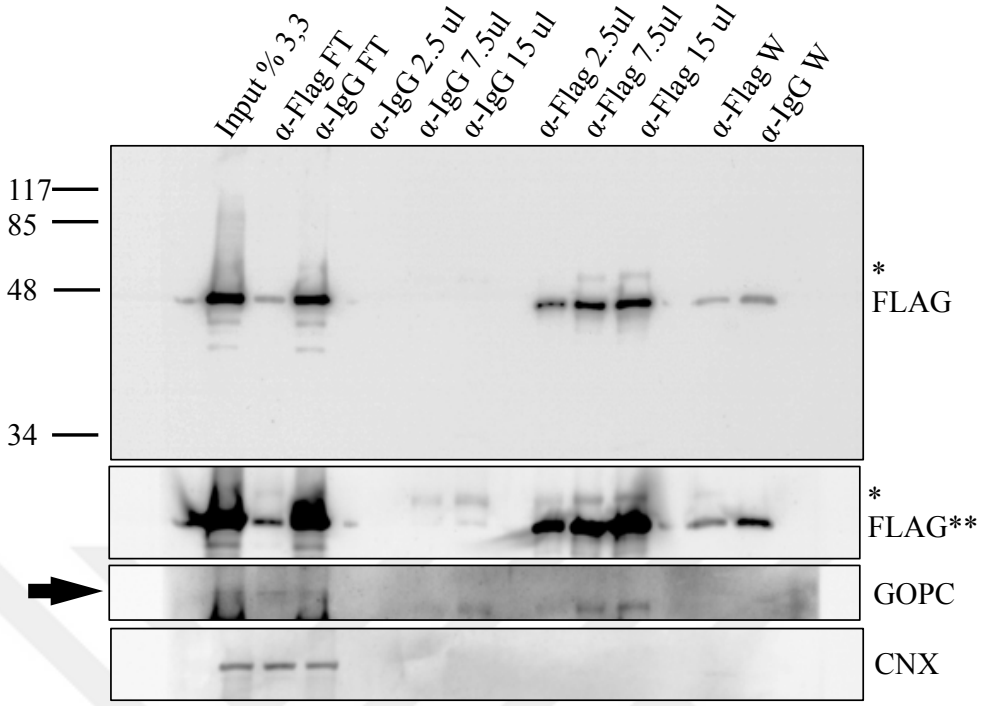


Figure 22: anti-FLAG antibody mediated pull down of FAM134B-2 in Hep3B-FAM134B-2-FLAG cells.

Asterisks show the antibody heavy chain. Arrow indicates protein bands of GOPC which are visible at input, FLAG and IgG flowthrough. Precipitated materials were loaded in 2.5µl, 7.5µl and 15µl in order to better compare protein amounts between input and precipitated samples. FT, flowthrough taken after primary binding of antigen to antibody; W, buffer after washing the beads.

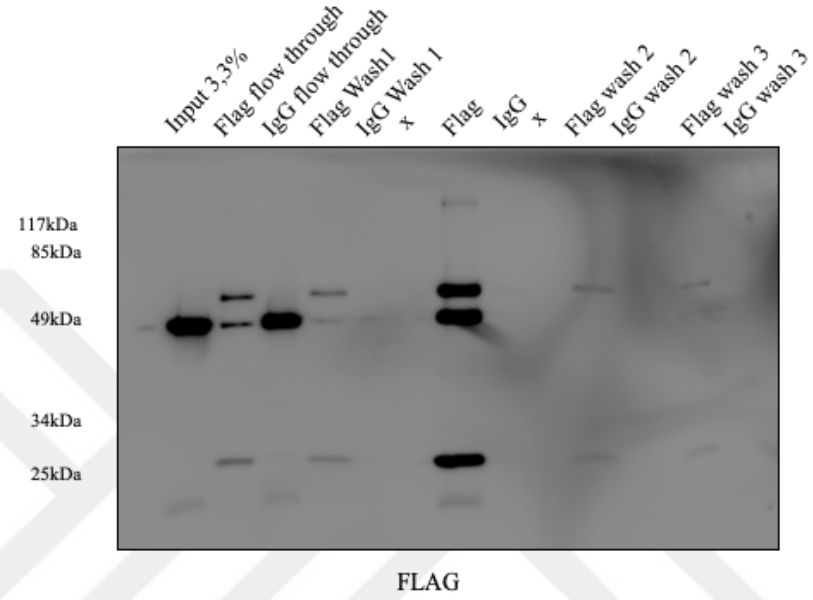
As shown in Figure 22, FAM134B-2 is retained by FLAG antibodies and yielded less protein in FT (flowthrough) while IgG isotype failed to retain FAM134B-2 and showed high amount of protein as in the input. Accordingly, we observed strong bands in a-FLAG lanes but not in a-IgG lanes. On the other hand, neither a-FLAG nor the a-IgG could pull down Calnexin indicating that they do not directly interact, at least in Hep3B cells.

4.11 FAM134B-2 localizes to Golgi

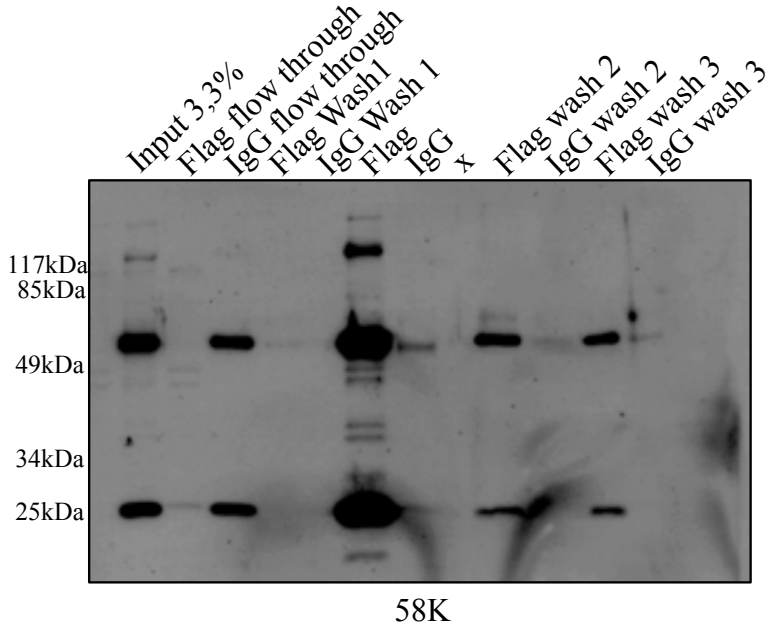
In parallel with previous studies on FAM134B, cell fractionation experiments indicated possible Golgi localization which could not be further verified by co-immunoprecipitation experiments using Golgi marker, GOPC. Hence, we sought possible Golgi localization of FAM134B using another Golgi marker, 58K.

For experimental procedure, we took advantage of Hep3B cells stably expressing FLAG tagged FAM134B-2, which was pulled-down using anti-FLAG antibody attached protein G agarose beads. The pulled down proteins were analyzed by immunoblotting against 58K protein.

A.



B.



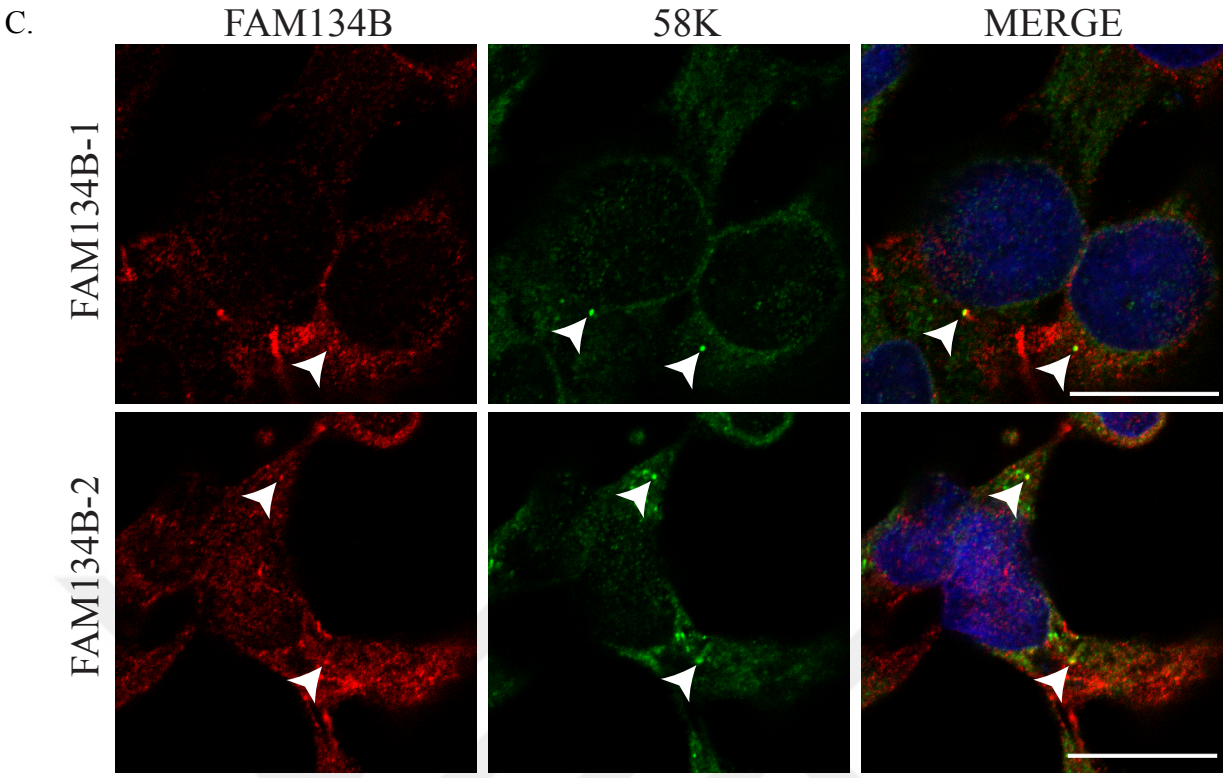


Figure 23: FAM134B-2 Co-immunoprecipitates with Golgi marker 58K

After precipitation, beads were washed three times with 50mM Tris-HCl buffer containing 150mM, 500mM and no NaCl subsequently. x, indicates empty wells. Loading volume of total protein lysate was determined as 3.3% (input) which corresponds to the loaded volume of buffer with beads. Asterisk indicates mouse antibody heavy chain. Flag and IgG lanes indicate specific proteins pulled down with agarose beads. Western blot images show two separate protein loading. A. Anti-FLAG; B. Anti-58K blotting. C. Colocalization of FAM134B isoforms and Golgi marker, 58K. Scalebar represents 20µm. White arrowheads show the FAM134B and 58K positive punctae.

FAM134B-2-FLAG protein was successfully pulled down, as demonstrated by presence of pronounced levels of the FLAG protein in Input and Flag lanes but not in IgG lane. Flowthrough lanes also clearly showed that isotype control IgG fails to retain FLAG protein, which was detected as high FLAG levels (Figure 23, A).

58K was also shown to be specifically pulled down along with FAM134B-2 as evidenced by a strong 58K signal at Flag lane, which was absent in Flag flowthrough, but present in IgG flowthrough. Of course, since 58K antibody is generated in mouse, we cannot rule out the possibility that the signal also come from mouse secondary antibody which recognize heavy chain of mouse anti-FLAG antibody. However, observing much stronger signal in Flag lane compared to input lane strengthen our hypothesis about direct binding of

FAM134B-2 and 58K protein. Interestingly, we also observed 58K specific bands at 120kDa and 25kDa which also become stronger in Flag lane (Figure 23, B).

Using immunofluorescence technique, we also showed that both FAM134B isoforms partially co-localized with Golgi marker 58K (Figure 23, C).

Together these data have shown that localization of FAM134B is not restricted to ER, but rather, it translocates to Golgi apparatus.

FAM134B RESPONSE TO STARVATION

4.12 Both FAM134B isoforms are degraded in response to nutrient starvation

In literature, full length FAM134B was shown to be gradually degraded in mouse embryonic fibroblasts (MEFs) upon nutrient starvation due to the consumption of ER fragments for energy recycling[16]. In another report, however, short isoform was shown to be stimulated in some cell lines, *in vitro*[77].

In hope of illuminating this contradiction, FOCUS and Hep40 cell lines which express both FAM134B isoforms were challenged by nutrient starvation. Cells were simply starved by replacing complete medium with EBSS (Earle's Balanced Salt Solution), which contains only low glucose and minerals, but no amino acid (Figure 24). We also took advantage of lysosomal degradation blocker, Bafilomycin A1, in order to demonstrate possible accumulation of FAM134B containing autophagosomes during the course of starvation. Using western blot method, cells were screened for FAM134B protein levels.

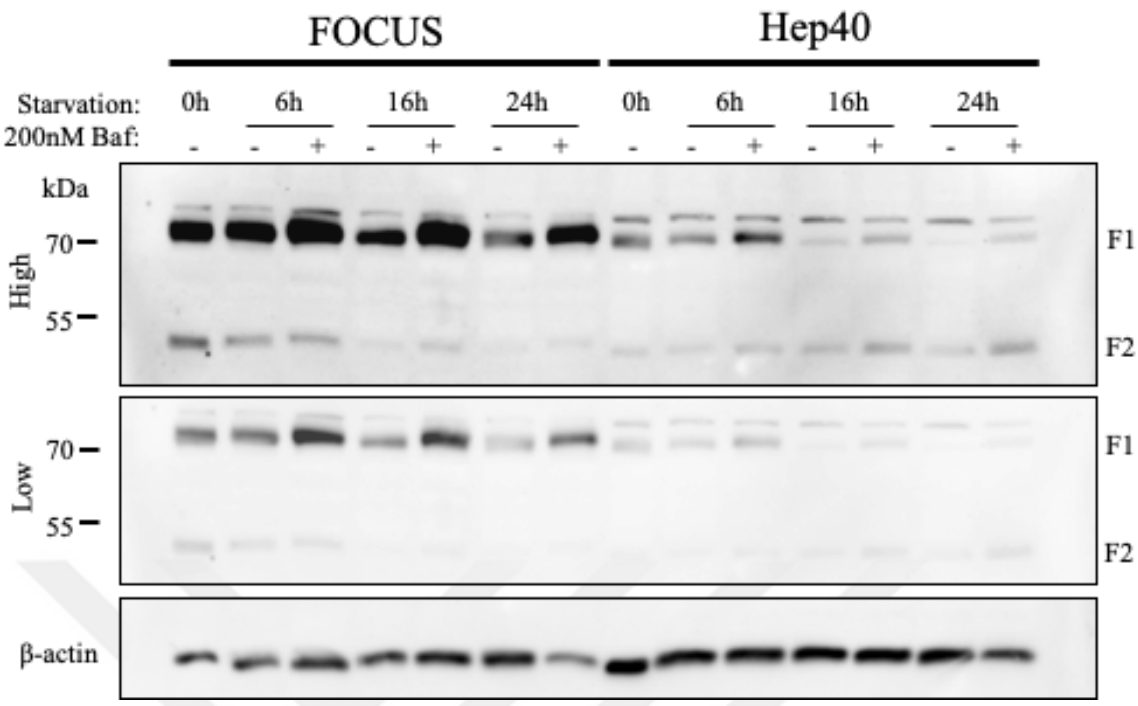


Figure 24: Response of FAM134B variants upon nutrient starvation.

Cells were starved for the indicated time periods by replacing complete medium with EBSS, either with or without 200nM Bafilomycin A1. Pictures were taken for 5 minutes (upper panel, high) and 1 minute (lower panel, low). F1 and F2 corresponds to FAM134B-1 and FAM134B-2 specific bands, respectively.

According to the immunoblotting results (Figure 24), the most dramatic change during starvation is observed in FAM134B-1, which apparently decreases over time in both cell lines; and, bafilomycin A1 treatment causes protein accumulation. FAM134B-1 was accumulated in Bafilomycin A1 treated FOCUS up to 16 hours, yielding higher amount of protein than starting point. However, FAM134B-1 accumulation in Hep40 cells only lasted up to 6 hours. Decreased protein levels of both isoforms in prolonged starvation even under Bafilomycin A1 treatment was noteworthy. Even though FAM134B-2 levels decrease over time, protein accumulation upon Bafilomycin A1 does not follow the similar trend; FAM134B-2 only slightly resists degradation in FOCUS cell line, while there was a gradual accumulation in Hep40 cells which peaks at 24 hours.

This data strongly suggests that FAM134B-1 and FAM134B-2 differs from each other partially, if not all, by degradation properties especially during starvation. In particular, FAM134B-2 seems to be slightly more resistant to starvation induced degradation.

4.13 Ectopic FAM134B-1 expression increases LC3BII formation

Since FAM134B has been described primarily as ER-phagy receptor, we hypothesized that its over expression would affect the autophagy machinery by shifting nutrient preference towards ER in addition to other macro molecules. In order to test our hypothesis, first, we generated stable HepG2 cell lines with inducible FAM134B-1 expression in order to observe cellular behavior upon different cellular stress inducers (Figure 25).

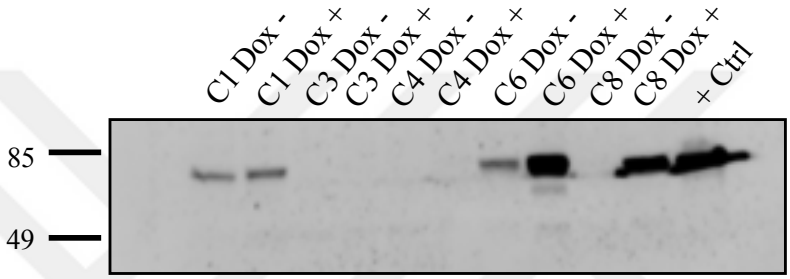


Figure 25: HepG2-FAM134B-1 clones are inducible for FAM134B-1 expression
Lanes with induced FAM134B-1 expression upon Doxycycline (a tetracycline analog) was accepted as positive clones. In this case, clone 6 and 8 were picked as positive clones and were used in following experiments.

Next, we starved HepG2-FAM134B-1 cells for 2, 4, 8, 16 and 24 hours with or without 24 hours of 1µg/ml Doxycycline treatment prior to starvation. The lysates were screened for autophagy-related and apoptotic changes using western blot method.

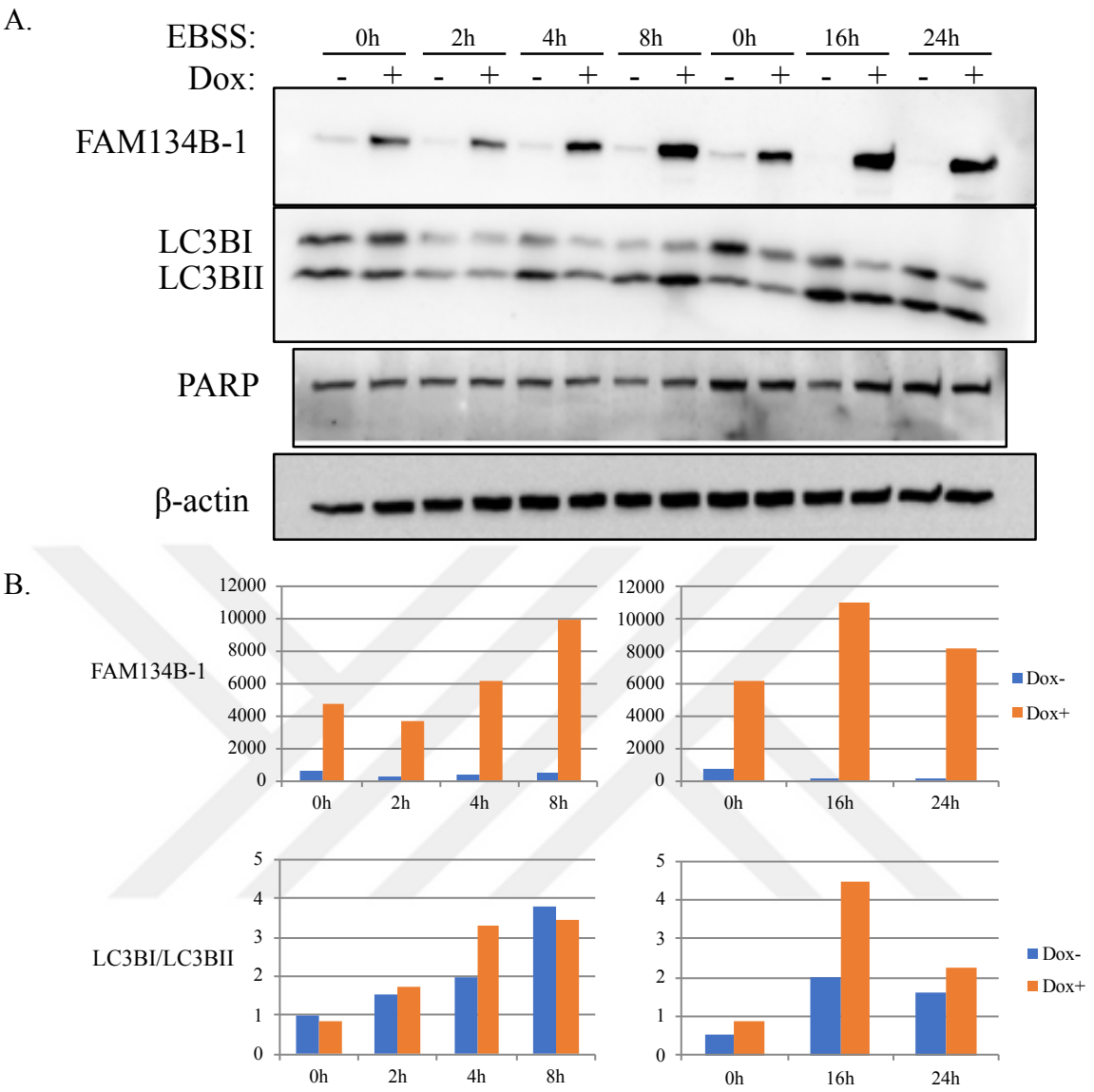


Figure 26: FAM134B-1 accumulates over time even under starvation

A. Western blot images of FAM134B-1 overexpressing HepG2 cells. Cells were starved for the indicated time periods. Autophagy flux and apoptosis levels were probed using anti-LC3B and anti-PARP antibodies, respectively. B. FAM134B-1 levels and LC3BII/LC3BI ratio were quantified in Fiji (Image J). The Y axis in FAM134B-1 represents arbitrary units. Short- and long-term starvation conditions were set in two different experiments.

Protein levels of FAM134B-1 was dramatically stimulated upon Doxycycline treatment, as expected. Interestingly, however, FAM134B-1 levels in Dox+ group kept accumulating gradually even under starvation, while protein levels remained same in Dox- group (Figure 26).

Proportional increase of LC3BII over LC3BI overtime in all groups also clearly indicates that the cells undergo an autophagy mediated catabolic metabolism. Early hours in starvation did not resulted in a clear effect of FAM134B-1 dependent change in LC3BII/LC3BI ratio. On the other hand, when starvation is prolonged, LC3BII/LC3BI ratio is clearly increased in Dox+ cells, with the most striking change at 16 hours. Furthermore, overall LC3B levels also tended to decrease in prolonged starvation in the presence of FAM134B-1.

Neither the presence of FAM134B-1 nor the starvation did not result in apoptosis as evidenced by PARP immunoblot, since no cleaved PARP was observed upon starvation.

Increased FAM134B-1 levels together with LC3BII accumulation during starvation suggests that cells respond starvation by stimulating the autophagosome formation; but, it fails to clear excessive amount of FAM134B-1 from ER. Furthermore, enhanced FAM134B expression is not lethal for cells and induction of starvation does not change the apoptotic response of the cells.

4.14 Upon starvation, *Fam134b*$^{-/-}$ mice display less weight loss and increased serum albumin levels along with disrupted amino acid release

FAM134B was discovered as an essential gene for central nervous system that its absence causes hereditary sensory neuropathy type 2 (HSANIIB). Although this phenotype had been nicely recapitulated in FAM134B knockout animals, to our knowledge, any other phenotypic effect was not defined in same mouse model previously. In fact, despite its discovery in ER-phagy process, the overall phenotypic effect has not been reported under stimulated autophagy. Therefore, we hypothesized that, a protein which take a critical role in selective autophagy, such as *Fam134b* (and its variants), would be much better understood under starvation conditions.

All animal groups composed of *Fam134b*$^{-/-}$ and *Fam134b*$^{+/+}$ mice were first synchronized by 24 hours starvation which is followed by free access to food for 3 hours. Then, *ad libitum* groups were fed until the experiment is terminated, while starvation groups were deprived of food for 36 hours. Access to water was free for all animals, during the experimentation. Experiment is terminated after 36 hours by cardiac puncture under deep anesthesia. Carcass and organ weights were measured immediately after euthanasia; and, serum samples were measured by serum analyzer.

A.


Body Weight Before 36h Starvation (g)
40
30
20
10
0
WT-AL
WT-ST
KO-AL
KO-ST

B.

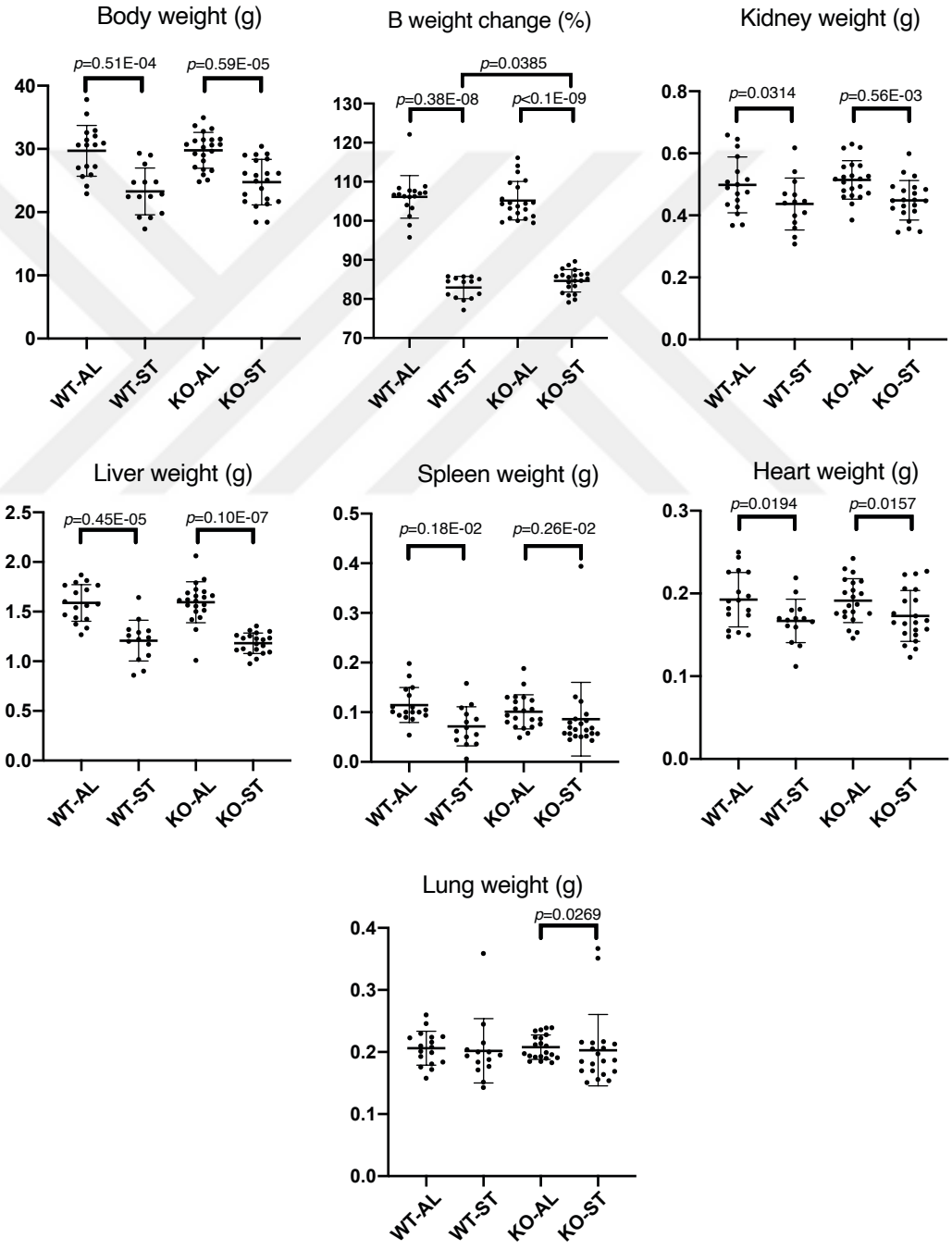

Body weight (g)
p=0.51E-04
p=0.59E-05
B weight change (%)
p=0.0385
p=0.38E-08
p<0.1E-09
Kidney weight (g)
p=0.0314
p=0.56E-03
Liver weight (g)
p=0.45E-05
p=0.10E-07
Spleen weight (g)
p=0.18E-02
p=0.26E-02
Heart weight (g)
p=0.0194
p=0.0157
Lung weight (g)
p=0.0269
WT-AL
WT-ST
KO-AL
KO-ST

Figure 27: *Fam134b*$^{-/-}$ animals resist starvation induced weight loss.

18-month-old mice (n=73) were used for body and organ weight calculation with following groups: *Fam134b*$^{+/+}$*-ad libitum* (WT-AL), n=17 (9 male, 8 female); *Fam134b*$^{+/+}$ Starvation (WT-ST), n=14 (8 male, 6 female); *Fam134b*$^{-/-}$*-Ad libitum* (KO-AL), n=21 (13 male, 8 female); *Fam134b*$^{-/-}$- Starvation (KO-ST), n=21 (13 male, 8 female). Mann-Whitney non-parametric test results are represented as mean and standard deviation. $p<0.05$ was considered as significant. Non-significant results are not indicated.

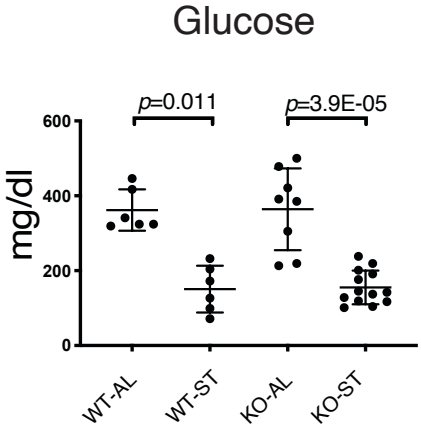
At basal levels, most of the organs did not show any difference between wild type and mutant groups. 36h starvation caused total body weight loss in both wild type and mutant groups, as expected. Although we could not observe any significant change in absolute weights between wild type and mutant groups, body weight loss percentages yielded a striking result: starved mutant group significantly resisted weight loss (Figure 27).

Liver and spleen weights decreased in both wild type and mutant groups upon starvation, without showing any significance resulting from the absence of the gene.

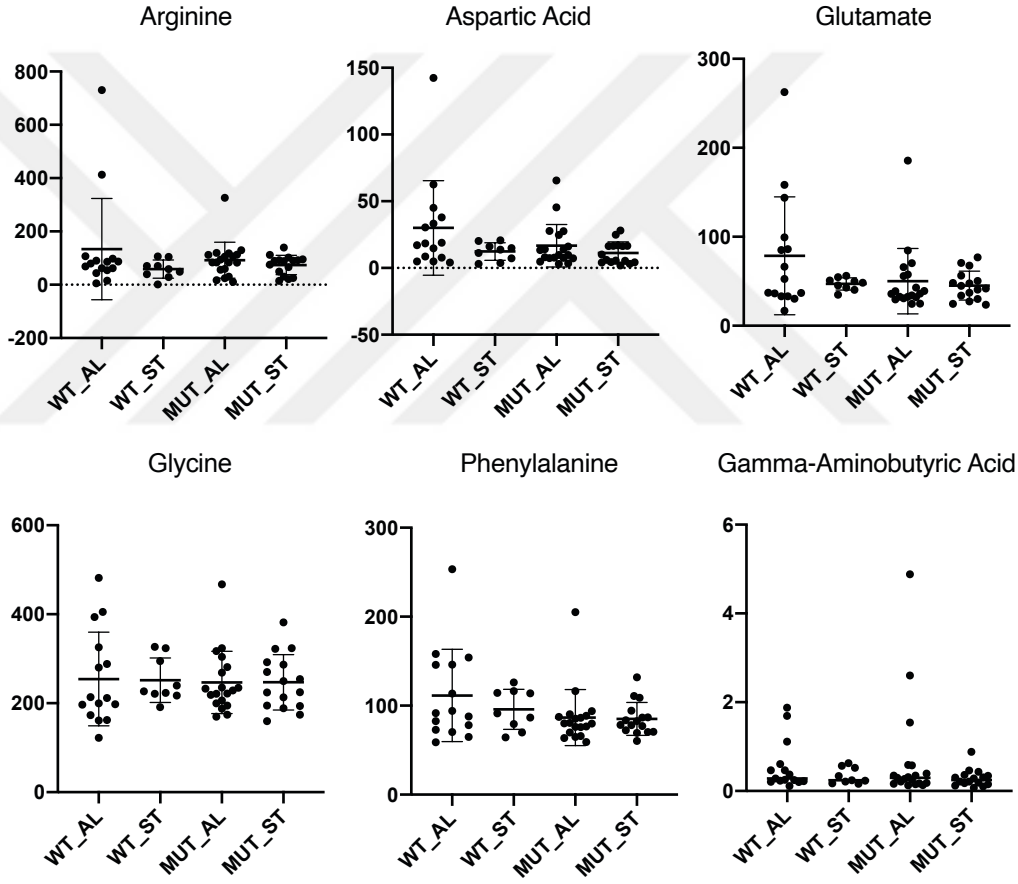
Autophagic proteolysis in the liver following starvation makes a significant contribution to the maintenance of blood glucose levels via conversion of amino acids to glucose, and accordingly, many amino acids are released into the blood by 24h of starvation. Therefore, we measured serum glucose and amino acid levels in both wild-type and *Fam134b*$^{-/-}$ mice after 36h of starvation. All starvation experiments performed on animals were set in two different times. Before the preparation of this thesis, the results from the initial serum amino acid analyses (from first experimental group) were submitted for publication and received acceptance. Second set of amino acid analyses were performed during the preparation of this thesis. Therefore, there are some differences in amino acid results mainly due to the number of samples used in article and thesis.

There was a significant decrease in serum glucose in both wild type and mutant mice, the fall in *Fam134b*$^{-/-}$ being more significant (Figure 28, A). There was no difference in amino acids arginine, aspartic acid, glutamate, phenylalanine, glycine and gamma aminobutyric acid in any group regardless of genotype or starvation conditions (Figure 28, B). Wild-type animals displayed a significant increase in serum levels of amino acids glutamine.

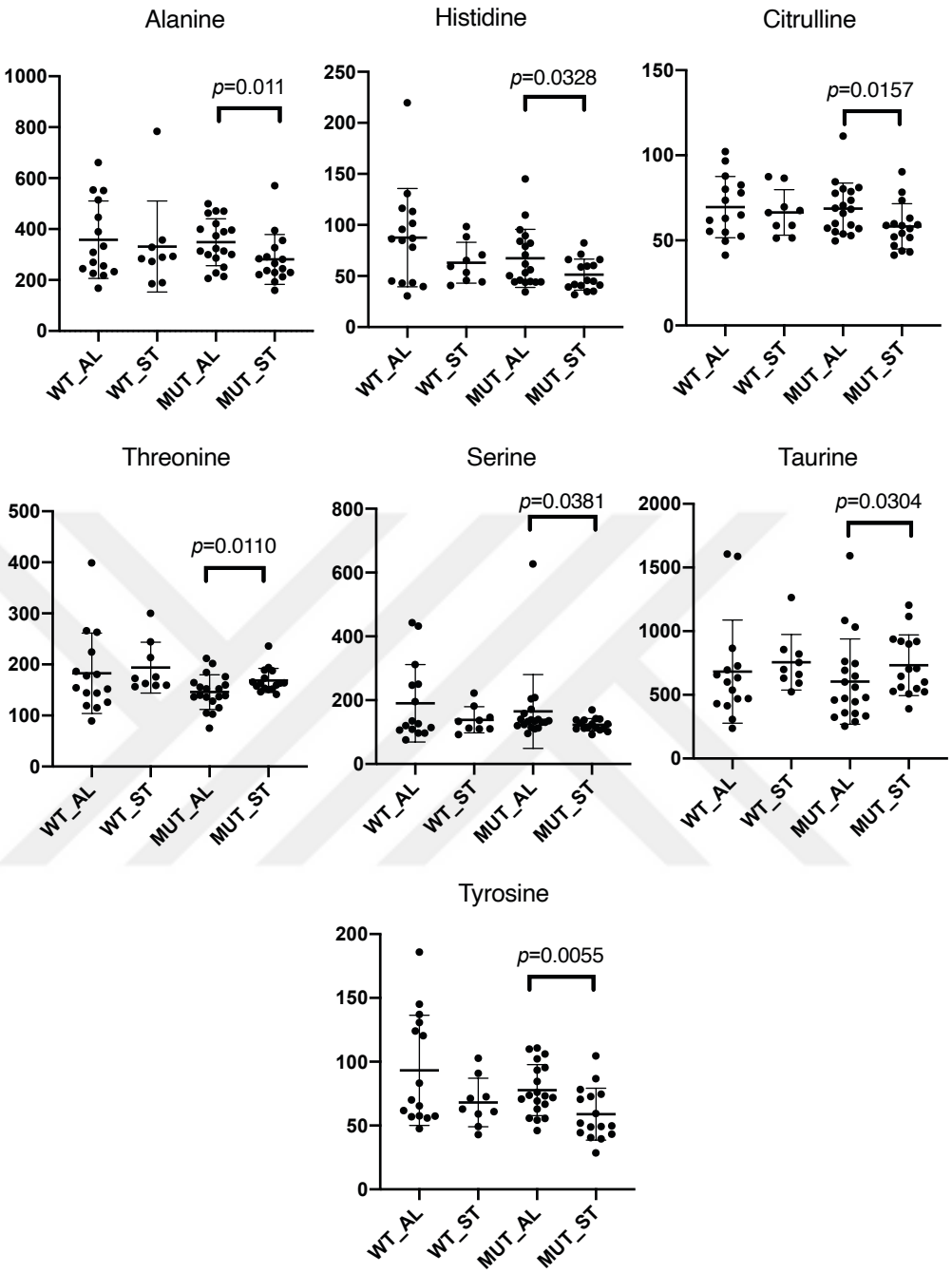
A.


Glucose
p=0.011
p=3.9E-05
mg/dl
600
400
200
0
WT-AL
WT-ST
KO-AL
KO-ST

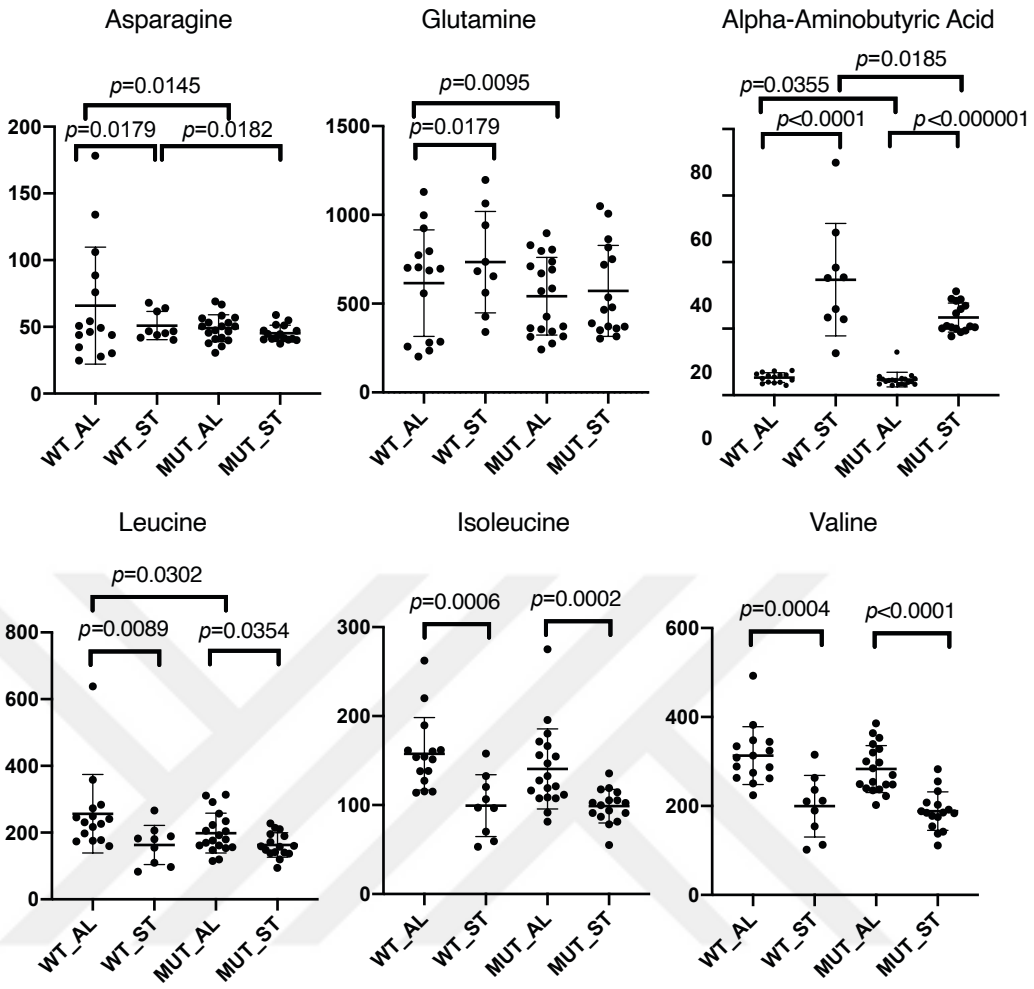
B.


Arginine
Aspartic Acid
Glutamate
Glycine
Phenylalanine
Gamma-Aminobutyric Acid
WT_AL
WT_ST
MUT_AL
MUT_ST

C.


Alanine
p=0.011
1000
800
600
400
200
0
WT_AL
WT_ST
MUT_AL
MUT_ST
Histidine
p=0.0328
250
200
150
100
50
0
WT_AL
WT_ST
MUT_AL
MUT_ST
Citrulline
p=0.0157
150
100
50
0
WT_AL
WT_ST
MUT_AL
MUT_ST
Threonine
p=0.0110
500
400
300
200
100
0
WT_AL
WT_ST
MUT_AL
MUT_ST
Serine
p=0.0381
800
600
400
200
0
WT_AL
WT_ST
MUT_AL
MUT_ST
Taurine
p=0.0304
2000
1500
1000
500
0
WT_AL
WT_ST
MUT_AL
MUT_ST
Tyrosine
p=0.0055
200
150
100
50
0
WT_AL
WT_ST
MUT_AL
MUT_ST

D.


Asparagine
p=0.0145
p=0.0179
p=0.0182
200
150
100
50
0
WT_AL
WT_ST
MUT_AL
MUT_ST
Glutamine
p=0.0095
p=0.0179
1500
1000
500
0
WT_AL
WT_ST
MUT_AL
MUT_ST
Alpha-Aminobutyric Acid
p=0.0185
p=0.0355
p<0.0001
p<0.000001
80
60
40
20
0
WT_AL
WT_ST
MUT_AL
MUT_ST
Leucine
p=0.0302
p=0.0089
p=0.0354
800
600
400
200
0
WT_AL
WT_ST
MUT_AL
MUT_ST
Isoleucine
p=0.0006
p=0.0002
300
200
100
0
WT_AL
WT_ST
MUT_AL
MUT_ST
Valine
p=0.0004
p<0.0001
600
400
200
0
WT_AL
WT_ST
MUT_AL
MUT_ST

E.

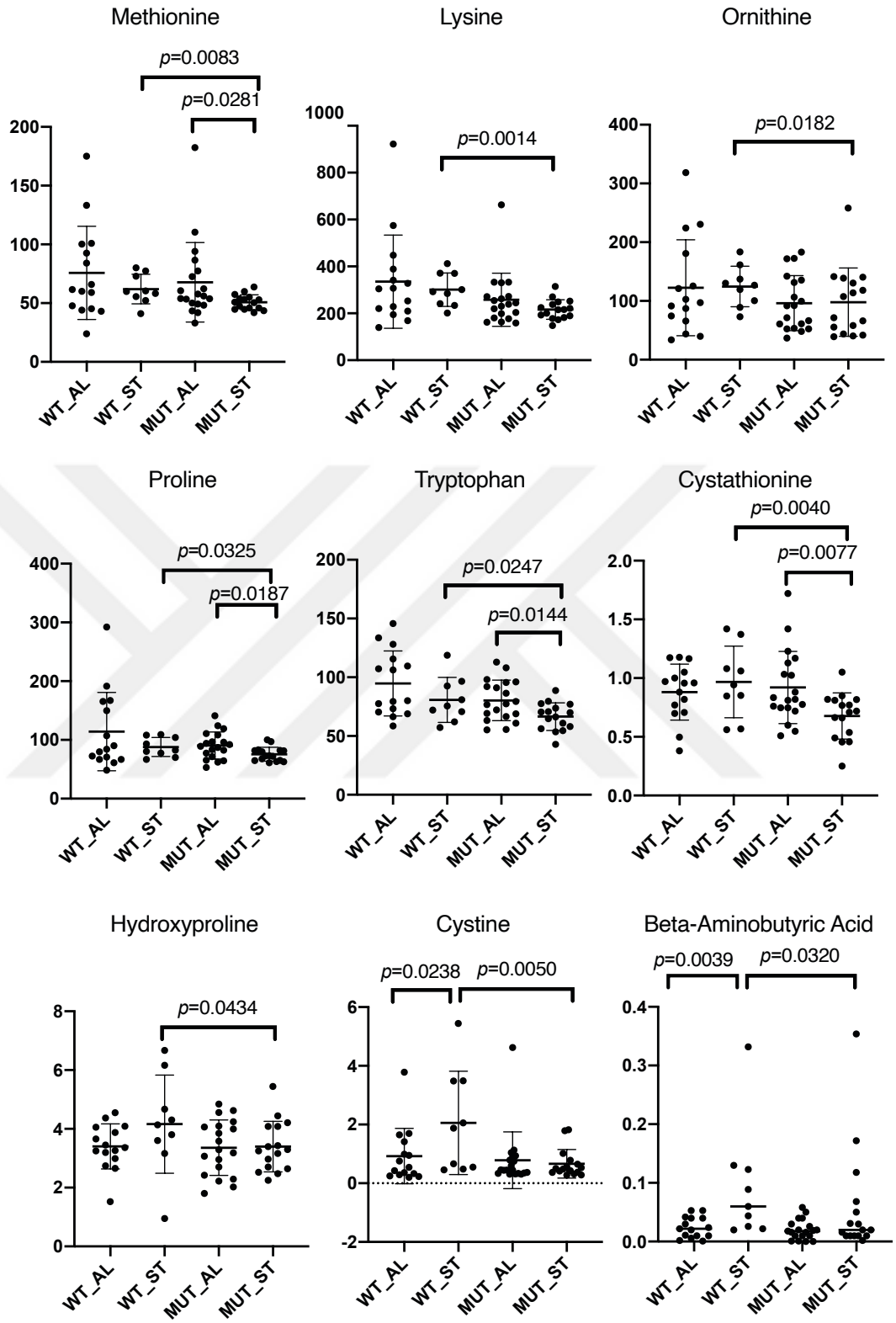


Figure 28: Starvation induces abrupted serum amino acid levels in *Fam134b*$^{-/-}$ mice.

A. serum glucose levels of wild type and *Fam134b*$^{-/-}$ mice. B. Unchanged amino acids after 36h of starvation. C. amino acids that significantly affected in mutant animals

after 36h of starvation. D and E. Various amino acids which are significantly altered between wild type and mutant animals as a physiological response to starvation. The animals tested for serum biochemistry were average 18 months old. Due to insufficient amount of serum for each animal amino acid analysis is organized as followed: WT-AL, n=15 (9 male, 6 female); WT-ST, n=9 (6 male, 3 female); KO-AL, n=19 (11 male, 8 female); KO-ST, n=16 (11 male, 5 female). Mann-Whitney non-parametric test results are represented as mean and standard deviation. $p<0.05$ was considered as significant. Non-significant results are not indicated.

There was no change in the levels of alanine, histidine, citrulline, threonine, serine, taurine and tyrosine amino acid in wild-type mice, but interestingly, all these amino acids underwent a significant drop in *Fam134b*$^{-/-}$ mice (Figure 28, C). At basal conditions, asparagine, glutamine, glycine, leucine and alpha-aminobutyric acid were significantly lower in mutants compared to wild type group (Figure 28, D). The branched chained amino acids, leucine, isoleucine, valine; and alpha-aminobutyric acid were dropped in both wild type and mutant groups after starvation.

The levels of methionine, lysine, ornithine, proline, tryptophan, cystathionine, hydroxyproline, cystine and Beta-aminobutyric acid were significantly lower in mutant starved animals as compared to wild type starvation. This clearly shows that mutant animals cannot effectively mobilize amino acids in circulation compared to wild type animals (Figure 28, E).

At serum biochemistry level, starvation clearly lowered the levels of LDL cholesterol and triglyceride, but elevated bilirubin levels in both wild type and mutant groups, as expected. Intriguingly, even though albumin and total protein levels did not change in wild type group, they significantly increased in mutant mice. On the contrary, Blood Urea Nitrogen (BUN) is elevated in wild type animals but remains statistically unchanged in mutant animals. Furthermore, serum parameters of wild type and mutant animals at *ad libitum* conditions showed a significance only in High Density Lipoprotein (HDL), which was lower in mutant mice (Figure 29).

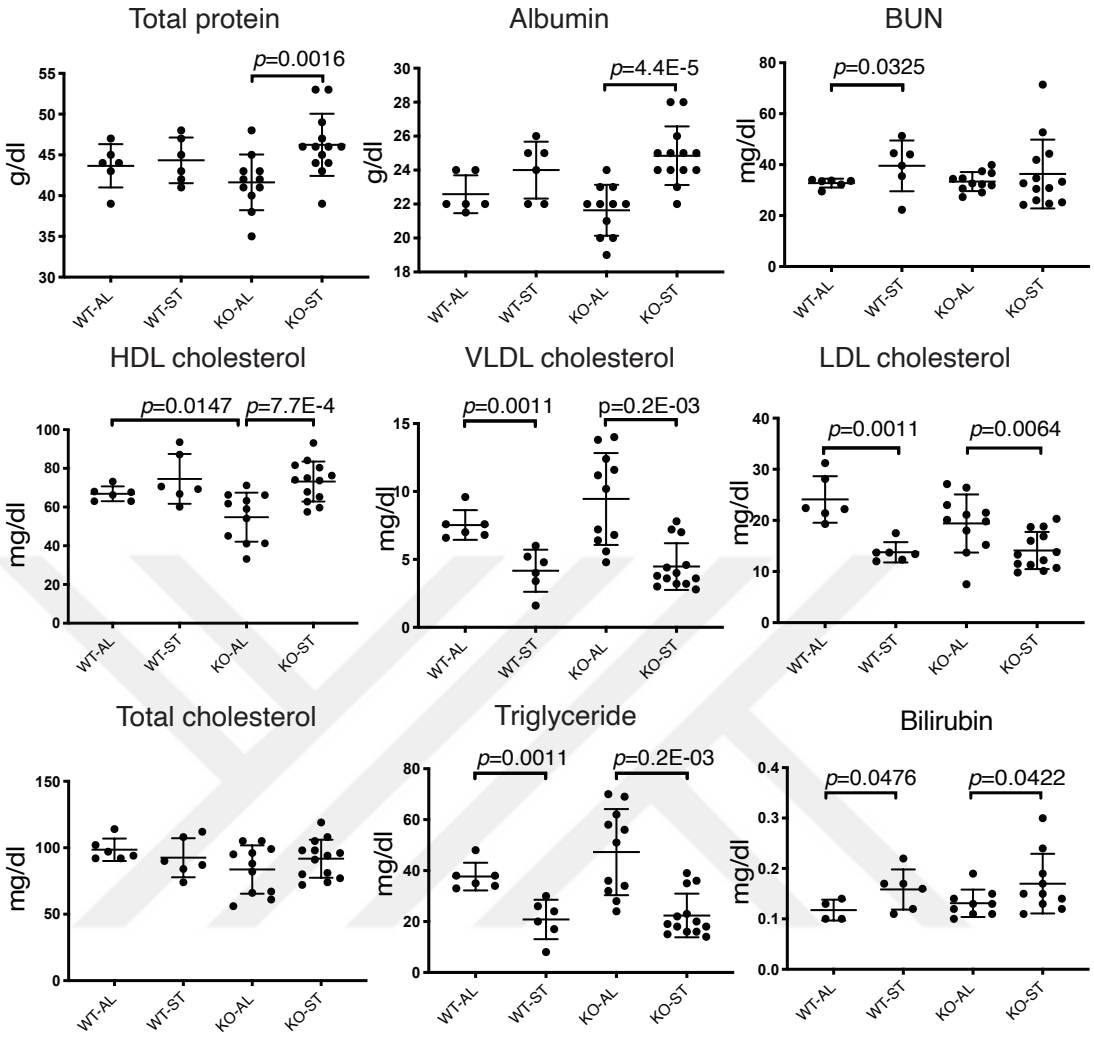


Figure 29: *Fam134b*$^{-/-}$ mice exhibits low basal levels of HDL cholesterol, and increased serum protein after starvation

Serum biochemistry of wild type and *Fam134B*$^{-/-}$ animals after 36h of starvation. The animals tested for serum biochemistry were average 18 months old and the groups are as follows: *Fam134b*$^{+/+}$-ad libitum (WT-AL), n=6 (4 male, 2 female); *Fam134b*$^{+/+}$ Starvation (WT-ST), n=6 (4 male, 2 female); *Fam134b*$^{-/-}$-Ad libitum (KO-AL), n=11 (8 male, 3 female); *Fam134b*$^{-/-}$- Starvation (KO-ST), n=13, (9 male, 4 female). BUN, Blood Urea Nitrogen; VLDL, Very Low-Density Lipoprotein; LDL, Low Density Lipoprotein; HDL, High Density Lipoprotein. Mann-Whitney non-parametric test results are represented as mean and standard deviation. $p<0.05$ was considered as significant. Non-significant results are not indicated.

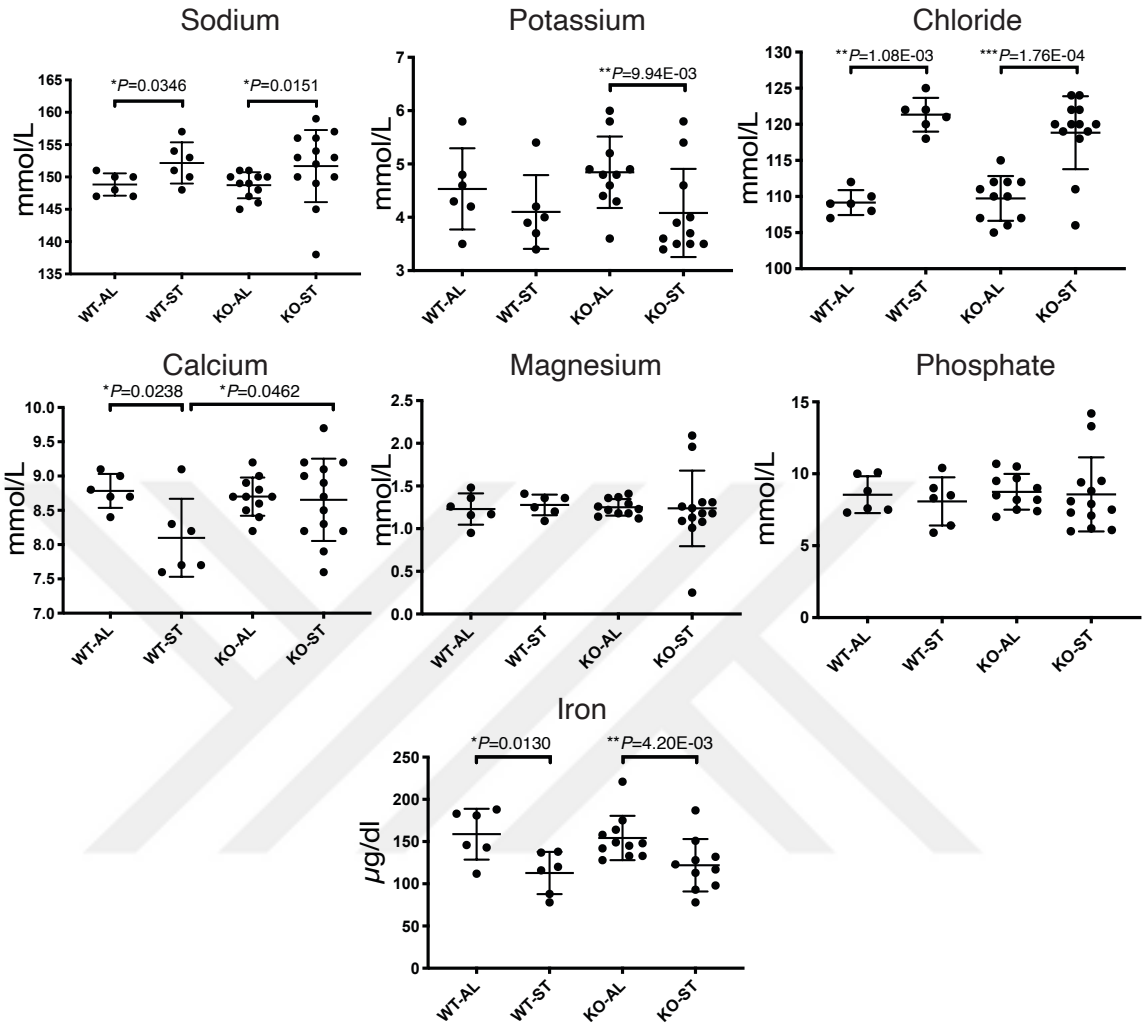


Figure 30: *Fam134b*$^{-/-}$ animals resisted starvation induced hypocalcemia.

Under *ad libitum* condition, there was no clear change in serum electrolyte levels in all groups. In fact, Magnesium and phosphate showed no change in any condition. Starvation induced increase in sodium and chloride, decrease in iron for both wild type and mutant groups. Nevertheless, we observed a significant decrease of potassium only in mutant animals. Furthermore, contrary to their wild type counterparts, mutant animals showed resistance to hypocalcemia.

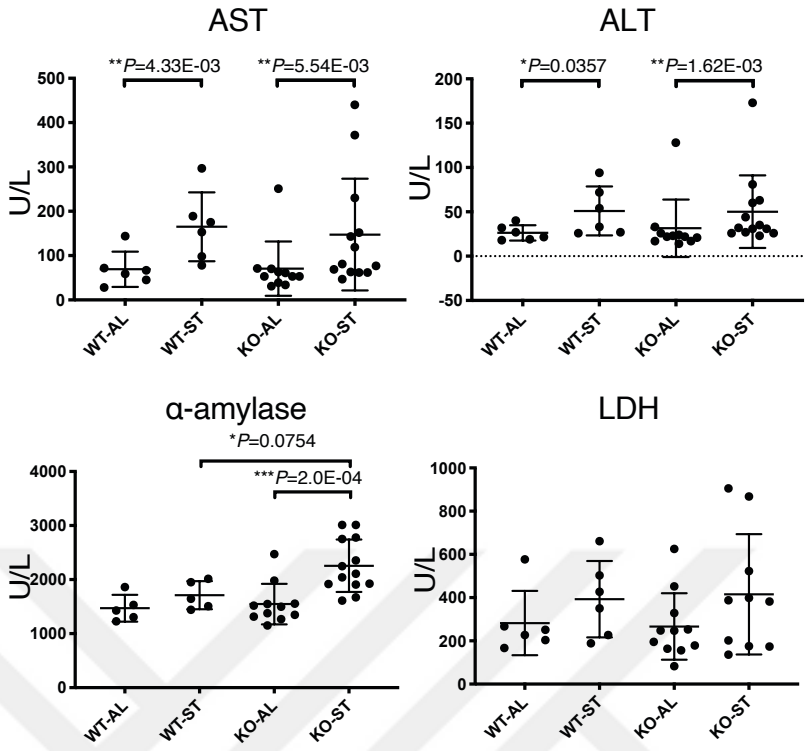


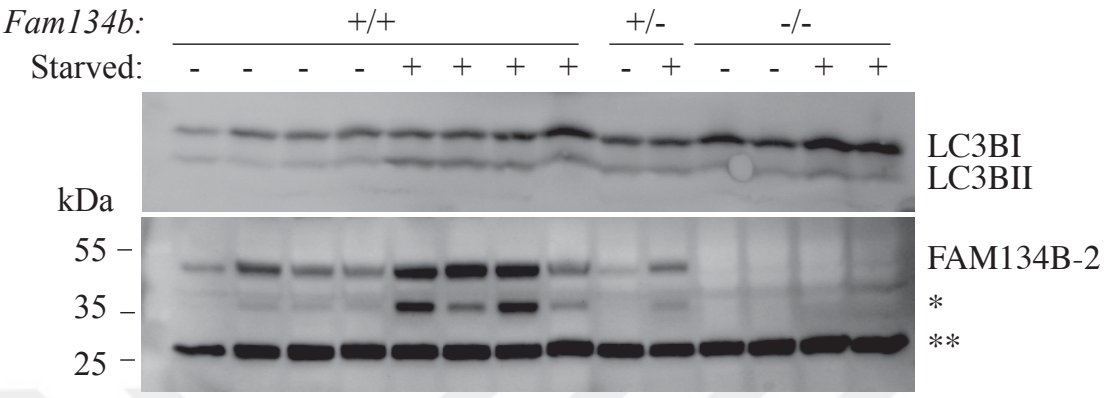
Figure 31: *Fam134b*$^{-/-}$ mice exhibits increased serum a-amylase levels upon 36h starvation

Mere absence of *Fam134b* without induction of starvation resulted in no change in serum enzymes. 36 hours fasting indeed caused elevated liver damage markers, Aspartate Transaminase (AST) and Alanine Transaminase (ALT), in both wild-type and mutant groups. Strikingly, however, serum alpha amylase levels dramatically increased in mutant group while same condition did not exhibit similar increase.

4.15 Starvation stimulates FAM134B-2 and another protein variant expression in liver

Despite the subtle changes, starvation indeed generated a set of observable effects in physiology of mutant animals. These changed encouraged us further look into FAM134B expression changes as a response to starvation. Since liver stands as a master regulator of energy homeostasis in body, we first analyzed starved liver in the context of starvation. To do so, wild type and mutant animals were starved for 48 hours; and, liver samples were subjected to western blot and Reverse Transcriptase-PCR analysis.

A.



B.

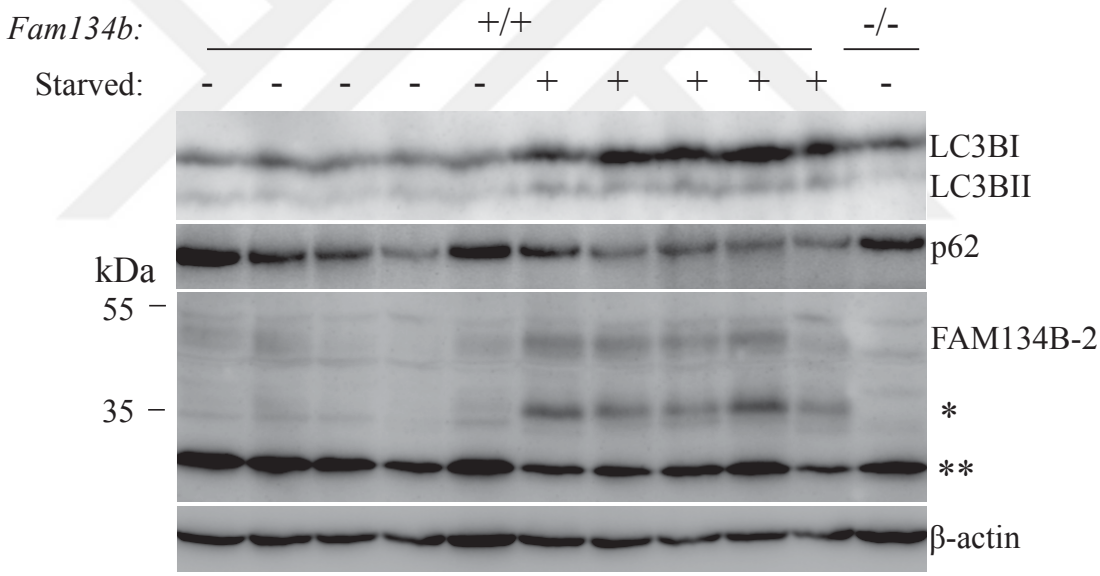


Figure 32: Starvation stimulates FAM134B-2 accumulation in liver.

A. and B. western blot images of starved mouse livers. Induction of autophagy was gauged by LC3B-II/ LC3B-I levels, as well as by p62 decrease. Single asterisk indicates additional 35kDa form of FAM134B-2. Double asterisk shows nonspecific antibody binding.

Wild type and heterozygous animals fed *ad libitum* has shown little expression of FAM134B-2 at 50kDa level. The correct place of indicated proteins were verified by liver protein lysates of mutant animals. Starvation has induced autophagic flux in all groups, as

shown by LC3B-II/LC3B-I ratio. Interestingly, basal levels of LC3B-I and LC3B-II were already stronger in mutant mice. Autophagy induction was also further verified by decreased levels of p62. Strikingly, FAM134B-2 is enhanced not only at 50kDa but also at 35kDa in both wild type and heterozygous animals after starvation.

Stimulation of FAM134B-2 in starvation came along with another question: which transcript isoforms give rise to the proteins we observe in western blot? We, therefore, performed RT-PCR with primers designed for six protein coding, two putative transcripts of mouse *Fam134b* on both *ad libitum* and starved animals.

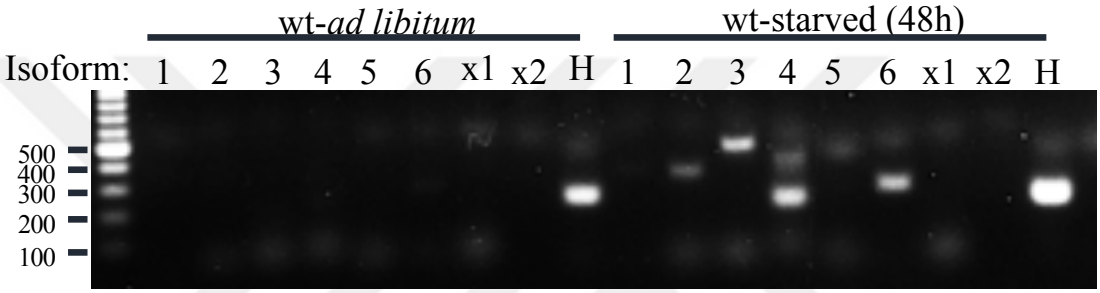


Figure 33: Expression of different mouse *Fam134b* isoforms in liver upon 48h starvation.

Under normal conditions, there was almost no visible amplification of *Fam134b* isoforms in liver. However, when animals were challenged with 48 hours starvation, *isoform-2*, *-3*, *-4* and *-6* dramatically increase. There was also very slight increase in isoform-1.

These results have clearly demonstrated that, short FAM134B-2 is dominant isoform in liver, but at low levels. However, liver dramatically responds to starvation by increasing FAM134B-2 levels along with an even shorter isoform. Furthemore, FAM134B-2 is most likely not a translation product of one variant, but rather *isoform-2*, *-3*, *-4* and *-6* all contributes to FAM134B-2 translation.

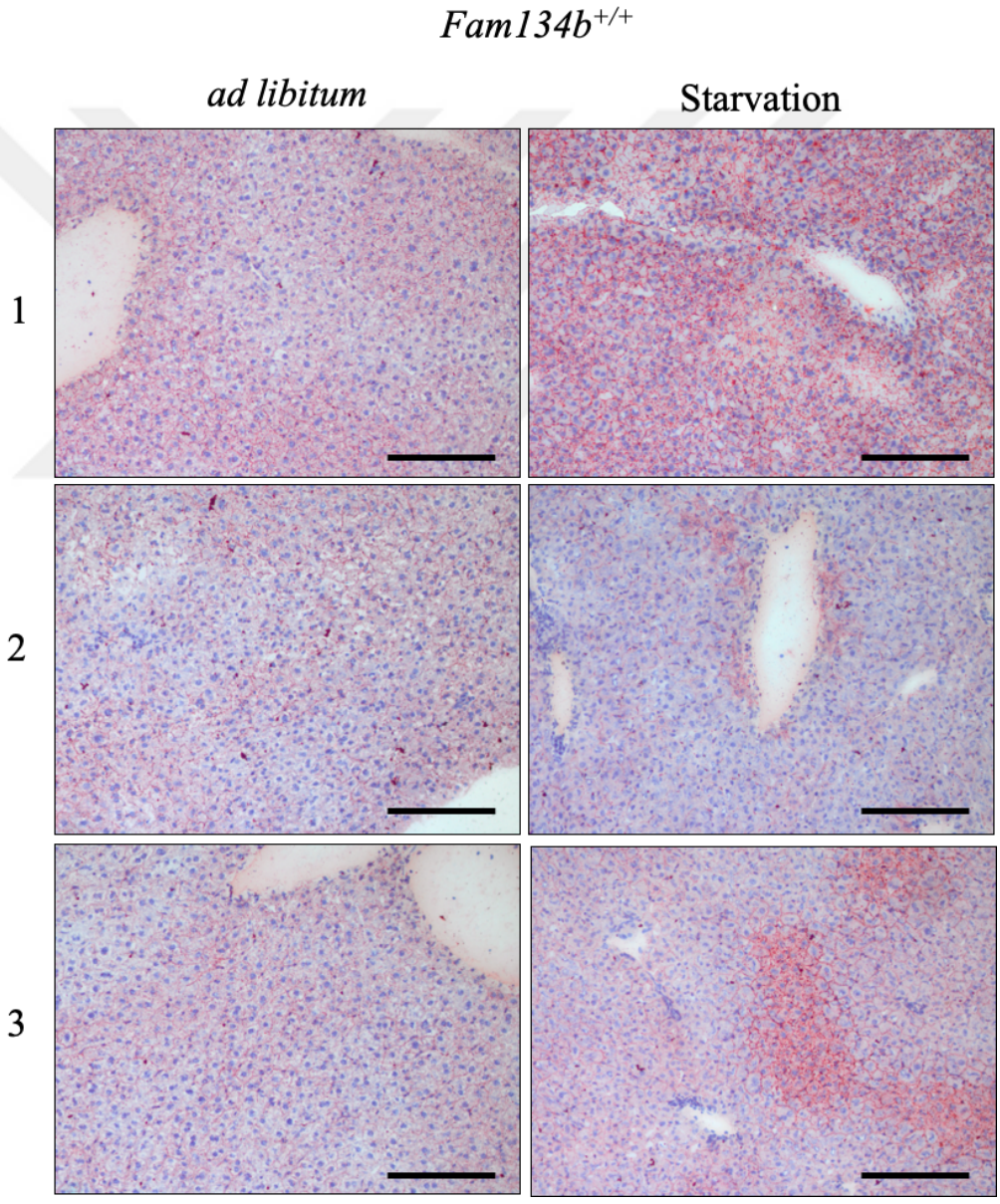
4.16 *Fam134b*$^{-/-}$ animals exhibit disrupted lipid storage in liver

Nutrient deficiency stimulates series of molecular changes in all living organisms. These responses usually cover critical organs which regulate energy homeostasis in higher mammals. Among those, liver is of particular interest since it strictly regulates collection and

redistribution of biological fuels. As the glycogen storages are depleted in early hours of starvation, peripheric lipids are mobilized and stored as lipid droplets in liver for generation of ketone bodies and gluconeogenesis. However, as the starvation progress, these energy reserves can also be depleted. Hence, FAM134B-2 increase in liver after starvation made us hypothesize that it might involve in metabolic processes in liver regulating lipid storage.

In order to test this hypothesis, we performed Oil-Red-O staining on 48 hours starved animal livers.

A.



B.

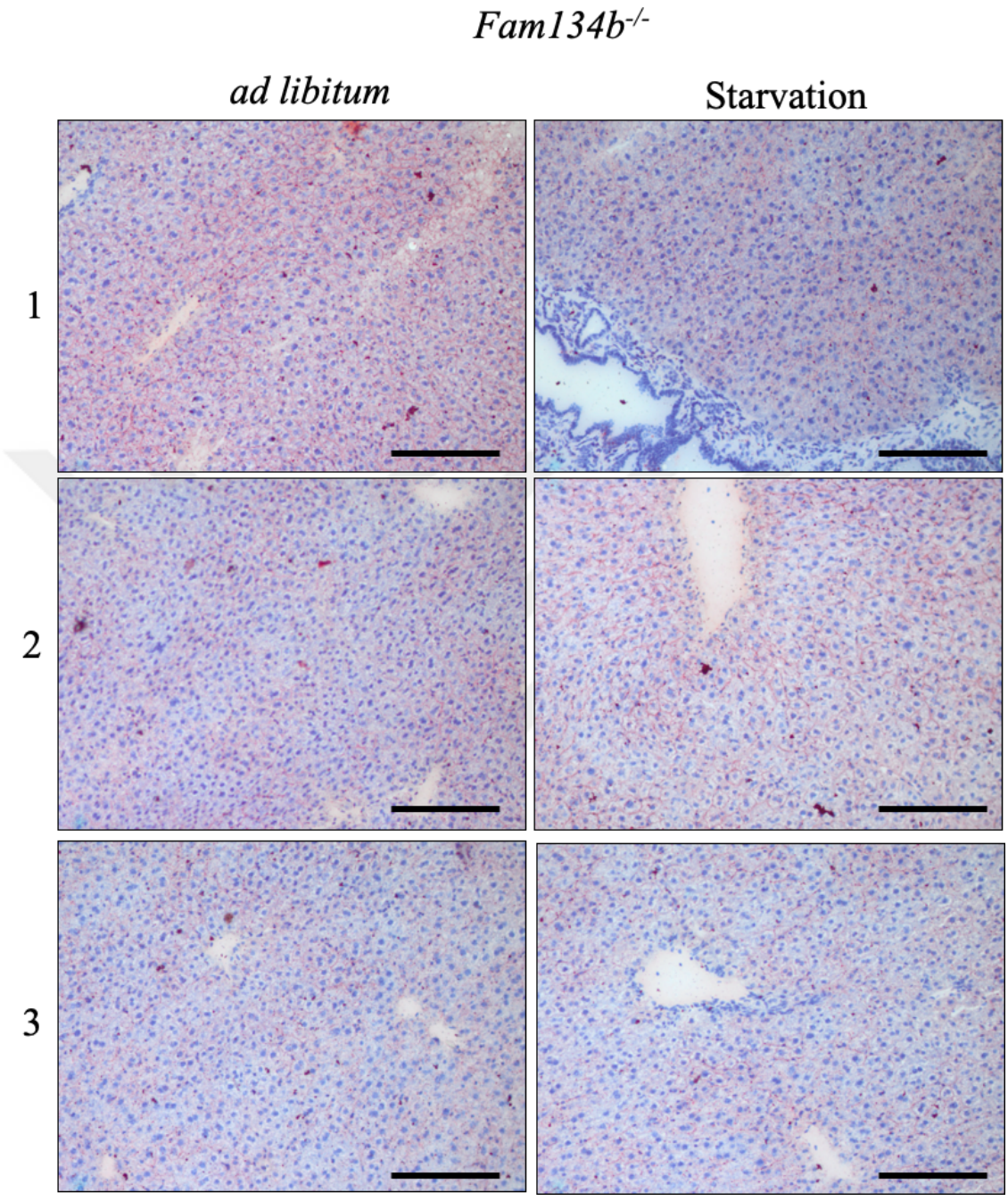


Figure 34: *Fam134b* deficiency lead to disrupted accumulation of lipid droplets

A. Livers of *Fam134b*$^{+/+}$ mice starved for 48 hours B. same experimental conditions applied to *Fam134b*$^{-/-}$. Corresponding numbers show liver samples from different animals (n=12). Samples were not aligned as pairs. Scale bar: 200µm

In basal conditions, slight accumulation of lipids was observed in liver sections of both genotypes. On the other hand, while wild type animals responded to starvation by strong increase of lipid droplet accumulation which is still visible at 48h hours (Figure 34, A), mutant animals failed to exhibit the similar accumulation (Figure 34, B).

Although there were low levels of lipid droplets in mutant liver in both conditions, this data shows that absence of *Fam134b* affects either deposition or mobilization of lipid contents of the liver.

4.17 FAM134B-2 is expressed in liver of different species

Starvation induced dynamic change and evolutionary conservation of FAM134B has made us hypothesize that we could detect FAM134B protein in liver other than mouse and bovine. Hence, we performed western blot analysis on liver of lower and higher eukaryotes such zebrafish, rat and human (Figure 35).

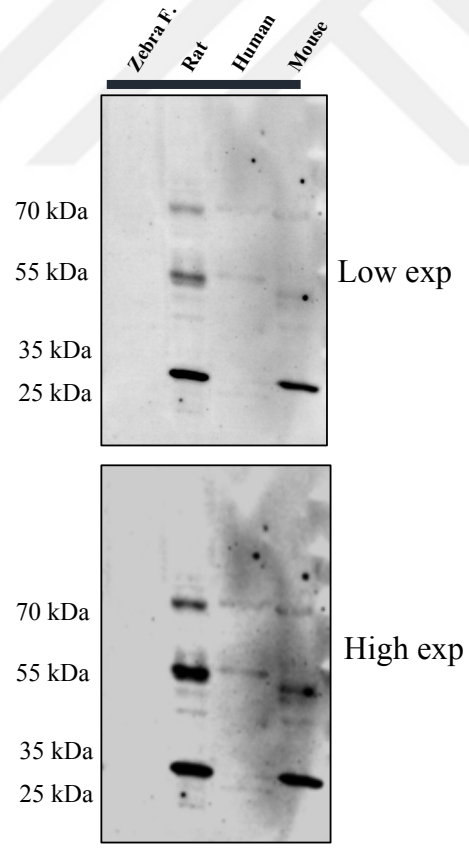


Figure 35: Liver FAM134B protein expression in zebrafish, rat, human and mouse.

Although we failed to detect any FAM134B in zebrafish, weak 50kDa expression in human and stronger 50kDa expression in rat were detected. When compared with the mouse control of the same and previous experiments, 70 kDa bands in all species are reminiscent of nonspecific antibody binding.

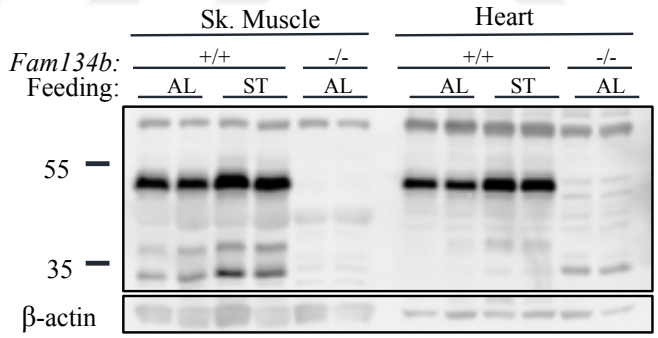
With these results, we showed that antibody we commonly use fails to detect zebrafish proteins, but can recognize rat, human and mouse FAM134B protein. We also showed that, in any species, FAM134B-2 is weakly expressed in liver.

4.18 Starvation stimulates FAM134B-2 expression in muscle and heart

The change of *Fam134b* levels in liver encouraged us to test whether same notion is also true for other organs which are known to be involved in energy homeostasis such as skeletal muscle and heart. As shown in previous sections, serum α-amylase levels are affected by the absence of FAM134B. Therefore, we included pancreas and stomach for screening the FAM134B expression levels.

Skeletal muscle, heart, pancreas and stomach tissues taken from starved animals were tested using western blot.

A.



B.

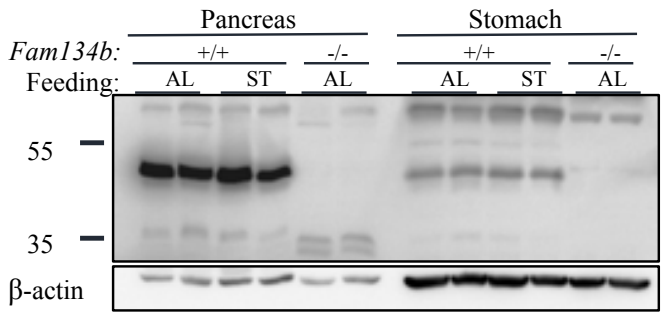


Figure 36: Response of *Fam134b* during 36h starvation shown in skeletal muscle, heart, pancreas and stomach.

A. FAM134B protein levels in skeletal muscle and heart. B. FAM134B protein levels in pancreas and stomach. AL, *ad libitum*; ST, starvation. Mutant animals were used as negative control.

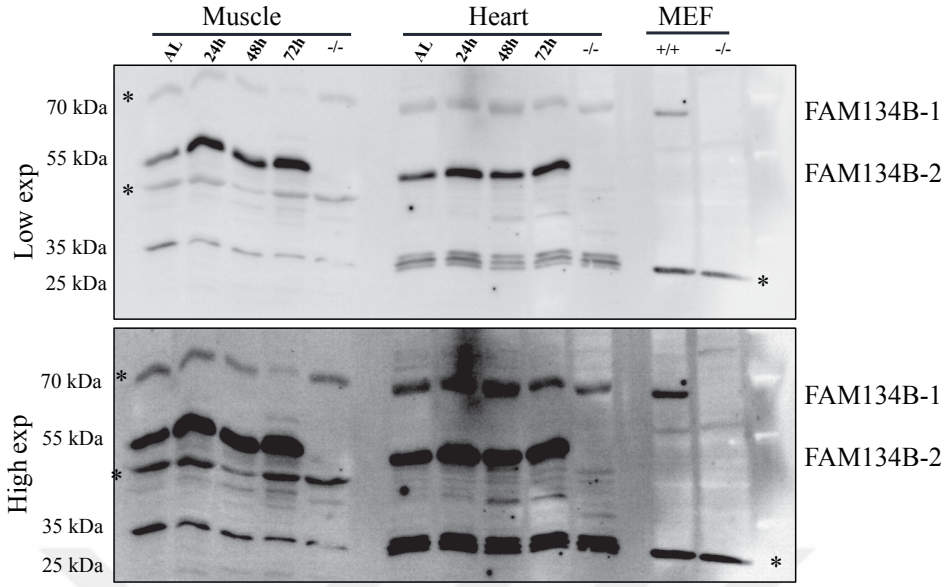
As previously shown, FAM134B-2 is already expressed strongly in skeletal muscle, heart and pancreas, but relatively weakly in stomach. Interestingly, however, starvation condition increased the protein level of FAM134B-2 even more in muscle and heart but not in pancreas and stomach (Figure 36).

This result has shown that muscle and heart respond to overall nutrient starvation in an organism by increasing FAM134B-2 but not FAM134B-1 levels.

4.19 Prolonged starvation further increases FAM134B-2 accumulation

Starvation induces cascade of events which fine tune the energy mobilization as well as the main fuel of the different organs throughout the body. Since these processes are not immediate events, but rather occur over time, we wondered whether the FAM134B-2 accumulation in heart, muscle and liver is ever increasing or a changing trend during the course of starvation. Therefore, we starved wild type animals according to schedule of 24, 48- and 72-hours periods and screened FAM134B-2 levels in heart, muscle, liver and kidney using western blot technique. We included kidney in this experimental set up, because it actively involves in energy mobilization during nutrient scarcity and stores energy as lipid droplets. In order to compare short and long isoforms (FAM134B-1 and -2) we performed western blot analyses with protein lysates taken from *Fam134b*$^{+/+}$ and *Fam134b*$^{-/-}$ Mouse Embryonic Fibroblasts (MEFs).

A.



B.

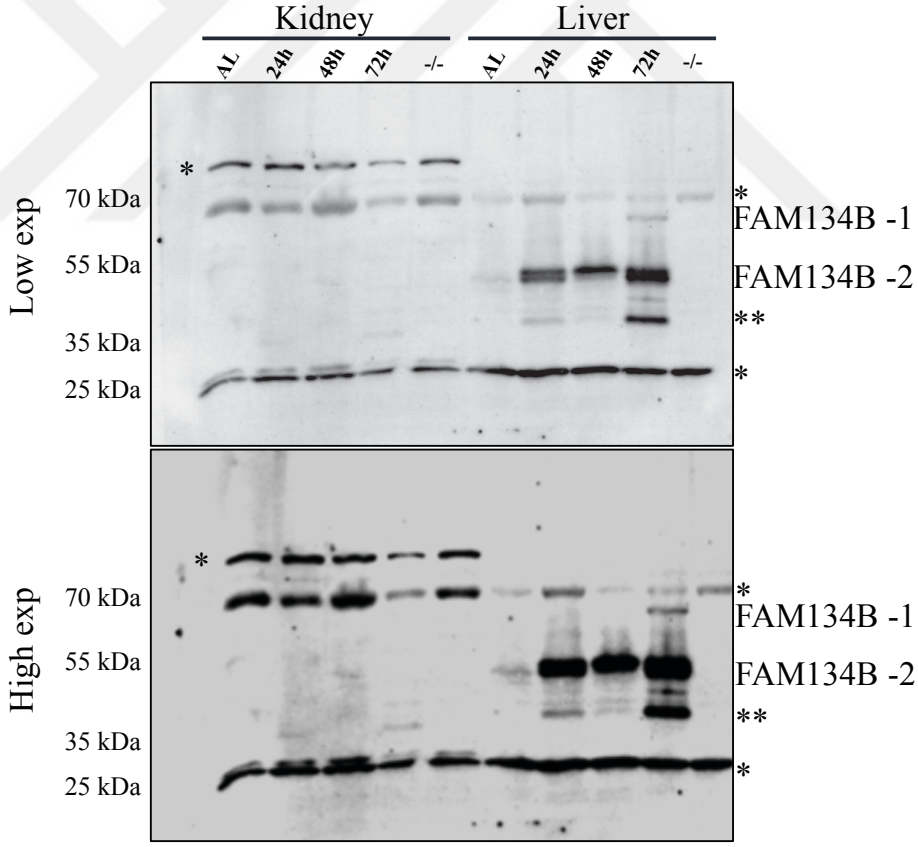


Figure 37: FAM134B-2 expression is further stimulated at 72h of starvation

A. Kidney and liver samples taken from starved animals. B.Muscle and heart samples taken from muscle, heart and MEF. AL, *ad libitum*; Mutant samples were used as negative control.

*, nonspecific bands; **, FAM134B specific band near 35kDa. MEF samples were used to show and compare protein size of FAM134B-1. High and low indicates digitally enhancement levels of the blot pictures.

According to the results, FAM134B could not be detected at kidney, neither at basal level nor during starvation. On the contrary, liver, heart and muscle exhibited strong FAM134B-2 increase at 72 hours. The most significant increase was observed in liver samples in which FAM134B-2 levels were almost absent at feeding conditions (Figure 37, B, Liver, AL). Intriguingly, FAM134B-2 levels at 24 hours are lower than 48 hours in muscle, heart and liver. However, at 72h, FAM134B-2 expression is much stronger, even more than 24h of starvation.

Shorter FAM134B-2 isoforms near 35kDa appear as early as 24 hours in liver and become strongest at 72 hours. Interestingly, the long isoform, FAM134B-1 also appeared at 72 hours. FAM134B-2 accumulation in muscle was more pronounced compared to heart, but 35kDa isoforms appeared in heart starting from 48 hours, which shows a clear difference of FAM134B expression between two muscle groups in response to starvation (Figure 37).

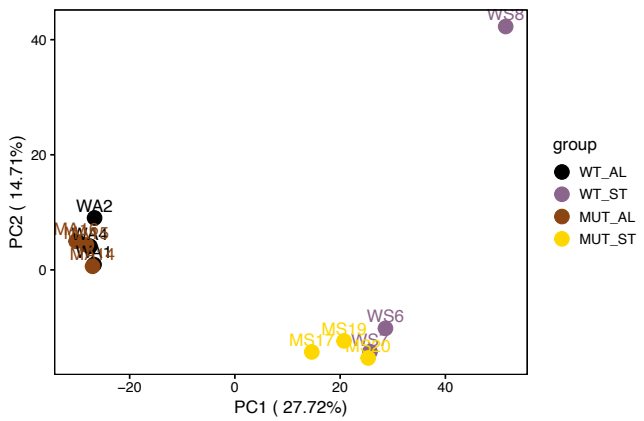
Together these results have shown that, as the starvation conditions prolonged, FAM134B-2 expression is further stimulated as a response.

4.20 Absence of *Fam134b*$^{-/-}$ alters liver gene expression related with lipid synthesis

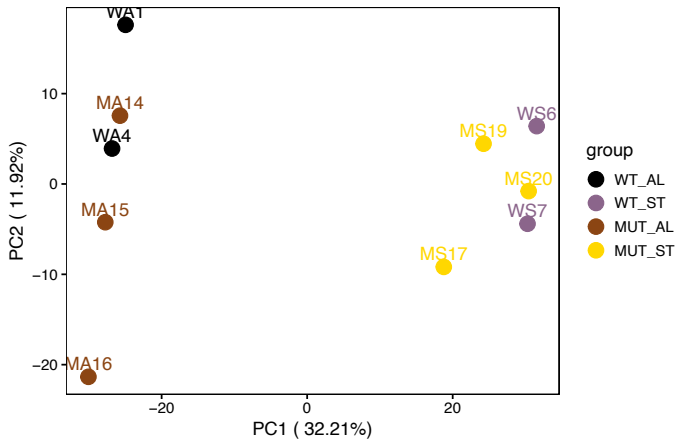
Among tissues that are responsive to starvation, most pronounced FAM134B increase was observed in liver which further intrigued us to further investigate other molecular alterations occurring globally. Decreased lipid deposition in mutant liver as a response to starvation and altered serum lipoprotein levels in *ad libitum* further encouraged us to perform a high-throughput analysis in order to reveal underlying mechanism at molecular level. Therefore, we performed RNA-sequencing on mouse liver samples (n=12) followed by bioinformatics analyze as described in methods section.

As a first step, we analyzed variability within and between groups by performing principle component and pearson's correlation analyses (Figure 38).

A.



B.



C.

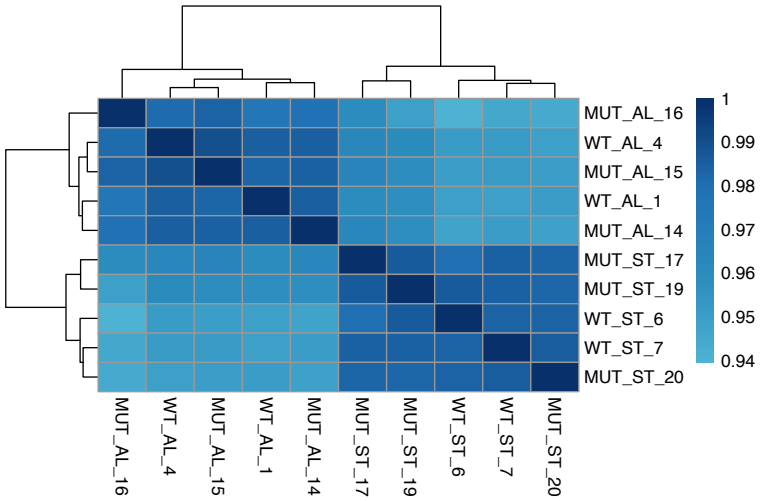


Figure 38: Principle component analyses and correlation heatmap of starved mouse livers

A. *Ad libitum* and starvation groups were perfectly segregated by PC1 axis. However, PC2 axis could not clearly divide wild type and mutant groups. B. Recalculation of principle component analyses without outlier samples, Wild type starvation 8 (WS8) and Wild type ad libitum 2 (WA2) C. Correlation heatmap of samples.

The first principle component analysis in which PC1 and PC2 represent 27.72% and 14.71% of the variability showed that *ad libitum* and starvation (PC1) samples are robustly determined as different variables. However, genotypic variation (PC2) showed that WT8 sample and WA2 samples represent outliers since they are located far away from other clusters. Hence, we eliminated these samples before proceeding further, making total number of samples analyzed (Figure 38). PCA without the outlier samples resulted in still very well separated clusters of *ad libitum* and starvation samples; but, wild type and mutant clusters were more convergent and it was difficult to differentiate samples genotypically.

In parallel with PCA analysis, Pearson's correlation heatmap showed that Ad libitum and starvation samples are distinctly clustered as evidenced by low coefficient scores; however, wild type and mutant samples did not show well demarcated clusters.

Next, we generated a scatter plot, where the significance (as -Log10) of differential expression is plotted against fold change, in order to identify significantly most altered genes at a first glance. This method also allowed us to see the abundance of significantly altered genes in four different experimental groups.

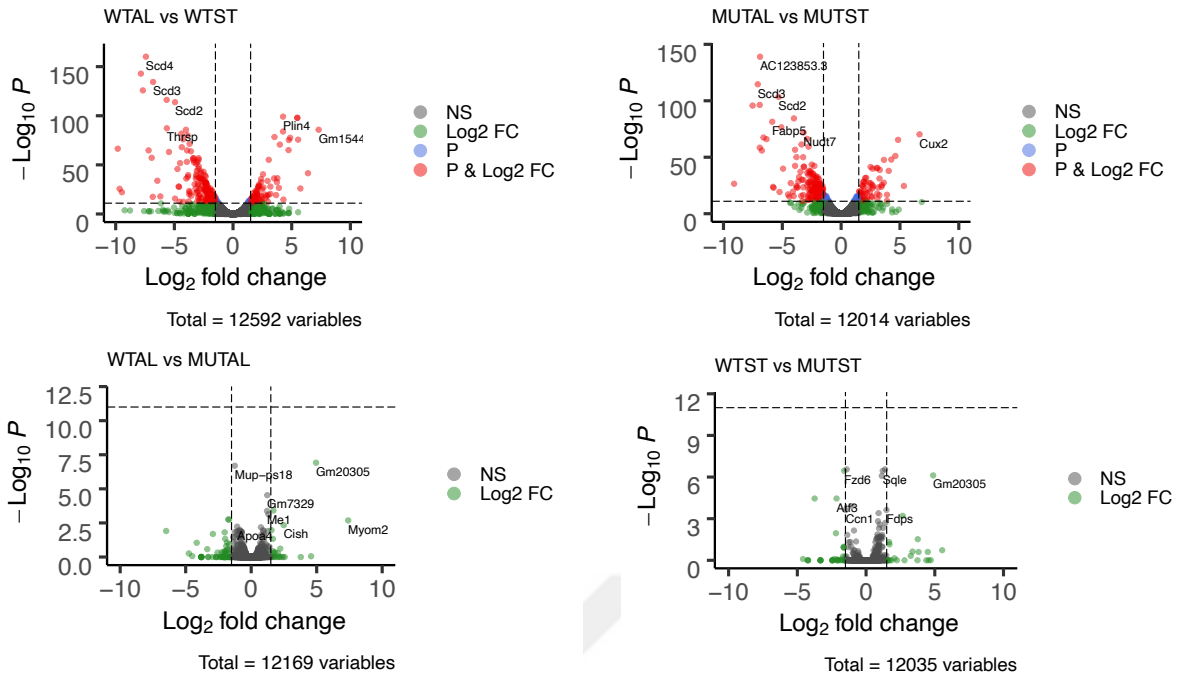


Figure 39: Volcano plot representing gene expression levels according to their P value and Log_2 fold change

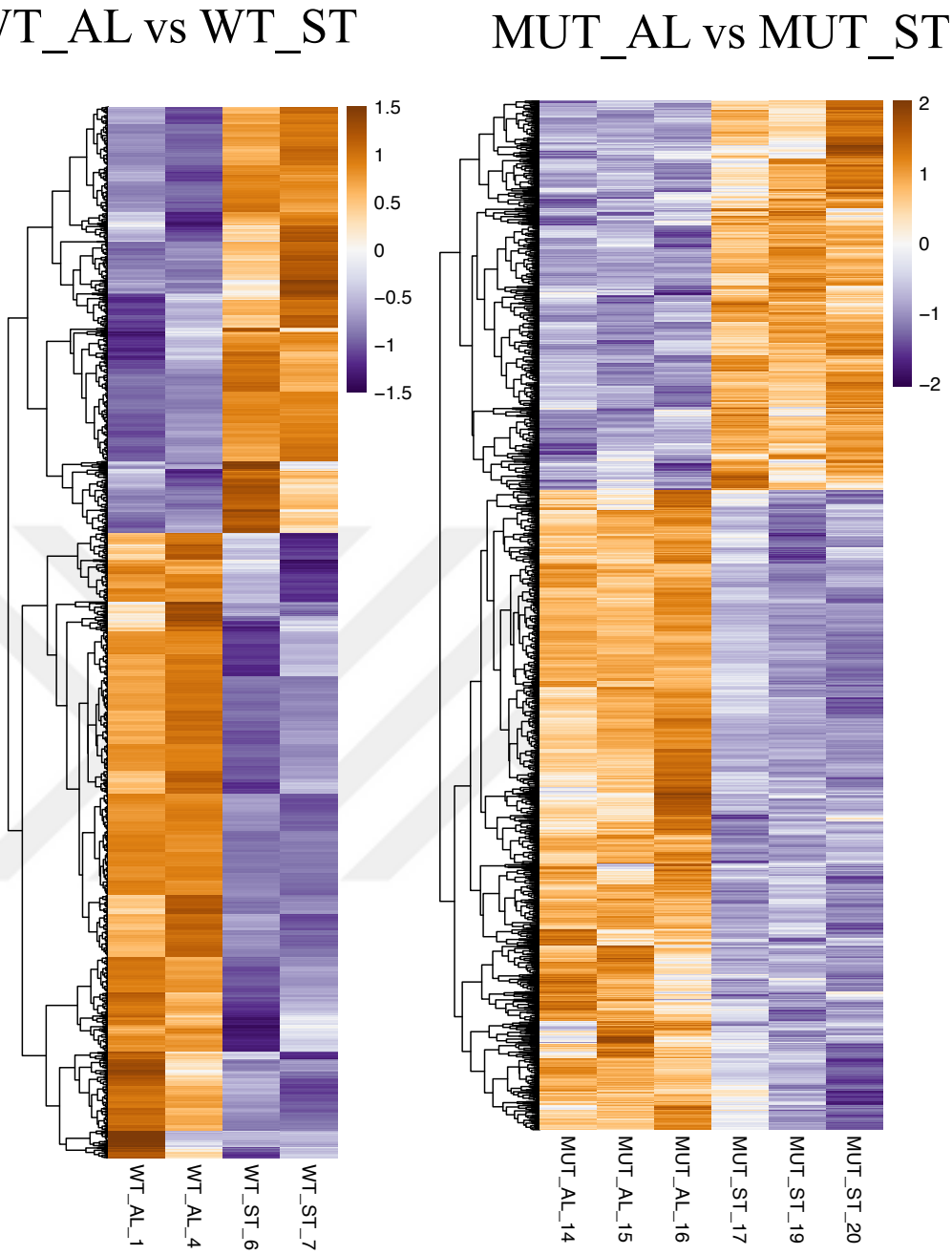
All four experimental groups were used to generate volcano scatter plot as written in the graph headings. Negative Log10 of P values are plotted against fold change (Log2). The grey dots located within two dashed lines perpendicular to each other shows insignificant results.

As shown in Figure 39, *ad libitum* and starvation groups showed the highest level of variance between groups as evidenced by the high number of genes which are significantly changed over two folds. However, wild type versus mutant samples both in ad libitum and starvation showed only few numbers of genes which are significantly altered. Generally speaking, this result indicates that gene expression profile of liver is dramatically altered when organism undergoes starvation as long as 36 hours, while it is not affected similar levels by the absence of *Fam134b*$^{-/-}$.

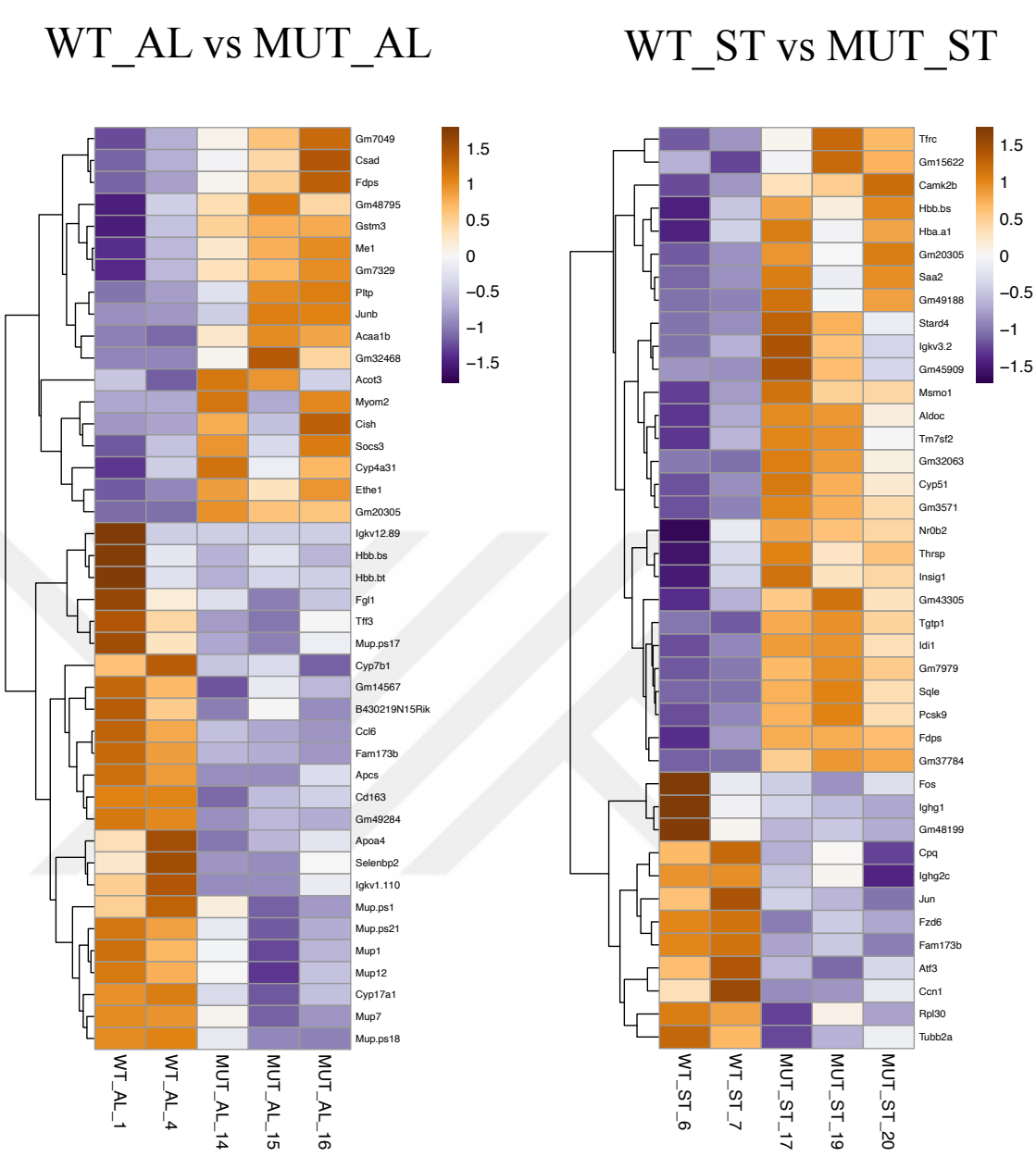
In order to compare expression profiles of experimental groups at gene level, first we excluded the genes which show False Discovery Rate values higher than 0.05, and fold changes below 1.6-fold which corresponds to ($Log_2$0.7). This finalized table was analyzed by hierarchical clustering and plotted as a heat map (Figure 40).

A

.


WT_AL vs WT_ST
MUT_AL vs MUT_ST
1.5
1
0.5
0
−0.5
−1
−1.5
2
1
0
−1
−2
WT_AL_1
WT_AL_4
WT_ST_6
WT_ST_7
MUT_AL_14
MUT_AL_15
MUT_AL_16
MUT_ST_17
MUT_ST_19
MUT_ST_20

B.


WT_AL vs MUT_AL
WT_ST vs MUT_ST
Gm7049
Csad
Fdps
Gm48795
Gstm3
Me1
Gm7329
Pltp
Junb
Acaa1b
Gm32468
Acot3
Myom2
Cish
Socs3
Cyp4a31
Ethe1
Gm20305
Igkv12.89
Hbb.bs
Hbb.bt
Fgl1
Tff3
Mup.ps17
Cyp7b1
Gm14567
B430219N15Rik
Ccl6
Fam173b
Apcs
Cd163
Gm49284
Apoa4
Selenbp2
Igkv1.110
Mup.ps1
Mup.ps21
Mup1
Mup12
Cyp17a1
Mup7
Mup.ps18
1.5
1
0.5
0
−0.5
−1
−1.5
WT_AL_1
WT_AL_4
MUT_AL_14
MUT_AL_15
MUT_AL_16
Tfrc
Gm15622
Camk2b
Hbb.bs
Hba.a1
Gm20305
Saa2
Gm49188
Stard4
Igkv3.2
Gm45909
Msmo1
Aldoc
Tm7sf2
Gm32063
Cyp51
Gm3571
Nr0b2
Thrsp
Insig1
Gm43305
Tgtp1
Idi1
Gm7979
Sqle
Pcsk9
Fdps
Gm37784
Fos
Ighg1
Gm48199
Cpq
Ighg2c
Jun
Fzd6
Fam173b
Atf3
Ccn1
Rpl30
Tubb2a
1.5
1
0.5
0
−0.5
−1
−1.5
WT_ST_6
WT_ST_7
MUT_ST_17
MUT_ST_19
MUT_ST_20

C.

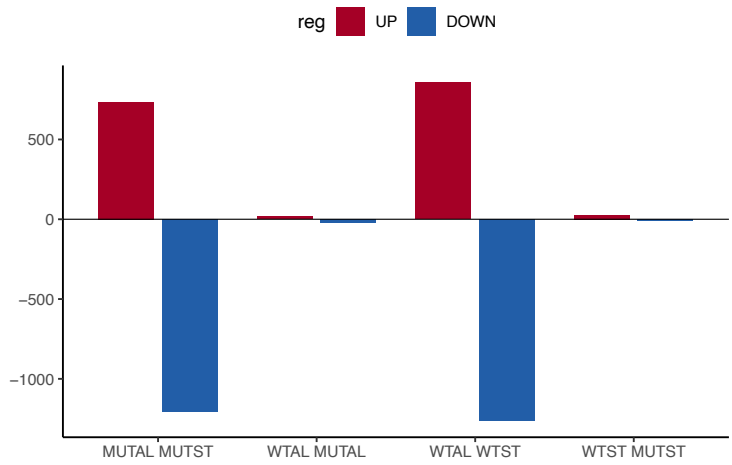


Figure 40: Absence of *Fam134b*$^{-/-}$ leads to alteration gene expression in both *ad libitum* and starvation groups

Gene expression analyses of ad libitum versus starvation samples (A) and wild type versus mutant samples (B) made by hierarchical clustering demonstrated as heat map. C. Bar graph of significantly altered genes remain within the criteria: False Discovery Rate (FDR)<0.05 and $Log_{2(}$Fold Change)> 0.7. In WT_AL vs MUT_AL (42) and WT_ST vs MUT_ST(39), gene names are indicated. Since there is high number of genes in WT_AL vs WT_ST (1700) and MUT_AL and MUT_ST (1500), no gene name is indicated on the side of the heat map. The gene names started with prefix "Gm-" are predicted genes and the ones end with suffix "-ps" are pseudogenes.

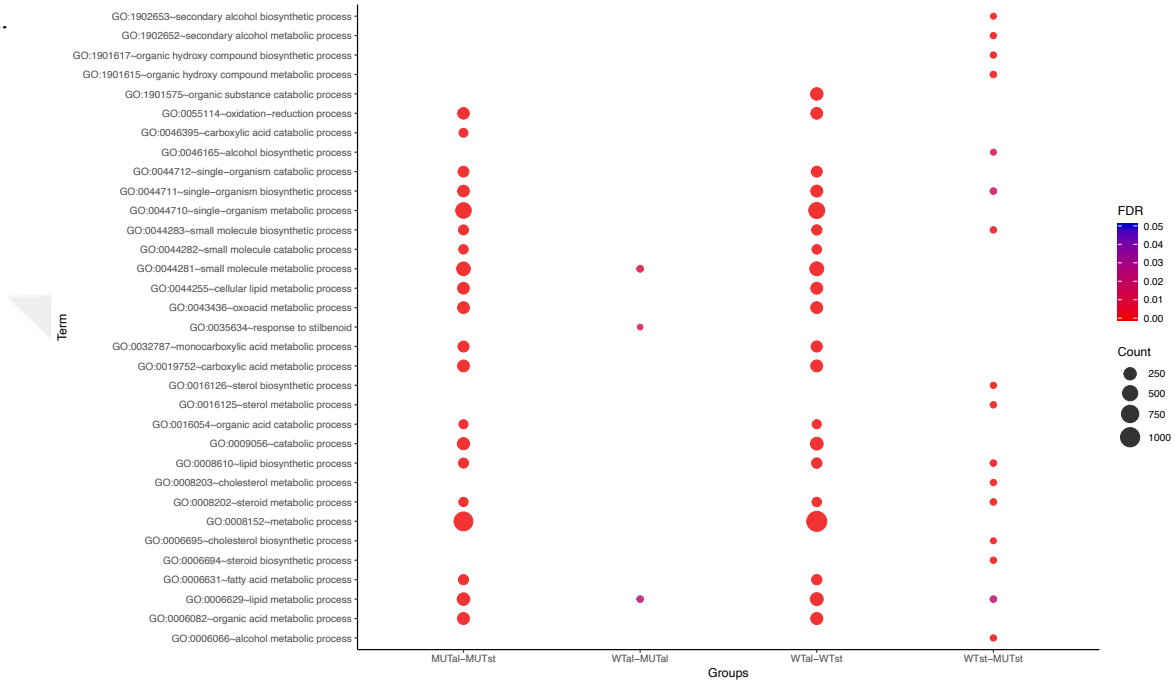
In support of previous results, *ad libitum* versus starvation exhibited differentially expressed more than 1700 genes in wild type samples (WT_AL vs WT_ST) and more than 1500 genes in mutant samples (MUT_AL vs MUT_ST) (Figure 40, A). However, altered gene number in genotypically analyzed samples were lower since in *ad libitum* samples (WT_AL vs WT_MUT) there were 42 genes and in starvation samples (WT_ST vs MUT_ST) there were only 39 genes. This difference was also clearly shown by cumulative data of significantly up- or down regulated genes plotted as bar graph (Figure 40, B).

Although there was a handful of genes, *Fam134b* absence resulted in significant differences in both *ad libitum* and starvation samples. At a first glance, the genes such as *fdps*, *Apoa4* in *ad libitum* group, and *pcsk9*, *sqle* and *fdps* in starved group shows that the expressional differences are likely to be relevant for cholesterol and lipid metabolism. However, obtaining

meaningful results from RNA sequencing data requires further functional clustering and annotation of selected genes.

Next, we submitted filtered gene groups to gene ontology and KEGG pathway database to functionally group genes.

A.



B.

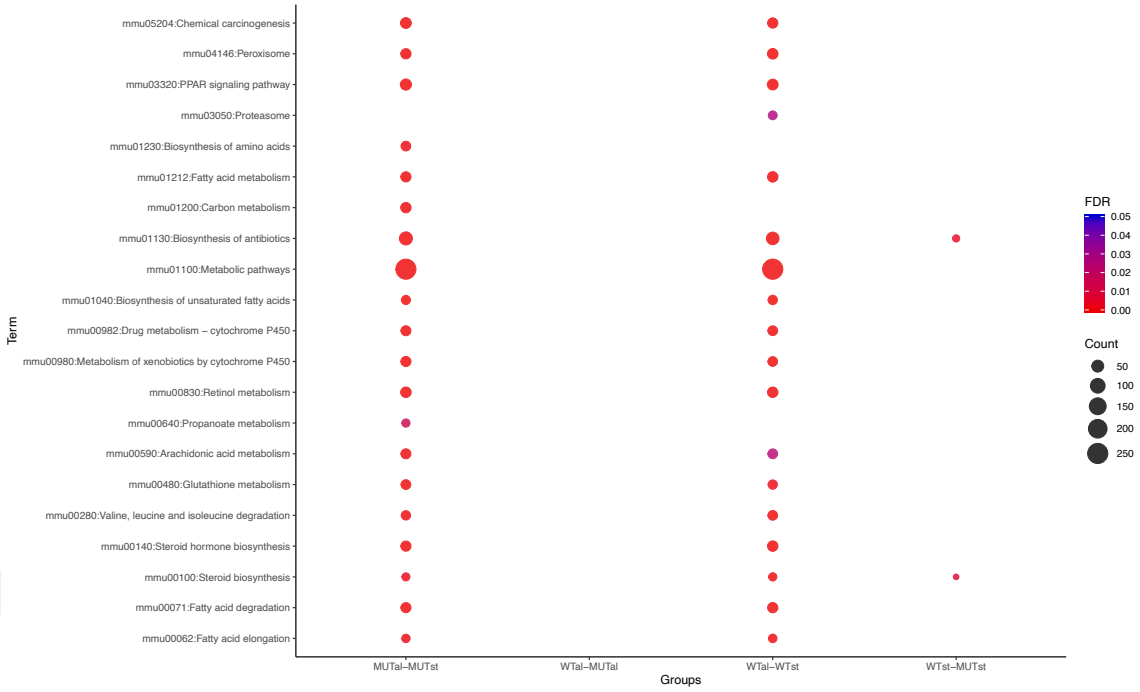


Figure 41: Absence of *Fam134b* alters expression of genes involved in lipid and cholesterol synthesis

Starvation responses in both wild type and mutant group robustly activated genes which are clustered in metabolic, catabolic and biosynthetic processes and pathways. *Fam134b* mutation on the other hand resulted in more limited numbers of functional clusters (Figure 41). Interestingly, in starvation conditions, there were more functional groups as shown by both gene ontology and KEGG pathway.

In gene ontology analyses, a subgroup of gene in WT_AL vs MUT_AL consisted of *Apoa4*, *Me1*, *Cyp7b1*, *Cyp17a1*, *Mup1*, *Csad*, *Fdps*, *Fgl1*, *Acaa1b*, *Pltp*, *Mup12*, *Acot3* are clustered in GO terms such as small molecule catabolic process, response to stilbenoids and lipid metabolic process (FDR<0.05). We failed to obtain any clusters of WT_AL vs MUT_AL group in KEGG pathway (FDR<0.05). On the other hand, WT_ST vs MUT_ST yielded a list of Gene Ontology clusters mostly represented by a gene list composed of *Tm7sf2, Cyp51, Stard4, Msmo1, Sqle, Insig1, Fdps, Pcsk9, Idi1*. The most prominent clusters were cholesterol and sterol-based processes, alcohol metabolic processes (process that end up with alcholol molecule production) and small molecular metabolic processes.

These data strongly suggest that the absence of *Fam134b* transcriptionally regulates the expression of genes which are involved in synthesis and bioprocess of molecules involved in energy regulation, such as lipids.

FAM134B RESPONSE TO ER-STRESS

4.21 Effects of ectopic FAM134B-1 expression upon Thapsigargin mediated ER-stress

The well-defined attribute of FAM134B as an ER-phagy receptor has urged us to hypothesize that FAM134B might also act as an ER-stress response gene by recycling ER fragments filled with unfolded proteins. Since all cellular activities were characterized in detail for FAM134B-1 we focused on this isoform during ER-stress experiments.

At initial experiments, we challenged inducible FAM134B-1 expressing HepG2 cells with a SERCA (ER calcium channel) blocker, Thapsigargin, which cause acute Calcium decrease in ER lumen but increase in cytosol [84]. Since most, if not all chaperones in ER lumen mediate their protein folding functions in the presence of Calcium, thapsigargin eventually causes Unfolded Protein Response (UPR). The HepG2-FAM134B-1 were induced with Doxycycline for 24 hours before and during the drug treatment. Cells were treated either with 10μM Thapsigargin for the indicated time points as two groups: 2,4 and 8 hours; 16 and 24 hours. The thapsigargin doses used in these experiments were taken from our previous studies[7,49,50]. DMSO treatment for 8 hours and 24 hours were used as negative controls. We performed a western blot experiment using total protein lysates (Figure 42, A).

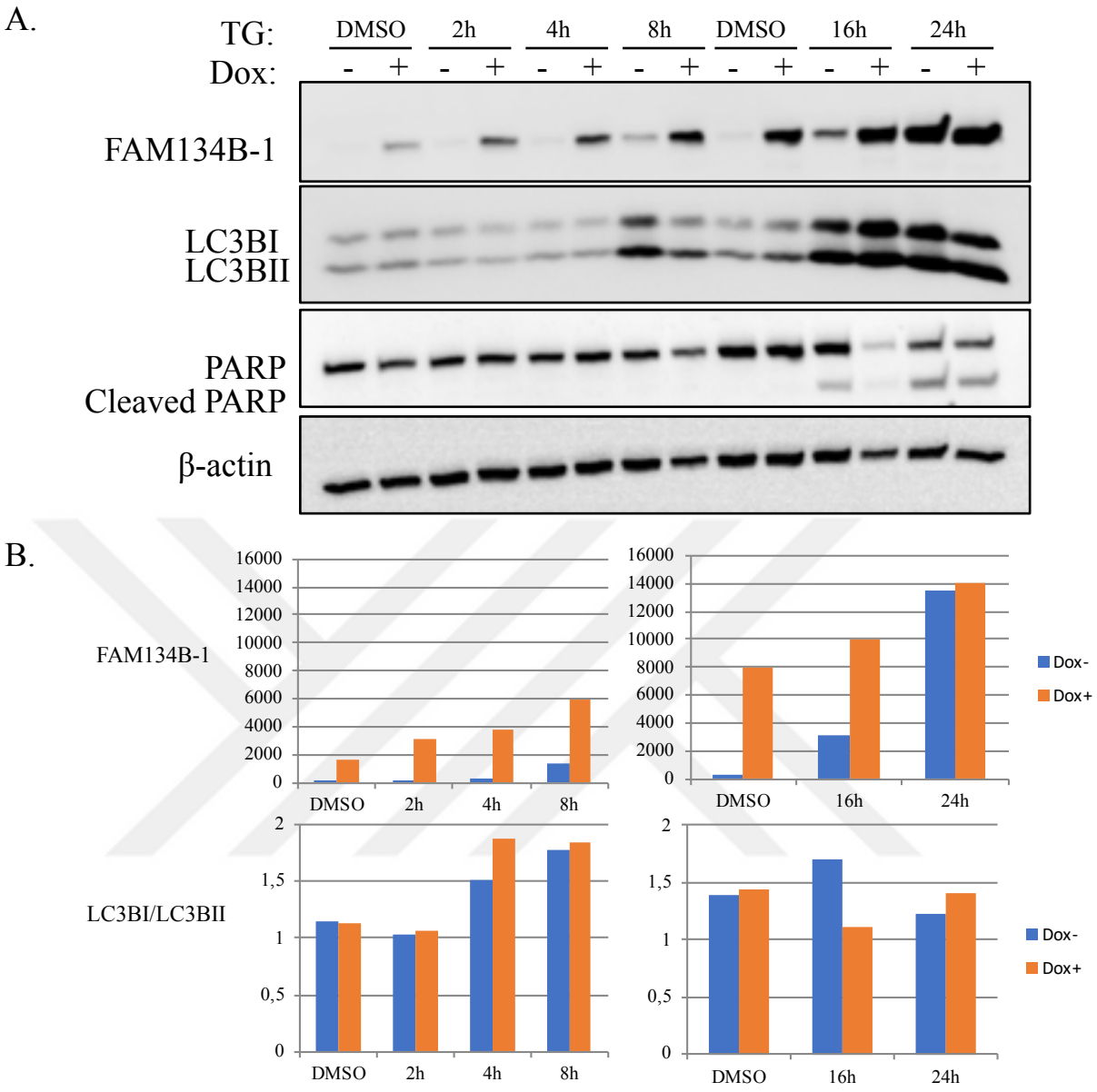


Figure 42: Thapsigargin treatment causes further accumulation of ectopically expressed FAM134B-1

A. western blot images of FAM134B-1 over-expressing HepG2 cells challenged with 10µM Thapsigargin (TG). B. Quantification of the western blot results. The Y axis in FAM134B-1 represents arbitrary units. Short- and long-term TG treatment conditions were set in two different experiments.

As seen in Figure 42, induced FAM134B-1 gradually accumulates in cell, which is visible as early as 2 hours. In addition, Dox- cells also start to accumulate FAM134B-1 starting from 8h, reaching peak level at 24h with nearly the same expression of 24h Dox+.

LC3BII/LC3BI ratios were upregulated upon thapsigargin treatment starting from 4 hours. Although, ratios did not change from this point, both LC3BI and LC3BII accumulation was noteworthy in 8h, 16h and 24h. Presence or absence of FAM134B did not dramatically affect LC3BII/LC3BI ratios in all groups; however, LC3BI and LC3BII protein levels were visibly lower in Dox+ group treated for 8 hours. This notion could not be observed in 16h and 24h (Figure 42, B).

Poly(ADP-ribose) polymerase (PARP) protein involves in vital cellular functions and its cleavage has long been used as an apoptosis marker [85]. Thapsigargin mediated apoptotic response became observable at 16 and 24 hours, as evidenced by cleaved PARP. However, we could not observe cleaved PARP in Dox+ cells at 16 hours.

When this experimental set up was repeated as seen in (Figure 43), Cleaved PARP appears at 16h and 24h in Dox- cells, but less visibly in Dox+ cells, which verifies the previous data (Figure 42). Furthermore, FAM134B-1 accumulation over time is also verified in both Dox- and Dox+.

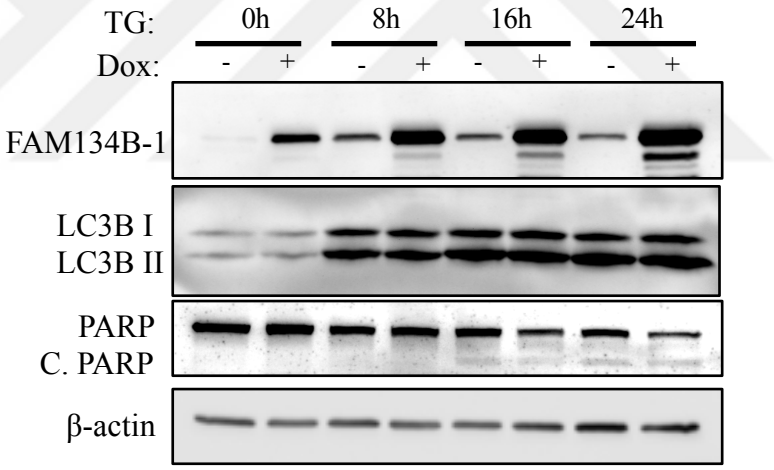


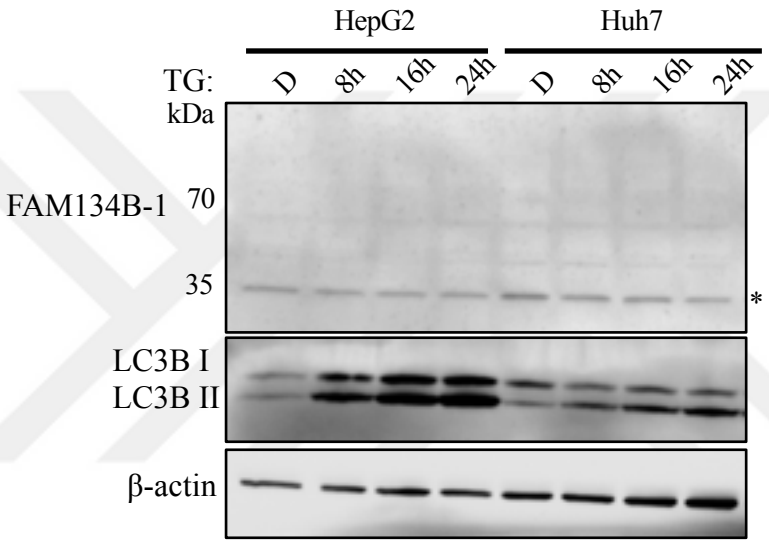
Figure 43: Accumulation of ectopically expressed FAM134B-1 was further verified in follow-up experiment.

These results have indicated that, Thapsigargin induces FAM134B-1 accumulation in cells especially when the protein is ectopically expressed. Increased levels of both LC3BI and LC3BII levels as well as LC3BII/LC3BI ratio clearly shows that Thapsigargin induces autophagy regardless of FAM134B-1 levels. In addition, presence of FAM134B-1 help cells cope with Thapsigargin induced apoptosis as long as 16 hours but fails to do so at 24 hours.

4.22 Thapsigargin fails to stimulate endogenous FAM134B expression in epithelial-like cells

Thapsigargin induced FAM134B-1 increase even in Dox- conditions has made us hypothesize that Thapsigargin alone might induce FAM134B induction in ancestral HepG2 cells which do not endogenously express FAM134B. To test this, we induced ancestral HepG2 cells and another FAM134B negative cell line Huh7 with Thapsigargin for 8, 16 and 24 hours.

A.



B.

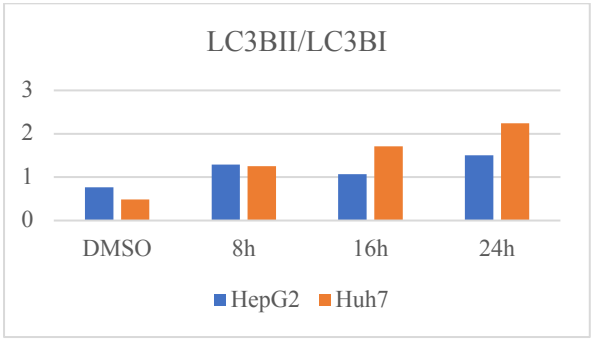


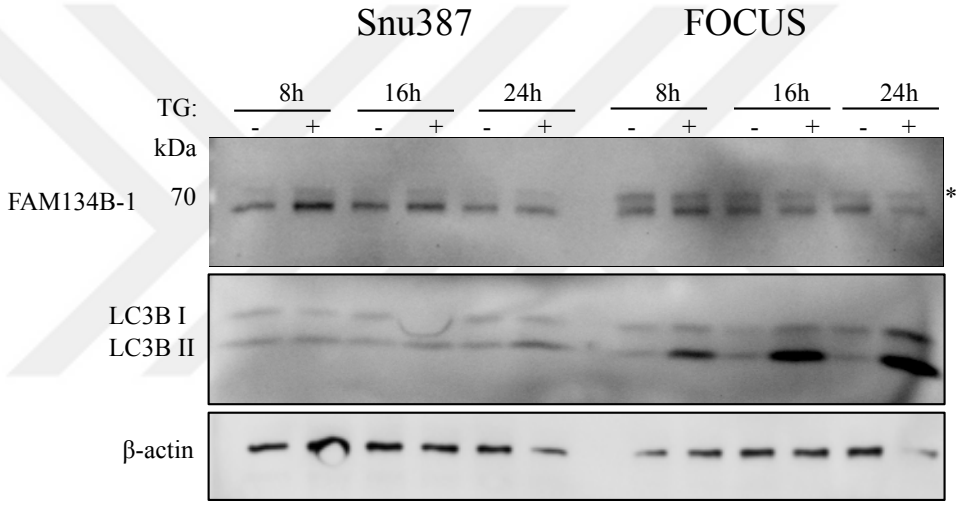
Figure 44: Thapsigargin treatment of ancestral cell lines with little or no FAM134B expression.

A. HepG2 and Huh7 cells were treated with 10µg and 2µg Thapsigargin respectively. The doses were determined based on the previous studies performed by our group. B. Quantification of LC3B bands using Image J software. D, DMSO.

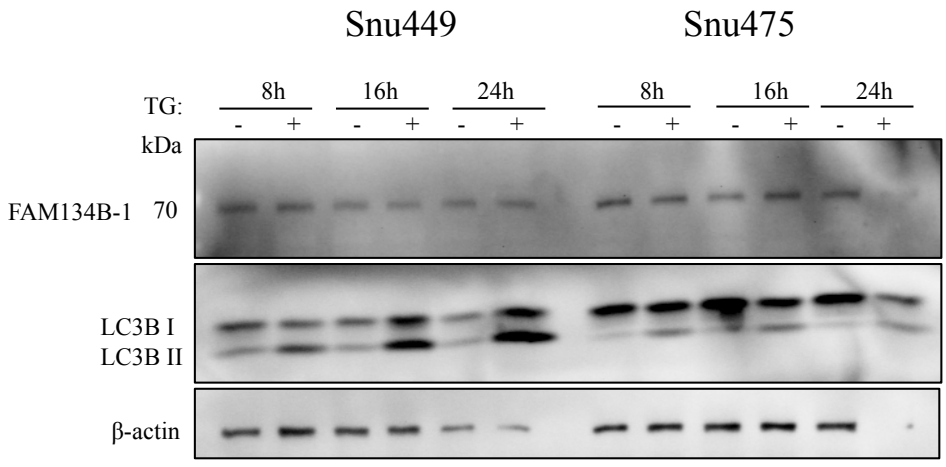
Thapsigargin treatment induced the accumulation of LC3BII and LC3BI as well as an increase in the ratio of LC3BII/LCBI in both HepG2 and Huh7. On the other hand, there was no FAM134B-1 levels increasing at any time point. This clearly shows that Thapsigargin cannot induce the protein expression of FAM134B in cell lines that do not endogenously expressing the protein (Figure 44).

Of course, these data raised the question how endogenous FAM134B is affected by thapsigargin treatment. Therefore, we tested the effect of thapsigargin on four different cell lines endogenously expressing FAM134B-1 (Figure 45).

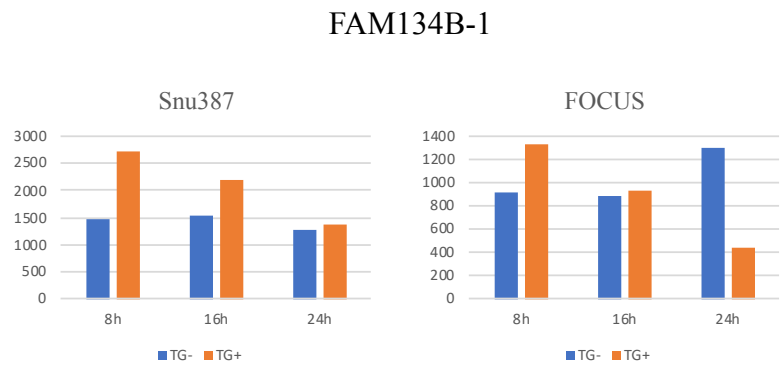
A.



B.



C.



D.

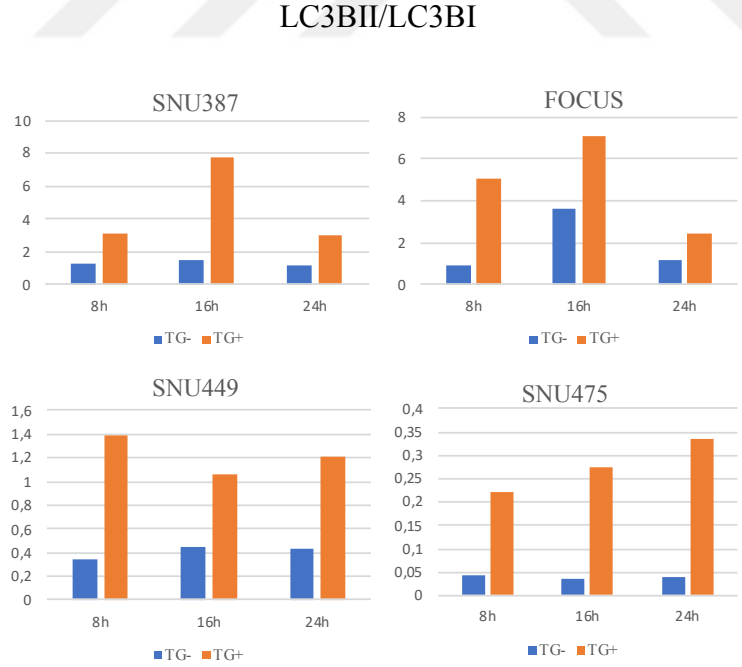


Figure 45: Thapsigargin induces FAM134B-1 expression at early time points

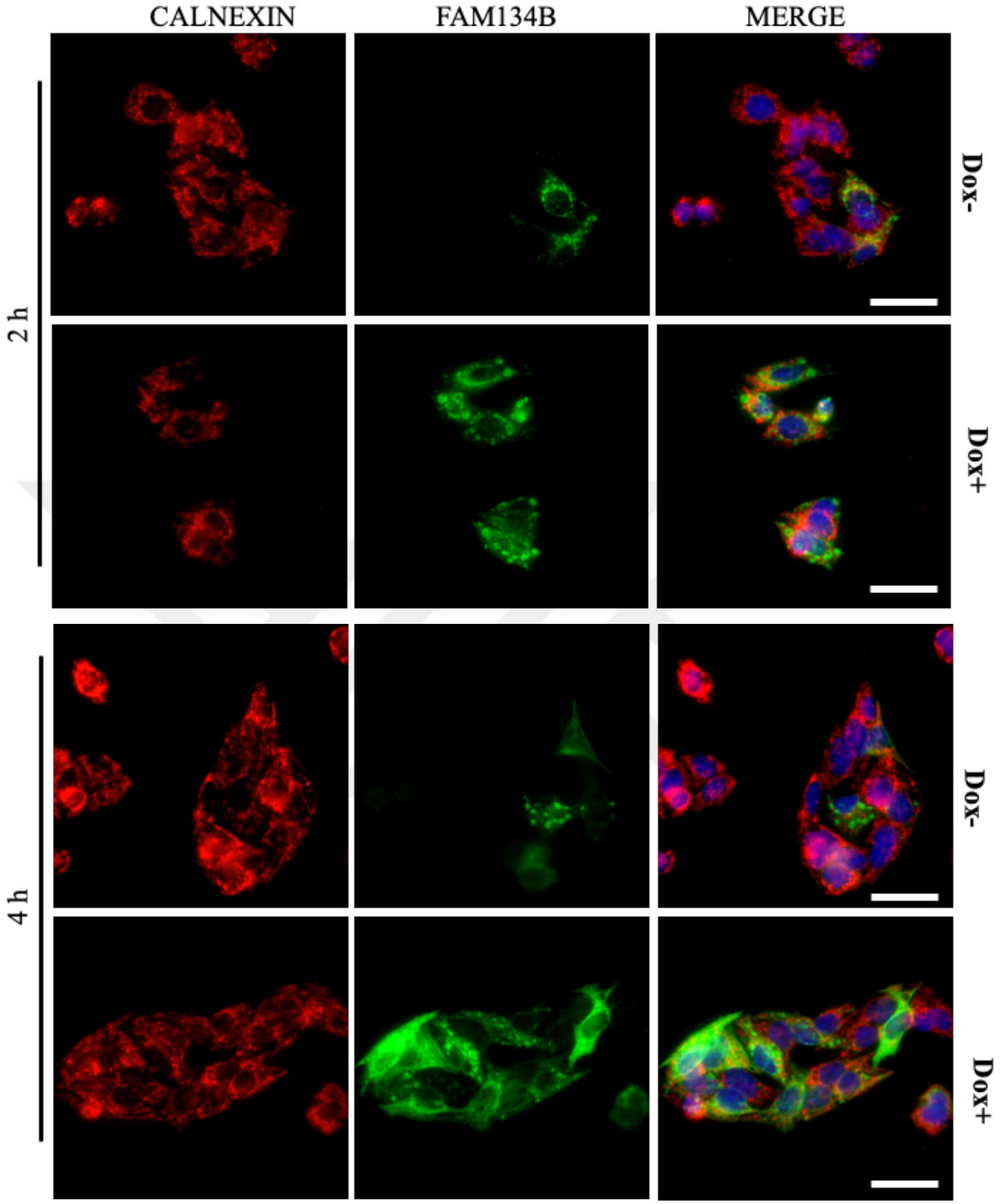
A. Snu387, FOCUS, Snu449 and Snu475 cells were either treated with 10μM Thapsigargin (TG) or DMSO for the indicated time periods. B. Densitometric quantification of endogenous FAM134B-1 levels in aforementioned cell lines. C. Densitometric quantification of LC3BII/LC3BI protein levels.

Similar to the cells with or without ectopically expressed FAM134B, both LC3B levels and LC3BII/LC3BI ratios were increased upon Thapsigargin treatment in Snu387, FOCUS, Snu449 and Snu475 cell lines, indicating the activation of autophagy (Figure 45, A, B and D). The most striking results were obtained with FAM134B-1 levels, since its increase is apparently stimulated at 8 hours as a response to Thapsigargin in Snu387, FOCUS and Snu449 cells (Figure 45, A, B and C). As the treatment prolong, however, FAM134B-1 levels gradually dropped for all cell lines and reached minimum at 24 hours, except Snu449.

Overall these data suggested that, Thapsigargin, an ER-stress inducer does not stimulate FAM134B-1 expression in cell lines without endogenous expression. However, its expression is enhanced in both endogenously and ectopically expressing cell lines as an early response. When treatment is prolonged, on the other hand, FAM134B-1 levels decrease in cell lines endogenously expressing FAM134B-1 but accumulates in ectopically expressed cell line.

4.23 Ectopically expressed FAM134B-1 accumulates in vesicles upon Thapsigargin treatment

Since FAM134B-1 localizes primarily in endoplasmic reticulum, accumulation of FAM134B-1 in both endogenously expressing and ectopically expressed cell lines upon thapsigargin induction at early time points has urged us to investigate this accumulation on cellular level. First, we have treated Dox inducible FAM134B-1 expressing HepG2 cells with 10μM thapsigargin for 2, 4 and 8 hours and performed immunofluorescent staining using FAM134B antibodies. In order to observe the changes in endoplasmic reticulum structure, we co-stained cells with Calnexin, an ER-chaperone (Figure 46).


CALNEXIN
FAM134B
MERGE
2 h
4 h
Dox-
Dox+
Dox-
Dox+

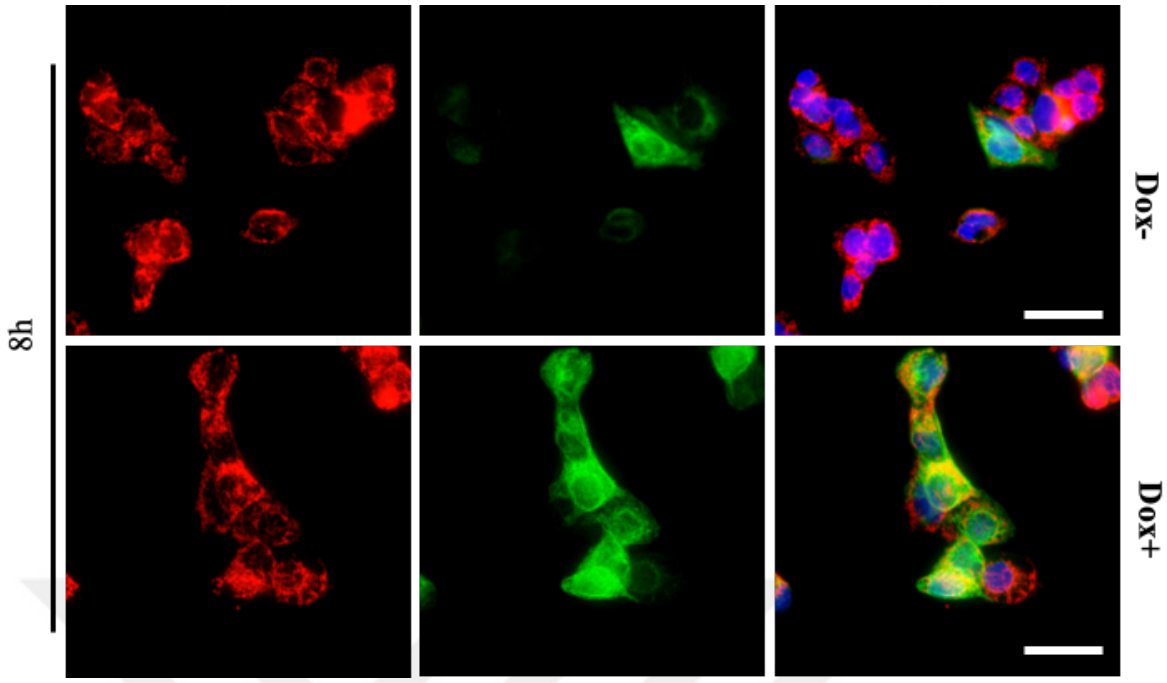


Figure 46: Time dependent accumulation of FAM134B-1 in HepG2-FAM134B-1 cells upon thapsigargin treatment

HepG2-FAM134B-1 cells were seeded on coverslips and induced with 1µM Doxycyclin for 24 hours, which is followed by 10µM thapsigargin treatment for the indicated time points and fixation of the cells by ice cold methanol, respectively. Scale bar represents 50µm.

Similar to the western blot results, after Thapsigargin treatment, FAM134B-1 levels increased over time in Dox + cells. Intriguingly, without getting diffused in the cell cytosol, FAM134B-1 staining started to accumulate as large vesicles (Figure 46) at as early as 2 hours. Despite low resolution in fluorescence imaging, it was visible that calnexin does not remarkably colocalize with FAM134B-1 on vesicles. As treatment period is prolonged (4h), cells with high FAM134B-1 signal density also increased, but without accumulation in vesicles. This cell type became dominant at 8h of treatment.

In order to verify the vesicular accumulation of FAM134B-1, we look closer to the 2h treatment of thapsigargin, where the vesicular formation occurs (Figure 47).

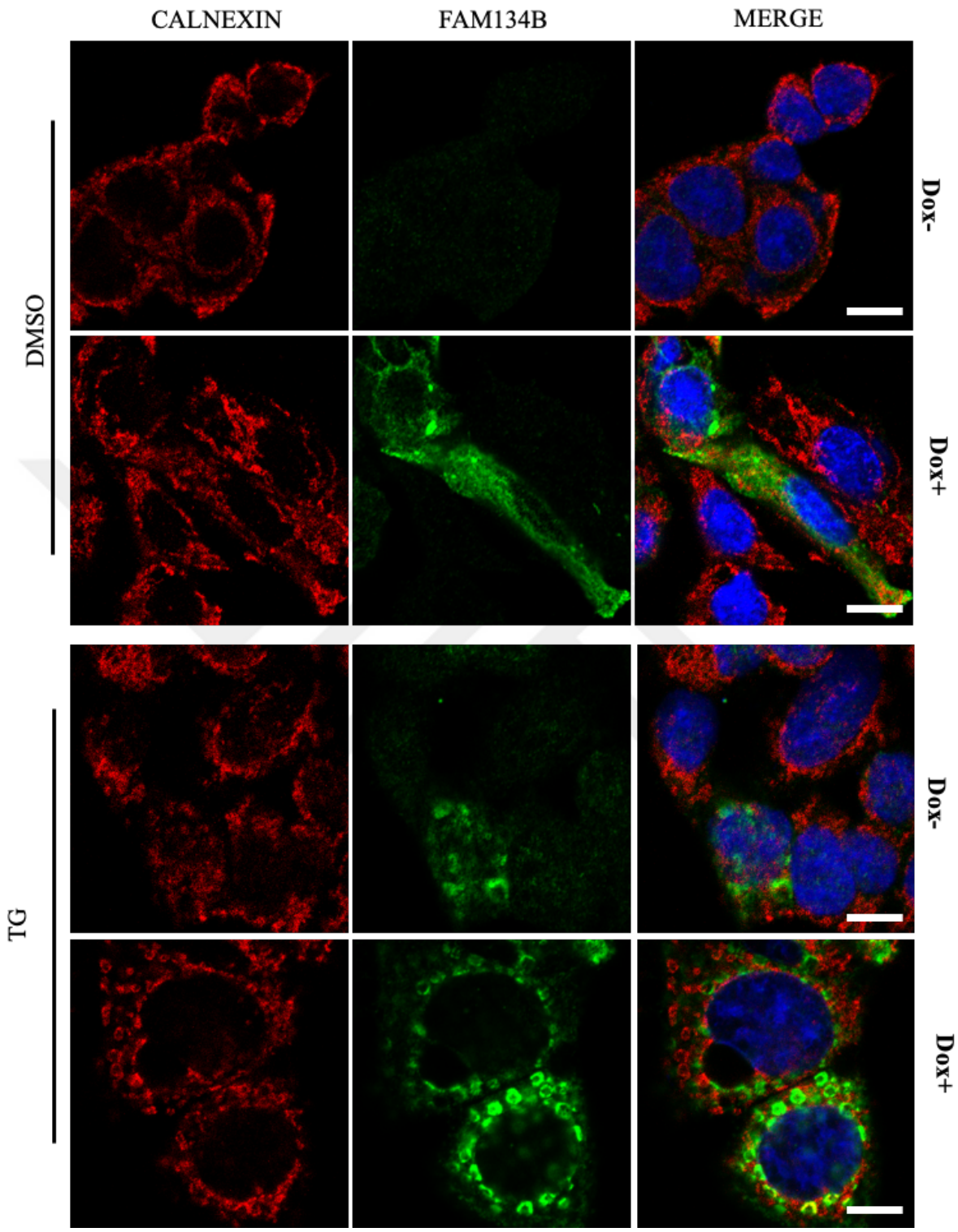


Figure 47: Vesicular accumulation of FAM134B-1 in HepG2-FAM134B-1 cells upon thapsigargin treatment

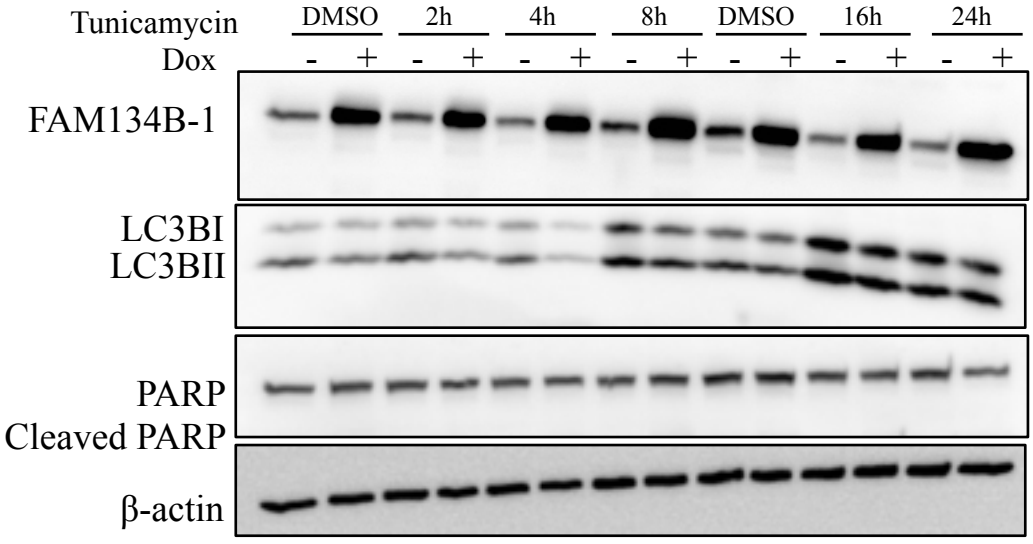
HepG2-FAM134B-1 cells were seeded on coverslips and induced with 1μM Doxycyclin for 24 hours, which is followed by either DMSO or 10μM thapsigargin treatment for 2 hours. The images were taken by confocal microscopy. Scale bar, 10μm.

Neither CNX nor FAM134B do not form any vesicular structures in DMSO group. On the other hand, 2h treatment of thapsigargin stimulated the formation of large FAM134B or CNX coated, mutually exclusive vesicles.

4.24 Ectopic FAM134B-1 expression alleviates Tunicamycin induced LC3B accumulation

Results obtained from Thapsigargin induced FAM134B-1 accumulation at different time points encouraged us to test another ER-stress inducing agent, Tunicamycin, which blocks N-linked glycosylation of ER-contained proteins, thereby causing ER-stress and unfolded protein response (UPR). We treated inducible HepG2 cells expressing FAM134B-1 with tunicamycin for 2, 4, 8, 16 and 24 hours. 24 hours prior to the tunicamycin treatment, cells were induced by 1μg/ml Doxycycline. Then, we performed western blot experiment to observe protein levels.

A.



B.

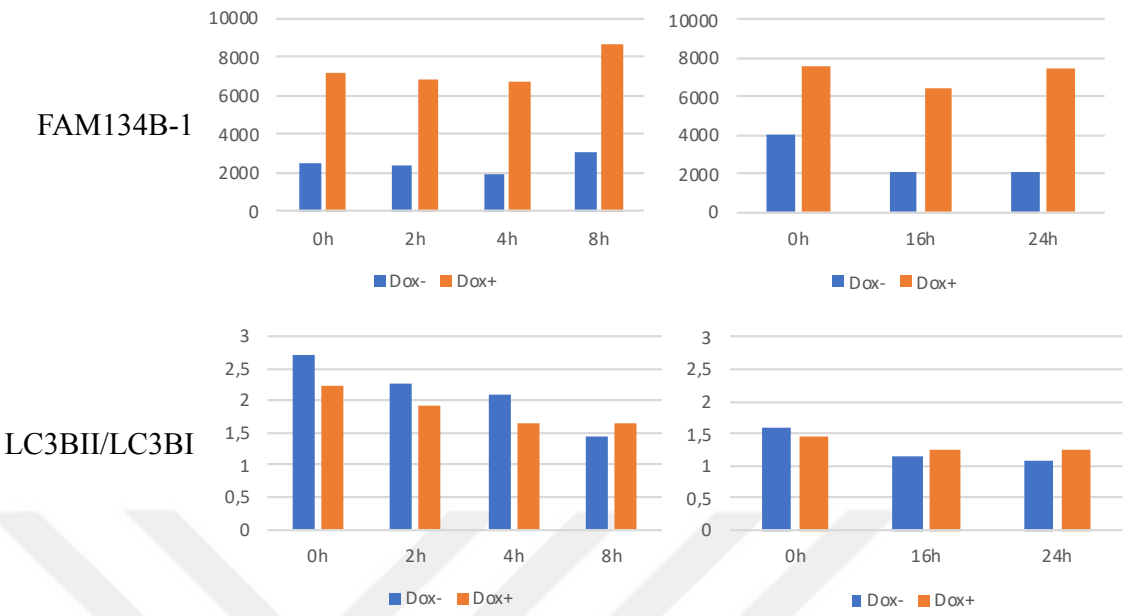


Figure 48: Expressional change of ectopically expressed FAM134B and LC3B upon treatment with Tunicamycin

A. Western blot images, B. densitometric analyses of both FAM134B and LC3BII/LC3BI ratio.

First of all, 10μM of tunicamycin treatment resulted in no apoptotic response, as demonstrated by the absence of cleaved PARP in treated cells. We also could not observe any dramatic accumulation of FAM134B-1 neither in Dox- or Dox+ groups. Interestingly, LC3BII/LC3BI ratios decreased gradually over time until 8 hours for both Dox- and Dox+ groups. Similar decrease was observed, but less remarkably, in 16- and 24-hour treatment. Strikingly, however, both LC3BI and LC3BII bands become weaker in Dox+ lanes, where FAM134B-1 is overexpressed, as long as 4 hours. This weakening of bands could not be observed at 8, 16 and 24 hours, where, in fact, both LC3B forms are strongly enhanced (Figure 48).

According to these results, FAM134B-1 overexpressed cells clearly prevented cells accumulating both LC3B forms as long as 4 hours but failed to do so after starting from 8 hours.

Based on these results, we also investigated the cellular localization of FAM134B-1 upon tunicamycin treatment using immunofluorescence method. HepG2-FAM134B-1 cells

were induced by 1µg/ml doxycycline 24h prior to 2h tunicamycin treatment, which is followed by staining with FAM134B-1 and CNX (Figure 49).

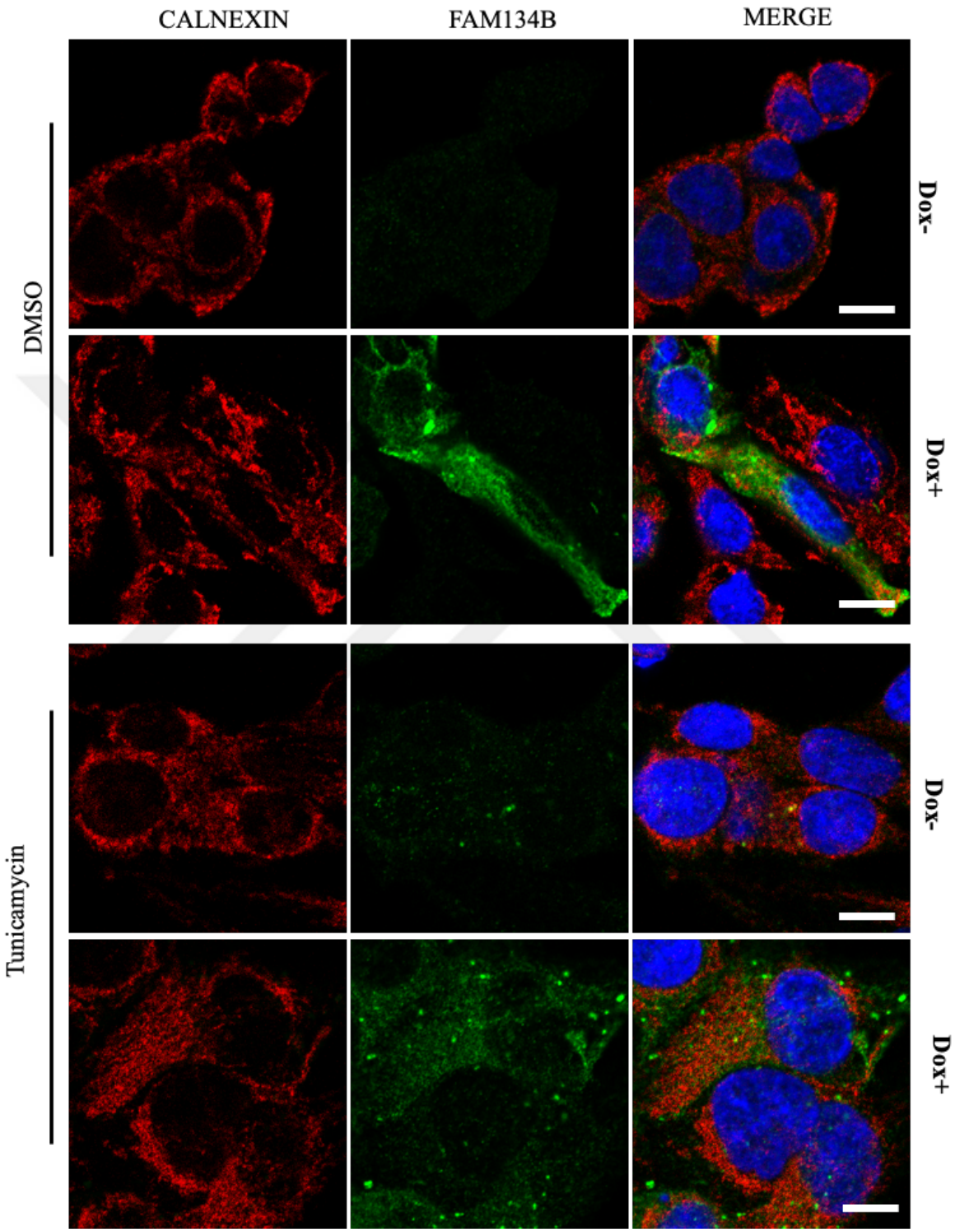


Figure 49: FAM134B-1 accumulates as punctae in response to Tunicamycin treatment

HepG2 cells were pre-treated with 1µg/ml doxycycline for 24 hours, and subjected to 10µM Tunicamycin treatment for 2 hours. Scale bar, 10µm.

Tunicamycin treatment induced accumulation FAM134B-1 containing punctae which was not co-stained with CNX.

Overall these results suggested that, in the presence of excessive FAM134B-1, Tunicamycin treatment does not fundamentally affect cellular death and the LC3BII/LC3BI ratio. On the other hand, overexpression of FAM134B-1 negatively affects accumulation of both LC3B forms as far as 4 hours, implying either a decreased preference on LC3B mediated autophagic pathway or relieved ER stress which do not enhance autophagy. Furthermore, Tunicamycin treatment do not cause an overall FAM134B-1 increase in protein level; but rather, it selectively induces formation of FAM134B-1 filled vesicles, in which Calnexin is excluded.

4.25 Tunicamycin enhances FAM134B-2 accumulation in liver

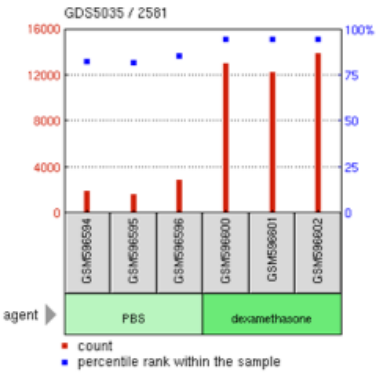
Lipid deposition in liver is affected by various factors including starvation, high caloric diet and by chemical insults. In light of our previous experiments, we hypothesized that other drugs that cause accumulation of lipids in liver might be directly associated with expressional alteration of *Fam134b* in mouse liver.

Being an ER-stress inducer, Tunicamycin is known to cause accumulation of lipid droplets in hepatocytes as a cellular response to chemical damage[86]. Another liver steatosis inducing agent is Dexamethasone, which is routinely utilized in clinics [8788]. In order to show association of these factors with *Fam134b* expression, we first analyzed publicly available Gene Expression Omnibus datasets. Previously published microarray analysis data of Dexamethasone treated animal livers showed that 2mg/kg treatment of Dexamethasone increases the FAM134B accumulation in both sexes of mice[89] (Figure 50, A).

Next, we tested both dexamethasone and tunicamycin in small number of animals in in order to observe possible changes in FAM134B levels. *Fam134b* heterozygous and wild type mice were treated either with 2mg/kg Dexamethasone or 1mg/kg Tunicamycin for 24 hours. Then, we performed western blot analyses on extracted liver samples.

A.

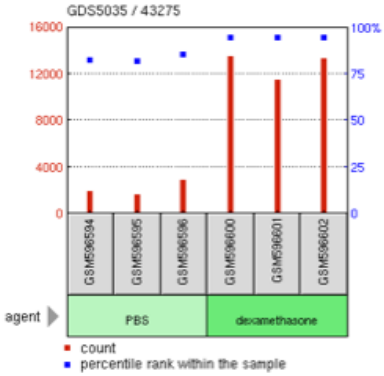
Profile GDS5035 / 2581
Title Glucocorticoid effect on the male liver
Organism Mus musculus



Graph caption help

Sample	Title	Value	Rank
GSM596594	Male PBS_rep1	1991.8	83
GSM596595	Male PBS_rep 2	1725.36	82
GSM596596	Male PBS_rep 3	2914.93	86
GSM596600	Male Dexamethasone 6 hr_rep 1	13089.9	95
GSM596601	Male Dexamethasone 6 hr_rep 2	12252.5	95
GSM596602	Male Dexamethasone 6 hr_rep 3	13964.2	95

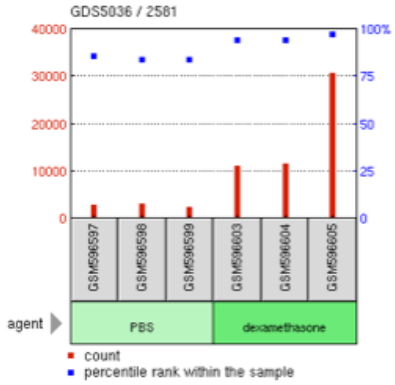
Profile GDS5035 / 43275
Title Glucocorticoid effect on the male liver
Organism Mus musculus



Graph caption help

Sample	Title	Value	Rank
GSM596594	Male PBS_rep1	1945.38	83
GSM596595	Male PBS_rep 2	1694.25	82
GSM596596	Male PBS_rep 3	2937.33	86
GSM596600	Male Dexamethasone 6 hr_rep 1	13569	95
GSM596601	Male Dexamethasone 6 hr_rep 2	11558.1	95
GSM596602	Male Dexamethasone 6 hr_rep 3	13357.4	95

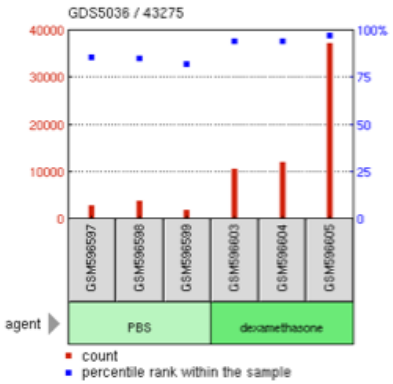
Profile GDS5036 / 2581
Title Glucocorticoid effect on the female liver
Organism Mus musculus



Graph caption help

Sample	Title	Value	Rank
GSM596597	Female PBS_rep 1	2935.15	86
GSM596598	Female PBS_rep 2	3294.9	84
GSM596599	Female PBS_rep3	2566	84
GSM596603	Female Dexamethasone 6 hr_rep 1	11091.9	94
GSM596604	Female Dexamethasone 6 hr_rep 2	11768.3	94
GSM596605	Female Dexamethasone 6 hr_rep 3	30831.6	97

Profile GDS5036 / 43275
Title Glucocorticoid effect on the female liver
Organism Mus musculus



Graph caption help

Sample	Title	Value	Rank
GSM596597	Female PBS_rep 1	2931.22	86
GSM596598	Female PBS_rep 2	3919.1	85
GSM596599	Female PBS_rep3	2094.53	82
GSM596603	Female Dexamethasone 6 hr_rep 1	10828.8	94
GSM596604	Female Dexamethasone 6 hr_rep 2	12115.1	94
GSM596605	Female Dexamethasone 6 hr_rep 3	37293	97

B.

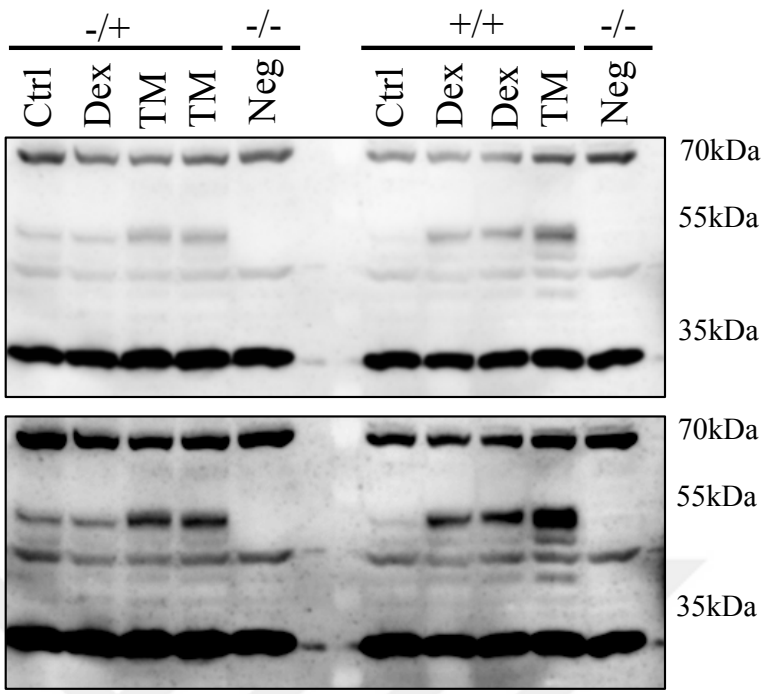


Figure 50: Effect of Tunicamycin and Dexamethasone on FAM134B-2 expression in liver.

A. Gene Expression Omnibus (GEO2) datasets showing male (top) and female (bottom) gene expression levels of mouse *Fam134b*. Figures in the left show FAM134B-1 while in the right show FAM134B-2. Red bars indicates relative mRNA expression of the gene. Heterozygous and homozygous wild type mice were treated with 1mg/kg tunicamycin and 2mg/kg dexamethasone. Ctrl, untreated control samples, TM, tunicamycin; Dex, dexamethasone; Neg, negative.

As seen in Figure 50, Tunicamycin stimulates FAM134B-2 protein expression in both heterozygous and wild type animals. Even though FAM134B-2 seems to be induced in response to Dexamethasone treatment in wild type samples, similar increase could not be observed in heterozygous samples. Of course, we cannot rule out the possibility that this contradiction is not a result of sample variability, since wild type control sample exhibited lower expression of FAM134B-2.

FAM134B IN CANCER

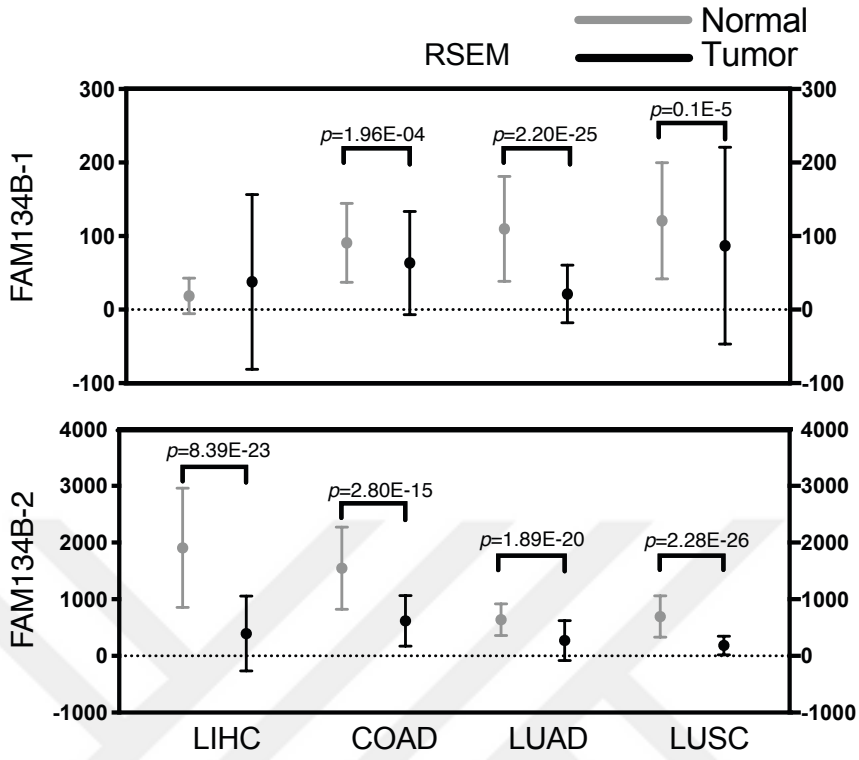
Early studies our group performed about FAM134B was mostly inspired by the results received from liver cancer[6], where FAM134B is significantly decreased during the course of

carcinogenesis. In the light of our experimental results from our previous studies and the results described above, we tried to further delineate the role of FAM134B and its variants in cancer.

4.26 *FAM134B* expression is altered during carcinogenesis

Our previous data demonstrating the relationship between liver cancer and *FAM134B* was generated by microarray studies. Although these data yielded critical data indicating possible tumor suppressor role of *FAM134B*, microarray studies usually may not specifically cover all transcript variants. Hence, we sought ways to analyze relevance of FAM134B variants not only in HCC but also in other cancer types. The Cancer Genome Atlas (TCGA) is a massive database harboring RNA sequencing data of various human cancer types; and, these data are represented in TCGA Splicing Variants Database (TSVdb) as transcript variants[81]. Using TSVdb, we first screened FAM134B expression in different cancer types at transcript variant level (Figure 51).

A.



B.

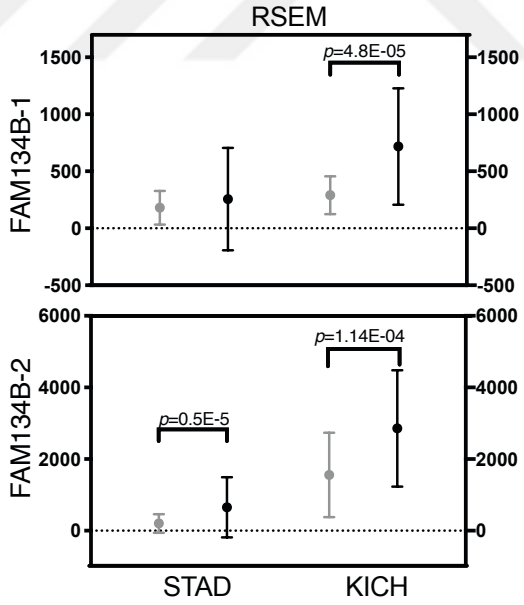


Figure 51: *FAM134B* is dramatically decreased in major human cancers

A. Dot whisker plot representing the expression of FAM134B isoforms in different cancers. LIHC, Liver Hepatocellular Carcinoma; COAD, Colon Adenocarcinoma; LUAD, Lung Adenocarcinoma; LUSC, Lung Squamous Carcinoma. B. Cancer types with increased expression of FAM134B isoforms: STAD, Stomach adenocarcinoma; KICH, Kidney

Chromophobe. Y axis represents transcript values as Transcript Per Million (TPM). $p<0.01$ accepted as significant.

The results have shown that low levels of *FAM134B-1* is expressed in non-tumor tissues, three of which decrease significantly in tumors, including Colon, Lung Adenocarcinoma and Lung Squamous carcinoma (Figure 51, A). These tissues, on the other hand, express stronger *FAM134B-2* expression at basal levels, which significantly decrease in tumors. On the contrary, Stomach Adenocarcinoma and kidney chromophobe (KICH) exhibited increased *FAM134B-2* levels in tumors. *FAM134B-1* was also increased in KICH but not in STAD tumors (Figure 51, B).

Concordant with our previous results, *FAM134B* is significantly decreased in Liver hepatocellular carcinoma but only as *FAM134B-2* isoform. Observing similar and opposite trends of expression in different cancers has clearly indicates that *FAM134B* expression is dynamically affected during the course of carcinogenesis.

4.27 *FAM134B* mRNA levels decrease during HCC development

In order to verify *in silico* data retrieved from public database we experimentally tested tissues from hepatocellular carcinoma patients. RNA extracted from non-tumor and tumor tissues were subjected to Reverse Transcriptase PCR using *FAM134B-1* and *FAM134B-2* specific primers. Only three non-tumor samples were retrieved from healthy livers, while the rest was taken from cirrhotic tissues.

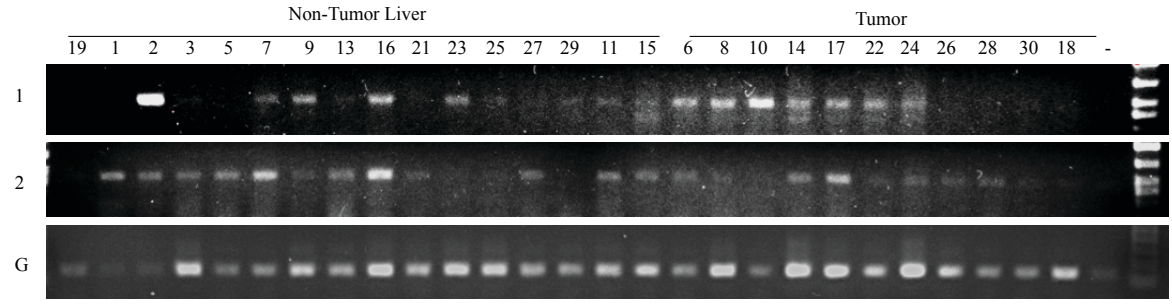


Figure 52: *FAM134B* isoform expressions of human hepatocellular carcinoma tissues shown by Reverse Transcriptase PCR.

Non-tumor and tumor liver tissues screened for the presence of *FAM134B* isoforms. Samples 1, 2 and 3 are taken from healthy liver. Samples numbered as 5 and 6; 7 and 8; 9 and 10; 13

and 14; 16 and 17; 21 and 22; 23 and 24; 25 and 26; 27 and 28; 29 and 30 are taken as pairs from non-tumor and tumor tissues, respectively. Numbers at the left side of the gel image represent isoforms: 1, *FAM134B-1*; 2, *FAM134B-2*. G, *GAPDH.*

As seen in Figure 52, both non-tumor and tumor samples showed the expression of *FAM134B-1* and *FAM134B-2* at different levels. However, FAM134B-2 was clearly downregulated in tumor tissues as shown by both paired and un-paired samples.

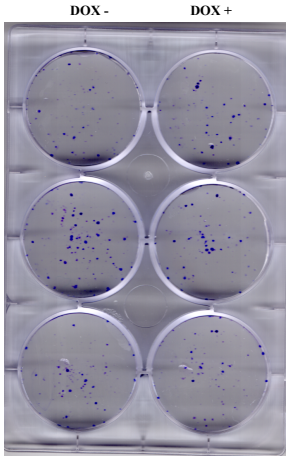
With this result, we supported the notion that during the liver carcinogenesis FAM134B-2 is tend to be suppressed indicating a potential role as tumor suppressor in liver cancer.

4.28 Effect of FAM134B ectopic expression on cell proliferation

The significant decrease of FAM134B not only in liver but also several other tumor types represents an important implication that the ectopic expression of FAM134B (and variants) would conversely affect tumor cell proliferation. To address this issue, first we performed colony forming assay using HepG2-FAM134B-1 cells, because: 1-HepG2 cells normally do not express FAM134B of any form; 2-This cell lines tend to form better demarcated colonies, which ease colony counting.

Briefly, cells were seeded to 6 well plate as 100 cells/well and induced with doxycycline for 15 days, which is followed by Crystal Violet staining. Pictures of plates were than taken and colonies were automatically counted by cell counter property of ImageJ.

A.



B.

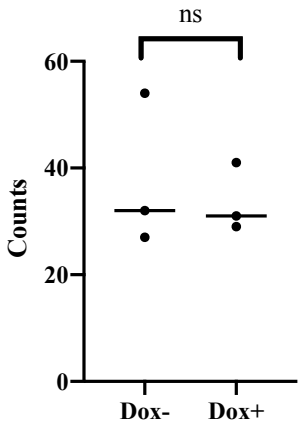


Figure 53: Colony formation assay of HepG2 cells inducible expressing FAM134B-1.

A. Picture of fixed and crystal violet stained HepG2 cells with or without 1µg/ml doxycycline. Each row represents the replicates of experiments. B. Plotting of colony counts statistically compared by student's t-test. ns, not significant.

The number of the colonies was not affected by presence of FAM134B-1, as seen in Figure 53, A.

Next, we screened and recalculated cell proliferation data of untreated control groups derived from other cell survival studies, which will be covered in following sections. We first statistically analyzed the SRB assay of HepG2-FAM134B-1 cells which were used to screen effect of various anti-cancer drugs and ER-stress inducers. The OD values of 24- and 72-hours proliferated cells without any drug treatment were statistically analyzed (Figure 54, B)

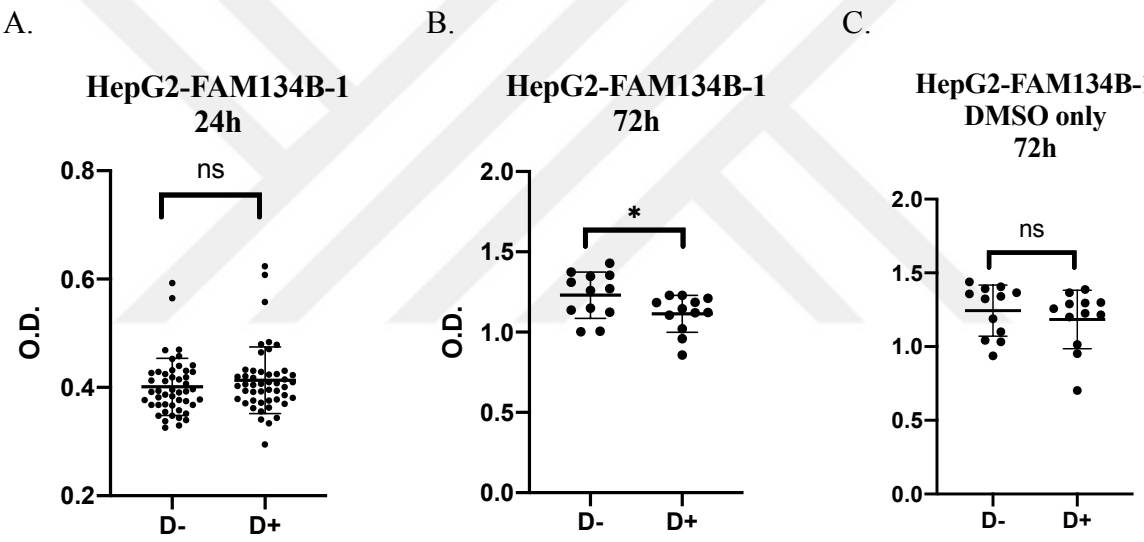


Figure 54: SRB experiments of HepG2-FAM134B-1 cells with or without doxycycline

A. HepG2-FAM134B-1 cells seeded in 96 well plate treated with doxycycline only for 24 hours. B. HepG2-FAM134B-1 cells seeded in 96 well plate treated with doxycycline only for 72 hours. C. HepG2-FAM134B-1 cells treated with DMSO only for 72 hours. Values were represented with mean and standard deviation. *, $p<0.05$; ns, not significant

The OD values shown that by 24 hours, cell density in both Dox- and Dox+ group does not statistically differ. However, cells which were not treated with any chemical shown that Dox+ group proliferated significantly less at 72h time point. The same drop could not be seen in DMSO-only treated group.

Next, we recalculated unchallenged inducible and stable Hep3B-FAM134B clones (Figure 55)

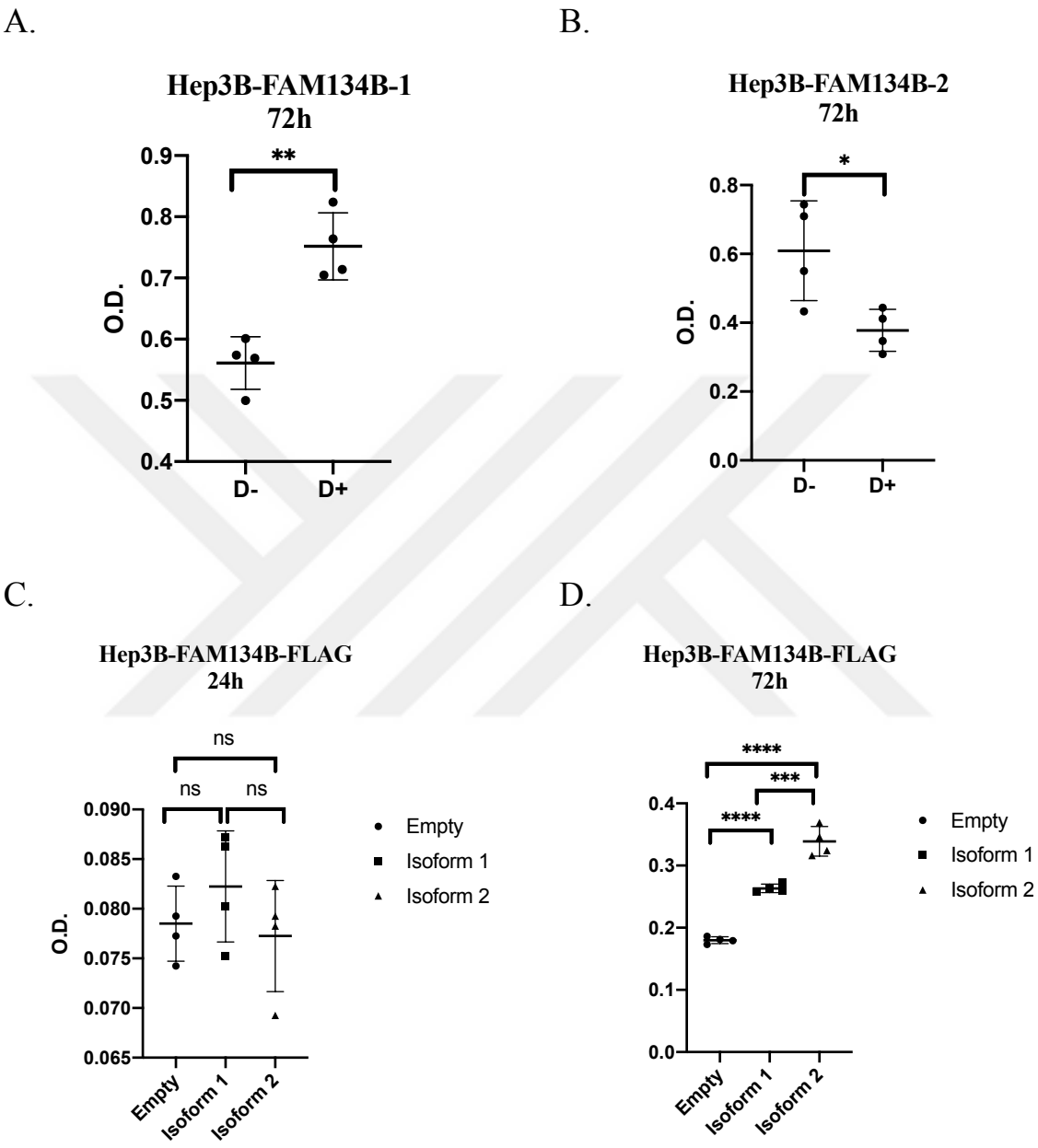


Figure 55: Ectopically expressed FAM134B isoforms *in vitro* caused contradicting proliferation rates in different systems

A. and B. Inducible FAM134B-1 and FAM134B-2 Hep3B cells seeded on 96 well plate were analyzed 72h after Dox induction without any drug treatment. C. and D. SRB assay of Hep3B cells proliferating for 24h and 72h. Cells stably express either FAM134B-1-FLAG or

FAM134B-2-FLAG, all of which are compared with empty vector transfected Hep3B cells. Values were represented with mean and standard deviation. *, $p<0.05$; **, $p<0.01$; ns, not significant

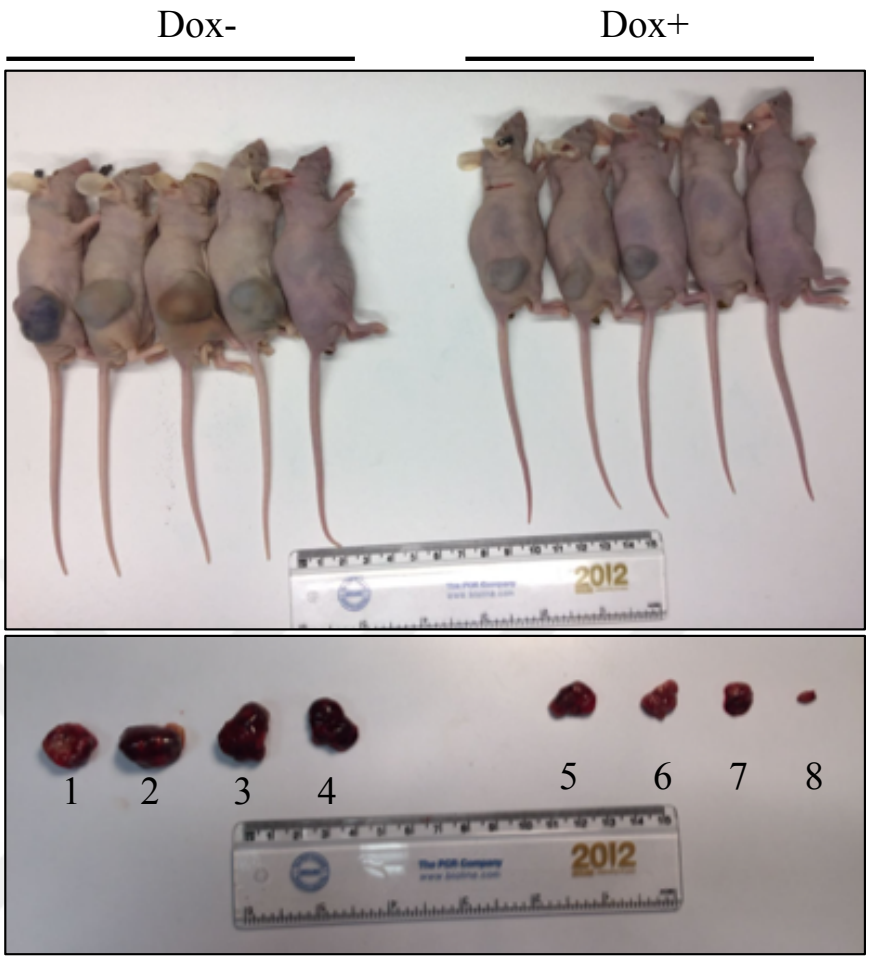
The results from inducible clones shown that FAM134B-1 presence favors cell proliferation at 72h, while FAM134B-2 induction inhibits cell proliferation at 72h (Figure 55). On the contrary, stable Hep3B-FAM134B-FLAG cells exhibited increased proliferation in both FAM134B-1 and FAM134B-2 cells compared to empty plasmid transfected cells, at 72 hours. This change could not be observed at 24 hours, which was used as starting point of the same experiment.

4.29 Ectopic FAM134B expression suppresses tumor formation *in vivo*

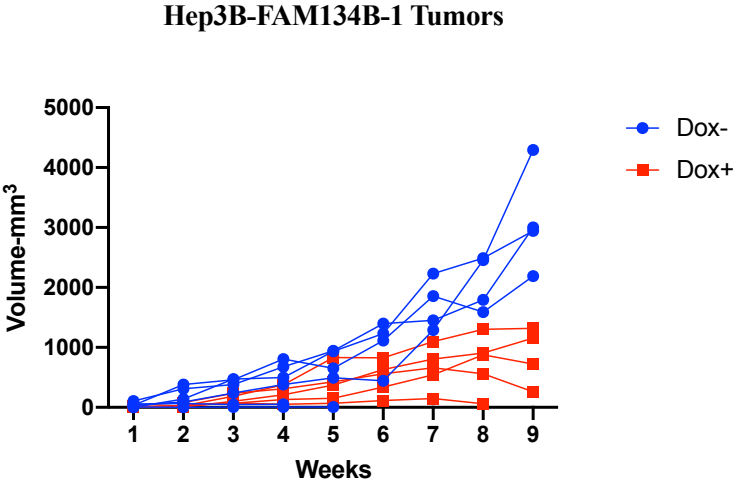
Despite its widespread use, *in vitro* studies have limited advantage for representing the dynamic tumor environment in cancer research. In the course of carcinogenesis, biological processes, such as three-dimensional interaction of tumor cells with each other and with microenvironment, progression of angiogenesis and local immune response, are usually not taken into consideration in *in vitro* studies. Furthermore, *in vitro* tumor growth studies are susceptible to experimental errors. Hence, we were not surprised to obtain contradicting results from *in vitro* studies.

In order to evaluate tumor formation properties of cancer cells ectopically expressing FAM134B, we took advantage of in vivo tumor xenograft studies. First, we subcutaneously injected tet-inducible Hep3B-FAM134B-1 cells to Nude mice. We preferred Hep3B cells over HepG2 cells, since the latter was reported as non-tumor forming cell line. Ectopic FAM134B-1 expression was induced by 2mg/ml doxycycline supplemented in drinking water.

A.


Dox-
Dox+
1
2
3
4
5
6
7
8

B.


Hep3B-FAM134B-1 Tumors
Volume-mm3
5000
4000
3000
2000
1000
0
1
2
3
4
5
6
7
8
9
Weeks
Dox-
Dox+

C.

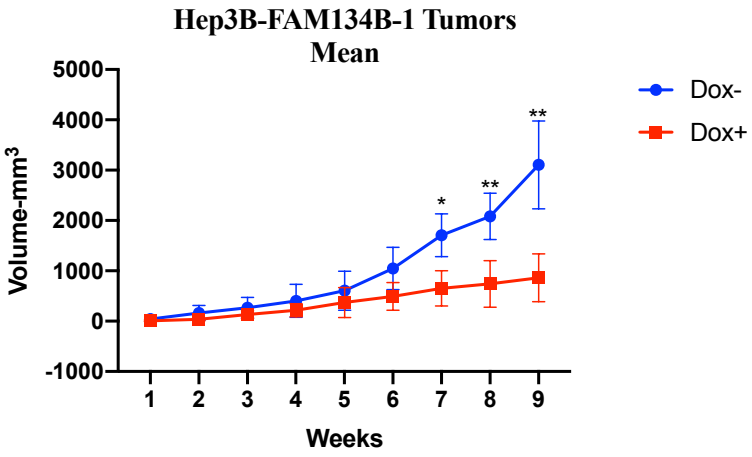


Figure 56: FAM134B-1 expression suppresses *in vivo* tumor development

Animals were given 5x10^6 Hep3B-FAM134B-1 cells subcutaneously. Dox+ group received 2mg/ml Doxycycline from drinking water. A. Fotographic images of tumors before (top) and after (bottom) excision. Tumors were numbered for downstream analyses. B. individual tumor growth over time. C. Tumor growth in Dox- and Dox+ groups over time. One animal from Dox- group exhibited no tumor development; therefore, it was excluded from statistical analyses.

As seen in Figure 56, A, one animal from Dox- group did not develop a tumor and one animal from Dox+ groups exhibited little to no tumor on the day of scarification. Individual tumor graph shown in Figure 56, B clearly demonstrates the differential clustering of Dox- and Dox+ during the tumor formation. This cluster was also statistically significant starting from week 7. This result clearly shows that ectopic expression of FAM134B-1 has a tumor inhibiting effect.

In order to make sure that the Dox+ tumors in animals express FAM134B-1, we performed western blot experiments on protein lysates of Hep3B-FAM134B-1 tumors.

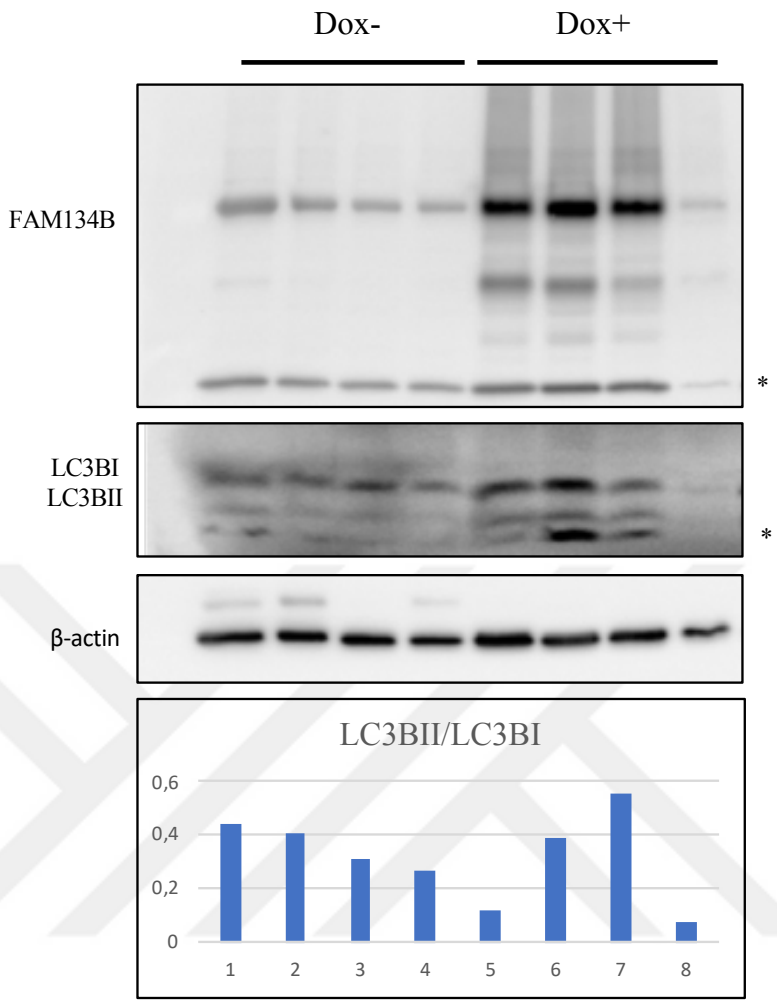


Figure 57: Doxycycline is capable of inducing FAM134B-1 *in vivo*

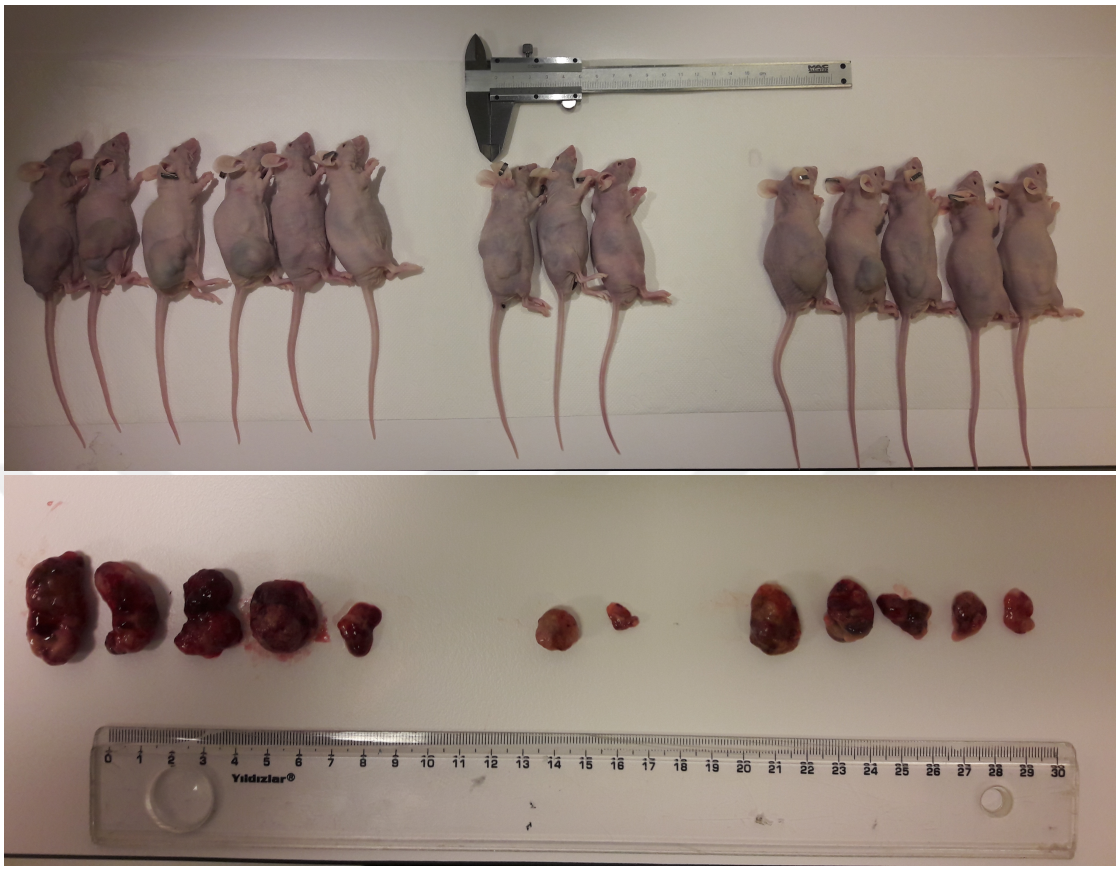
Immunoblotting of FAM134B, LC3B and western blot. Bar plot shows the LC3BII/LC3BI ratio in the same order of samples. Asterisks indicate the non-specific antibody bindings.

Although there was low level of FAM134B-1 expression in Dox- group, Doxycycline treatment by drinking water has clearly enhanced FAM134B-1 expression Figure 57. Unfortunately, we failed to observe similar stimulation in last tumor (8th), possibly due to insufficient amount of total protein, which is supported by the low expression levels of β-actin and LC3B of the same. In addition, we also observed weaker FAM134B specific bands corresponding to 55kDa (Tumor number 5, 6, 7), possibly indicating a leaky FAM134B expression from human cells or from host tissue. Interestingly, LC3BII/LC3BI ratio was not dramatically altered in Dox+; but, levels of both LC3BI and its lipidated form, LC3BII, were visibly enhanced.

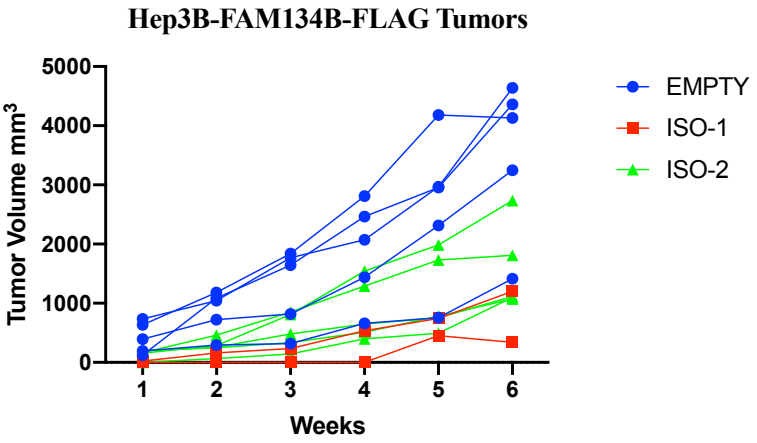
Based on these results, we performed another xenograft experiment in which both FAM134B-1 and FAM134B-2 are included. In this experimental set up, we utilized stable Hep3B cell lines expressing flag tagged versions of FAM134B-1 and FAM134B-2 for two reasons: 1- Doxycycline uptake may differ between animals, which would yield variable results; 2- FLAG tagged proteins allow many robust downstream applications such as co-immunoprecipitation assays, immunofluorescence.

We injected EMPTY, FAM134B-1-FLAG and FAM134B-2-FLAG plasmid containing cells subcutaneously to nude mice. Emtpy vector, FAM134B-1 and FAM134B-2 containing cells were injected 6 mice per group (n=18).

A.


EMPTY
FAM134B-1
FAM134B-2

B.


Hep3B-FAM134B-FLAG Tumors
Tumor Volume mm3
5000
4000
3000
2000
1000
0
1
2
3
4
5
6
Weeks
EMPTY
ISO-1
ISO-2

C.

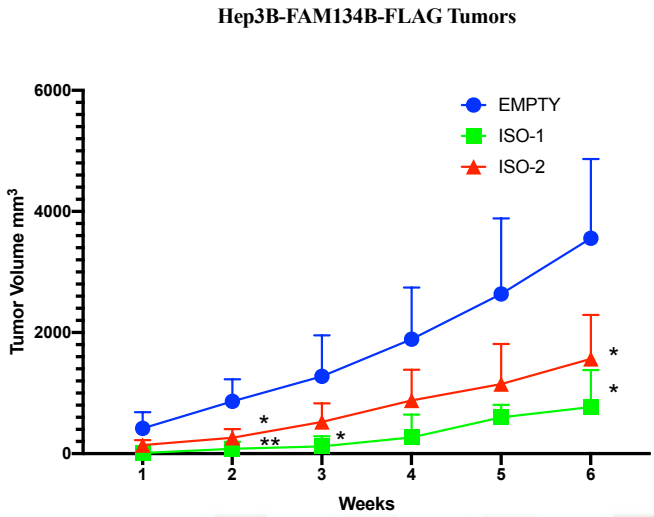


Figure 58: Both FAM134B isoforms suppresses tumor development *in vivo*

A. Photographic images of tumors before and after tumor excision. 2.5x10^6 cells were injected right flanks of nude mice. B. Individiual tumor growth of three tumor groups. C. Tumor growth of three tumor growths as shown by mean±SD. P<0.05, *; p<0.01, **

One day after injection, two animals from FAM134B-1 group; after one week, one animal from FAM134B-1 and one animal from FAM134B-2 died; therefore, they were not included in calculations. Five out of six animals in EMPTY, two out of three animals in FAM134B-1 groups failed to develop tumors, while all animals in FAM134B-2 group developed excisable tumors (Figure 58). Animals which did not develop tumors were not included in tumor volume calculations.

Similar to the xenograft experiment performed by inducible cells, FAM134B-1-FLAG expressing cells developed significantly smaller tumors compared to Hep3B-Empty cells. Interestingly, despite their larger mean size compared to FAM134B-1, FAM134B-2 cells yielded significantly smaller tumor size compared to EMPTY group.

Together these data of xenograft studies indicated that both FAM134B isoforms have tumor suppressive effect in HCC tumors.

4.30 Ectopic expression of FAM134B-1 suppresses inflammatory response *in vivo*

Observing the tumor inhibiting effect of FAM134B overexpression *in vivo* but not *in vitro* forced us to suppose that FAM134B might facilitate cross-talk between tumor cells and host cells, which critically determines whether tumor growth is favored. One of the most critical microenvironmental determinant is inflammatory response of the host organism, activation of which usually favor the tumor growth by increasing tumor-promoting cytokines. Native immune cells are known to be key players in tumor microenvironment and secrete cytokines such as IL-6 and TNF-a to promote tumor by protecting Cancer Stem Cells (CSCs)[90]. Since FAM134B has previously been shown to regulate secreted proteins[91], we hypothesized that presence of FAM134B might directly affect the cross-talk between tumor and stroma.

Based on information, we desired to test whether tumor favoring cytokines are expressed in tumor microenvironment when FAM134B is overexpressed in tumor cells. Hence tumors expressing FAM134B-1 (Section 4.2.4) were analyzed for expression of mouse TNF-α and IL-6 using Reverse Transcriptase PCR.

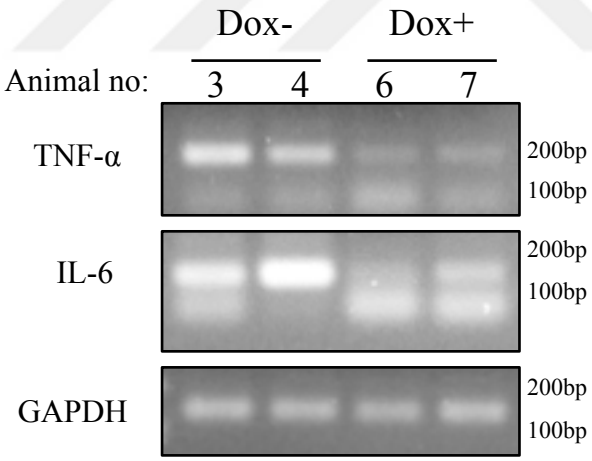


Figure 59: Mouse native immune response against Hep3B-FAM134B-1 cells

Reverse transcriptase PCR performed by specific primers designed for mouse Tumor necrosis factor alpha (TNF-α) and Interleukin-6 (IL-6). The numbers indicate labels of tumor used in this experiment.

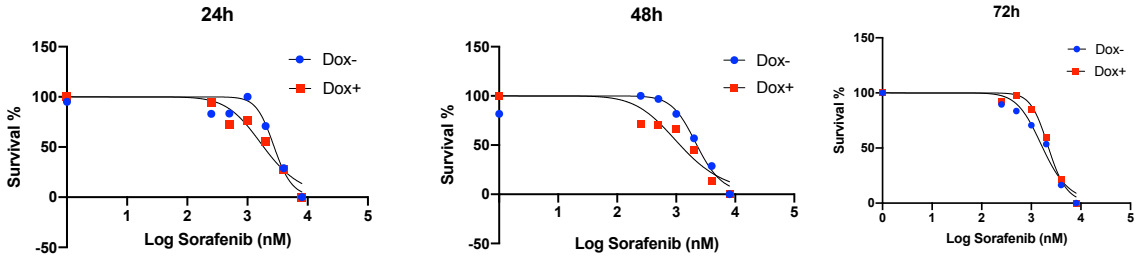
Mouse specific primers used to detect TNF-α and IL-6 clearly amplified its target cDNA sequence strongly in Dox- tumors. However, cDNA amount of these cytokines was strikingly low in Dox+ tumors (Figure 59), which suggest that forced expression of FAM134B-1 in tumor cells involves in direct interaction between tumor and its microenvironment, possibly by regulating secreted signal molecules during ER-Golgi maturation.

4.31 Ectopic expression of FAM134B-1 slightly alters survival response against anti-cancer agents

Cancer patients progressing to late HCC stages usually undergo chemotherapy regimen, which is mostly mediated by use of multi-kinase inhibitor Sorafenib. Unfortunately, sorafenib prolongs overall survival time around only two months[92] and other potential alternatives still do not offer a substantial treatment option. Since during the progression of HCC, cells tend to lose their FAM134B expression, we hypothesized that overexpression of the same would make a difference in chemotherapeutic response of cells. Therefore, we performed cell Sulforhodamine B (SRB) based survival assays by challenging FAM134B expressing HCC cell lines by two chemotherapeutic agents: Sorafenib and Bortezomib.

Bortezomib is a 20S proteasome inhibitor and intensively used to treat multiple myeloma patients[93]. The main reason of selection of this molecule to perform in vitro assays is that it blocks proteasomal degradation pathway and leaves autophagy pathway as the only protein degradation option for the cells. Therefore, we hypothesized that FAM134B mediated autophagy degradation would become more pronounced in Bortezomib treated FAM134B expressing cells.

A. Sorafenib



R^2 values (fitness to non-linear curve)

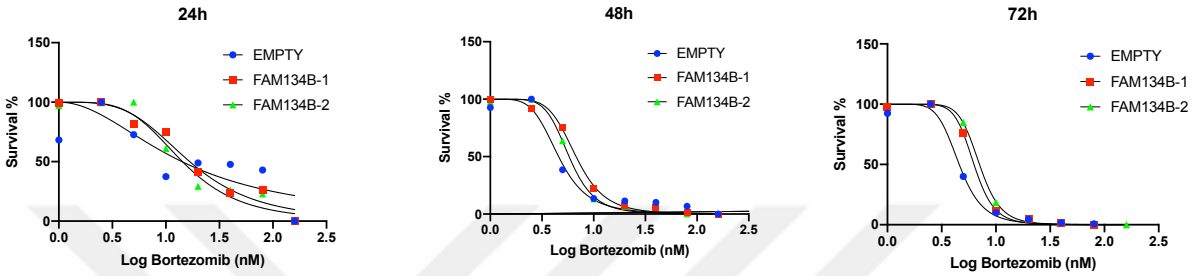
Dox-: 0.6907 Dox-:0.7523 Dox-:0.9029

Dox+:0.6050	Dox+:0.7887	Dox+:0.9745

IC50 values

Dox-: 2.8µM	Dox-:2.2µM	Dox-:1.7µM
Dox+:1.9µM	Dox+:1.2µM	Dox+:2.2µM

B. Bortezomib



R^2 values (fitness to non-linear curve)

Empty: 0.2251	Empty: 0.9578	Empty: 0.9802
FAM134B-1: 0.5867	FAM134B-1: 0.9861	FAM134B-1: 0.9945
FAM134B-2: 0.7552	FAM134B-2: 0.9682	FAM134B-2: 0.9942

IC50 values

Empty: 14.2nM	Empty: 4.6nM	Empty: 4.6nM
FAM134B-1: 16.7nM	FAM134B-1: 6.8nM	FAM134B-1: 6.3nM
FAM134B-2: 14.3nM	FAM134B-2: 5.8nM	FAM134B-2: 7.1nM

Figure 60: Effect of Sorafenib and Bortezomib on FAM134B expressing HCC cell lines A. HepG2-FAM134B-1 cells challenged by varying doses of Sorafenib for 24, 48 and 72 hours. B. Hep3B-FAM134B-FLAG cells challenged by varying doses of Bortezomib for 24, 48 and 72 hours. Fitness to the kill curve and IC50 values are indicated in boxes below the graphs of each time point.

Sorafenib SRB experiments yielded the best fitness of kill curve at 72 hours (R^2: 0.9029 and 0.9725 for Dox- and Dox+ respectively), at which FAM134B expression favored cell survival over non-expressing cells, evidenced by IC50 values (2.2µM to 1.7µM). Kill curves at earlier time points (24 and 48 hours) exhibited contradicting IC50 values along with poorer curve fitness values (

Figure 60).

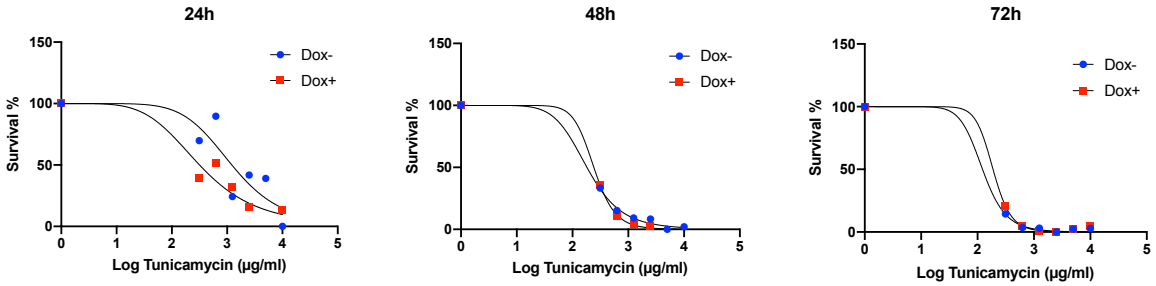
Similar to Sorafenib, Hep3B-FAM134B-FLAG cells treated with Bortezomib showed better survival profile compared to Empty plasmid transfected cells starting from 48 hours, at which FAM134B-1 and FAM134B-2 cells showed IC50 values of 6.8nM and 5.8nM over control cells (4.6nM). Similar trend is also followed at 72 hours, where IC50 values of FAM134B-1 and FAM134B-2 cells were 6.3nM and 7.1nM over control cells (4.6nM).

Overall these results suggest that, ectopic expression of FAM134B in epithelial like cells such as HepG2 and Hep3B leads to slight increase in drug resistance against treatment of sorafenib and bortezomib.

4.32 FAM134B-1 slightly alters survival response against ER-stress agents

The drugs Sorafenib and Bortezomib are also well known for their potential to induce ER-stress while exerting molecular effects. Keeping this in mind, we hypothesized that ectopic FAM134B expression would also affect cell survival against ER-stress inducing agents. Therefore, we performed SRB experiment by treating inducible HepG2-FAM134B cells with Tunicamycin and Dithioteritol (DTT).

A. Tunicamycin



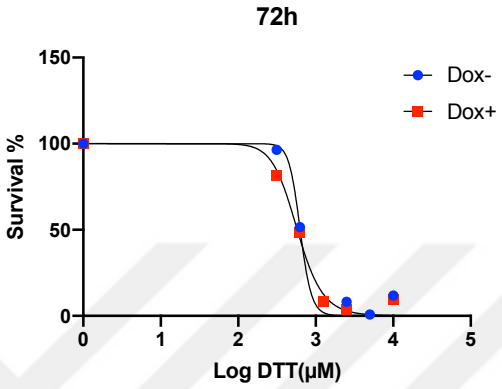
R^2 values (fitness to non-linear curve)

Dox-: 0.5030	Dox-:0.9622	Dox-:0.9954
Dox+: 0.6353	Dox+:0.9913	Dox+:0.9888

IC50 values

Dox-:1.22mg/ml	Dox-:0.18mg/ml	Dox-:0.12mg/ml
Dox+:0.32mg/ml	Dox+:0.24mg/ml	Dox+:0.19mg/ml

B. DTT



R^2 values (fitness to non-linear curve)	IC50 values
Dox-:0.9368	Dox-:3.28mM
Dox+:0.9649	Dox+:2.76mM

Figure 61: Effect of Tunicamycin and DTT on FAM134B expressing HCC cell lines
Inducible HepG2-FAM134B-1 cells challenged with Tunicamycin (A) and DTT (B). 24- and 48-hours treatment of DTT could not be fitted in kill curve, therefore, not shown.

Ectopic expression of FAM134B-1 cells lead to increased resistance against Tunicamycin starting from 48 to 72 hours as evidenced by IC50 values (Figure 61).

Contrary to other ER-stress inducers, HepG2-FAM134B-1 cells showed slightly less survival score when treated with DTT, as demonstrated by IC50 values (3.28mM and 2.76mM of Dox- and Dox+, respectively)

4.33 Proteasomal blockage leads to accumulation of FAM134B

Cellular recycling of macro- and micronutrients are mediated either through lysosomal or proteasomal degradation. Bortezomib exerts its effect via blocking 20S subunit of proteasome machinery, thereby blocking proteasome mediated protein degradation. We

hypothesized that, treating cells with anticancer drug bortezomib might indirectly switch protein degradation mechanism to lysosomal degradation, which in turn exaggerate the effect of FAM134B. Therefore, we treated Hep3B-FAM134B-1 and Hep3B-FAM134B-2 cells with 10nM Bortezomib for 72 hours. The cell lysates were analyzed using western blot (Figure 62).

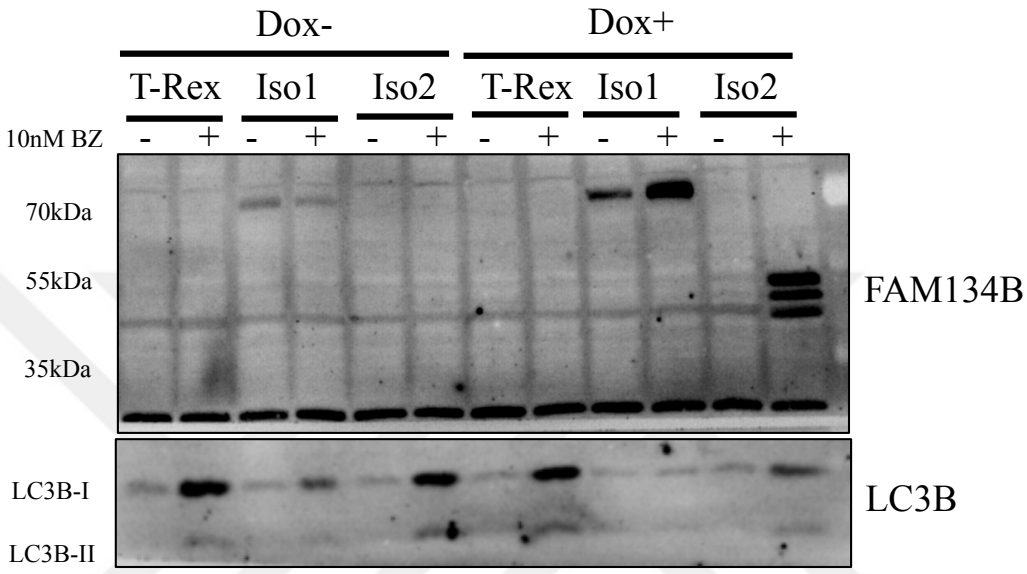


Figure 62: Bortezomib induced FAM134B expression
T-Rex (untransfected), FAM134B-1 and FAM134B-2 expressing cells were treated with 10nM bortezomib for 72 hours.

Although Bortezomib treatment resulted in no change of FAM134B expression in cells without Doxycycline induction (FAM134B negative), it clearly induced accumulation of both LC3BI and LC3BII. However, induction of FAM134B expression via Doxycycline strikingly resulted in even more increased levels of both FAM134B isoforms. Furthermore, accumulation of LC3BI and LC3BII is lost FAM134B positive cells.

4.34 FAM134B-2 is suppressed during epithelial to mesenchymal transition

Metastasis is one of the hallmarks of cancer and represents an important cause of mortality in cancer patients. In metastasis, cancer cells undergo fundamental molecular and morphological changes facilitating their escape from tumor site, which is a phenomenon called Epithelial to Mesenchymal Transition (EMT). These cells highly specialized on mobilization

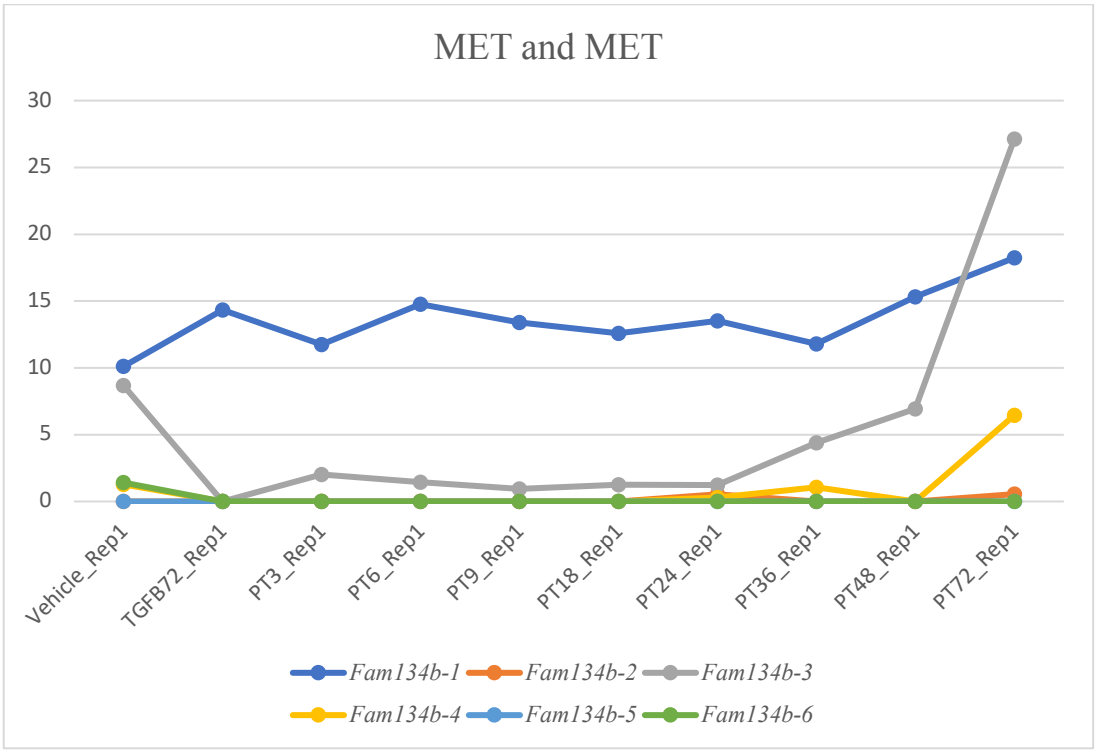
are also able to reverse the process and settle in distant tissues called Mesenchymal to Epithelial Transition (MET).

In order to monitor the relationship between EMT/MET and Fam134b expression, we picked NMuMG cells as an *in vitro* study model. NMuMG cells are murine mammary epithelial cells which can easily be transformed into mesenchymal state by TGF- β stimulation and this process can be reversed simply by removing TGF-β from cell culture media. These EMT/MET experiments have been performed in İBG, and both the RNA-sequencing and protein lysates were kindly provided by Hani Alotaibi.

Briefly, RNA sequencing results as TPM values were obtained from NMuMG cells treated with TGF-β for 72 hours which is followed by removal of TGF-β for 3, 6, 9, 18, 24, 36, 48 and 72 hours (Figure 63, A). Protein lysates used for screening FAM134B proteins were obtained from NMuMG cells which were treated with 24, 48 and 72 hours with TGF-β, followed by TGF-β removal for 24, 48 and 72 hours (Figure 63, B). In order to observe any TGF-β induced resistance against EMT, cells were also treated for 150 days with TGF-β without interruption.

We analyzed RNA-sequencing data and performed western blotting to observe expression levels of *Fam134b* isoforms at RNA and protein levels.

A.



B.

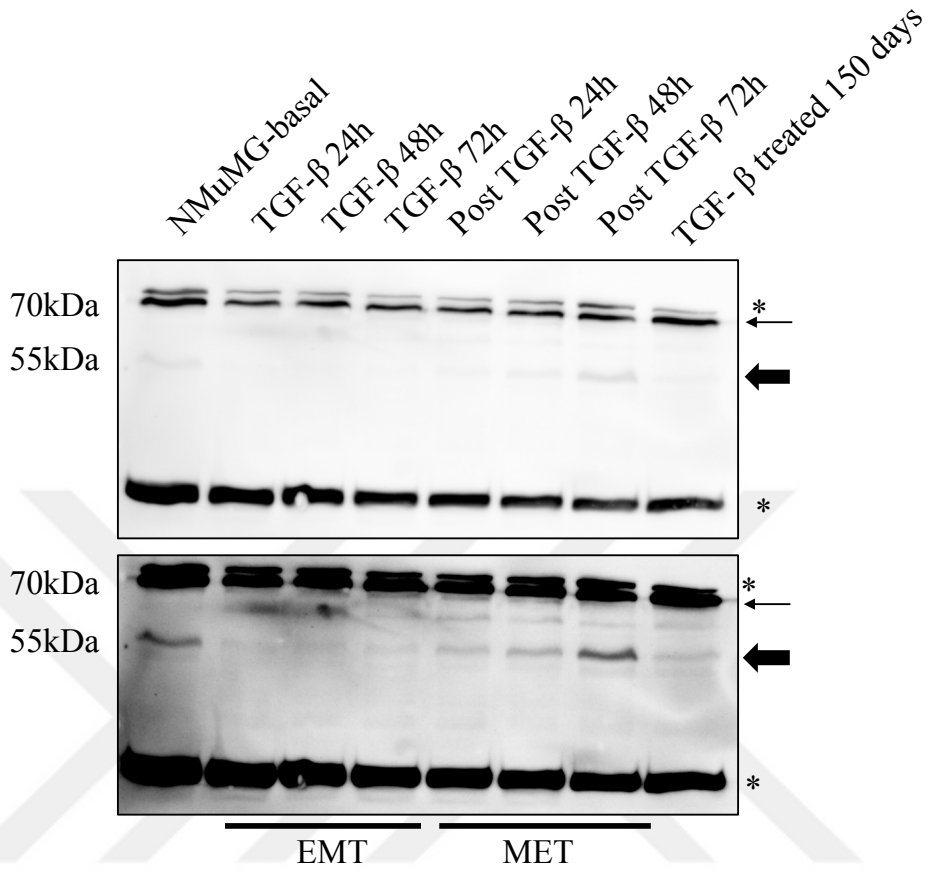


Figure 63: RNA sequencing and western blot results of NMuMG cells which undergo to EMT and MET

A.RNA sequencing results of mouse *Fam134b* variants (for each group, n=2). The y axis shows expression values as TPM. B. Protein levels of FAM134B variants.

At RNA level, TGF-β induced EMT progression did not resulted in any clear change in full length *Fam134b-1*, but caused a sharp decrease of short isoform *Fam134b-3*. After TGF-β removal, *Fam134b-3* expression started to rise back as early as 24 hours and reached basal levels after 48 hours (Figure 63, A).

The similar expression pattern was also observed in western blot, where TGF-β treatment leads to a sudden drop of short isoform (Mesenchymal state), FAM134B-2, which started to appear 24 hours after TGF-β was removed and reached its basal level at 72 hours (Epithelial state). Interestingly, however, FAM134B-1 level also shows a slight decrease upon TGF-β treatment (mesenchymal state). Furthermore, chronic TGF-β treatment lead to slight

increase of FAM134B-2 level in NMuMG cells. Another intriguing observation was that, despite similar expression levels of *Fam134b* isoforms, protein of short isoform is much less pronounced compared to long isoform (Figure 63, B).

These results clearly showed that FAM134B-2 is associated with functional state of cells and is lost upon induction of Mesenchymal transition. Differential protein expression of each isoform also indicates that RNA product of each variant is either translated or degraded at different rates.

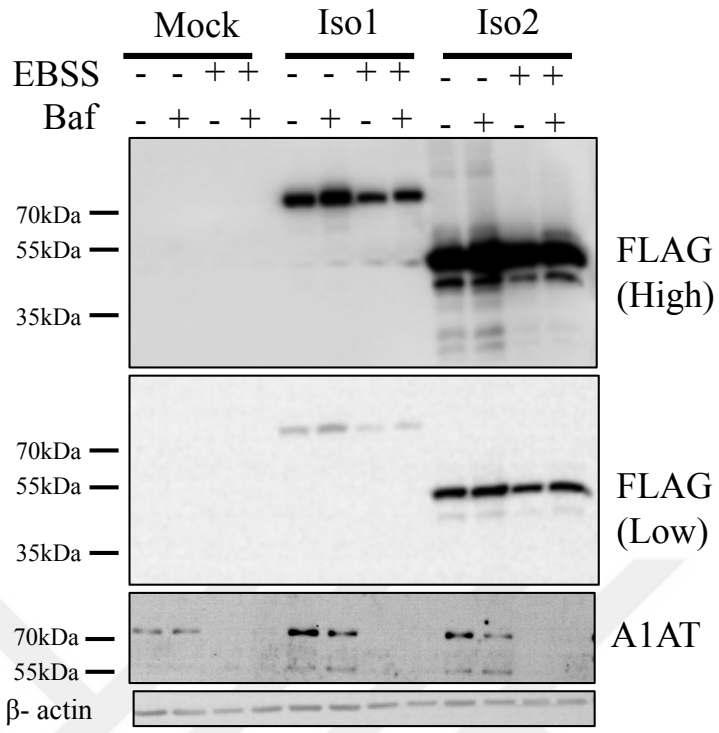
4.35 Ectopic FAM134B expression alters hepatocyte lineage specific markers

Development of liver cancer is a multistep process in which usually de-differentiation of hepatocytes into progenitor-like state takes place. This usually accompanied by loss of hepatocyte specific markers. Therefore, we suggested that loss of FAM134B during the course of carcinogenesis might affect this dedifferentiation process.

In parallel with this hypothesis, we screened series of hepatocyte and progenitor markers which are known to be secreted to extracellular space, in Hep3B-FAM134B-FLAG cells. We selected secreted molecules, since their intracellular process is obliged to pass through reticular system for maturation, which is likely to be affected by FAM134B expression. We also challenged cells with starvation and Bafilomycin A1 in order to observe possible intracellular accumulation or degradation of proteins of interest.

Briefly, Hep3B-FAM134B-FLAG cells were treated with 16 hours starvation and/or 100nM Bafilomycin A1 and subjected to Western blot analyses (Figure 64).

A.



B.

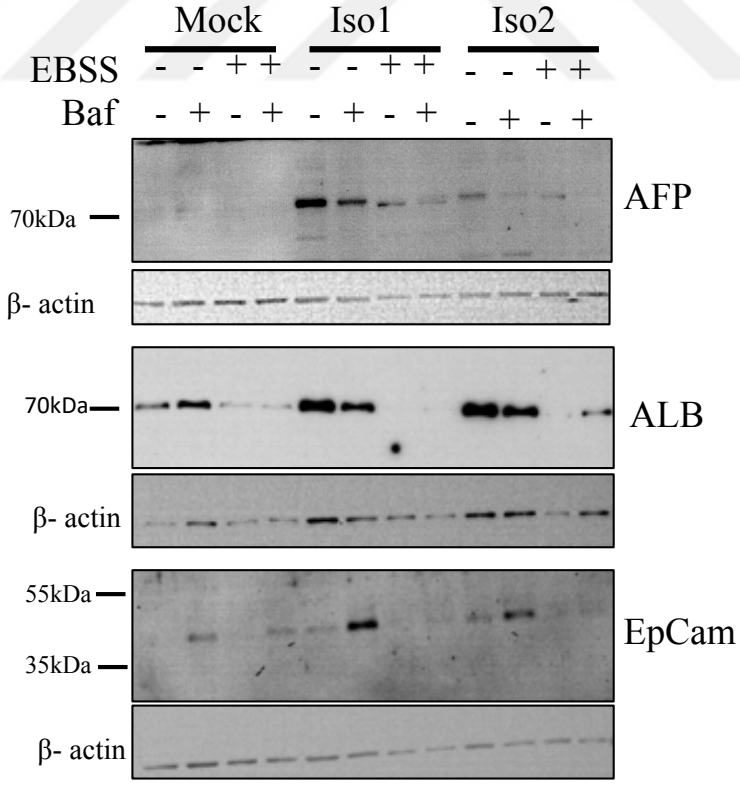


Figure 64: Ectopic expression of both isoforms alters hepatocyte lineage specific markers

A. Western blot images of Hep3B cells expressing FLAG tagged FAM134B isoforms. Membranes were blotted by FLAG, A1AT. B. Bloting results of AFP, ALB and EpCAM. Each blot image was accompanied with their corresponding β-actin image. Starvation induced by 16h treatment of EBSS. EBSS, earl's buffer saline; Baf, 100nM Bafilomycin A1

FLAG western blot results clearly show that FAM134B-1 and FAM134B-2 are robustly expressed at basal levels, with higher expression of the latter. Starvation alone caused decrease of FAM134B-1 and FAM134B-2, and Bafilomycin A1 alone induced accumulation of both isoforms. In both isoforms, Starvation treatment with Bafilomycin A1 caused only limited amount of protein accumulation, without bringing proteins to basal level. We did not observe any signal in Empty vector transfected Hep3B cells, as expected (Figure 64, A).

Alpha-1-Antitrypsin (A1AT) is one of the hepatocyte specific marker and secreted into the bloodstream. Strikingly, basal A1AT levels in Hep3B-EMPTY cells were low, but strongly stimulated in both FAM134B-1-FLAG and FAM134B-2-FLAG cells at basal levels. It was also interesting to see that despite FAM134B isoform increase in Bafilomycin A1 treated-only cells, A1AT levels decrease in same conditions. Starvation alone wiped out expression of both FAM134B isoforms which could not be rescued by Bafilomycin A1 treatment (Figure 64, A).

Presence of FAM134B-1-FLAG and FAM134B-2 FLAG was also associated with strong AFP expression, higher in former and weaker in latter, at basal conditions. Similar to A1AT, Bafilomycin A1 treatment resulted decrease in protein levels. Starvation caused a visible degradation of proteins which could not be reversed by Bafilomycin A1(Figure 64, B).

Similar expression pattern was also observed in ALB levels with the exception that Bafilomycin A1 induced slight accumulation of ALB in Hep3B-EMPTY cells but not FAM134B expressing cells, in which chemical intervention lead to decrease in ALB. Although ALB findings are quite exciting, we kept in mind that the protein equal loading control showed somewhat variance (Figure 64, B).

Although, FAM134B-1 and FAM134B-2 overexpression lead to slight increase of EpCAM levels compared to EMPTY transfected cells, Bafilomycin A1 treatment caused a pronounced expression of EpCAM in FAM134B-1, and with a lesser extent, FAM134B-2. Starvation caused a complete protein degradation; but, Bafilomycin A1 treatment brought expression back in EMPTY cells (Figure 64, B).

Overall these results strongly suggest that both FAM134B isoform expression affect accumulation of secreted proteins inside the cells instead of targeting them to degradation. The

only marker following the canonical lysosomal degradation pathway is EpCAM. Overexpression of FAM134B variants degrades progenitor marker EpCAM at basal conditions but blockage of autophagy cause rapid accumulation of the protein. All these findings are interpreted considering the possibility that differences in protein levels might be simply because of single clone derived Hep3B-FAM134B cells which endogenously express hepatocyte and progenitor markers.

4.36 Induced FAM134B expression increases albumin levels

To rule out the single cell derived variabilities, we checked ALB levels in Doxycycline inducible Hep3B cells. In order to mimic long term exposure to FAM134B overexpression, inducible cells were passaged 21 days and cells were collected at each time point. Cell lysates were analyzed in western blot to detect FAM134B and ALB (Figure 65).

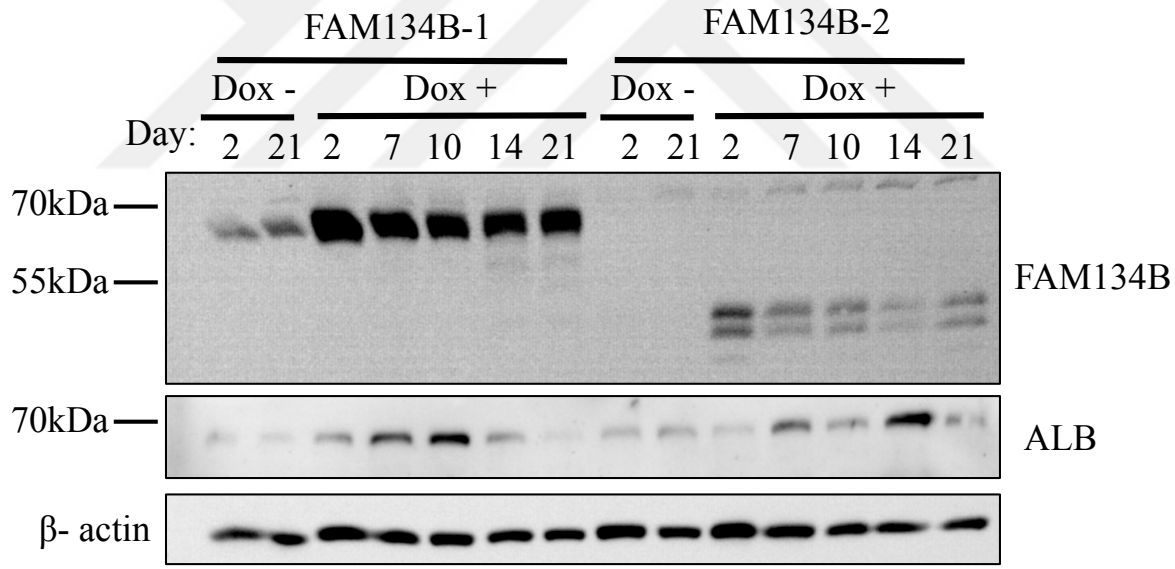


Figure 65: Liver specific differentiation markers under the inducible expression of FAM134B isoforms

Hep3B-FAM134B-1 and Hep3B-FAM134B-2 cells with or without induction of doxycyline were passaged for 21 days. In dox- conditions, only first and last day of experimental conditions were added.

Doxycycline negative and positive lanes showed clear induction of FAM134B isoforms. However, after day 2, FAM134B levels slightly decreased even under constant Doxycycline induction. Interestingly, ALB expression was also induced in FAM134B-1 cells starting from Day 2 reaching highest level at day 10 and started to decrease thereafter. FAM134B-2 cells, on the other hand, exhibited low ALB levels at day 2, but showed an increasing trend reaching top at day 14 (Figure 65).

Since inducible cell lines are single cell derived clones and also represent a paired experimental model where gene expression is stimulated in same cells, evaluation of marker expression would be considered more reliable. Therefore, enhanced ALB expression in FAM134B induced cells supported the previous data.

4.37 Ectopic FAM134B expression does not alters tumoroid formation *in vitro*

Ectopic expression of FAM134B variants in Hep3B cells did not cause a dramatic change in morphology or colony forming abilities. This might be due to lack of any morphological change in cells; however, there may be phenotypic effects on microscopic level going unnoticed due to the limitation of monolayer cell culture technique. Organoid based cell culture methods are commonly used to grow tumor cells in three-dimensional environment which allows tumor cells to form colonies and exhibit different phenotypes than monolayer methods such as cell-cell interaction, cell polarity, invasiveness etc.

Results showing the altered expression of hepatocyte associated traits combined with the advantages of organoid culture techniques have urged us to generate Hep3B organoid cell culture in order to observe possible effect of FAM134B expression. Briefly, cells were seeded in Matrigel:Complete Medium mixture (20:80%) and cells were induced by docycyline at day 4. After ten day of incubation hematoxylin and eosin staining was performed (Figure 66).

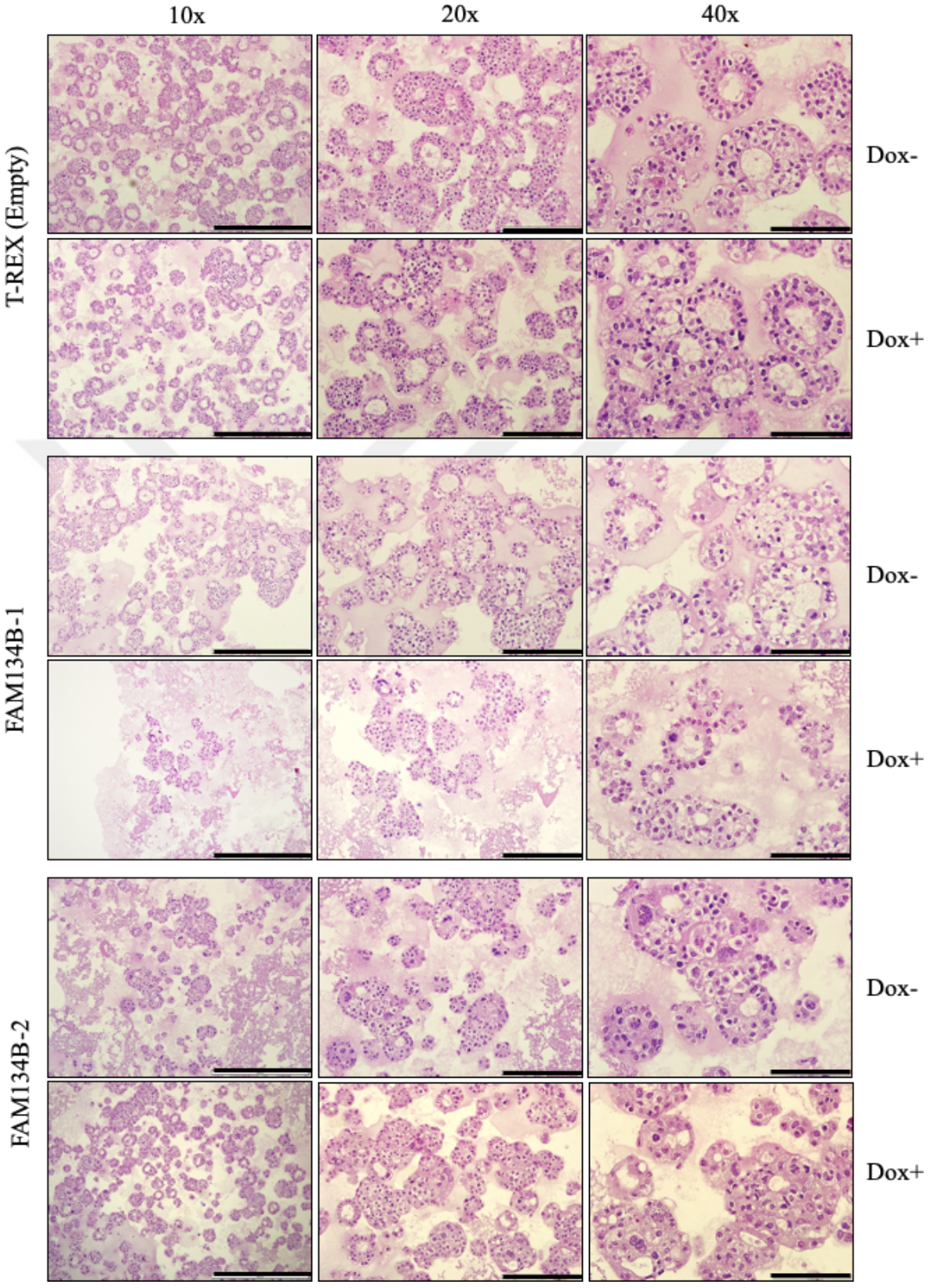


Figure 66: Ectopic FAM134B expression does not affect tumoroid formation

Scalebars of 10x, 20x and 40x corresponds 500µm, 200µm and 100µm respectively.

All conditions made by Hep3B cells formed round shaped organoid structures most of which had cell free area in the center. Cells were tended to align as single layer at the periphery of organoids, reminiscent of epithelial cell organization. Most of the cell cytoplasm exhibited low staining of eosin possibly due to cytosolic lipid or glycogen contents.

Hep3B-T-Rex cells treated with doxycycline did not presented any change in colony formation as well as morphology. FAM134B-1 and FAM134B-2 expression also did not dramatically change any of these traits, but it slightly increases cytosolic eosin staining.

5 DISCUSSION

The role of FAM134B has gained great attention of the scientific community and the number of publications has dramatically increased since the early descriptive studies and theses defining its functional properties. Despite the recent mechanistic discoveries, there are still many questions to be answered with regard to FAM134B variants and their functions not only in nervous tissues as shown by Khaminets et al.[16], but also in other tissues, and in different physiological and pathological contexts.

In this thesis, we focused primarily on definition of FAM134B isoforms, their functional insights in other organs *in vivo* as well as in cell culture, and implications in cancer. Although our findings together should be considered as integrative in the context of the role of FAM134B, we grouped our work under two headlines: 1- FAM134B in physiology; 2- FAM134B in cancer.

5.1 FAM134B in physiology

Gene structure of FAM134B

Our group members previously investigated the evolutionary conservation of FAM134B across different species[7]. Therefore, we narrowed down the number of species to human, mouse and bovine, which were more readily available to study in molecular biology laboratories.

As an initial study, we revisited *in silico* analyses of FAM134B gene and protein structure across species under the light of recent findings in literature. The verified datasets we benefited from (GTEx) have demonstrated the expected similarity between human and mouse *FAM134B* in terms of exon number, genomic location, and alternative transcripts. Of course, besides the long-known isoform, FAM134B-1, mouse expresses at least 5 more transcripts, all of which are short version of the genes, and their transcription is mediated by alternative transcription start sites. Although exon 4, 5, 6, 7, 8 and 9 are common in all isoforms, each variant has different transcription start site. This strongly indicates different gene regulatory elements at 5' UTR of each short isoforms (Figure 8). In line with this, one of the mouse short isoforms, namely FAM134B-2, was previously shown to be regulated by CEBPα and CEBPβ transcription factors in liver, [77]. Even though other transcript variants were not mentioned in the article, the defined short isoform (FAM134B-2) corresponded to *isoform-3,* which was

defined in this thesis. Furthermore, our RT-PCR results from starved mouse livers has shown that, FAM134B-2 increase in western blot is a result of increased mRNA levels of *isoform-2, -3, -4 and -6* combined (Figure 32 and 33). Differentially expressed *Fam134b* isoforms in brain, testis, heart and muscle verified by our RT-PCR analysis has also indicated that transcription of isoforms is under control of tissue specific factors (Figure 12).

The reason why mouse has multiple versions of short isoform compared to human and bovine could be partially explained by genomic architecture of mouse. Compared to mouse, alternative splicing profile of human is conserved only by 15% [94] despite 85% similarity of protein coding genomic sequence[95]. Slight differences at N-terminal of mouse FAM134B-2 proteins strongly suggests possible roles of these nuances (Figure 9 and 10). This is partially supported by the fact that, short isoform of FAM134B in all species are not generated by a mere post-translational truncation of the protein, but rather, a short peptide replaces the large transmembrane domain (TM12) by alternative splicing. This new FAM134B-2 specific N-terminal sequence replacing the large TM12 might suggest new functional feature. For example, this exchange eliminates previously identified phosphorylation sites S149 and S151, but not S153[17], all of which mediate FAM134B oligomerization, required for ER scission.. Hence, re-arrangement of these phosphorylation sites through alternative splicing along with the loss of TM12 would deeply affect its function. Another example could be the CNX binding ability of TM-12, which is peculiar to full length FAM134B[18] and its deletion abrogates CNX binding.

It is also noteworthy that, FAM134B-1 and FAM134B-2 (human) proteins are identical for their C-terminal 345 amino acids. This also strongly suggests that, C-terminal of all short FAM134B-2 isoforms must retain the functions of highly conserved [16] TM34 and LIR motif.

Expression profile of FAM134B variants in vivo

In order to better characterize the roles of FAM134B variants we screened the presence of these transcript variants in healthy tissues of human, bovine and mouse. Human derived Genotype Tissue Expression (GTEx) data further supported with RT-PCR results has nicely shown the distinct nature of transcript variant expression (Figure 11 and 12). In addition, using western blot and RT-PCR techniques similar expression profile was observed in both mouse

and bovine tissues. Long FAM134B-1 predominantly expressed in brain, testis, fat and to a lower extend lung, while FAM134B-2 is almost exclusively expressed in muscle, heart, liver, pancreas (Figure 13, 15, 16 and 67).

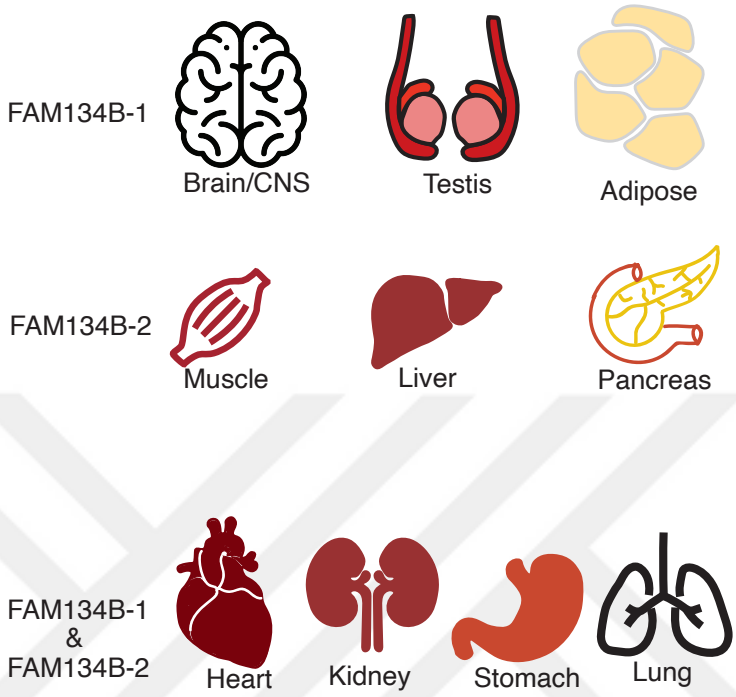


Figure 67: Tissues classified according to their expression levels of FAM134B isoforms

What does selective isoform expression in various tissues would possibly mean? The canonical role of FAM134B-1 has been defined, for the first time, on peripheric nerves, where its absence was shown to cause ER expansion and eventually decreased cell survival in peripheric neurons[16]. Similarly, since the protein quality control is essential in brain, it is logical to hypothesize that FAM134B aberration would result in gross clinical outcomes. However, to our knowledge, FAM134B has not been functionally linked with the central nervous system, where FAM134B-1 is the almost exclusively expressed isoform as both mRNA and protein. This indicates that the absence of FAM134B-1 in CNS might be robustly compensated by other mechanisms[96].

Besides the defined neurological functions, there are only a handful of studies describing the role of FAM134B in other tissues. One example is the excessive lipid deposition in adipose tissue upon overexpression of FAM134B, which was demonstrated by others[76,97]. In our *in vivo* studies, FAM134B-1 was shown as the main isoform expressed in adipose tissue

and mutant mice slightly resisted to starvation induced weight loss. Although this data suggests that FAM134B-1 plays important roles on lipid deposition in adipose tissue, slowed down weight loss could also be due to muscle mass affected by absence of FAM134B.

Another interesting tissue that shows high FAM134B-1 expression is testis. Due to the spatial restrictions, sperms do not have a functional endoplasmic reticulum[98]. However, spermatogenesis is highly demanding process in terms of protein synthesis. This usually requires a finely tuned ER homeostasis, perturbation of which may easily cause ER-stress induced Unfolded Protein Response (UPR)[99]. Robust FAM134B-1 expression in testis (Figure 16) might be playing an important role as a counter balancing agent in this process by keeping ER size in physiological shape. However, it is important to keep in mind that *Fam134b* mice were fertile and did not exhibited in any embryonic defect. This indicates that, similar to CNS, absence of the protein is compensated by other mechanisms.

Our western blot analyses have revealed that, FAM134B-2 is the dominantly expressed isoform in muscle and heart tissues (Figure 16). In previous reports, association of FAM134B with cytoskeletal elements and calcium channels were shown in high throughout interactome data [32]. Therefore, it is tempting to speculate that FAM134B-2 is playing critical roles in maintaining architectural structure of endoplasmic reticulum or Ca^{2+} homeostasis via directly interacting with such cellular structures. Nevertheless, loss of FAM134B has resulted in no prominent phenotype either in muscle or in heart, indicating that the absence of FAM134B is tolerated by some unknown compensatory mechanisms.

Besides its tissue specific transcriptional expression, translation of FAM134B isoforms needs to be mentioned. For example, mouse brain and heart showed strong and weak expression of all isoforms on mRNA levels. However, brain and heart selectively expressed protein of FAM134B-1 and FAM134B-2 respectively. This suggests that mRNA reserves of FAM134B variants are tightly regulated for translation, at least in some of the tissues such as heart and testis. Indeed, this notion could also be attributed to protein degradation rate, such that testis might rapidly degrade short isoforms while heart selectively inhibits degradation of short isoforms.

While interpreting all these results, it is also critical to keep in mind that deletion of *Fam134b* alone does not induce mortality in mice; therefore, functional effects of all isoforms could be either subtle to detect or somehow compensated by some other mechanisms[100]. Therefore, a protein band emerged in mutant testis but not in wild type was not surprising

(Figure 15). Immun recognition of this newly emerged protein by FAM134B antibody strongly suggests a compensatory expression of a closely related homolog gene.

In vitro Expression profile of FAM134B variants

Characterization experiments performed on cancer cell lines have shown that FAM134B-1 is almost always peculiar to mesenchymal-like cell lines (Figure 17), all of which exhibits fibroblast-like cell morphology along with expression of mesenchymal-like molecular markers[72]. Furthermore, primary wild type Mouse Embryonic Fibroblasts (MEFs) has also predominantly expressed FAM134B-1 (Figure 37). FAM134B-2 expression, on the other hand, could be only weakly visible in some cell lines such as FOCUS, Huh7, and even weaker in Hep40 and Mahlavu (Figure 17). Autophagosome blocking experiments performed with Bafilomycin A1 has shown that low endogenous FAM134B-2 expression compared to FAM134B-1 is not due to high amount of lysosomal degradation (Figure 24).

One possible explanation for almost exclusive expression of FAM134B-1 in mesenchymal-like cells could be the ER status of the cell types. Among HCC cell lines, most of the mesenchymal-like cells were previously shown to have elevated ER stress levels and UPR[49,50]. Growing tumor usually faces a constant ER-stress, which help cells gain a survival advantage through activation of UPR. Hence, it is tempting to speculate that tumor promoting effect of ER-stress is accompanied with FAM134B-1 expression, which in turn alleviates ER-stress and prevents cellular death. In fact this was shown by knockdown experiments, where Snu449 cells silenced for FAM134B-1 were much more susceptible to ER-stress induced cell death[49]. As mentioned in other sections, FAM134B-1 was shown to be the part of protein quality control mechanism and helps eliminate misfolded procollagen proteins by targeting them to lysosomes[18]. Similarly, mesenchymal-like cells tend to secrete vast amount of extracellular matrix proteins. Therefore, keeping FAM134B-1 would be extremely advantageous especially when the cell is adapting to its surroundings, and having an increased demand for protein folding quality control (Figure 68).

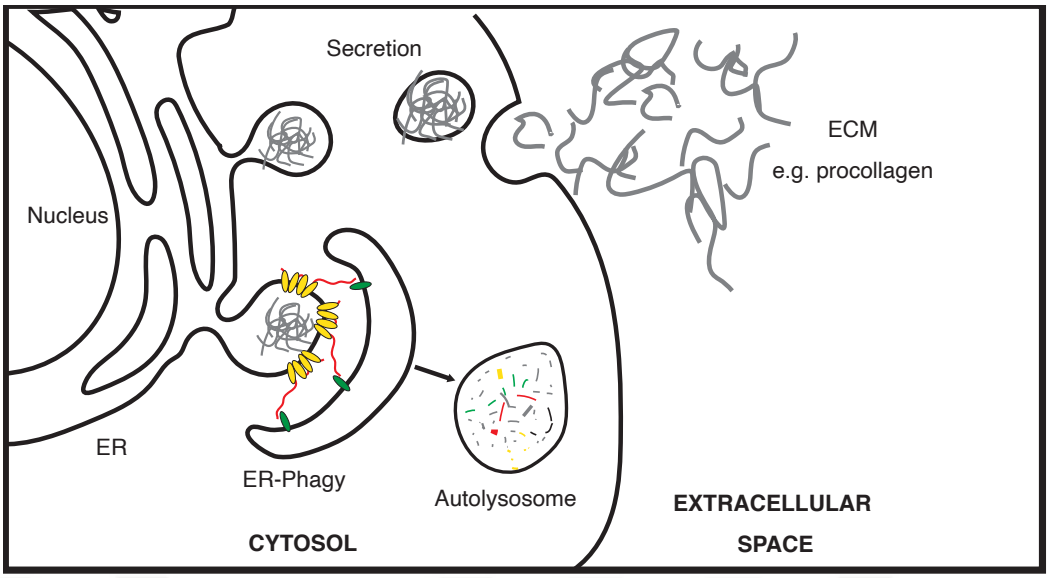


Figure 68: FAM134B-1 involves in protein control mechanism of extracellular matrix

In addition to collagen, mesenchymal like cells secrete bulk amount of extracellular matrix components. FAM134B-1 is likely to be involved in quality control mechanism of other ECM elements.

Localization and function of FAM134B in vitro

Three-dimensional structure of FAM134B isoforms suggests a fundamental difference: short isoform lacks a long unstructured N-terminal tail and a large transmembrane domain (TM12). Hence, we speculated that the truncated version of the protein would be impaired for the capabilities of the full-length protein. However, starvation experiments performed on Huh7-FAM134B cells have shown that both isoforms are capable of sequestering ER fragments via LC3B and are similarly affected by starvation and Bafilomycin A1 treatment. This result was not surprising, since the remaining transmembrane domain (TM34) was previously shown to be essential and TM34 domain alone is sufficient to form smaller liposomes [15]. Although two isoforms exhibited similar co-staining pattern with CNX, cell fractionation experiment has shown that FAM134B-2 corresponded to slightly lighter fractions than FAM134B-1. Besides the CNX[101] and Atlastin-2[102], FAM134B-2 fractions better colocalized with peak of Golgi marker GOPC[103] (Figure 21 and 69). Furthermore, co-immunoprecipitation of FAM134B-2 with another Golgi marker FTCD (58K)[104] strongly suggest that FAM134B-2 is also directly associated with Golgi apparatus (Figure 23).

İmmunofluorescence imaging demonstrating both isoforms colocalized with FTCD indicates that FAM134B isoforms are also endogenous to Golgi apparatus (Figure 23). FTCD protein is located at Golgi membranes and binds to cytoskeleton elements such as vimentin[105]. Therefore, direct interaction of FAM134B-2 and FTCD would propose a role in architectural organization of Golgi apparatus, as well as endoplasmic reticulum.

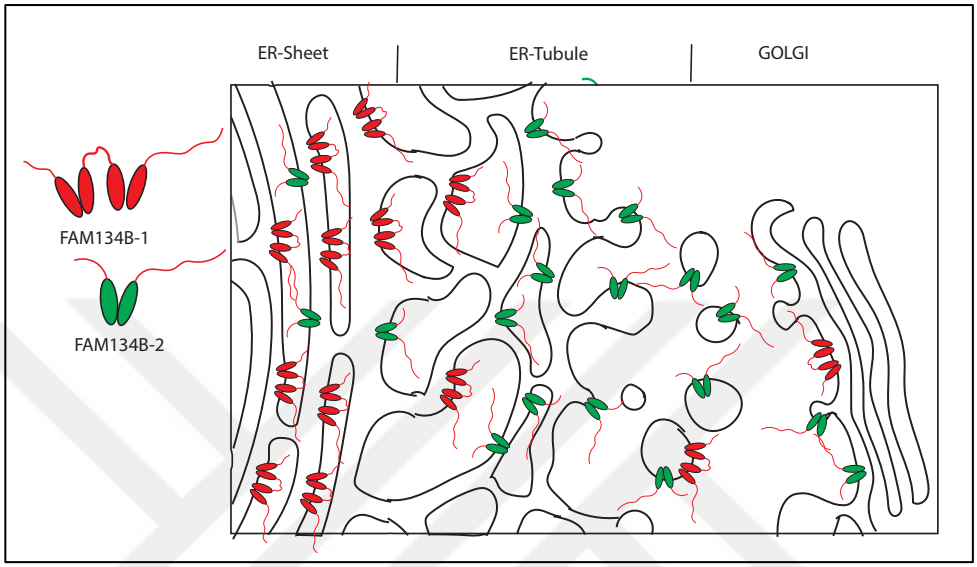


Figure 69: Proposed localization of FAM134B-1 and FAM134B-2

TM12 of FAM134B-1 was shown to mediate direct binding with different molecules such as CNX. Although both FAM134B-1 and FAM134B-2 harbor partial or whole RHD, which favors the bending of ER membrane, FAM134B-1 might be retained in ER-sheets due to direct binding to ER-sheet resident proteins such as CNX. Since FAM134B-2 is not strictly retained in ER-sheets, it might freely move to ER tubules and Golgi.

Direct and functional interaction of FAM134B-1 with CNX has been previously shown. In the study, procollagen proteins were shown to accumulate in ER lumen due to unmet folding requirements, and requires assistance of FAM134B-1 for lysosomal degradation[18]. Furthermore, they described that FAM134B-1 interacts with CNX through hydrophobic transmembrane motif of the TM12, which is lacking in FAM134B-2. In support of this notion, FAM134B-2 failed to precipitate with CNX (Figure 22), which shows that FAM134B-2 is unable to interact with CNX. Therefore, FAM134B-2 might not be a direct partner for relieving ER stress through CNX mediated ER degradation (Figure 70).

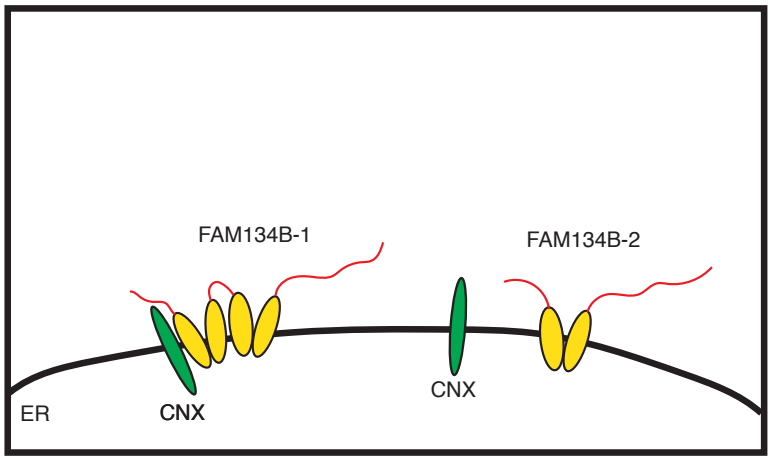


Figure 70: FAM134B-2 is not a partner of CNX

Since FAM134B-1 but not FAM134B-2 was shown to be a partner of CNX, it is likely that FAM134B-2 is not directly involved in quality control of misfolded proteins in similar to FAM134B-1

FAM134B was discovered as a target determining protein of the autophagy machinery, which is evolutionarily perfected to regulate energy recycling and expenditure. Therefore, we performed series of nutrient starvation experiments; one of the most simple and effective way to stimulate general autophagy by creating nutrient deficient environment[106]. Initial starvation experiments have shown that two isoforms do not always behave similarly *in vitro* (Figure 24). Particularly, in contrast with decrease of FAM134B-1 during starvation, FAM134B-2 clearly resisted degradation and even accumulated when treated with Bafilomycin A1 in Hep40 cells, which was not observed in FOCUS. This strongly suggests a selection mechanism for FAM134B isoforms under starvation conditions. During prolonged starvation, loss of FAM134B proteins even when treated with Bafilomycin A1 strongly implies that FAM134B-2 is eliminated in other degradation pathways (Figure 24).

LC3B has long been approved as a key marker for the evaluation of autophagy flux [106]. Co-localization of both FAM134B-1 and FAM134B-2 with LC3B in immunofluorescence experiments (Figure 19) strongly suggest that LIR motif of truncated FAM134B-2 is able to attract autophagosomes. Increased LC3BII/LC3BI ratio in starved cells ectopically expressing FAM134B-1 implies that FAM134B-1 stimulates total autophagy machinery or somehow enhance LC3B lipidation (Figure 26). Although we cannot rule out the possibility that FAM134B-1 does not affect upstream of autophagy machinery, decrease of total LC3B levels

in prolonged starvation (both LC3B-I and -II) would be attributed to LC3B biogenesis or degradation[106], affected by FAM134B-1 overexpression. Strong existence of inducible FAM134B-1 in HepG2 cells even in prolonged starvation may be associated with enhanced degradation of LC3BII, which depletes LC3B reserves.

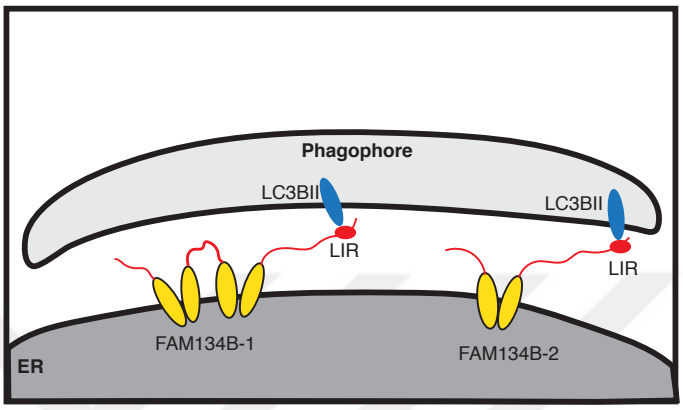


Figure 71: Both FAM134B-1 and FAM134B-2 is able to attract expanding phagophore

FAM134B dependent LC3B changes were also further supported with *in vivo* experiments where the absence of *Fam134b* caused increase in both LC3B-I and -II in protein level (Figure 32). Therefore, FAM134B may play important roles not only as ER-phagy receptor but also as rate limiting protein in autophagy flux.

Function of FAM134B in vivo

Experimental settings were further expanded with *in vivo* starvation experiments using *Fam134b*$^{-/-}$. The effect of *Fam134b* deficiency could be observed even in basal conditions. Significantly low HDL levels in fed (*ad libitum*) mutant mice yielded important clues regarding the *Fam134b* phenotype. HDL production and clearance from blood are primarily mediated by the liver, suggesting that FAM134B-2 in liver might be involved in quality control of lipoprotein particles[107]. However, with given data, we cannot rule out the possibility whether HDL uptake mechanisms by the peripheric tissues is disrupted due to *Fam134b* absence.

Starvation was well tolerated by mutant animals even in the aged condition. During starvation, most of the physical and physiological parameters underwent dramatic changes in both wild type and transgenic groups, in line with the literature [108–110]. In addition to the

expected changes, we also observed remarkable alterations in particular parameters of mutant mice. First and foremost, the staggered decrease of body weight change (Figure 27), accompanied by the unchanged blood urea nitrogen values (Figure 28), indicates impaired amino acid mobilization from peripheral tissues.

As reported previously, starvation-induced hypoglycemia and a decrease in insulin levels with maintained glucagon levels triggers an autophagic response in the liver, resulting in a surge of amino acids released into the blood at around 24h of fasting [39]. Accordingly, for most of the serum amino acids, starved mutant animals exhibited lowest amino acid levels, indicating a disrupted amino acid mobilization (Figure 28). This observation strongly suggests that in the absence of FAM134B-2, liver tissue cannot undergo sufficient autophagic proteolysis to produce these amino acids. Another interesting observation with *Fam134b*$^{-/-}$ mice was a decrease in the serum levels of methionine, valine, tyrosine, histidine and proline. Thus, it appears that these normal constituents of serum are depleted during starvation, probably because they are converted to glucose. Such a compensation may be necessary when autophagic degradation of proteins is defective.

Although liver weights between wild type and mutant group did not show any difference, increased serum albumin as well as the total protein in mutant mice indicates that fine tuning of albumin secretion during starvation is regulated by FAM134B-2.

Increase of glucagon in circulation is one of the earliest responses for energy mobilization upon nutrient starvation[39]. Glucagon was previously shown to downregulate serum calcium levels by altering gastrointestinal uptake [111]. The steady state calcium levels in mutant mice during starvation strongly suggests a function in calcium homeostasis, likely through intestinal absorption. Finally, *Fam134b*$^{-/-}$, but not wild-type mice, displayed abnormal increases in blood α-amylase levels upon starvation, an indication of pancreatic injury, salivary gland malfunction or other intraabdominal inflammations [112]. As demonstrated in western blot experiments, FAM134B-2 is predominantly expressed in the pancreas in which basal autophagy is necessary to maintain α-amylase secreting acinar cells [113]. Furthermore, another ER-phagy receptor, CCPG-1, was shown to critically involve in secretive acinar cells and its absence increases serum α-amylase levels [34]. Therefore, α-amylase increase in *Fam134b*$^{-/-}$ could be partially attributed to lack of ER-phagy, which lead to discharge of excessive α-amylase to bloodstream.

Closer look to the liver during starvation has revealed a strong FAM134B-2 stimulation along with smaller protein variant near 35kDa (Figure 32). The antibody used to detect FAM134B in immunoblot recognizes amino acid sequence of C-terminal tail of the protein. Considering its small size, this shorter isoform is highly likely to be a soluble isoform, lacking its transmembrane domain, either produced from an unknown transcript variant or generated by posttranslational cleavage of the protein (Figure 72). Of course, this shorter isoform could also be a product of one of 4 different transcript variants (*isoform-2, -3, -4* and -*6*) expression of which is enhanced upon starvation (Figure 33). This result also indicated that FAM134B-2 in mice is not product of a single transcript, but rather, it is translated from at least four transcript variants.

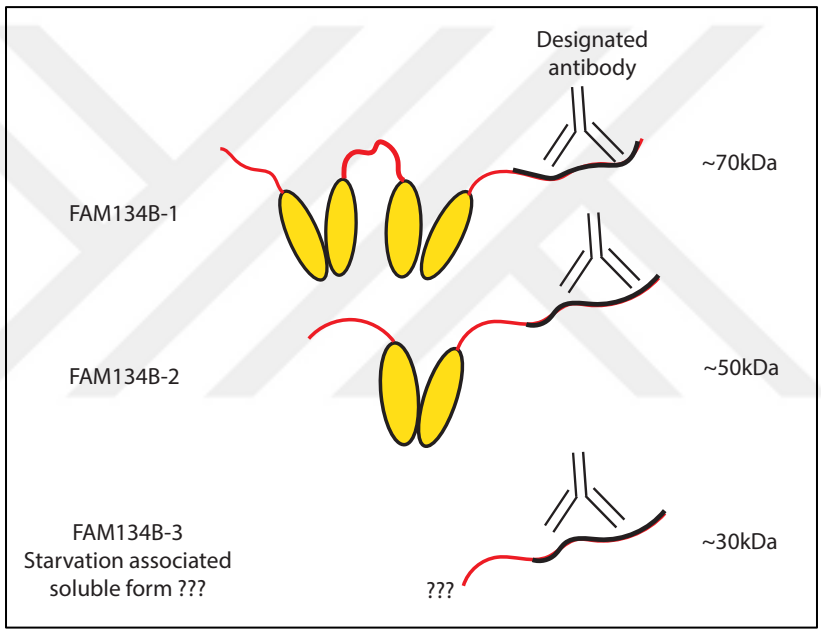


Figure 72: Shorter FAM134B isoform might be associated directly with starvation

Designated FAM134B antibody (Sigma: HPA012077) recognizes FAM134B protein at sequence closer to C-terminal end. The shorter isoform at 30kDa is therefore is likely to lack any transmembrane domain. If it is so, it is also likely for FAM134B-3 to be a soluble protein which could either be generated as a post-translational cleavage or translated from one of the transcript isoforms. This potential protein isoform is named as FAM134B-3.

FAM134B-2 expression was enhanced at 48 hours, and enhanced even further at 72 hours of starvation in muscle and heart, but not in pancreas and stomach (Figure 36). It is indeed tempting to link this with energy metabolism, since heart and muscle have been shown to also store glycogen in basal conditions and lipid droplets during starvation[114–117].

During nutrient starvation, series of strictly regulated events occur in order to redistribute stored energy in the form of micronutrients. For instance, liver glycogen is released into bloodstream in the form of glucose under the control of glucagon. Although higher mammals are equipped with complex cellular mechanisms to obtain glucose from various carbon sources, namely gluconeogenesis, brain does not completely rely on glucose consumption in prolonged starvation. This is mainly due to demanding nature of gluconeogenesis, which can rapidly deplete amino acid reserves, eventually causing muscle wasting and or organ failure[118] Since glycogen storages of the liver could only be utilized for few hours in men, fatty acids from adipose tissue are released to the bloodstream, which could be utilized primarily by muscle and heart[118]. As a response to prolonged starvation, free fatty acid in the circulation is accumulated in the liver in the form of lipid droplets[119,120]. Lipids stored in liver during starvation, are utilized to generate ketone bodies, which could be used as fuels for brain, muscle, heart and kidney[118].

In line with this background information, we have screened the lipid droplet storage of *Fam134b*$^{-/-}$ mice under starvation conditions. Lipid content of mouse liver was previously shown to increase and reach peak level at around 24 hours of starvation and decrease thereafter due to lipid storage depletion [119]. While lipid droplet remnants were still visible for wild type liver after 48 hours of starvation, there was no visible lipid droplets in *Fam134b*$^{-/-}$ animals (Figure 34). Strikingly, even in basal conditions (*ad libitum*), mutant liver exhibited lower Oil Red-O staining. This result indicates that *Fam134b*$^{-/-}$ mice somehow fails to store lipids in the liver or depletes stored lipids faster than its accumulation. The former hypothesis is less likely to be the accepted, since there are still residual stored lipids in basal and starved conditions; and, absence of such accumulation would abrogate ketone body formation which in turn would affect animal survival due to abrogated energy homeostasis. Here, lower basal levels of HDL would be directly linked to low liver lipids during starvation, since HDL acts as a scavenger system for peripheral lipids. Of course, we could not have tested similar starvation conditions in other organisms; however, detection of low basal levels of FAM134B-2 expression in human and rat tissues is an indicator of similar functional roles in these species (Figure 35).

These intriguing results urged us to further investigate metabolic changes of starvation in liver at transcriptome level. Initial principle component analysis clearly shows that absence of *Fam134b* does not fundamentally alters transcriptomics of the liver (Figure 38). As expected, starvation dramatically changes the transcriptome of both wild type and mutant groups, in

which energy homeostasis related metabolic processes are primarily involved. When wild type and mutant groups of *ad libitum* and starvation groups were analyzed for differential expression, we obtained less than 50 protein coding genes. However, these genes in both *ad libitum* and starvation group have clustered under functional annotation groups, which are primarily having roles in energy metabolism and lipid processing. Furthermore, Gene Ontology (GO) terms and KEGG pathways have revealed possible implications in cholesterol synthesis and metabolism. Among the affected genes, *Fdps*[121], *Idi1*[122] and *Sqle*[123] were upregulated upon *Fam134b* deletion and are known to be rate limiting enzymes in cholesterol biosynthesis. *Pcsk9* gene, which is upregulated in starved mutant group, is also known to be a critical gene having role in controlling serum LDL levels. Its increase was associated with decreased LDL uptake by the liver, thereby increasing serum LDL levels[124,125]. The reason why we have not detected any changes of LDL in starved mutant mice, could be attributed to global effect of starvation which already depletes these particles from circulation. In addition, slight increase of *Pcsk9* in mutant animals might affect the liver uptake of LDL particles thereby reducing total liver cholesterol, which concordant with decreased natural lipid content of mutant liver.

Of course, the affected genes related with lipid metabolism are not limited with those described above. There are other genes involved in lipid synthesis such as *Me1*, *Acot3*, *Cyp4a31* and *Thrsp*; and genes involved in cholesterol mechanisms such as *Stard4*, *Msmo1*, *Cyp51*, *Insig1*, *Pltp* and *Apoa4*. Mouse *Cyp4a31* is ortholog of human CYP4A22 which is primarily found in endoplasmic reticulum and extracellular space, and is hypothesized to catalyze omega hydroxylation of fatty acids[126]. Although its primary role is still unclear, increase in *Fam134b* absence could be interpreted as increased responsiveness to extracellular lipids in liver.

Mouse *Cyp51* is an ortholog of human CYP51A1, which is primarily localize to endoplasmic reticulum and catalyzes removal of 14α-methyl group from lanosterol, which is necessary for cholesterol synthesis[127]. Furthermore, its expression has been found to be stimulated during cholesterol insufficiency. Therefore, increased *Cyp51* expression in animals strongly suggests that there is a slight cholesterol insufficiency in starved *Fam134b* mutant mice. This can further be supported by the early depletion of lipid droplets in mutant mouse during starvation.

Among the genes significantly altered in livers of *ad libitum* fed *Fam134b* knockout animals was *Me1*(Malic Enzyme1). Malic Enzyme 1 (*Me1*) is known to convert Malate into pyruvate and NADPH through pentose phosphate pathway, products of which are used for fatty

acid synthesis[128,129]. In these reports, *Me1* upregulation was associated either with diets containing high carbohydrate, low fat and/or thyroxine hormone. Treating animals with starvation or high fat diet, on the other hand, dramatically decrease this enzyme. Therefore, *Fam134b* deletion would have an indirect impact on either increased energy flow to liver (most likely as glucose) or decreased lipid synthesis, which is compensated by increase of *Me1* enzyme.

Human *THRSP* was previously shown as a partner of Throid hormone receptor both as positive and negative regulator. More importantly, this regulation has been shown to affect malic enzyme levels in tissues[130]. In mouse, *Thrsp* levels were upregulated in mutant starved mice, but *Me1* levels remained unchanged in same conditions, which is discordant with this information. This could be partially explained by the results that in basal conditions *Me1* levels were significantly higher in mutant mice and starvation decreased its level to near-basal levels, possibly due to increased *Thrsp* levels in starved animals.

Although there is no ortholog of mouse *Acot3* gene in human, ACOTs (Acyl Coenzyme Tioesterases) represent a set of genes which are involved in recycling fatty acid from fatty acyl CoA into free Fatty acids and Coenzyme A primarily in mitochondria and peroxisomes[131]. Even though the role of these enzymes is still not well understood, increased *Acot3* activation in *Fam134b* mutant mice could possibly be a compensatory mechanism to maintain intracellular free fatty acid in certain levels.

PLTP protein has previously been associated with phospholipid transfer from VLDL to HDL molecules, and its over expression was shown to decrease HDL levels[132]. In addition, deletion of *Pltp* resulted in destabilized atherosclerotic plaques[133]. Therefore, increased *Pltp* levels in mutant mouse liver strongly implies an association with decreased serum HDL levels in mutant mice fed *ad libitum*.

Insig1 is known to be located on endoplasmic reticulum and forms a complex along with CREBP and SCAP proteins. In response to cholesterol deficiency, CREBP is processed in Golgi for nuclear localization and initiates transcription of cholesterol synthesis genes, as well as *Insig1* for inducing a negative feedback loop to suppress CREBP function after cholesterol levels are recovered [134]. *Insig1* expression is stimulated in starved mutant mice which indicates a cellular response to lack of cholesterol.

Among these genes, *Apoa4* decrease in mutant mice fed *ad libitum* is of particular importance, since this gene has been defined as a critical component of HDL particles[135]. Here,

it is important to state that *Apoa4* has been shown to be component of HDL only in rodents. In human, however, APOA4 is prominently produced in intestines upon digestion and plays important role in forming VLDL particles[136].

There are of course other significantly altered genes worth investigating in the perspective of ER-phagy and *Fam134b*. However, since most of them are less efficiently clustered in gene ontology terms, the regarding interpretation will be left for future research.

FAM134B in ER-Stress response

The ER localization of FAM134B and its function as organelle specific autophagy receptor urged us to research its possible roles in ER-stress. Induction of ER stress has been shown to activate autophagy machinery[137] and induction of ER-phagy has been associated with ER stress recovery[33]. In line with this, regardless of their FAM134B-1 expression levels, cells treated with thapsigargin exhibited stimulation of autophagy cascade, even stronger in prolonged treatments, as shown by LC3B levels Figure 42 and Figure 43). Similar effect has been shown in TM treated cells (Figure 44). TG induced FAM134B-1 accumulation in cells ectopically expressing FAM134B-1 but not in ancestral cells strongly suggest an abrogated lysosomal degradation mechanism rather than expressional induction of FAM134B.

Under same TG conditions, we performed immunofluorescence experiments and critically observed that FAM134B-1 accumulates in the form of large vesicles inside the cells, excluding CNX protein, at 2 hours of TG treatment. This was followed by increase in more diffuse FAM134B-1 signal along with the loss of FAM134B-1 coated vesicles (Figure 46 and 47). In many ER-phagy papers, selectively fragmented cargo has been demonstrated as immunofluorescence staining of receptor as punctae, which is surrounded by lysosomal markers such as LAMP1 as small circles. This canonical notion briefly describes that autophagy receptors, along with their specific cargo, is subjected to degradation via lysosomal enzymes. However, TG treated HepG2-FAM134B-1 cells show large vesicles instead of punctae, implying a mechanism regarding FAM134-1 mediated vesicle formation. Even if this explains the results of 2h of TG treatment, it is still to be explained why FAM134B-1 keeps accumulating after 2h of treatment into ER like structures but not as vesicles. One possible explanation could be returning of FAM134B-1 vesicles back to ER sheets or tubules after their function as vesicle was completed.

Resolving of ER-stress is essential for cell viability, such that, unresolved ER-stress eventually leads to cellular death[138]. Indeed, 24 hours treatment of TG induced cellular death starting from 16 hours, shown by cleaved PARP (Figure 42 and 43). However, FAM134B-1 expressing cells exhibited slightly lower PARP cleavage, suggesting a role in ER-stress resolution. The reason why we observe only little difference between two conditions could be due to constant TG treatment. Sec62, a component of translocon complex for example, has been demonstrated to act in ER resolution after cells were treated with ER stress agent cyclopiazonic acid (CPA), a mild SERCA blocker, for 12 hours followed by removal of the reagent[33].

In contrast with the cells ectopically expressing FAM134B-1, cells endogenously expressing FAM134B exhibited increased levels of protein at 8 hours, which is followed by a decrease during extended TG treatment. At 24h of treatment, FAM134B-1 levels were even lower than the untreated cells. Gradual decrease of FAM134B-1 in these cells could be a result of cellular response to TG possibly by degrading ER fragments via FAM134B mediated autophagy. This clearly indicates that FAM134B has a critical role in relieving ER-stress, possibly by degrading ER fragments loaded with unfolded proteins.

Obviously, endogenously and ectopically expressed FAM134B-1 exhibits different behavior in a response to TG treatment. Despite having been demonstrated as stimulator of autophagy, TG has been previously shown to block autophagy[139] by preventing recruitment of Rab7 decorated endosomes to autophagosomes. This clearly contradicted with the slight increase followed by a decrease of FAM134B-1 in endogenously expressing cells. On the other hand, both conditions exhibited increased LC3B response which indicates autophagy stimulation. One possible explanation for this contradiction is that, in both condition, autophagy machinery could be activated; but, in ectopic expression, due to increased load of FAM134B-1, ER might be fragmented and transferred to other type of cellular vesicles (e.g. endosomes) instead of lysosomes. A similar notion was previously proposed in a study, which elaborates detachment of FAM134B-1 coated vesicles from ER and fusion with endolysosomes[29]. Although the FAM134B-1 lead cargo stemmed from ER is lysed through lysosomal enzymes in endolysosomes, FAM134B-1 might be protected from this degradation due to its localization at outer leaflet of the vesicle, facing towards the cytosol.

Cellular response to TM (Tunicamycin) induced ER-stress in FAM134B expressing cells were apparently different than TG induced response, which clearly shows that FAM134B differentially responds to stress stimuli depending on the ER stress agent. First of all, FAM134B

did not further accumulate as a response to TM treatment in HepG2 cells, which shows that, at least in part, FAM134B-1 decorated endoplasmic reticulum turnover is not disrupted by TM as is by TG.

Although LC3BII/LC3BI ratio seems to decrease in prolonged TM treatment, both LC3B variants were accumulated suggesting the induction of core autophagy machinery[106]. However, during the treatment, both variants of LC3B accumulation was always much lower in FAM134B expressed cells treated with TM. Of course, this could be interpreted as decreased autophagy flux. However, it is also possible that enhanced FAM134B expression would alleviate the stress load on endoplasmic reticulum, thereby autophagy machinery, simply by acting as an ER-phagy receptor (Figure 48, 49 and 73). This is further supported by western blot data of prolonged TM treatment, which clearly indicates that FAM134B overexpression fails to alleviate LC3B accumulation.

In order to observe the behavior of FAM134B variants in a more complex systems, we performed mouse oriented *in vivo* studies. We picked Tunicamycin as ER insulting agent for mice, because it had been intensively studied for in vivo ER stress studies and many transcriptome data were available at GEO. Furthermore, TM had been shown to induce ER stress in liver and mediates steatosis. We also picked dexamethasone as another agent, since dexamethasone is a potent agonist of cortisol which is known to directly act on energy metabolism and liver lipid composition[88,140]. Therefore, we extracted GEO dataset in which FAM134B is induced as a response to 24h DEX treatment (Figure 50) [89].

TM treatment of mouse liver has shown that, induction of ER-stress for 24 hours in liver was responded by increase in FAM134B-2 but not FAM134B-1. Although it is tempting to acknowledge this data as a direct result of ER stress, we cannot rule out the possibility that FAM134B accumulation could be mere result of temporary steatosis caused by tunicamycin[141]. However, in either case, protein level of FAM134B-2 is enhanced in response to cellular stress. For DEX treatment, increase of FAM134B in homozygous wild type but not in hemizygous animals might be difficult to interpret due to low number of animals in groups.

Proteasome machinery plays critical role in ER homeostasis, particularly during ER Associated Protein Degradation (ERAD) of [149], in which ER resident proteins are retro-translocated to cytosol and degraded by proteasome machinery. Effect of bortezomib in FAM134B cells might be partially rescued due to re-direction of degradation pathway into autophagosome associated mechanism where ER proteins are also degraded. However, western

blot results have shown that FAM134B overexpression of either isoform resulted in further FAM134B accumulation, but decreased LC3B induction (Figure 62). Cells not expressing FAM134B, on the other hand, exhibited strong accumulation of LC3BI, and to a lesser extent, LC3BII, suggesting an enhanced stimulation of autophagy. On the other hand, since Bortezomib is known to inhibit autophagy machinery by a mechanism, which was only partially explained, this accumulation can also be attributed to blocked autophagy[150]. In either case, autophagy flux seemed to be relieved by the presence of FAM134B isoforms. During the progress, degradation of FAM134B in the autophagolysosomes are less likely, because its expression is further increased in the presence of BZ, which was not observed in Empty (T-Rex only) or Dox- cells. Then, how does FAM134B relieves the induction of autophagy? One plausible explanation is fragmentation of FAM134B coated ER vesicles without help of LC3B and its fusion with endo-lysosomes, which was previously reported for ATZ-polymer filled ER fragments[29]. In this scenario, FAM134B is not directly engulfed, therefore, does not remain and degrade inside the autophagosomes. Of course, this hypothesis needs to be tested by other experimental set ups such as immunofluorescence and co-immunoprecipitation.

Taken together, both FAM134B isoforms are apparently involved in ER stress response. Cells take advantage of FAM134B expression in order to cope with ER stress with a mechanism yet to be understood. The outline describing the role of FAM134B in ER stress is shown in Figure 73.

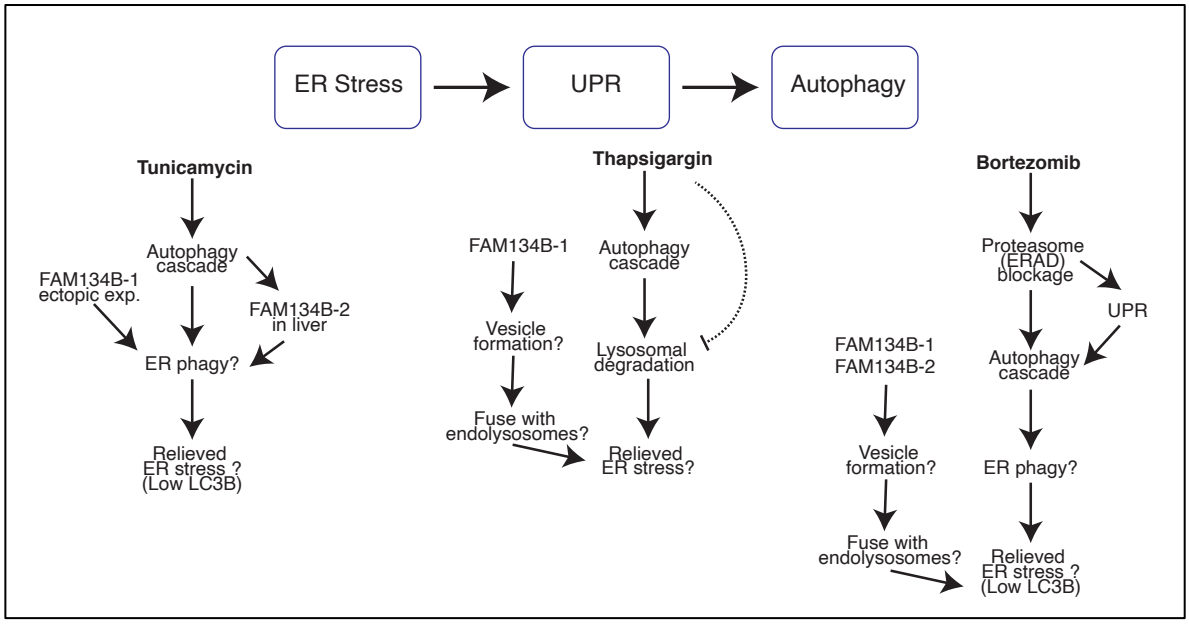


Figure 73: Both FAM134B-1 and FAM134B-2 are possible actors in alleviating ER stress

Activation of autophagy pathway is one of the outcomes of ER-stress induced unfolded protein response. Although three ER stress agents act through different mechanisms, autophagy flux marker LC3B is somewhat negatively affected in all conditions.

5.2 FAM134B in cancer

Earliest data regarding the significance of FAM134B in hepatocellular carcinoma has come with microarray analyses of carcinogenesis progression from cirrhotic liver to hepatocellular carcinoma[6]. Its decrease during carcinogenesis strongly suggests a tumor suppressive role, which were further supported by various research papers[64–66,68,142]. Therefore, with the aforementioned implications in physiology, we revisited the role of FAM134B in liver cancer.

We started our research by investigating public datasets in order to verify expression of FAM134B in various tumors, including Hepatocellular Carcinoma. TCGA Splicing Variant Database (TSVdb) harbors RNA-sequencing data obtained from massive tumor archive at isoform level. First of all, expression levels in both normal and tumor tissues have shown that FAM134B-2 is the dominant isoform in most of the normal tissues, and tend to decrease during carcinogenesis (Figure 51). This clearly demonstrates that the decreased transcript levels during hepatocellular carcinoma development is largely due to FAM134B-2 isoform levels. Even though colon (COAD), lung squamous (LUSC) and lung adenocarcinoma (LUAD) tissues showed similar pattern, Stomach (STAD) and Kidney (KICH) samples expressed increased FAM134B-1 and FAM134B-2 levels. This obviously contradicts the role of FAM134B as a tumor suppressor, which was also shown for Esophageal Squamous Cell Carcinoma (ESCC) in the literature[59,143]. FAM134B-2 specific decrease in Hepatocellular Carcinoma has also been shown by RT-PCR experiments performed on patient samples.

We further investigated the phenotypic effect of FAM134B expression in cancer using colony formation and cell proliferation assays. FAM134B-1 ectopic expression did not enhance colony forming capacity of HepG2 cells. However, proliferation assays performed by SRB has yielded slightly repressed growth rate of FAM134B-1 expressing cells. Although similar trend was observed in Hep3B-FAM134B-2 cells, data contradiction between inducible and stable cell lines might indicate experimental errors or cell colony specific behavior of the expressed gene. Of course, these *in vitro* data were not central for the original design of the experiment,

therefore, need to be further validated by other methods such as flow cytometry analysis of BrdU labeled cells in order to accurately measure proliferation rates.

Effects of FAM134B on tumor growth were further investigated by *in vivo* tumor xenograft experiments. Tumor forming potential of Hep3B cells expressing either isoform clearly demonstrated a tumor suppressive role, at least in part, for hepatocellular carcinoma. On the contrary, FAM134B has been previously associated with increased tumor rates in hepatocellular carcinoma cell line derived xenografts[60]. This obvious contradiction can be addressed by two major explanations: 1- In the reference paper, decreased tumor growth of sh-FAM134B cells used for xenograft experiments HLF cells, which exhibits mesenchymal-like characteristics[144]. As described above, FAM134B-1 is endogenously expressed in mesenchymal-like cell lines and its downregulation in these cell lines severely disrupts cell proliferation[49]. Therefore, it is likely that FAM134B expression behaves differently in epithelial like cells than mesenchymal like cells. 2- Tumor growth upon ectopic FAM134B expression had been demonstrated with Bel-7402 cell line. However, this cell line was accepted as a problematic model, since it was reported as possibly contaminated with other cell lines[145], which would deeply affect the cell phenotype and interpretation of data.

As mentioned above, inhibition of *in vivo* tumor growth, which was not clearly supported by *in vitro* experiments, has demonstrated the importance of tumor microenvironment. This notion was shown by decreased inflammation marker in mouse stroma cells in Hep3B-FAM134B-1 xenografts. On the perspective of ER-phagy, FAM134B-1 might involve in this process by sequestering pro-inflammatory chemokines before secretion, which prevents mouse stroma from synthesizing inflammatory cytokines such as IL6 and TNF-α before releasing into extracellular space.

By nature, *in vivo* tumor development occurs under various stress factors such as hypoxia, lack of nutrient and inflammation. Since the protein folding environment is extremely delicate, these conditions easily disrupt ER homeostasis and results in ER-stress. As much as these conditions seems to lead troublesome cancer cells to undergo apoptosis, constantly activated UPR helps cancer cells adapt and survive in hostile a surrounding[146].

Next, we investigated the survival of HCC cell lines against various ER-stress inducing agents and chemotherapeutics via SRB evaluation experiments in order to observe the effect of ectopic FAM134B expression. In all treatment conditions except DTT, overexpression of both variants slightly increased survival at 72h of treatment. In particular, TM results further

supported the previously stated western blot results, where FAM134B overexpression was shown to relieve autophagy flux (Figure 61). However, care must be taken when interpreting the result since at 48- and 72 hours, smallest dose of TM resulted in sudden drop of cell survival in both conditions, which could be misleading. Therefore, further experimentation with intermediary doses is required for tunicamycin. Although DTT treatment on FAM134B expressing cells exhibited slight decrease in cell survival, relatively poor curve fitness might cause some interpretation mistakes. Both Sorafenib and Bortezomib are known to induce ER stress via different mechanisms[147,148], and their use as insulting agent resulted in increased cell survival in FAM134B expressed cells. However, curve fitness of Sorafenib in cells not expressing FAM134B was also poor which could also be misleading (

Figure 60). Cells treated with Bortezomib, on the other hand, exhibited slight but consistent resistance.

Patient mortality from cancer is not a mere result of uncontrolled proliferation of tumor cells, but rather, gaining new set of skills allowing them to travel distant tissues, which is called metastasis. This new phenotype of tumor cells is usually acquired through the process called Epithelial to Mesenchymal Transition (EMT), and the process is reversed when cells need to settle down in a favorable niche (MET)[151]. We, therefore, investigated the behavior of FAM134B variants in a designated epithelial-like cell line NMuMG, which acquire mesenchymal phenotype by TGF-β treatment and return to original epithelial-like phenotype simply by removing of TGF-β[152]. Sharp decrease of FAM134B-2 upon TGF-β treatment followed by increase upon TGF-β removal strongly suggest that FAM134B-2, but not full length FAM134B-1, is less compatible with mesenchymal phenotype (Figure 74). Although the underlying reason needs to be delineated by further research, we speculate that EMT-Associated Secretory Phenotype[153] (EASP) would require special arrangement of endoplasmic reticulum state which would be intervened by expression of short FAM134B-2 isoform. Of course, we should carefully interpret these results, since FAM134B-2 is also detected in mesenchymal like cells such as FOCUS and, to a lesser extent, Mahlavu.

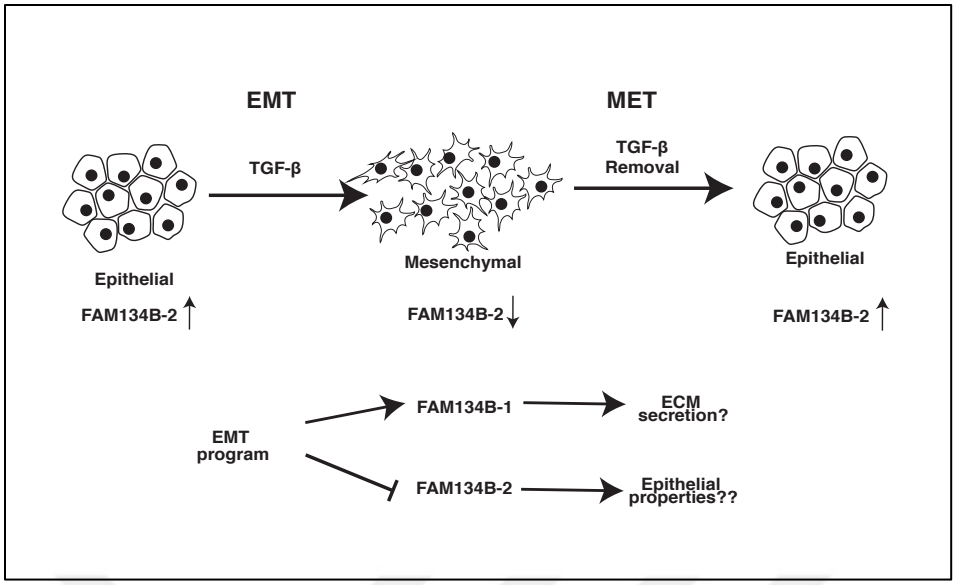


Figure 74: Mesenchymal transition is compatible with FAM134B-1 but not FAM134B-2

During the course of carcinogenesis, hepatocyte specific markers are usually altered due to reprogramming of the transformed cells. Some of these markers are proteins secreted into extracellular space or displayed on cell surface. But first, these proteins are processed through endoplasmic reticulum for proper protein folding. Since FAM134B variants had been shown to fine tune quality of some secreted proteins (e.g. APOIIIC[77]), we screened FAM134B expressing cells for their expression status of hepatocyte and liver progenitor cell markers. At basal conditions, pronounced expression of AFP, ALB, A1AT and EpCAM in Hep3B-FAM134B-FLAG cells (Figure 64) suggested acquisition of both hepatocyte-like and progenitor-like phenotype thanks to FAM134B-1, and to a lesser extent, FAM134B-2[154]. This result is obviously contradicting with existing literature, where liver associated Albumin was shown to be degraded in the presence of *Fam134b*[77]. Furthermore, the question regarding how a protein, which is known to target fragments for lysosomal degradation, would favor the cells to accumulate such proteins? One possible answer is that FAM134B variants might affect the maturation of secreted/displayed protein, thereby causing their retention inside the cell in a similar way how procollagen secretion is controlled[18]. Another explanation could be clonality of the stable cell lines; cell clones subjected to experimentation might have been selected as a lineage from differentiated/marginal subset of Hep3B cell line, which resulted in increased marker expression regardless of FAM134B expression. Of course, we tried to eliminate this

possibility by repeating experiment in Hep3B cells inducibly expressing FAM134B isoforms (Figure 65). Prolonged culture of cells under FAM134B expression showed fluctuating levels of Albumin which supports the data retrieved from stable cell line (Figure 64). However, there is still a possibility that the fluctuation of ALB expression is due to changes in dominating cell types in culture conditions when cells are repeatedly passanged. Even though cells are considered to be derived from single cell, cellular plasticity might rearrange cellular phenotype in group of cells.

Finally, we have tested the tumoroid formation potential of FAM134B expressing Hep3B cells (Figure 66). Although there was no striking difference between Dox+ and Dox- groups in terms of capability to form organoids, cytosols of Dox+ groups exhibited slightly higher eosin staining which could be attributed to a different cytosolic composition. As mentioned in *in vivo* starvation experiments, energy reserves such as lipids might affect staining pattern of these cells. Of course, further experimentation of immunostaining and western blot experiments are necessary to reveal molecular response of the cells especially under elevated FAM134B expression.

6 CONCLUSION & FUTURE PERSPECTIVES

First, we have characterized the transcript variants of *FAM134B* in human, bovine and mouse. We clearly showed that FAM134B has at least two major isoforms: long (FAM134B-1) and short (FAM134B-2). Differing from the human and bovine FAM134B, mouse *Fam134b* was shown to express at least six isoforms, all of which is controlled supposedly by different regulatory elements. FAM134B-2, lacks N-terminal hydrophobic tail as well as TM12 transmembrane structure. These isoform variants were also shown to be differentially regulated as shown in human GTEx data and experimental results of bovine and mouse samples. According to these results, muscle and heart exhibits the highest expression profile of FAM134B-2; while long isoform, FAM134B-1 is expressed in brain, adipose and testis tissue in addition to peripheric nerves[16]. For deeper understanding of the gene structure and function of FAM134B, further experimentation is required to characterize transcriptional control of FAM134B variants. Moreover, it would be extremely helpful to perform a comprehensive interactome analysis of FAM134B variants through mass spectrometry. This would expose all possible interactors of protein and give detailed implications about how these two proteins differ in terms of function. Grumati et al. has performed a comprehensive proteomics analysis on full length FAM134B [32]. This would be an excellent starting point since they have shown that FAM134B is also in contact with various other molecules localized in different structures such as microtubule and mitochondria.

In addition to its well-known localization in ER, both FAM134B isoforms clearly translocate to the Golgi apparatus. Although CNX had been shown as a functional partner of FAM134B, we found that FAM134B-2 does not directly interact with CNX under basal conditions. Although the localization of FAM134B and its variants were associated either with ER or Golgi, its association with other free vesicles shuttling between different endomembrane system would greatly help us gain further insights.

Early functional *in vitro* studies have clearly shown that FAM134B-1 is almost peculiar to mesenchymal-like cells, which mostly exhibits fibroblast-like characteristics. Similarly, even *de facto* fibroblasts, MEFs, exhibited FAM134B-1 as predominant isoform. On the other hand, FAM134B-2 was not clearly segregated with a certain cell type, since both

epithelial- and mesenchymal-like cells exhibited low levels of FAM134B-2. Although we could not associate FAM134B-2 with a certain cell status, its dramatic decrease during TGF-β mediated EMT showed that FAM134B-2 is less compatible with mesenchymal-like cell state. A follow up study on discovering FAM134B-1 and FAM134B-2 regulatory elements which are controlled by transcription factors involved epithelial or mesenchymal specific would be highly helpful. Comparing the secretome of wild type and FAM134B-silenced mesenchymal cells would show important clues on how paracrine factors are affected.

In vitro induction of autophagy through nutrient starvation has shown that endogenous FAM134B isoforms tend to decrease during starvation; however, ectopically expressed FAM134B-1 resist starvation induced degradation. Moreover, ectopic FAM134B expression leads to persistence of lipidated form of LC3B (LC3BII) either through enhancing lipidation of LC3BI or decreasing its degradation. This could be best answered by blocking autophagy machinery at upstream (e.g. mTOR) in the presence of excessive FAM134B.

ER-stress induced by TG of FAM134B-1 expressing cell has exhibited non-canonical vesicle formation coated with FAM134B-1, which rapidly dissolves after 2 hours of treatment. During prolonged treatment, ectopically expressed FAM134B-1 provides a slight survival advantage to TG treated cells. Similarly, effects of both TG and TM mediated autophagy induction is somehow relieved by FAM134B expression as shown by LC3B levels. Similar effect was also observed in BZ treated cells. FAM134B-2 in liver was also shown to be responsive to TM treatment *in vivo,* possibly involving in ER-stress response. A future study examining the FAM134B regulatory elements through luciferase-based assay would be important to determine selective responsiveness of *FAM134B* gene promoters to ER-stress stimulators. However, such experiments should be designed in accordance with previous reports, such that, cells should be only briefly treated with ER-stress agent and should be observed during recovery phase[33].

In vivo functional studies have shown that *Fam134b*$^{-/-}$ has no gross phenotype even in aged animals in both sexes. Although organ weights did not exhibit any gross change, mutant mice slightly resisted body weight loss after 36h nutrient starvation. This was further supported with disrupted amino acid release in mutant animals. Therefore, absence of *Fam134b* in clearly alters peripheric autophagy response. Transcriptome analyses along with disrupted HDL levels indicates slightly disrupted cholesterol and lipid synthesis. Significant increase of serum a-amylase in starved mutants also indicates that FAM134B-2, a predominant form in pancreas,

fine tunes the exocrine function. Transmission electron microscopy approach for different *Fam134b* knockout mouse tissues under both physiological and stress conditions would reveal important cellular functions. Muscle, heart, liver, pancreas and adipose tissue would be of particular interest due to their importance in energy homeostasis and their expression profile of FAM134B isoforms.

Verifying the literature, FAM134B isoforms were found to be both tumor promoting and tumor suppressing gene, depending on the context. Ectopic expression of FAM134B variants did not cause a clear phenotype on cell proliferation *in vitro*. However, cells ectopically expressing FAM134B has clearly shown a tumor suppressor effect. Suppression of host cell specific proinflammatory factors indicates that FAM134B expression contributes not only intracellular homeostasis but also extracellular communication between tumor cells and its surroundings. The proposed mechanism for the FAM134B involvement in cancer is described in Figure 75.

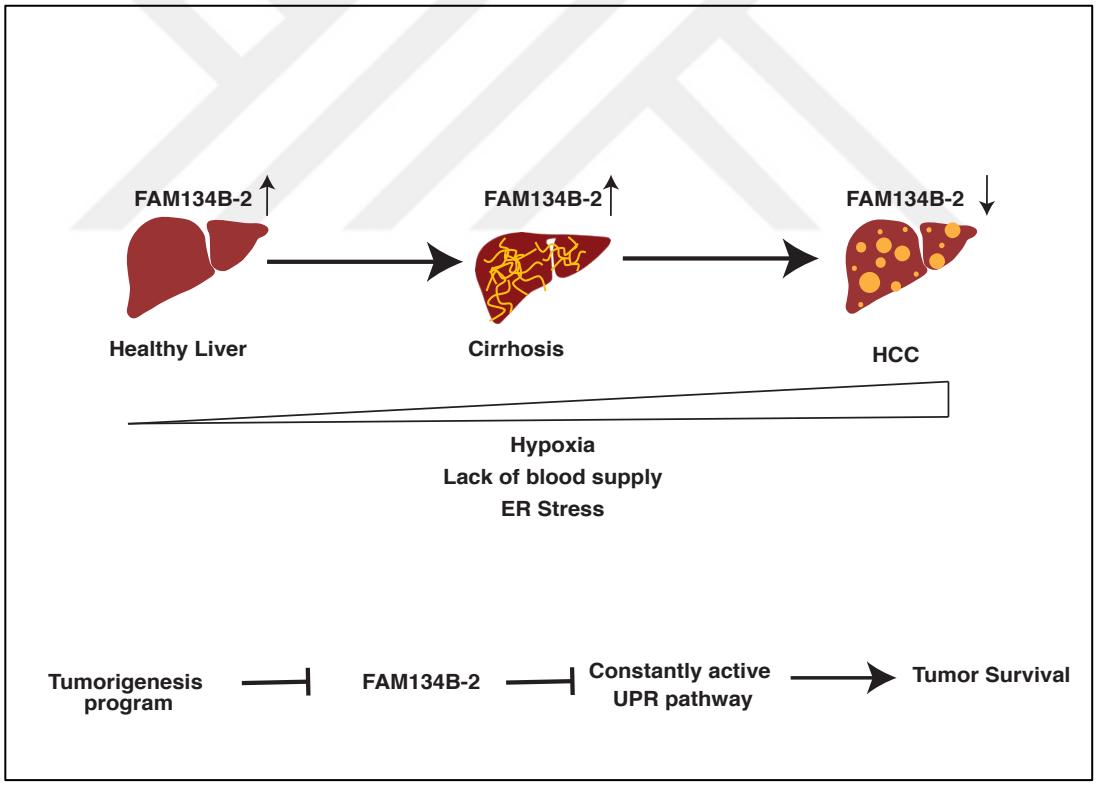


Figure 75: Proposed mechanism for FAM134B mediated tumor suppression

Hepatocellular carcinogenesis is a multistep process and usually occurs on the background of cirrhosis. As the disease progresses, tissue blood supply is mostly disrupted due to increased fibrotic scar tissue. This leads to hypoxia, lack of nutrient supply and ER stress. FAM134B-2 could be helping hepatocytes by alleviating ER-stress and suppressing constant

activation of UPR. Therefore, tumor cells might be suppressing FAM134B-2 in order to maintain UPR.

UPR is one of the factors that facilitate tumor development by helping tumor cells to cope with a challenging microenvironment. Although the direct link between UPR and FAM134B isoforms is yet to be discovered, it is likely that FAM134B presence help recover from ER-stress induced UPR. Therefore, during HCC development, an unknown mechanism shuts the expression of FAM134B down. An initial study of analyzing various UPR markers along with FAM134B expression on human or animal liver tumor samples would be informative for association of ER-phagy with ER-stress.

The past few years have been fruitful for the understanding of the molecular roles of *FAM134B,* but without defining its isoforms and their relevance in the whole organism. To our knowledge, this is the first paper to define the differential expression of *FAM134B* isoforms in various tissues under normal and starved conditions, as well as in cancer. These findings will help us further understand the functional roles of *FAM134B* isoforms in diseases such as cancer.

7 REFERENCES

1. Ferlay J, Colombet M, Soerjomataram I, et al. Estimating the global cancer incidence and mortality in 2018: GLOBOCAN sources and methods. *Int. J. Cancer*. 2019;144(8):1941–1953.
2. Ramakrishna G, Rastogi A, Trehanpati N, et al. From Cirrhosis to Hepatocellular Carcinoma: New Molecular Insights on Inflammation and Cellular Senescence. *Liver Cancer*. 2013;2(3–4):367–383.
3. Aravinthan AD, Alexander GJM. Senescence in chronic liver disease: Is the future in aging? *J. Hepatol.* 2016;65(4):825–834.
4. Mudbhary R, Hoshida Y, Chernyavskaya Y, et al. UHRF1 Overexpression Drives DNA Hypomethylation and Hepatocellular Carcinoma. *Cancer Cell*. 2014;
5. Ozturk N, Erdal E, Mumcuoglu M, et al. Reprogramming of replicative senescence in hepatocellular carcinoma-derived cells. *Proc. Natl. Acad. Sci. U. S. A.* 2006;103(7):2178–83.
6. Yildiz G, Arslan-Ergul A, Bagislar S, et al. Genome-Wide Transcriptional Reorganization Associated with Senescence-to-Immortality Switch during Human Hepatocellular Carcinogenesis. *PLoS One*. 2013;8(5):.
7. Taşdemir N. Identification and characterization of two endoplasmic reticulum protein isoforms encoded by senescence- associated fam134b gene (Mater's Thesis). Ankara: Bilkent University; 2008.
8. Kurth I, Pamminger T, Hennings JC, et al. Mutations in FAM134B, encoding a newly identified Golgi protein, cause severe sensory and autonomic neuropathy. *Nat. Genet.* 2009;41(11):1179–1181.
9. Axelrod FB, Gold-Von Simson G. Hereditary sensory and autonomic neuropathies: Types II, III, and IV. *Orphanet J. Rare Dis.* 2007;
10. Schwarz DS, Blower MD. The endoplasmic reticulum: Structure, function and response to cellular signaling. *Cell. Mol. Life Sci.* 2016;73(1):79–94.
11. Wang Y, Huang S. Golgi structure formation, function, and post-translational modifications in mammalian cells. *F1000Research*. 2017;
12. Fagone P, Jackowski S. Membrane phospholipid synthesis and endoplasmic reticulum

function. *J. Lipid Res.* 2009;50(SUPPL.):311–316.

13. Zhang H, Hu J. Shaping the Endoplasmic Reticulum into a Social Network. *Trends Cell Biol.* 2016;
14. Zhou X, He Y, Huang X, et al. Reciprocal regulation between lunapark and atlastin facilitates ER three-way junction formation. *Protein Cell*. 2019;
15. Bhaskara RM, Grumati P, Garcia-Pardo J, et al. Curvature induction and membrane remodeling by FAM134B reticulon homology domain assist selective ER-phagy. *Nat. Commun.* 2019;10(1):.
16. Khaminets A, Heinrich T, Mari M, et al. Regulation of endoplasmic reticulum turnover by selective autophagy. *Nature*. 2015;522(7556):354–358.
17. Jiang X, Wang X, Ding X, et al. FAM134B oligomerization drives endoplasmic reticulum membrane scission for ER-phagy. *EMBO J.* 2020;e102608.
18. Forrester A, De Leonibus C, Grumati P, et al. A selective ER -phagy exerts procollagen quality control via a Calnexin- FAM 134B complex . *EMBO J.* 2019;38(2):1–16.
19. Ohsumi Y. Protein turnover. *IUBMB Life*. 2006;58(5–6):363–369.
20. Lilienbaum A. Relationship between the proteasomal system and autophagy. *Int. J. Biochem. Mol. Biol.* 2013;4(1):1–26.
21. Luzio JP, Pryor PR, Bright NA. Lysosomes: Fusion and function. *Nat. Rev. Mol. Cell Biol.* 2007;8(8):622–632.
22. Yim WWY, Mizushima N. Lysosome biology in autophagy. *Cell Discov.* 2020;
23. Parzych KR, Klionsky DJ. An overview of autophagy: Morphology, mechanism, and regulation. *Antioxidants Redox Signal.* 2014;20(3):460–473.
24. Dikic I, Elazar Z. Mechanism and medical implications of mammalian autophagy. *Nat. Rev. Mol. Cell Biol.* 2018;
25. Johansen T, Lamark T. Selective Autophagy: ATG8 Family Proteins, LIR Motifs and Cargo Receptors. *J. Mol. Biol.* 2020;
26. Bolender RP, Weibel ER. A morphometric study of the removal of phenobarbital-induced membranes from hepatocytes after cessation of threatment. *J. Cell Biol.* 1973;56(3):746–61.
27. Bernales S, McDonald KL, Walter P. Autophagy counterbalances endoplasmic reticulum expansion during the unfolded protein response. *PLoS Biol.* 2006;

28. Mochida K, Oikawa Y, Kimura Y, et al. Receptor-mediated selective autophagy degrades the endoplasmic reticulum and the nucleus. *Nature*. 2015;522(7556):359–362.
29. Fregno I, Fasana E, Bergmann TJ, et al. ER -to-lysosome-associated degradation of proteasome-resistant ATZ polymers occurs via receptor-mediated vesicular transport . *EMBO J.* 2018;37(17):1–18.
30. Lennemann NJ, Coyne CB. Dengue and Zika viruses subvert reticulophagy by NS2B3-mediated cleavage of FAM134B. *Autophagy*. 2017;13(2):322–332.
31. Chino H, Mizushima N. ER-Phagy: Quality Control and Turnover of Endoplasmic Reticulum. *Trends Cell Biol.* 2020;
32. Grumati P, Morozzi G, Hölper S, et al. Full length RTN3 regulates turnover of tubular endoplasmic reticulum via selective autophagy. *Elife*. 2017;6:1–32.
33. Fumagalli F, Noack J, Bergmann TJ, et al. Translocon component Sec62 acts in endoplasmic reticulum turnover during stress recovery. *Nat. Cell Biol.* 2016;18(11):1173–1184.
34. Smith MD, Harley ME, Kemp AJ, et al. CCPG1 Is a Non-canonical Autophagy Cargo Receptor Essential for ER-Phagy and Pancreatic ER Proteostasis. *Dev. Cell*. 2018;44(2):217-232.e11.
35. Chino H, Hatta T, Natsume T, Mizushima N. Intrinsically Disordered Protein TEX264 Mediates ER-phagy. *Mol. Cell*. 2019;74(5):909-921.e6.
36. Chen Q, Xiao Y, Chai P, et al. ATL3 Is a Tubular ER-Phagy Receptor for GABARAP-Mediated Selective Autophagy. *Curr. Biol.* 2019;29(5):846-855.e6.
37. Mizushima N, Yoshimori T, Levine B. Methods in Mammalian Autophagy Research. *Cell*. 2010;
38. Cahill GF. Fuel Metabolism in Starvation. *Annu. Rev. Nutr.* 2006;26(1):1–22.
39. Ezaki J, Matsumoto N, Takeda-Ezaki M, et al. Liver autophagy contributes to the maintenance of blood glucose and amino acid levels. *Autophagy*. 2011;7(7):727–736.
40. Clinical OF. Amino Acid Metabolism of Glucone ogenesis in the Regulation. 1970;
41. The I, Bloor WR, Stoneburg A, Oleson C. Lipids of Fasting Mouse.
42. Shen Y, Ballar P, Apostolou A, Doong H, Fang S. ER stress differentially regulates the stabilities of ERAD ubiquitin ligases and their substrates. *Biochem. Biophys. Res. Commun.* 2007;

43. Fenteany G, Standaert RF, Lane WS, et al. Inhibition of proteasome activities and subunit-specific amino-terminal threonine modification by lactacystin. *Science (80-.).* 1995;
44. Sicari D, Delaunay-Moisan A, Combettes L, Chevet E, Igbaria A. A guide to assessing endoplasmic reticulum homeostasis and stress in mammalian systems. *FEBS J.* 2020;
45. Schuck S, Prinz WA, Thorn KS, Voss C, Walter P. Membrane expansion alleviates endoplasmic reticulum stress independently of the unfolded protein response. *J. Cell Biol.* 2009;187(4):525–536.
46. Hetz C. The unfolded protein response: Controlling cell fate decisions under ER stress and beyond. *Nat. Rev. Mol. Cell Biol.* 2012;13(2):89–102.
47. Bagola K, Mehnert M, Jarosch E, Sommer T. Protein dislocation from the ER. *Biochim. Biophys. Acta - Biomembr.* 2011;1808(3):925–936.
48. Song S, Tan J, Miao Y, Zhang Q. Crosstalk of ER stress-mediated autophagy and ER-phagy: Involvement of UPR and the core autophagy machinery. *J. Cell. Physiol.* 2018;233(5):3867–3874.
49. Soner D. Role of Fam134B in Liver Cancer (Mater's Thesis). Ankara: Bilkent University; 2013.
50. Yilmaz M. Characterization Of Fam134b In The Context Of Hepatocellular Carcinoma And Endoplasmic Reticulum Stress (Master's Thesis). Ankara: Bilkent University; 2011.
51. Xie N, Li Y, Wang C, et al. FAM134B Attenuates Seizure-Induced Apoptosis and Endoplasmic Reticulum Stress in Hippocampal Neurons by Promoting Autophagy. *Cell. Mol. Neurobiol.* 2020;
52. Viswanath P, Radoul M, Izquierdo-Garcia JL, et al. 2-hydroxyglutarate-mediated autophagy of the endoplasmic reticulum leads to an unusual downregulation of phospholipid biosynthesis in mutant idh1 gliomas. *Cancer Res.* 2018;
53. Liao Y, Duan B, Zhang Y, Zhang X, Xia B. Excessive ER-phagy mediated by the autophagy receptor FAM134B results in ER stress, the unfolded protein response, and cell death in HeLa cells. *J. Biol. Chem.* 2019;294(52):20009–20023.
54. Bray F, Ferlay J, Soerjomataram I, et al. Global cancer statistics 2018: GLOBOCAN estimates of incidence and mortality worldwide for 36 cancers in 185 countries. *CA. Cancer J. Clin.* 2018;68(6):394–424.

55. Hanahan D, Weinberg RA. Hallmarks of cancer: The next generation. *Cell*. 2011;144(5):646–674.
56. Wang M, Kaufman RJ. The impact of the endoplasmic reticulum protein-folding environment on cancer development. *Nat. Rev. Cancer*. 2014;14(9):581–597.
57. Tang WK, Chui CH, Fatima S, et al. Oncogenic properties of a novel gene JK-1 located in chromosome 5p and its overexpression in human esophageal squamous cell carcinoma. *Int. J. Mol. Med.* 2007;19(6):915–923.
58. Fatima S, Chui CH, Tang WK, et al. Transforming capacity of two novel genes JS-1 and JS-2 located in chromosome 5p and their overexpression in human esophageal squamous cell carcinoma. *Int. J. Mol. Med.* 2006;
59. Islam F, Gopalan V, Law S, Tang JC on, Lam AK yin. FAM134B promotes esophageal squamous cell carcinoma in vitro and its correlations with clinicopathologic features. *Hum. Pathol.* 2019;87:1–10.
60. Zhang Z qi, Chen J, Huang W qiu, et al. FAM134B induces tumorigenesis and epithelial-to-mesenchymal transition via Akt signaling in hepatocellular carcinoma. *Mol. Oncol.* 2019;13(4):792–810.
61. Kasem K, Gopalan V, Salajegheh A, et al. JK1 (FAM134B) gene and colorectal cancer: A pilot study on the gene copy number alterations and correlations with clinicopathological parameters. *Exp. Mol. Pathol.* 2014;
62. Kasem K, Gopalan V, Salajegheh A, et al. The roles of JK-1 (FAM134B) expressions in colorectal cancer. *Exp. Cell Res.* 2014;
63. Islam F, Gopalan V, Wahab R, et al. Novel FAM134B mutations and their clinicopathological significance in colorectal cancer. *Hum. Genet.* 2017;
64. Kasem K, Sullivan E, Gopalan V, et al. JK1 (FAM134B) represses cell migration in colon cancer: A functional study of a novel gene. *Exp. Mol. Pathol.* 2014;
65. Islam F, Gopalan V, Wahab R, et al. Stage dependent expression and tumor suppressive function of FAM134B (JK1) in colon cancer. *Mol. Carcinog.* 2017;56(1):238–249.
66. Islam F, Gopalan V, Pillai S, et al. Promoter hypermethylation inactivate tumor suppressor FAM134B and is associated with poor prognosis in colorectal cancer. *Genes Chromosom. Cancer*. 2018;
67. Islam F, Gopalan V, Vider J, Lu C tai, Lam AKY. MiR-142-5p act as an oncogenic

microRNA in colorectal cancer: Clinicopathological and functional insights. *Exp. Mol. Pathol.* 2018;104(1):98–107.

68. Islam F, Gopalan V, Vider J, et al. MicroRNA-186-5p overexpression modulates colon cancer growth by repressing the expression of the FAM134B tumour inhibitor. *Exp. Cell Res.* 2017;
69. Islam F, Haque MH, Yadav S, et al. An electrochemical method for sensitive and rapid detection of FAM134B protein in colon cancer samples. *Sci. Rep.* 2017;
70. Boriachek K, Islam MN, Gopalan V, et al. Quantum dot-based sensitive detection of disease specific exosome in serum. *Analyst*. 2017;142(12):2211–2219.
71. Haque MH, Gopalan V, Chan KW, et al. Identification of Novel FAM134B (JK1) Mutations in Oesophageal Squamous Cell Carcinoma. *Sci. Rep.* 2016;6:1–11.
72. Yuzugullu H, Benhaj K, Ozturk N, et al. Canonical Wnt signaling is antagonized by noncanonical Wnt5a in hepatocellular carcinoma cells. *Mol. Cancer*. 2009;8:90.
73. Cai M, Liu Q, Jiang Q, et al. Loss of m 6 A on FAM134B promotes adipogenesis in porcine adipocytes through m 6 A-YTHDF2-dependent way. *IUBMB Life*. 2019;71(5):580–586.
74. Yuan Z, Song D, Wang Y. The novel gene pFAM134B positively regulates fat deposition in the subcutaneous fat of Sus scrofa. *Biochem. Biophys. Res. Commun.* 2014;454(4):554–559.
75. Cai M, Chen J, Yu C, et al. FAM134B promotes adipogenesis by increasing vesicular activity in porcine and 3T3-L1 adipocytes. 2018;(866):1–10.
76. Cai M, Zhao J, Liu Q, Wang X, Wang Y. FAM134B improves preadipocytes differentiation by enhancing mitophagy. *Biochim. Biophys. Acta - Mol. Cell Biol. Lipids*. 2019;1864(12):.
77. Kohno S, Shiozaki Y, Keenan AL, Miyazaki-Anzai S, Miyazaki M. An N-terminal-truncated isoform of FAM134B (FAM134B-2) regulates starvation-induced hepatic selective ER-phagy. *Life Sci. Alliance*. 2019;2(3):1–13.
78. Gangalum RK, Horwitz J, Kohan SA, Bhat SP. αA-crystallin and αB-crystallin reside in separate subcellular compartments in the developing ocular lens. *J. Biol. Chem.* 2012;287(50):42407–42416.
79. Mehlem A, Hagberg CE, Muhl L, Eriksson U, Falkevall A. Imaging of neutral lipids by oil red O for analyzing the metabolic status in health and disease. *Nat. Protoc.*

2013;8(6):1149–1154.

80. Ardlie KG, DeLuca DS, Segrè A V., et al. The Genotype-Tissue Expression (GTEx) pilot analysis: Multitissue gene regulation in humans. *Science (80-.).* 2015;348(6235):648–660.
81. Sun W, Duan T, Ye P, et al. TSVdb: A web-tool for TCGA splicing variants analysis. *BMC Genomics*. 2018;19(1):1–7.
82. Khaminets A, Heinrich T, Mari M, et al. Regulation of endoplasmic reticulum turnover by selective autophagy. *Nature*. 2015;522(7556):354–358.
83. Kurth I, Pamminger T, Hennings JC, et al. Mutations in FAM134B, encoding a newly identified Golgi protein, cause severe sensory and autonomic neuropathy. *Nat. Genet.* 2009;41(11):1179–1181.
84. Thastrup O, Cullen PJ, Drobak BK, Hanley MR, Dawson AP. Thapsigargin, a tumor promoter, discharges intracellular Ca2+ stores by specific inhibition of the endoplasmic reticulum Ca2+-ATPase. *Proc. Natl. Acad. Sci. U. S. A.* 1990;87(7):2466–2470.
85. Oliver FJ, De La Rubia G, Rolli V, et al. Importance of poly(ADP-ribose) polymerase and its cleavage in apoptosis: Lesson from an uncleavable mutant. *J. Biol. Chem.* 1998;
86. Feng B, Huang X, Jiang D, et al. Endoplasmic reticulum stress inducer tunicamycin alters hepatic energy homeostasis in mice. *Int. J. Mol. Sci.* 2017;18(8):.
87. Brenner RR, Ayala S, Garda HA. Effect of dexamethasone on the fatty acid composition of total liver microsomal lipids and phosphatidylcholine molecular species. *Lipids*. 2001;36(12):1337–1345.
88. Cole TG, Wilcox HG, Heimberg M. Effects of adrenalectomy and dexamethasone on hepatic lipid metabolism. *J. Lipid Res.* 1982;23(1):81–91.
89. Duma D, Collins JB, Chou JW, Cidlowski JA. Sexually dimorphic actions of glucocorticoids provide a link to inflammatory diseases with gender differences in prevalence. *Sci. Signal.* 2010;3(143):1–11.
90. Zhang S, Yang X, Wang L, Zhang C. Interplay between inflammatory tumor microenvironment and cancer stem cells (Review). *Oncol. Lett.* 2018;16(1):679–686.
91. Kohno S, Shiozaki Y, Keenan AL, Miyazaki-Anzai S, Miyazaki M. An N-terminal-truncated isoform of FAM134B (FAM134B-2) regulates starvation-induced hepatic selective ER-phagy. *Life Sci. Alliance*. 2019;2(3):1–13.
92. Copur MS. Sorafenib in advanced hepatocellular carcinoma [3]. *N. Engl. J. Med.*

2008;359(23):2498.

93. Boccadoro M, Morgan G, Cavenagh J. Preclinical evaluation of the proteasome inhbitor bortezomib in cancer therapy. *Cancer Cell Int.* 2005;5:1–9.
94. Thanaraj TA, Clark F, Muilu J. Conservation of human alternative splice events in mouse. *Nucleic Acids Res.* 2003;31(10):2544–2552.
95. Brudno M, Poliakov A, Salamov A, et al. Automated whole-genome multiple alignment of rat, mouse, and human. *Genome Res.* 2004;14(4):685–692.
96. Yamanaka T, Nukina N. ER dynamics and derangement in neurological diseases. *Front. Neurosci.* 2018;12(FEB):1–7.
97. Yuan Z, Song D, Wang Y. The novel gene pFAM134B positively regulates fat deposition in the subcutaneous fat of Sus scrofa. *Biochem. Biophys. Res. Commun.* 2014;454(4):554–559.
98. Marx F, Training O, Training P, et al. Molecular Biology of the Cell 6 edition by Bruce Alberts. 2014.
99. Guzel E, Arlier S, Guzeloglu-Kayisli O, et al. Endoplasmic reticulum stress and homeostasis in reproductive physiology and pathology. *Int. J. Mol. Sci.* 2017;18(4):.
100. El-Brolosy MA, Kontarakis Z, Rossi A, et al. Genetic compensation triggered by mutant mRNA degradation. *Nature*. 2019;568(7751):193–197.
101. Okazaki Y, Ohno H, Takase K, Ochiai T, Saito T. Cell surface expression of calnexin, a molecular chaperone in the endoplasmic reticulum. *J. Biol. Chem.* 2000;275(46):35751–35758.
102. Rismanchi N, Soderblom C, Stadler J, Zhu PP, Blackstone C. Atlastin GTPases are required for Golgi apparatus and ER morphogenesis. *Hum. Mol. Genet.* 2008;17(11):1591–1604.
103. Charest A, Lane K, McMahon K, Housman DE. Association of a Novel PDZ Domain-containing Peripheral Golgi Protein with the Q-SNARE (Q-soluble N-Ethylmaleimide-sensitive Fusion Protein (NSF) Attachment Protein Receptor) Protein Syntaxin 6. *J. Biol. Chem.* 2001;276(31):29456–29465.
104. Gao YS, Alvarez C, Nelson DS, Sztul E. Molecular cloning, characterization, and dynamics of rat formiminotransferase cyclodeaminase, a Golgi-associated 58-kDa protein. *J. Biol. Chem.* 1998;273(50):33825–33834.
105. Gao YS, Sztul E. A novel interaction of the Golgi complex with the vimentin

intermediate filament cytoskeleton. *J. Cell Biol.* 2001;152(5):877–893.

106. Klionsky DJ, Abdelmohsen K, Abe A, et al. Guidelines for the use and interpretation of assays for monitoring autophagy (3rd edition). *Autophagy*. 2016;
107. Zhou L, Li C, Gao L, Wang A. High-density lipoprotein synthesis and metabolism (Review). *Mol. Med. Rep.* 2015;
108. Namazi F, Omidi A, Abbasi S, et al. Starvation and refeeding in rats: Effect on some parameters of energy metabolism and electrolytes and changes of hepatic tissue. *Pesqui. Vet. Bras.* 2016;36:101–105.
109. Yamamoto J, Kamata S, Miura A, et al. Differential adaptive responses to 1- or 2-day fasting in various mouse tissues revealed by quantitative PCR analysis. *FEBS Open Bio*. 2015;5:357–368.
110. Jensen TL, Kiersgaard MK, Sørensen DB, Mikkelsen LF. Fasting of mice: A review. *Lab. Anim.* 2013;47(4):225–240.
111. Aliapoulios MA, Morain WD, Kacoyanis GP. Glucagon as a hypocalcemic and hypophosphatemic agent in the rat. *Gastroenterology*. 1973;65(6):912–918.
112. Matull WR, Pereira SP, O'Donohue JW. Biochemical markers of acute pancreatitis. *J. Clin. Pathol.* 2006;59(4):340–344.
113. Antonucci L, Fagman JB, Kim JY, et al. Basal autophagy maintains pancreatic acinar cell homeostasis and protein synthesis and prevents ER stress. *Proc. Natl. Acad. Sci. U. S. A.* 2015;112(45):E6166–E6174.
114. Heijboer AC, Donga E, Voshol PJ, et al. Sixteen hours of fasting differentially affects hepatic and muscle insulin sensitivity in mice. *J. Lipid Res.* 2005;46(3):582–588.
115. Jaromowska M. Effect of fasting on skeletal muscle triglyceride content Department of Clinical Physiology , Medical School , uL Miekiewicza 2 , 15-230 Biatystok (Poland), 15 February 1984 o Vastus deepest. 1985;41(February 1984):357–358.
116. Takagi A, Kume S, Kondo M, et al. Mammalian autophagy is essential for hepatic and renal ketogenesis during starvation. *Sci. Rep.* 2016;6(December 2015):1–9.
117. Jacob S. Lipid droplet accumulation in the heart during fasting. *Acta Histochem.* 1987;82(2):149–152.
118. Sherwood LM, Parris EE, Cahill GF. Starvation in Man. *N. Engl. J. Med.* 1970;
119. Lipoids of the fasting mouse. 1. The relation between carcass lipids and liver lipids. *Lipoids fasting mouse. 1. Relat. between carcass lipids liver lipids.* 1941;

120. Guan HP, Goldstein JL, Brown MS, Liang G. Accelerated fatty acid oxidation in muscle averts fasting-induced hepatic steatosis in SJL/J mice. *J. Biol. Chem.* 2009;284(36):24644–24652.
121. Wilkin D, Kutsunai S, Edwards P. Isolation and sequence of the human farnesyl pyrophosphate synthetase cDNA. Coordinate regulation of the mRNAs for farnesyl pyrophosphate synthetase, 3-. *J. Biol. Chem.* 1990;265(8):4607–4614.
122. Agranoff BW, Eggerer H, Henning U, Lynen F. Isopentenol pyrophosphate isomerase. *J. Am. Chem. Soc.* 1959;
123. Tai HH, Bloch K. Squalene epoxidase of rat liver. *J. Biol. Chem.* 1972;
124. Chaudhary R, Garg J, Shah N, Sumner A. PCSK9 inhibitors: A new era of lipid lowering therapy. *World J. Cardiol.* 2017;9(2):76.
125. Evison BJ, Palmer JT, Lambert G, et al. A small molecule inhibitor of PCSK9 that antagonizes LDL receptor binding via interaction with a cryptic PCSK9 binding groove. *Bioorganic Med. Chem.* 2020;28(6):115344.
126. Kawashima H, Naganuma T, Kusunose E, et al. Human fatty acid ω-hydroxylase, CYP4A11: Determination of complete genomic sequence and characterization of purified recombinant protein. *Arch. Biochem. Biophys.* 2000;378(2):333–339.
127. Strömstedt M, Rozman D, Waterman MR. The ubiquitously expressed human CYP51 encodes lanosterol 14α-demethylase, a cytochrome P450 whose expression is regulated by oxysterols. *Arch. Biochem. Biophys.* 1996;329(1):73–81.
128. WISE EM, BALL EG. Malic Enzyme and Lipogenesis. *Proc. Natl. Acad. Sci. United States*. 1964;52(1933):1255–1263.
129. TEPPERMAN HM, TEPPERMAN J. Patterns of Dietary and Hormonal Induction of Certain Nadp-Linked Liver. *Am. J. Physiol.* 1964;206:357–361.
130. Chou WY, Cheng YS, Ho CL, et al. Human spot 14 protein interacts physically and functionally with the thyroid receptor. *Biochem. Biophys. Res. Commun.* 2007;357(1):133–138.
131. Westin MAK, Hunt MC, Alexson SEH. The identification of a succinyl-CoA thioesterase suggests a novel pathway for succinate production in peroxisomes. *J. Biol. Chem.* 2005;280(46):38125–38132.
132. Lie J, De Crom R, Van Gent T, et al. Elevation of plasma phospholipid transfer protein increases the risk of atherosclerosis despite lower apolipoprotein B-containing

lipoproteins. *J. Lipid Res.* 2004;

133. Zhang K, Liu X, Yu Y, et al. Phospholipid transfer protein destabilizes mouse atherosclerotic plaque. *Arterioscler. Thromb. Vasc. Biol.* 2014;
134. Gong Y, Lee JN, Lee PCW, et al. Sterol-regulated ubiquitination and degradation of Insig-1 creates a convergent mechanism for feedback control of cholesterol synthesis and uptake. *Cell Metab.* 2006;
135. Mahley RW, Innerarity TL, Rall SC, Weisgraber KH. Plasma lipoproteins: Apolipoprotein structure and function. *J. Lipid Res.* 1984;
136. Qu J, Ko C, Tso P, Bhargava A. Apolipoprotein A-IV : A Multifunctional Protein. 2019;
137. Rashid HO, Yadav RK, Kim HR, Chae HJ. ER stress: Autophagy induction, inhibition and selection. *Autophagy*. 2015;11(11):1956–1977.
138. Sano R, Reed JC. ER stress-induced cell death mechanisms. *Biochim. Biophys. Acta - Mol. Cell Res.* 2013;
139. Ganley IG, Wong PM, Gammoh N, Jiang X. Distinct Autophagosomal-Lysosomal Fusion Mechanism Revealed by Thapsigargin-Induced Autophagy Arrest. *Mol. Cell*. 2011;42(6):731–743.
140. Du WW, Liu F, Shan SW, et al. Inhibition of dexamethasone-induced fatty liver development by reducing miR-17-5p levels. *Mol. Ther.* 2015;23(7):1222–1233.
141. Jo H, Choe SS, Shin KC, et al. Endoplasmic reticulum stress induces hepatic steatosis via increased expression of the hepatic very low-density lipoprotein receptor. *Hepatology*. 2013;57(4):1366–1377.
142. Kasem K, Gopalan V, Salajegheh A, et al. The roles of JK-1 (FAM134B) expressions in colorectal cancer. *Exp. Cell Res.* 2014;326(1):166–173.
143. Song T-J. Characterization of hepatocellular carcinoma cell lines based on cell adhesion molecules. *Int. J. Mol. Med.* 2012;1158–1164.
144. Doi I, Namba M, Sato J. Establishment and some biological characteristics of human hepatoma cell lines. *Gann, Japanese J. Cancer Res.* 1975;
145. Rebouissou S, Zucman-Rossi J, Moreau R, Qiu Z, Hui L. Note of caution: Contaminations of hepatocellular cell lines. *J. Hepatol.* 2017;
146. Clarke HJ, Chambers JE, Liniker E, Marciniak SJ. Endoplasmic Reticulum Stress in Malignancy. *Cancer Cell*. 2014;25(5):563–573.

147. Brüning A, Rahmeh M, Friese K. Nelfinavir and bortezomib inhibit mTOR activity via ATF4-mediated sestrin-2 regulation. *Mol. Oncol.* 2013;
148. Rahmani M, Davis EM, Crabtree TR, et al. The Kinase Inhibitor Sorafenib Induces Cell Death through a Process Involving Induction of Endoplasmic Reticulum Stress. *Mol. Cell. Biol.* 2007;
149. Wu X, Rapoport TA. Mechanistic insights into ER-associated protein degradation. *Curr. Opin. Cell Biol.* 2018;
150. Kao C, Chao A, Tsai CL, et al. Bortezomib enhances cancer cell death by blocking the autophagic flux through stimulating ERK phosphorylation. *Cell Death Dis.* 2014;
151. Banyard J, Bielenberg DR. The role of EMT and MET in cancer dissemination. *Connect. Tissue Res.* 2015;
152. Xu J, Lamouille S, Derynck R. TGF-B-induced epithelial to mesenchymal transition. *Cell Res.* 2009;
153. Reka AK, Chen G, Jones RC, et al. Epithelial-mesenchymal transition-associated secretory phenotype predicts survival in lung cancer patients. *Carcinogenesis*. 2014;
154. Chaudhari P, Tian L, Deshmukh A, Jang YY. Expression kinetics of hepatic progenitor markers in cellular models of human liver development recapitulating hepatocyte and biliary cell fate commitment. *Exp. Biol. Med.* 2016;

8 APPENDIX

8.1 Ethics Approval from İBG Animal Experiments Local Ethics Committee (İBG-AELEC)

İZMİR BİYOTIP VE GENOM MERKEZİ
HAYVAN DENEYLERİ YEREL ETİK KURULU (İBG-HADYEK)
KARARI

Toplantı Tarihi	: 26/02/2020	**Toplantı Günü**	: Çarşamba
Toplantı Sayısı	: 3	**Toplantı Saati**	: 15:30

Sayın Doç. Dr. Güneş ÖZHAN,

2020-011 Protokol No'lu; yürütücüsü olduğunuz "Fam134B'nin biyolojik işlevleri ve kanserle ilişkisi" başlıklı projenin uygulanmasında etik açıdan sakınca olmadığına oy birliği ile karar verilmiştir.

Bilgilerinizi ve gereğini rica ederiz.

(Proje yürütücüsü) **Doç. Dr. Güneş ÖZHAN BAYKAN** **Başkan**	**Vet. Hek. Kerem ESMEN** **Başkan Yardımcısı**
Prof. Dr. H. Alper BAGRIYANIK **Üye**	**Prof. Dr. Ensari GÜNELİ** **Üye**
Doç. Dr. Kasım DİRİL **Üye** (Katılmadı)	**Dr. Öğr. Üyesi Ayşe Banu DEMİR** **Üye** (Katılmadı)
Dr. Gülçin ÇAKAN AKDOĞAN **Üye**	(Projede araştırmacı) **Vet. Hek. Umur KELEŞ** **Üye**
None H. Muammer KARAGÖZ **Üye**	

8.2 Curriculum Vitae in ARBIS format



UMUR KELEŞ

Kişisel Bilgiler

İletişim Bilgileri

Doğum Tarihi	05/08/1988
İletişim Adresi	İzmir Biyotıp ve Genom Merkezi (İBG)
Telefon	(505) 897 61 09
E-posta	umur.keles@ibg.edu.tr
Web Adresi	

Öğrenim Bilgileri

01 Mart 2017 - Şu Anda (3 yıl 5 ay)
Doktora, Doktora, DOKUZ EYLÜL ÜNİVERSİTESİ, TÜRKİYE
İZMİR ULUSLARARASI BİYOTIP VE GENOM ENSTİTÜSÜ, MOLEKÜLER BİYOLOJİ VE GENETİK (DR) (İNGİLİZCE)
Diploma Numarası: -
Ağırlıklı Genel Not Ortalaması: 3.85 / 4.0

06 Haziran 2014 - 30 Ocak 2015 (8 ay)
Yüksek Lisans, Tezli Program, İHSAN DOĞRAMACI BİLKENT ÜNİVERSİTESİ, TÜRKİYE
MÜHENDİSLİK VE FEN BİLİMLERİ ENSTİTÜSÜ, MOLEKÜLER BİYOLOJİ VE GENETİK (YL) (TEZLİ)
Diploma Numarası: 150076657
Ağırlıklı Genel Not Ortalaması: 3.82 / 4.0

05 Eylül 2005 - 10 Haziran 2011 (5 yıl 10 ay)
Lisans, Anadal/Normal Öğretim, ANKARA ÜNİVERSİTESİ, TÜRKİYE
VETERİNER FAKÜLTESİ, VETERİNER PR.
Diploma Numarası: 2011-10-0047
Ağırlıklı Genel Not Ortalaması: 3.37 / 4.0

Deneyim / İşyeri Bilgileri

01 Ocak 2014 - Şu Anda (6 yıl 7 ay) (Tam Zamanlı)
ARAŞTIRMACI, ÖĞRETİM GÖREVLİSİ, İZMİR BİYOTIP VE GENOM MERKEZİ

Yabancı Dil Bilgileri

İNGİLİZCE (Okuma: İyi, Yazma: İyi, Konuşma: İyi)

Bilimsel Teknolojik Faaliyet Alanları

Bilimsel Teknolojik Faaliyet Alanı Bilgileri

Temel Bilimler -- Yaşam Bilimleri -- Moleküler Biyoloji ve Genetik -- Kanser Moleküler Biyolojisi

Temel Bilimler -- Yaşam Bilimleri -- Moleküler Biyoloji ve Genetik -- Genetik Mühendisliği

Oluşturma Zamanı: 21 Temmuz 2020 23:35:48

Temel Bilimler -- Yaşam Bilimleri -- Moleküler Biyoloji ve Genetik -- Hayvan Moleküler Genetiği

Temel Bilimler -- Yaşam Bilimleri -- Hayvan Biyolojisi -- Hayvan Doku Kültürü

Anahtar Kelimeler

Karaciğer Kanseri

Hepatoselüler Karsinoma

Kanser Genetiği

Otofaji

Deney Hayvanları

Transgenik Fare

Hücre Kültürü Teknikleri

Primer Hücre Kültürü

Ksenogreft

Moleküler Klonlama

Gen Transfeksiyonu

Hibridoma

Ar-Ge Yetkinlik

Makaleler

M. ÖZTÜRK, T. BATUR, U. EKİN, A. ERDOĞAN, E. İŞCAN, U. KELEŞ, Ö. ÖZ & Ç. ÖZEN, Molecular pathogenesis of liver cancer, Journal of gastrointestinal cancer, 2017, 1941-6628, 48, 3, 222-224.

C. OZEN, C. OZEN, G. YİLDİZ, G. YİLDİZ, A. T. DAGCAN, A. T. DAGCAN, D. CEVİK, D. CEVİK, A. ORS, A. ORS, U. KELES, U. KELES, H. TOPEL, H. TOPEL, M. OZTURK & M. OZTURK, Genetics and epigenetics of liver cancer, NEW BIOTECHNOLOGY, 2013, 1871-6784, 30, 4, 381-384.

Bildiriler

U. KELEŞ, G. KARAKÜLAH, E. İŞCAN, H. ERBAK YILMAZ & M. ÖZTÜRK, Hepatoselüler karsinomanın gelişiminde FAM134B: dost mu?, düşman mı?, Sözlü Sunum, Onkolojide İz Bırakanlar, 14 Kasım 2019, 17 Kasım 2019.

U. KELEŞ, E. İŞCAN, E. BAL & M. ÖZTÜRK, HEPATOSELÜLER KARSİNOMADA FAM134B'NİN MEZENKİMAL FENOTİP BELİRTECİ OLARAK BELİRLENMESİ, Sözlü Sunum, 3. ÇUKUROVA HEPATOSELÜLER KARSİNOMA KONGRESİ, 21 Şubat 2019, 23 Şubat 2019.

U. KELEŞ, Ç. ÖZEN, A. ÖRS, K. PADMANABHAN, S. DİMİTROV & M. ÖZTÜRK, DIFFERENTIATION OF HEPATOCYTE LIKE CELLS FROM IMMORTALIZED MOUSE EMBRYONIC FIBROBLASTS HARBORING LARGE T ANTIGEN, Poster Sunumu, MOLBİYOKON, 27 Kasım 2015, 29 Kasım 2015.

Projeler

PIA-BOSPHORUS-FRANSA, BURSİYER, HİSTON VARYANTLARININ KARACİĞERİN GELİŞİMİ, REJENERASYONU VE KANSERLEŞMESİNDEKİ ROLÜ, Yürütülen Kuruluş: KURULUŞ GÜNCELLENMESİ GEREKİYOR, Destek Alınan Kuruluş: , 15 Şubat 2012, 15 Ağustos 2014.

TÜBİTAK Burs ve Destekleri

Proje Bilgileri

111T558, Histon Varyantlarının Karaciğerin Gelişimi, Rejenerasyonu ve Kanserleşmesindeki Rolü, Uluslararası, Burslu, Sonuçlandı, ARDEB, KBAG - Kimya Biyoloji Araştırma Destek Grubu, Projeye Katılma/Ayrılma Tarihleri: 01.03.2012 - 15.08.2014, Proje Başlangıç/Bitiş Tarihleri: 15.02.2012 - 15.08.2014.

BİDEB Destekleri

UMUR KELEŞ, Etkinlik Destekleri ve Eğitim Bursları Müdürlüğü, 2211-A Genel Yurt İçi Doktora Burs Programı, Başvurusu Reddedildi, 2011 - 3, 01.10.2011 - 31.08.2016.
UMUR KELEŞ, Etkinlik Destekleri ve Eğitim Bursları Müdürlüğü, 2211-A Genel Yurt İçi Doktora Burs Programı, Başvurusu Reddedildi, 2013 - 1, 01.03.2013 - 28.02.2017.

Panelistlik/İzleyicilik/Raportörlük Sayısı

Panelistlik/Dış Danışmanlık Sayısı	ARDEB/BİDEB 0	TEYDEB 0	Toplam 0
İzleyicilik/Danışmanlık Sayısı	ARDEB/BİDEB 0	TEYDEB 0	Toplam 0
Raportörlük Sayısı	ARDEB/BİDEB 0	TEYDEB 0	Toplam 0